Chalk putty:

Specimen preparation and aging properties

C. Sanchez Alonso

Master of Science in Applied Earth Sciences
December 16, 2019

TU Delft

Chalk putty: specimen preparation and aging properties

by

C. Sanchez Alonso

to obtain the degree of Master of Science
at the Delft University of Technology,
to be defended publicly on Monday December 16, 2019 at 16:00 PM.

Student number:	4728645	
Project duration:	April 1, 2019 – December 16, 2019	
Thesis committee:	Dr. ir. D.J.M. Ngan-Tillard,	TU Delft, supervisor
	Prof. Dr. C. Jommi,	TU Delft
	Prof. Dr. P.L.J. Zitha,	TU Delft

An electronic version of this thesis is available at `http://repository.tudelft.nl/`.

TU Delft FUGRO

Preface

This research was conducted under the sponsorship and and supervision of Fugro GB Marine Limited in their test facilities in Wallingford, UK. I would like to express gratitude for providing the technical support, material, testing resources and housing. Recognition is given to the laboratory staff for the assistance in the preparation of the material, performance of the tests and data processing. Special mention to T. Nee for the mentorship and support throughout the project, N. Cottrell for the training in advanced soil laboratory testing and B. Sampurno for the overview of the project.

In TU Delft, I would like to thank D. Ngan-Tillard for the ongoing support and guidance and C. Jommi, whose valuable input and assistance contributed towards accomplishing the final result of this project. Finally, special thanks to all the academic staff in the MSc in Geo-engineering for the knowledge and abilities provided during these two years.

C. Sanchez Alonso
Delft, December 2019

Summary

Chalk putty is a soil-like material formed when intact chalk is disturbed. Its characteristics are known to improve over time. Chalk layers have recently been encountered in the North and Baltic Seas in the context of designing turbine foundations for offshore wind developments, and consequently awareness of the current lack of expertise concerning the characteristics of remolded chalk created around driven piles has increased. Offshore and onshore pile tests have shown that axial capacity increases more than five times after three months (referred to in the literature as "set-up"). Despite this evidence, laboratory replications of this phenomenon are scarce and the results inconclusive. In addition, specimen preparation techniques are not fully reported in the existing literature.

Preparing specimens and setting up tests without disturbing the material is therefore challenging since chalk putty is a very soft material, with undrained shear strength below 10 kPa, which behaves as a slurry even at medium densities. This thesis develops a preparation method that minimizes such disturbance and is suitable for commercial purposes. Dry crushed chalk specimens were compacted and saturated in the triaxial apparatus at target water content and subsequently stored in watertight containers for aging. Evolution of the characteristics of chalk putty over time was then assessed using laboratory tests. Triaxial tests with Bender elements, Direct Simple Shear, Constant Rate of Strain and Thixotropy tests were conducted on specimens aged up to three months.

The results show that the behavior of chalk putty cannot be classified with classic soil types. Constant Rate of Strain tests demonstrated a response comparable to silty soil, with a gradual transition between reloading and virgin compression lines leading to difficulty in determining the yield point. On the other hand, the critical state friction angle in shear tests was in the range of dense sand, while the stress-strain behavior presented a linear region followed by a destructuration phase which finally reached a hardening or softening phase at strains larger than 2%. In the volumetric response, this translated to an initial compressive response, succeeded by a constant volume phase during destructuration and eventual dilation or contraction at larger strains. Furthermore, it was further determined that the material possesses thixotropic properties when mixed with de-ionized water. Finally, the effect of time on the "set-up" seems to be limited. No increase in shear strength was recorded, while the initial shear stiffness decreased with aging time, due to unconfined preservation of the samples. However, the ultimate dilatancy of the specimens increased over time, which may be a result either of dissolved calcium carbonate during crushing and saturation reprecipitating or of recementation occurring around the grains.

Contents

1 Introduction

1.1. Motivation

Field experience shows that the mechanical properties of crushed and compacted chalk, also known as chalk putty, improve with time (Lord et al., 2002). In the 1970s, studies of chalk focused on its use as a fill material for embankments (Clayton, 1977).

After the discovery, exploitation and subsequent subsidence of the Ekofisk oil field in a chalk reservoir, attention was turned to the lack of knowledge about the properties and behavior of chalk (Hermansen et al., 1997). Subsidence originated from compaction of the reservoir rock due to the increase in effective stress upon the material as pore pressure decreased with production (Johnson et al., 1988). Injecting water to avoid the effect of subsidence resulted in further compaction, against the predictions (Hermansen et al., 1997). This phenomenon is explained by the weakening of the structure of chalk when it is in contact with non-equilibrium cold seawater, in addition to the degradation of the strength of this type of rock which is cause by increasing water saturation and is not only as function of stress (Johnson et al., 1988).

Today, with the expansion of the offshore wind industry, especially in the North and Baltic Seas. Chalk strata are found in the layers where the turbine foundations are designed in offshore projects in countries such as France, United Kingdom, Denmark, Germany and Poland awareness of the lack of knowledge about the evolution of chalk characteristics, particularly when chalk putty is involved. The design of structures in this type of rock is highly conservative due to the limited data about the behavior of the crushed material, which is formed when chalk is submitted to stresses. While field evidence shows an increase of the axial capacity over time of piles driven in chalk (Buckley et al., 2017, Ciavaglia et al., 2017, Jardine et al., 2018), the laboratory test results are unclear, not seeming to identify the mechanisms taking place within the putty samples.

Chalk is a calcareous rock of organic origin, North Sea chalk was formed in the Cretaceous period under shallow seas in Northwestern Europe (Lord et al., 2002). It is mainly composed of coccoliths, for this reason, it has a high percentage of calcium carbonate, while clay and silt are minor components (Bundy, 2013). When chalk present in any environment with enough energy to break any inter-particulate bonds, then chalk putty is formed. In pile driving, the increase of the local shear stresses around the shaft leads to puttification.

The characteristics of chalk putty mean that testing is problematic when following the existing standards given the characteristics of this material, at low dry densities the liquid limit is reached before full saturation and the plasticity index is very low, around 6%, which means that the change of consistency occurs swiftly (Clayton, 1977). This complicates the handling of undisturbed samples as well as the setup on the testing apparatuses.

The aim of this thesis is to develop a representative sample preparation method optimal in commercial applications. This means finding a technique that can be reproduced in commercial laboratories, specifying the steps taken and controlling all the variables, such as compression processes, so that these can be isolated in order to study the effect of each mechanism taking place in the specimens. Once this is achieved, the effect of aging in chalk putties will be studied by means of isolating the sample from external physical or chemical processes: drainage, redox reactions with the pile material and interaction with the ions in the porewater. This way, the extent of the cementation mechanisms in the reported gain of strength of the samples in the literature can be well understood.

Chalk samples were obtained from a site (referred to in this document as 'the site') by Fugro (Fugro, 2012). Belonging to the same geological unit, this chalk is reported to be composed by $CaCO_3$ in a 98.6%, and low to medium dry density (lower than 1.70 Mg/m^3). The samples have been stored in Fugro facilities and batches of reconstituted specimens will be prepared and tested after air drying and crushing. The method and justification are presented in this report.

1.2. Research questions

- What is the best sample preparation method of chalk putty for commercial purposes, to develop a representative, standardized and repeatable technique.
- What are the effects of aging mechanisms when samples are preserved in undrained conditions and isolated from external physical and chemical processes.

1.3. Content of this report

This report presents the work done towards answering the questions above, and is structured as follows:

- **Chapter 2**: Evidence regarding the increased axial strength over time of piles driven into chalk, analysis of the existing literature related to chalk putty, review of specimen preparation techniques, and conclusion.
- **Chapter 3**: Further elaboration of the objectives of the specimen preparation and the test program, description of the test types.
- **Chapter 4**: Report of the specimen preparation trials, description of the selected preparation technique, results of the tests from the initial phase.
- **Chapter 5**: Results and analysis of the tests from the main scope of the project.
- **Chapter 6**: Discussion of the results from specimen preparation and the testing program in terms of the material characteristics (compression, thixotropy, strength, stiffness).
- **Chapter 7**: Conclusions about the specimen preparation and the testing program, recommendations for further research.
- **Appendix A**: Test results from the initial scope.
- **Appendix B**: Test results from the main scope, presented by test type and aging time.
- **Appendix C**: Sample pictures after testing.

2

Literature review

2.1. Chalk: formation and characteristics

Chalk is a type of limestone with a high calcite content, up to 98%, which is made of the nanofossils of coccolithophores, known as coccoliths, deposited in a deep-sea environment. Te Latin term for chalk *"creta"*, and the Cretaceous Period takes its name from this type of rock since it is the period when North Sea and Baltic Sea chalk was formed. In-depth study of the properties of this rock was motivated initially by the discovery of the Ekofisk reservoir in the central sector of the North Sea. This, together with the outcropping of the material in the south of England and northwest of France led to research focusing on the properties of North Sea chalk formations although this type of limestone is also present in the Ontong Java plateau and the Caribbean Sea (Fabricius, 2007).

The diagenesis of North Sea chalk is related to a transgression period during the early Upper Cretaceous at the West European continental shelf (Figure 2.1). As the sources of sand and clay decreased with ongoing transgression, deposition of sediments with up to 98% carbonate content occurred (Carrington et al., 2011).

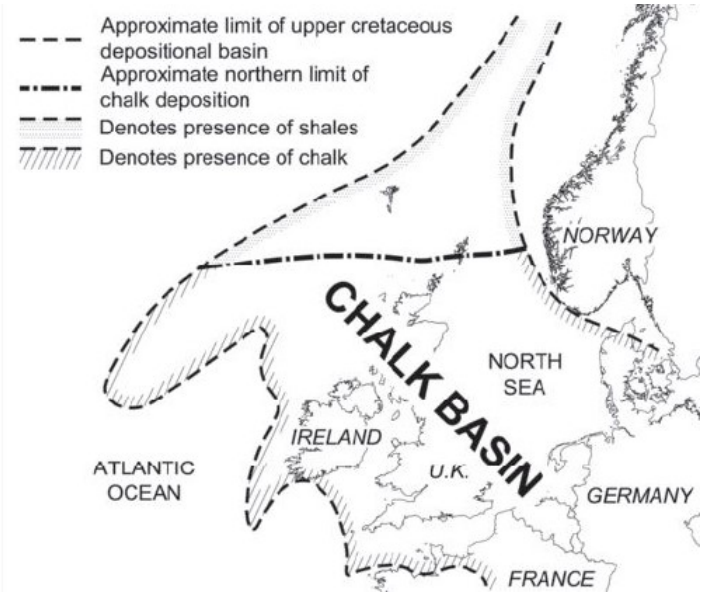

Figure 2.1: Chalk basin in North West European Continental Shelf. Source Anderton (1979)

Coccolithe nanofossils are the main component of this rock with sizes generally ranging from silt to clay, giving the texture of a mudstone. The microstructure is shown in Figure 2.2, where complete microphossils are blended with fragments. Occasionally, calcareous macrofossils can be identified but these features do not influence the physical properties as a whole. The silicious fraction of chalk comes from material transported from the continent by the wind or via rivers in the vicinity of the coast (Fabricius, 2007). Cementation in chalk occurs at a slower rate than in calcitep, this is the reason why the coccoliths remain distinguishable in SEM images (Lakshtanov et al., 2018). Clayton (1978) states that this cement may be originated from a supersaturated solution of calcium carbonate precipitating on the original grains, welding them together.

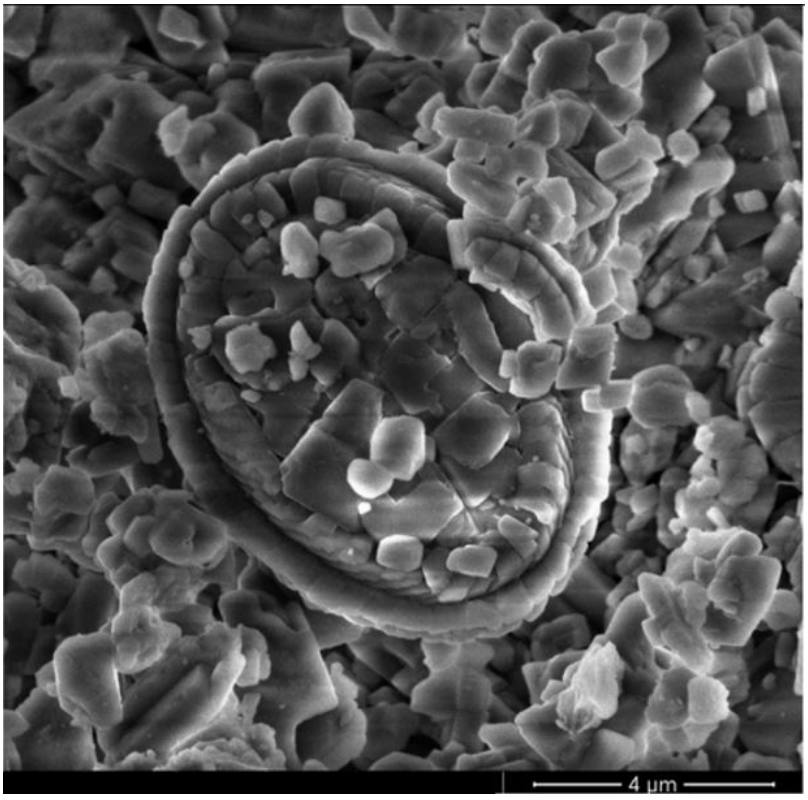

Figure 2.2: Scanning Electron Microscope image of chalk. Source Lakshtanov et al. (2018)

Bedding is typical in chalk formations and it ranges from 0.1 m-1 m thickness. Another remarkable feature in chalk deposits is the presence of flint. Formation of this feature results from a series of replacement and void filling process by deposition of dissolved biogenic silica (Madsen and Stemmerik, 2010). The presence of flint is of engineering relevance as it is highly influential in pile driveability and excavability of chalk

Regarding the engineering properties, these are mainly influenced by the dry density. The Unconfined Compressive Strength (UCS) ranges from 5 MPa to 27 MPa in low (less than 1.5 Mg/cm^3) and high (more than 1.9 Mg/cm^3) density chalk, respectively, but it is reduced to 50% - 70% when saturated (Waltham, 2002). Natural weathering is commonly due to frezee-thaw cycles or salt action. This, together with other processes such as undergoing shear stresses when chalk is used as a fill material and civil engineering works like tunneling, pile driving or rotary drilling produce a weak debris -chalk putty (Bundy, 2013)- whose properties will be discussed in the next section. For engineering purposes, chalk is classified in different grades based on the structure and weathering of the geotechnical unit, this classification is described at CIRIA PR 11 (et al. Lord, 1994) and further elaborated in Lord et al. (2002).

2.2. Chalk putty: definition and formation

Chalk putty, also referenced in the literature as 'crushed chalk', 'chalk slurry', 'remolded chalk' or 'destructured chalk', is defined by Bundy (2013) as a form of this sedimentary calcareous rock that results when the intact material is broken down into finer particles, and consequently losing the cementation between grains, behaving as a soil. In Figure 2.3 the microscopic structure of chalk putty is shown.

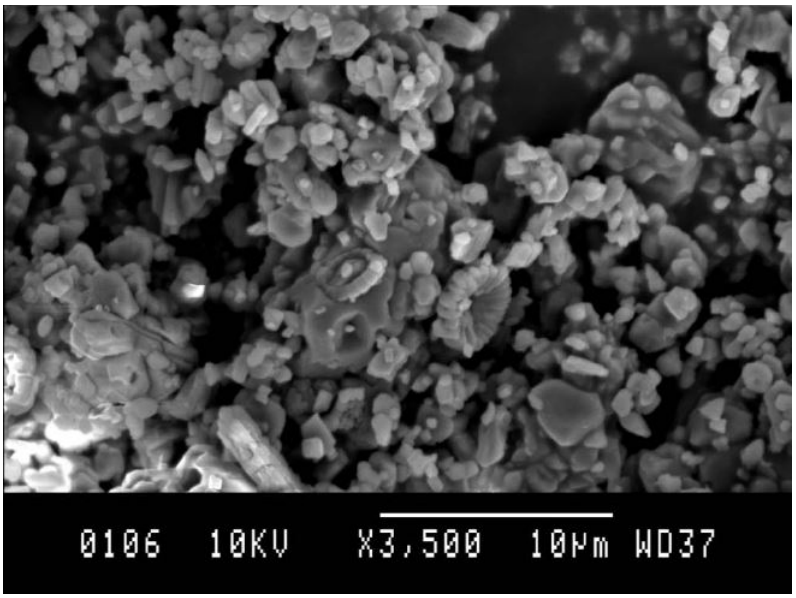

Figure 2.3: Scanning Electron Microscope image of crushed chalk, cement infilling can be observed in the center of the image. Source Bundy (2013)

Occurrence of this process is reported by Bundy (2013) to take place in any environment where energy is enough to break down any inter-particulate cement bonds. This weakening may be a result of shearing, crushing, vibration or degradation of the cementation by weathering processes (Ciantia, 2018). Therefore, some putties are a result of natural processes such as local shear stress or weathering but many are a result of handling intact chalk during civil engineering projects like embankments (Clayton, 1977), tunneling (Razoaki, 2000) or pile driving (Buckley et al., 2017, Ciavaglia et al., 2017, Muir Wood et al., 2015). The behavior of chalk as a particulate material is also referred by Leddra and Jones (1990) in chalk reservoir wells.

The extent of the disturbed area around a pile was studied by Muir Wood et al. (2015) driving plates into low to medium density chalk (up to values of 1.70 Mg/m^3). The typical width of the disturbed area is reported to be of 40% of the plate width. Moreover, Ciavaglia et al. (2017), in a test program aiming to quantify the development of axial resistance of piles driven in chalk, measured the disturbed annulus around an open-ended driven pile (shown in Figure 2.4), which was reported to have 20 mm-40 mm thickness around the shaft on piles with an outer diameter of 762 mm and a pile wall thickness of 44.5 mm. Buckley et al. (2017) measured a disturbance up to 14 mm away from the pile shaft of 139 mm in diameter and 8.5 mm wall thickness.

2.3. Field evidence of monotonic axial pile set-up in chalk

As reported by Lord et al. (2002), it is generally known from field experience that the mechanical properties of crushed and compacted chalk improve with time.The factors controlling the rate of mechanical property improvement are not well understood in the academic literature. Authors attribute this to water content loss through drainage and cementation from calcium carbonate released during compaction.

With the purpose of quantifying the positive gain in capacity (referred in the literature as set-up) and, therefore improving the pile design methods in chalk, studies on the behavior of piles driven in chalk have been

Figure 2.4: Evidence of the remoulded annulus around a driven pile in chalk. Source Ciavaglia et al. (2017)

carried out as a part of the Joint Industry research project (JIP) that took place between 2015 and 2016 involving Scottish Power Renewables, Imperial College London and Geotechnical Consulting Group. These testing programs included offshore pile testing at the Wikinger offshore wind farm project site and testing of onshore piles driven in chalk at a site located in a previous chalk quarry close to St-Nicholas-at-Wade in Kent, UK. It was reported that after 80 days, the measured water content in the disturbed area formed during pile driving is lower than the average in the field (Buckley et al., 2017).

Buckley et al. (2017) undertook the first pile testing program as a part of the JIP. Seven open-ended uninstrumented steel pipe piles of 139 mm diameter and 8.5 mm thick were driven into chalk. The monotonic axial set-up factors -ratio of the shaft capacity on aged piles against initial shaft capacity- exceed those observed in sands (Gavin et al., 2015) allowing to draw an aging trend which the author affirms that follows a curve as the one presented in Figure 2.5. Possible reasons for this capacity increase were determined as consolidation of the chalk putty formed around the interface, redox reactions of the pile steel and the chalk or recementation of the chalk putty.

As a continuation of the testing program described above, Buckley et al. (2018) reported the tests on two instrumented close-ended piles with an outer diameter of 102 mm. These piles were slowly jacked and subjected to tension testing after full reconsolidation, 23 days and 80 days of aging. The results of those tests, presented in Figure 2.5, show the loss in capacity due to the decrease of the chalk specific volume and therefore the effective stress around the pile. No puttified zone was observed on the extraction of the close-ended jacked piles. In the conclusions, it is stated that the aging mechanisms and loading behavior in time might be more related to the pile geometry or installation method rather than the recementation process or redox reactions between the pile and the soil.

Remotely controlled full-scale seabed pile load static tension tests were done by Jardine et al. (2018) 11 weeks to 15 weeks after driving 3 steel tubular piles of 1.37 m of diameter. The soil of the site is made of a superficial layer of clay, overlaying glacial till of variable thickness and then chalk is found at depths ranging 30 m to 60 m. The test site is in the location of an offshore wind farm where piles of the foundations are driven up to the chalk layer on 50 out of the 70 turbine locations. The gain of shaft capacity was observed in time due to the aging of chalk as well as the slow pore pressure dissipation mechanisms taking place in the glacial till. This set-up in chalk exceeded the predictions of the model developed by Buckley et al. (2017). The specifications of the tests and results can be found in Figure 2.6.

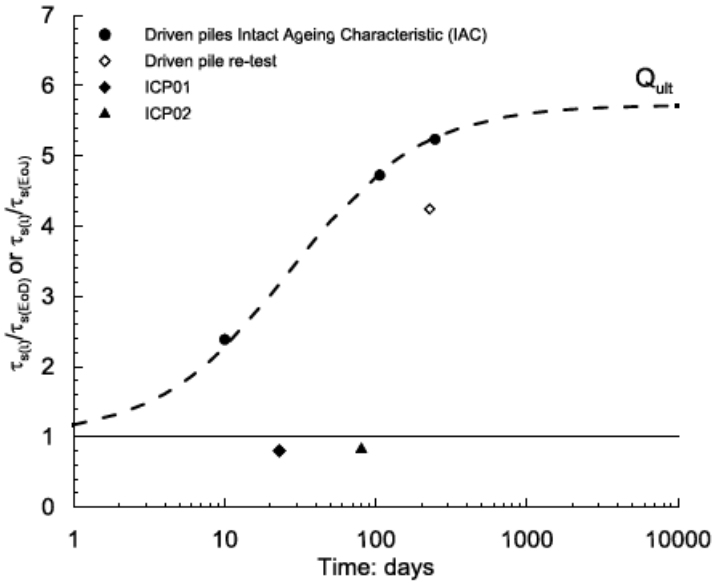

Figure 2.5: Set-up factors from Buckley et al. (2017) and Buckley et al. (2018) compared in time after the equalization periods. The horizontal axis shows the elapsed time in days, while the vertical axis shows the ratio of the shaft capacity measured at each test over the shaft capacity at the end of driving ($\tau_{s(EoD)}$) for the driven pile tests Buckley et al. (2017) and at the end of jacking ($\tau_{s(EoJ)}$)for the instrumented jacked pile tests (Buckley et al., 2018). Source Buckley et al. (2018)

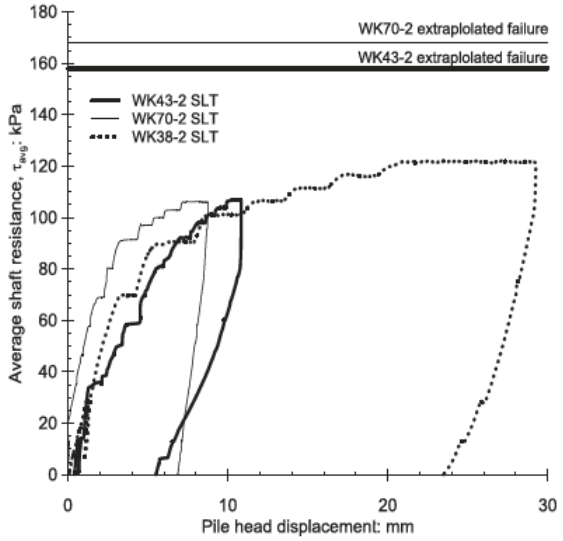

Figure 2.6: Offshore static load tests at Wikinger site including extrapolated failure points for chalk-dominated locations. The curves show the shaft resistance as a function of pile head displacement from tests preformed after 38 days, 43 days and 70 days. On the last two tests, the failure shaft resistance is extrapolated. Source Jardine et al. (2018)

Finally, Ciavaglia et al. (2017) carried out uplift tests on two instrumented tubular driven steel piles shortly after driving (2-6 days), after 7 weeks and after 4 months. One of them was not subjected to load while the other was used to determine the effect of lateral loading in the build-up of shaft resistance over time. The testing program and results are presented in Figure 2.7. showing the set-up of unit shaft resistance over time for both piles.

In summary, although the build-up of strength in axial pile capacity has been reported in the literature about both onshore and offshore driven piles, the mechanisms are fairly unclear. Authors attribute this set-up to different mechanisms among which the dissipation of excess pore pressure and the structural changes within

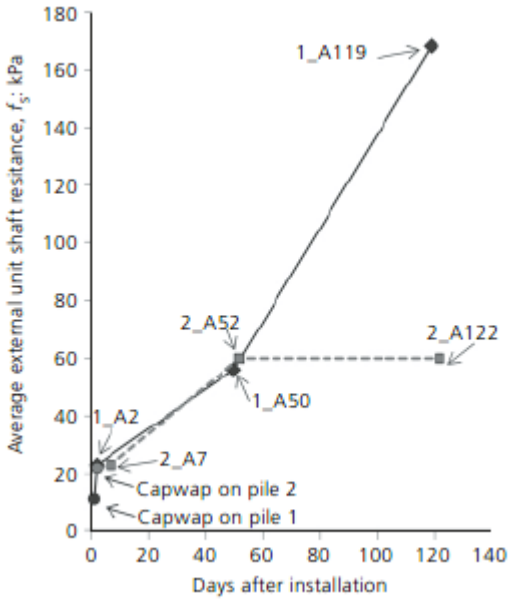

Figure 2.7: Average unit shaft resistance against time elapsed since pile installation. Full line shows the results of the tests on a pile without the action of lateral loading after 2 days, 52 days and 119 days. Dashed line shows the results of the tests on piles subjected to lateral load up to 10% of the lateral capacity before uplift tests after 7 days and 52 days and 50% of the lateral capacity up to 122 days. Source Ciavaglia et al. (2017)

the chalk putty are found. However, Buckley et al. (2018) characterized the porewater dissipation process as rapid, due to the small thickness of the puttified annulus, while the piles continue gaining in capacity even four months after driving (Ciavaglia et al., 2017).

2.4. Laboratory work on chalk putty

In the literature, scarce laboratory testing on chalk putty can be found. The early works focus on the behavior of chalk as a fill material (Clayton, 1977, Razoaki, 2000), to understand the behavior of putty in general. Bundy (2013) looks for an overview of the behavior of chalk putties in any type of earthwork. Finally, recent literature is centered on offshore applications (Bialowas et al., 2018, Doughty et al., 2018).

2.4.1. Sample preparation and test setup

In the mentioned publications, there are two main types of techniques reported used to prepare the samples: The first one involves drying the rock material before crushing and sieving it. Differences in these first type of methods are found in the way of saturating the samples that will be subsequently described (Bialowas et al., 2018, Bundy, 2013, Clayton, 1977, Razoaki, 2000). The other technique involves compaction of the chalk sample without addition of water using a proctor compactor (Doughty et al., 2018).

There is not much information in the early literature about the way the specimens were saturated at desired water content. Clayton (1977) described that the samples were prepared in two days to a 25% water content and 1.95 Mg/m^3 bulk density making sure that there was no loss of water between the preparation and testing. No further details on the test setup are given.

On the other hand, Razoaki (2000) obtained samples from slurries from a tunneling project, this slurry produced by the Tunnel Boring Machine (TBM) had a very high water content. The particle size of the material was silt to clay-sized. Preparation was done by washing the material through a 425 μm sieve (retaining mainly flint), the material was air-dried, crushed and sieved another time. Mixing all of the material thoroughly to

ensure uniform properties. Then, the dry obtained material was mixed to a water content of 28%, equal to liquid limit. Afterward, the resulting slurry was deposited in a consolidometer device in three layers in order to avoid trapped air, no standardized method was specified, vibrating the consolidometer while mixing the slurry with a glass rod to release air bubbles. Specimens were stored for aging under full saturation condition in a relatively constant temperature room. This drained aging took place with a constant load of 10 kg, the area is not specified so the pressure cannot be calculated. Undrained aged test specimens were prepared, compressed for a few hours, sealed, waxed and stored for aging. To ensure that there was no loss in water during undrained aging the weight of the samples were checked at a regular basis.

Bundy (2013) describes in more depth the process followed to prepare for triaxial testing. The raw samples were first dried, after being broke into gravel-sized pieces. Then a Tema mill is used with different grinding times in order to achieve different particle sizes. A method named the 'dry press' technique was used in his work. In summary, the dry powder from the mill is placed on a manufactured 'suction' split former with a triaxial test membrane placed in a load frame. The material is placed in ten layers and compacted with a plunger. Once the sample was formed, the setup was placed on the triaxial cell with a suction cap keeping the integrity of the sample during setup. Subsequently, the samples were saturated using flushing de-aired distilled water, without using carbon dioxide as it is customary in this technique because it creates acidic conditions within the sample possibly leading to dissolution. Instead, an upward flush of water was created until a volume greater than the sample had passed from the top line. After this, increases in cell pressure and back pressure were introduced in order to achieve saturation of the sample, keeping an effective cell pressure of 15 kPa. Neither the water content not the bulk density of the samples achieved by this method is specified in this study.

Bialowas et al. (2018), fabricated the chalk samples using one large batch of homogeneously crushed chalk. To do so, small blocks of chalk were oven-dried at 105° for 48 h, crushed, first gross with a plastic mallet and soil grinder then fine with a Jaw Crusher and subsequently mixed. The water used in the sample preparation was infused with chalk particles for 30 days. Then the slurry was created by means of mixing the dry chalk with the infused water and degassed under vacuum for 2 hours with some gentle vibrations, moved into a funnel with a ball valve at the end of the neck to remove air pockets and finally the slurry was degassed for an additional 30 minutes in order to reach a high degree of saturation prior to consolidation. The water content targeted was 2.2 times the liquid limit. Finally, the samples were placed in a consolidometer device with a vertical pressure of 300 kPa, the mode of application of this load is not specified. For triaxial setup, the samples were extruded and placed on the pedestal and a vacuum of -10 kPa was placed after the membrane was applied. The water content of the sample after consolidation was not measured.

Finally, Doughty et al. (2018) tried a different preparation method that would maintain the water content from the field. To do so, chalk putty was formed by compaction without the addition of water. 2.5 kg Proctor compactor applying 270 blows or until no further compaction can take place. No drying or sieving took place in order to reproduce site conditions. It was the objective to maintain the natural water content of the undisturbed samples. Samples were aged in drained and undrained conditions. Undrained aging took up to 28 days while drained aging 0, 7 and 14 days, after the consolidation of the samples, aging was done under constant isotropic stress (100 kPa and 200 kPa).

As described in Doughty (2016), the setup of the drained aged samples in the triaxial apparatus was achieved after three attempts. The first was the installation of the sample with no porous stone at the top and with suction until the mold was removed. Once the mold was detached, the top cap was placed and suction turned up at the bottom, the low permeability of the chalk lead to an inconsistency of the properties within the sample because the suction only affected the bottom third of the sample. The second contemplated placing the sample in a consolidometer under a small load before extruding it onto the pedestal, this method involved consolidation before testing on day 1, therefore missing some processes that may take place during consolidation. Finally, the third involved installation of the putty using a split mold that allowed controlled draining, with no suction and adding a porous stone on the top.

Table 2.1: Summary of the specimen preparation methods described above.

Author	Crushing	Specimen preparation	Ageing condition
Clayton (1977)	Crushed and sieved	Not specified. 25% water content and 1.95 Mg/m^3 bulk density	Not specified
Razoaki (2000)	Crushed and sieved	Mix material to 28% water content. Prepare specimens in consolidometer device with 10 kg constant load	Drained with constant load, undrained in wax
Bundy (2013)	Crushed with different grinding times	'Dry press' technique, sample is prepared in the split mold with test membrane, suction cap is placed on top for test setup. Saturation by flushing water and cell and back pressure increments.	Drained
Bialowas and Diambra (2018)	Crushed with plastic mallet and soil grinder and Jaw Crusher	Not specified final water content. Mixed dry material with water infused with chalk to a water content 2.2 times the liquid limit and set in a consolidometer device at 300 kPa. Specimens extruded on the triaxial pedestal	Drained
Doughty (2018)	Proctor compacted	Place samples in split mold with membrane, compacting the putty while placing it in layers. Weight on top placed for consolidation. Water ejected is given but no values of final water content.	Drained for triaxial testing, undrained for fall cone tests

2.4.2. Testing regime

Clayton (1977) undertook consolidated triaxial undrained with pore water pressure measurement. Assuming that the effective friction angle remains constant in time, he studied the evolution of the effective cohesion with time.

Razoaki (2000), performed different batches of tests on the drained aged slurry and the undrained aged slurry. With drained and undrained triaxial tests on the unaged slurry, he proved that the behavior of the chalk putty is similar to granular soils that have dilative behavior in shear. To do so, the samples were preconsolidated for 4 hours, before testing. On the aged slurry triaxial drained and undrained tests were conducted, where the changes of behavior during isotropic compression and shear deformation were recorded. It was concluded that creep of the drained aged slurry increases the small strain stiffness and yield, which does not happen in undrained aging.

Bundy (2013), undertook a thorough research on the behavior of the chalk putty including index testing as well as strength tests, all these are hereby listed: unconsolidated undrained triaxial (UU), consolidated triaxial testing with pore pressure measurement, particle size distribution (PSD), porosity and dry density, Atterberg limits, shear strength with fall cone of putty, shear box (with effect of time-dependent volume changes) and ring shear.

In their research Bialowas et al. (2018) developed a testing program involving 21 triaxial tests were performed on the reconstituted samples aged up to 71 days, after isotropic consolidation with different overconsolidation ratios at final cell pressures of 100 kPa, 200 kPa, 300 kPa and 400 kPa. Additionally, two oedometer consolidation tests (K_0 condition) were carried out to test the loosest state possible of the samples and achieve higher pressures.

At last, Doughty et al. (2018) carried out a program involving thixotropy tests on undrained aged samples and triaxial tests on drained aged samples. The falling cone measured an increase of C_u from 2 kPa to 6 kPa was measured, which was related to thixotropic hardening. Triaxial tests were performed after different times of drained aging under 100 kPa and 200 kPa for 7 days and 14 days. The results from triaxial tests show ductile samples after 0 days of consolidation. During the test, sample first shows compaction and dilation afterward, this is explained by the fact that no structure was formed within the soil. On the aged samples, a higher initial stiffness is shown due to the formation of a stable structure and recementation. The behavior of the sample is dilative under shear, with a strain-hardening response.

2.5. Measured properties of chalk putty

The chalk used in this study, as well as the chalk encountered in offshore projects (Barbosa et al., 2015, Carrington et al., 2011, **?**), studies referenced in literature (Buckley et al., 2017, Ciavaglia et al., 2017, Sorgi and De Gennaro, 2011) are mostly low to medium density chalks in their intact form. The properties of this material are presented in the following sections.

2.5.1. Index properties

- Particle size distribution

When chalk is crushed for testing, the grain size distribution evolves with grinding time (Bundy, 2013, Clayton, 1978), the fine proportion increases with longer crushing time. Moreover, the type of mill influences the particle size distribution for a given grinding time (Clayton, 1978). For instance, Bundy (2013) created specimens of particle sizes between the basic coccolithic lath and collections of entire coccolith shields and shields at various stages of disintegration. The predominant particle size is 2 μm-4 μm. Crushed chalk by Bialowas et al. (2018) contained 80% of fines (particles of a size below 63 μm), being the mean grain size 6.74 μm, these fine particles are, however, chemically inactive (Figure 2.8.). In contrast, Puig (1973) created chalk putties by means of disintegration of the natural material by vibration, Clayton (1978) found that the particle size distribution of those is similar to the measured from field samples.

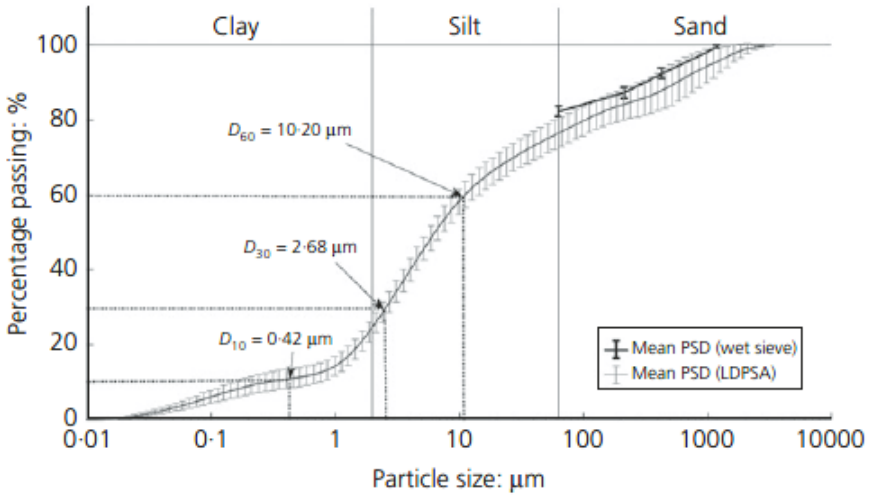

Figure 2.8: Particle size distribution of crushed chalk. In this plot clay refers to a particle size rather than a type of particle. Source Bialowas et al. (2018)

- Atterberg limits

Bundy (2013) measured the value of the Atterberg Limits on crushed samples from different chalk formation. These chalk putties were classified as low plasticity silt soils in the Casagrande chart, with liquid limits from

19% to 26% and measuring a plasticity index equal to 4% in the samples from the four different formations. Also Clayton (1977) found that the plasticity index of chalk lies close to 6% in the studied samples. Additionally, it was reported that the clay mineral content does not significantly affect the Atterberg limits due to the high content in calcium carbonate. Furthermore, Puig (1973) found a relationship between the *in-situ* dry density and the plasticity of chalk, with low strength chalk having a higher liquid limit than harder chalks.

On the pile site presented previously in this chapter, the low to medium density Margate chalk in St-Nicholas-at-Wade in Kent, was found to have a liquid limit between 30 and 31% with a plasticity index of 6.4% on average by Buckley et al. (2017). Bialowas et al. (2018) measured a liquid limit of 29.4% and 7.4% plastic index on samples from the same site.

- Hydraulic conductivity

The hydraulic conductivity is dependent on the dry density of the chalk slurry, the packing of the particles determines this parameter, chalk putties with decreasing dry densities have higher hydraulic conductivity.

2.5.2. Thixotropy

Although the concept of thixotropy is nominally defined for clays, it can also be extended to other slurries such as chalk slurries. McGraw-Hill and Parker (2003) defines this phenomenon as "Property of certain gels which liquefy when subjected to vibratory forces, such as ultrasonic waves or even shaking, and then solidify again when left standing". It is an isothermal, reversible, time-dependent process which normally takes place under undrained conditions (Mitchell, 1961). Usually, the thixotropy strength ratio -the ratio between the shear strength after time with thixotropic strength gain and the shear strength just after remolding- depends on the mineralogical composition of the clay (Yang and Andersen, 2015).

Boswell (1948) studied the thixotropy of sedimentary rocks, among which chalk can be found. In this research, Sendonian Chalk was characterized as 'moderately thixotropic', as much as other clay/silt materials. Furthermore, Doughty et al. (2018) measured the evolution of the thixotropic properties of chalk putty in a 24-day time span. The undrained shear strength of the specimens measured with falling cone increased from 2.4 kPa to 7.4 kPa in the elapsed time (Figure 2.9.), this increase follows a log-linear trend in time although the correlation of the measurements is qualitatively low. Bundy (2013) also shows an increase in undrained shear strength of chalk putty in time, measured with fall cone.

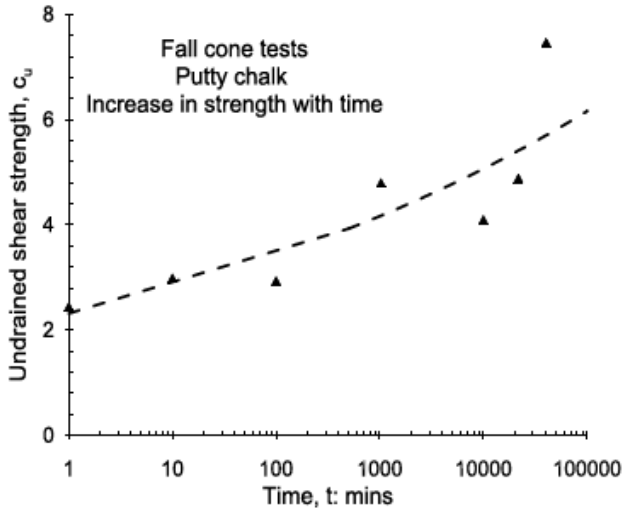

Figure 2.9: Measured undrained shear strength with fall cone test on aged chalk putty. Source Doughty et al. (2018)

2.5.3. Compression

No comprehensive studies on the compression response of chalk putties have been developed to date. Bundy (2013) reported a fast primary consolidation of the material and negligible creep effects. For this reason, no further investigation of these effects was undertaken. In agreement with this, Buckley et al. (2017) affirms that the dissipation of excess porewater pressure around driven piles occurs in a rapid manner, which is also due to the fact that the putty annulus has a small thickness.

Bialowas et al. (2018) carried out oedometer tests on reconstituted crushed chalk samples up to 10 MPa of vertical stress giving the compression curve shown in Figure 2.10. The results of these tests show that particle crushing occurs beyond 2 MPa axial stress. During isotropic consolidation in the triaxial cell, the small-strain shear stiffness was measured with Bender Elements, which has a logarithmic relation with consolidation stress. Regarding secondary consolidation, creep deformation is inversely proportional to the overconsolidation ratio (OCR), this means that normally consolidated samples experience a larger amount of deformation.

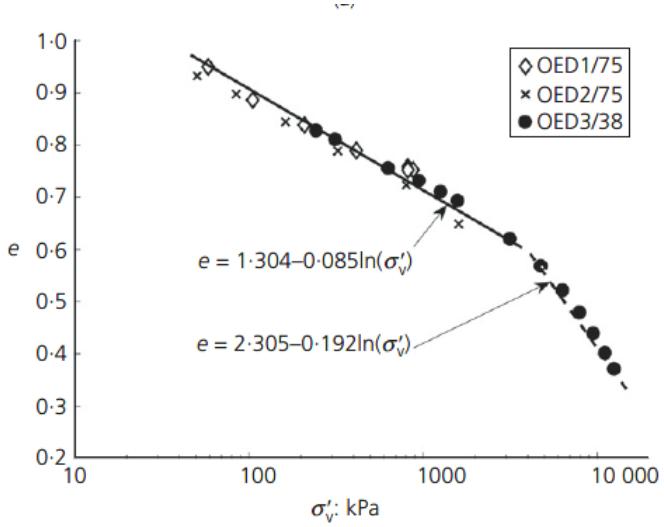

Figure 2.10: Consolidation paths from oedometer tests. Source Bialowas et al. (2018)

2.5.4. Stiffness

Alvarez-Borges et al. (2019) investigated the stiffness of chalk putty by means of undrained triaxial tests with Bender Elements, finding out that the mean effective stress is the dominant parameter affecting small-strain stiffness. Large strain stiffness was found to be nonlinear with strain-softening behavior in samples prepared at a water content equal to the liquid limit and strain hardening behavior in specimens prepared at a water content equal to the plastic limit. However, no increase in large strain stiffness with larger consolidation pressures is recorded.

Bialowas et al. (2018) tested the evolution of the small-strain stiffness during secondary consolidation, an increase of small-strain stiffness was found, this increase is larger with decreasing OCR. These authors have found additionally, that the initial stiffness of chalk putty specimens increases with OCR when tested in the triaxial cell at 300 kPa.

2.5.5. Strength

Clayton (1977) reports a dependence of the undrained shear strength with the water content, this is related to the swift change of consistency within a small range of specimen water contents.

Several values for the friction angle are recorded in the literature for chalk putties, although the general agreement is that the value ranges between 30° and 36°. Clayton (1977) assumes a constant value of 35.5° for the friction angle, with a cohesion equal to 0 kPa at time 0 and evolution of the effective cohesion in time. Bundy (2013) found non-linearity in drained shear failure envelopes, the effective friction angle evolves with the grading from 29° to 37°. Bialowas et al. (2018) measured an ultimate friction angle $\phi = 31°$.

2.5.6. Time dependency of properties

Clayton (1977) concluded that there is an increase of effective cohesion in time from 4.0 kPa to 13 kPa after 85 days then reaching a plateau as shown in Figure 2.11. Clayton (1977) reports additionally an increase of strength with increasing confining pressure.

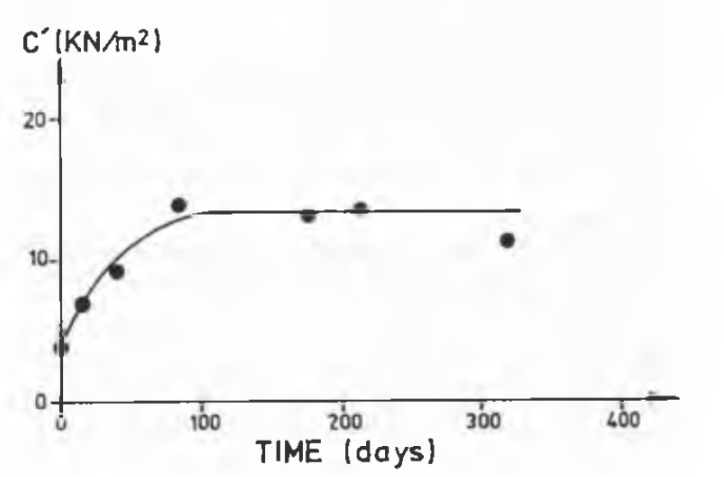

Figure 2.11: Evolution of the effective cohesion with age on chalk putty specimens. Source Clayton (1977)

On the other hand, Razoaki (2000) concludes that creep deformation and subsequent densification during drained aging allows the material to develop structure. Creep also increases small strain stiffness and yield of the material. In undrained aging, where no creep densification occurs, no changes in the stiffness and yield of the material are measured. Razoaki (2000) suggests that aging is a creep-related phenomenon. And states that the increase in post-yield volume contractions during drained and undrained aging signifies that changes other than creep effects have occurred in the fabrics of the soil.

Bundy (2013) measured the strengthening of the putty samples in time using fall cone testing. Even though loss of water during aging was reported, the results corrected for water content show an increase in the strength at a constant water content, which is not specified. The decrease in penetration in time is plotted in Figure 2.12, which shows an increase in undrained shear strength, since the units or the size of the fall cone are unknown, the value cannot be determined. However, in this study, the contribution of cementation or re-cementation to the strength is found negligible when the samples are tested in the shear box, this is depicted in the results presented in Table 2.2. The fact that no change in sample fabric, observed with the scanning electron microscope (SEM), was found is additionally used to support this argument. The data presented by Bundy (2013) is admittedly limited, with triaxial tests performed only during a three-week period.

Bialowas et al. (2018) Found age-related strength gains to be negligible although a consistent increase of small-strain shear stiffness in time was observed measuring the shear wave velocity with Bender Elements, the reason to this increase is related to creep deformations. As a matter of fact, the samples were found to have a considerable amount of creep, lasting beyond the 72 days of aging to which the samples were subjected during the experimental program, creep aging is described by a linear law with respect to the logarithm of time. Besides consolidation related changes in stiffness, the specimens do not appear affected by the aging. In the

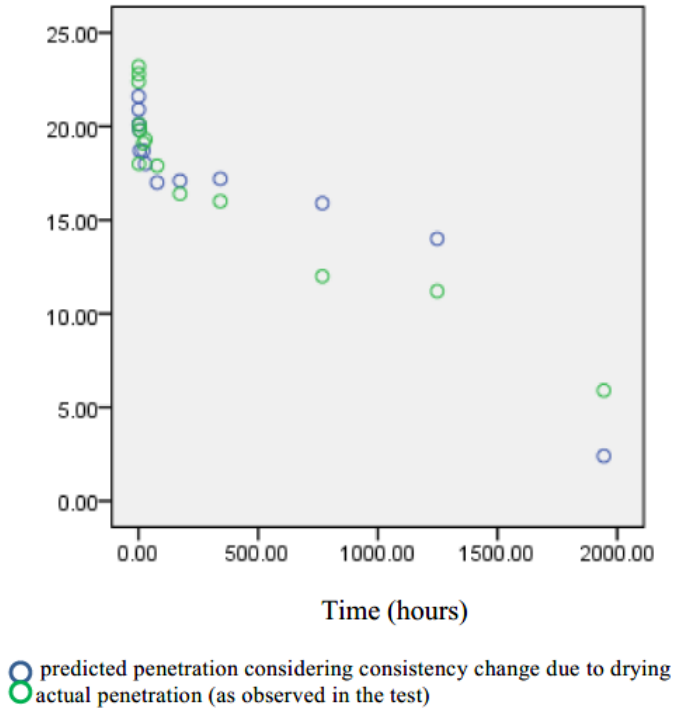

Figure 2.12: Measured penetration and corrected for consistency change with water content testing with cone penetrometer on aged chalk putty. Units of the Y axis not specified by the author, it is assumed it shows the penetration of the fall cone in mm. Source Bundy (2013)

Table 2.2: Results of the ageing effects on strength of chalk putty, tested on drained direct shear box apparatus under 100 kPa vertical stress. Source Bundy (2013)

Test period (days)	Peak strength (kPa)	Residual strength (kPa)
3	75.1	69.4
25	73.1	68.3
50	72.8	67.5

conclusions, it is affirmed that the recementation process described by Clayton (1977) may have an effect on this increase of stiffness during secondary consolidation.

Doughty et al. (2018), contrary to the previous authors, finds an increase in undrained shear strength of chalk putty due to a combination of thixotropic hardening, recementation, and consolidation. Regarding the samples subjected to undrained aging, thixotropic hardening was measured with fall cone tests. The results shown in Figure 2.9 show an increase of the undrained shear strength from 2.4 kPa to 7.4 kPa after 28 days. The results from the triaxial tests of samples consolidated to 100 kPa and 200 kPa and subjected to undrained testing show that the aged shear strength increases but not with the same magnitude as in the field tests.

2.6. Cementation in chalk putty

Cementation, according to Lord et al. (2002) is accepted in the engineering community to be one of the mechanisms taking place in chalk putty. Chalk putty is formed due to the compaction and shear of chalk, these mechanisms generate finer particles of $CaCO_3$ that accumulate around the grain boundaries providing cement for growth. Over time, cementation and recrystallization processes occur. Evidence of this process is provided by Clayton and Matthews (1987), aragonite crystals which were not present prior to construction were found on a chalk fill through SEM imaging (Figure 2.13).

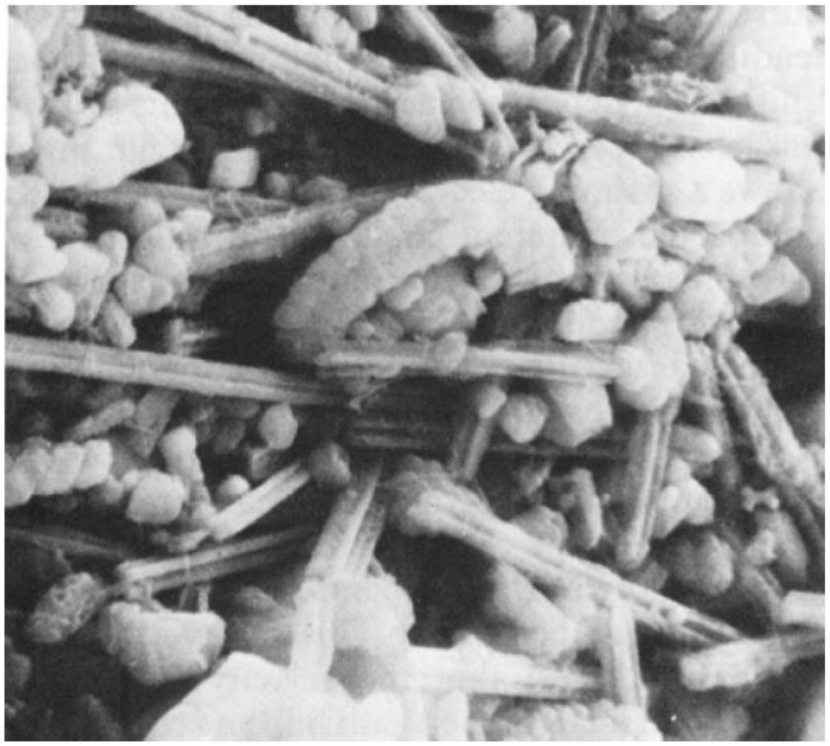

Figure 2.13: SEM image showing aragonite crystals within the chalk fill microstructure. Unknown scale. Source Clayton and Matthews (1987)

In diagenesis of chalk, the cementation process is described by Neugebauer (1974). When chalk is subjected to high burial pressures, the calcium carbonate at the points of contact is dissolved, migrating to the pore fluid. Once the pressure in the fluid decreases, the concentration of $CaCO_3$ in the pore fliud is in a state of oversaturation, as a result, the cement deposits allowing recrystallization.

2.7. Behavior of chalk and chalk putty

The mechanical behavior of chalk has been modelled by Ciantia (2018) as strain hardening elasto-plastic material with tensile strength which comes from the bond between particles of the soft rock. Figure 2.14. shows the expansion of the yield locus resulting from this tensile strength and the increase in isotropic pre-consolidation pressure due to interparticle bonding (p'$_t$ and p'$_m$, respectively). The shape of the uncemented yield locus isshown in green.

Leddra and Jones (1990) conclude that low-density chalk deforms under shear in an equivalent way to soil at critical state condition. Chalk at small consolidation pressures exhibits strain-softening behavior, while large consolidation stresses lead to a strain-hardening response, which is common to soils. This is caused by the damage to the cement bonds between grains making the chalk behave like a particulate material with critical state behavior.

In agreement with this, Lagioia and Nova (1995) proved the critical state behavior of calcarenite through laboratory tests. This material has a stage called the destructuration phase, where it transitions from rock to soil-like material named as destructuration phase. In this stage, the deviatoric stress is constant while the strain increases, it is followed by a hardening or softening phase which concludes in the critical state.

Consequently, it can be assumed that the behavior of the chalk subjected to high pressures is comparable to that of unaged chalk putty since the bond between grains has been lost in both cases. The behavior of saturated chalk putty can be modeled according to constitutive models of sand (i.e. strain-hardening models).

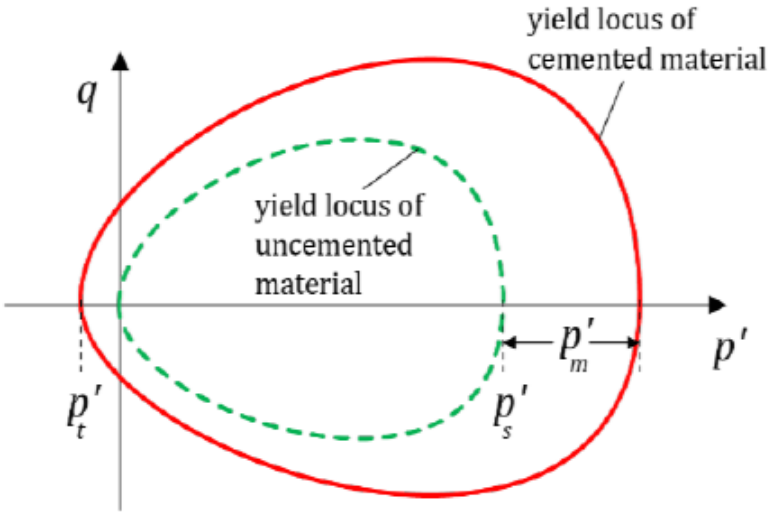

Figure 2.14: Yield locus of soft rocks, including the effect of cementation. Source Ciantia (2018)

2.8. Sand/silt sample preparation techniques

Several sample preparation techniques are reported in the literature, the suitability of each of them depends on the targeted dry density of the sample. The maximum dry density corresponds to the British Standard (BS) 'ordinary' compaction while low relative densities are achieved by means of pouring the sample, either dry or through water (Head, 1980).

2.8.1. British Standard

BS 1337:1990-1 (BSI, 1990) proposes a method for the preparation of disturbed samples suitable for different types of tests. This technique is used in order to prepare disturbed samples with a dry density in the medium to high range. Usually, it is performed at a water content close to the optimum, which can be obtained with BS 1337-4:1990 Dry density-water content relationship test (BSI, 1990). In the material, it is specified to use a sieve of the suitable particle size, mortar and rubber pestle, a cylindrical split mold with clamping device among other preparation molds and a tamping rod of ½ to 1/3 of the diameter of the sample. The sample aggregates are broke down using the rubber pestle so that the grains themselves are not damaged.

Prior to compaction, the sample is mixed with the necessary amount of water to achieve the suitable water content, then the sample is sealed and stored for 24 hours and the water content is checked. There are two compaction methods described, either subjecting the sample to a specific compactive effort or achieving a specified dry density. The last one involved filling the mold volume with the weight corresponding to that density and the number of blows and/or compactive effort is determined by trial and error. If the sample is prepared for triaxial testing then the number of layers and blows is indicated in the standard depending on the specimen dimension.

2.8.2. ASTM

ASTM D5311-92 (ASTM, 2004) proposes three methods for the preparation of reconstituted samples: the Poring method, dry or moist vibration method and tamping method. These methods are further described in the following paragraphs as the standard only collects major guidelines. Therefore, the methods reported subsequently re in agreement with this standard.

2.8.3. Ladd undercompaction

This method, proposed by Ladd (1978) takes into account the fact that by compacting the overlaying layers of soil inside the mold will compact the bottom layers. Therefore the first layers have a lower density, how much lower depends on the targeted relative density of the sample, being the undercompaction 0 for very dense samples to 15% for very loose specimens. At the end of the process, the structure and water content are uniform throughout the specimen. The recommended water content for the soil depends on the particle size majority of the sample. The indicated water content will lead to achieving a degree of saturation of 20%-70%.

The method states that the material must be air-dried and sieved to avoid soil clumps. Then it is placed in a plastic bag and mixed with the necessary amount of water to achieve the target water content, the sample may be compacted after a waiting period that ranges from two hours to one night, for coarse to fine material respectively.

For the compaction process, the material is separated in bags with the mass required for each layer. Then each layer is placed in the mold and tamped to the specified height with an adjustable tamping rod following a diagonal scheme that ensures homogeneity in the horizontal direction. If necessary, in the last layers of a dense sample, the tamping rod can be hit with a plastic mallet.

2.8.4. Pluviation method

Vaid and Negussey (1988) describe this technique that consists of pouring the soil of the sample in the mold, either through air or water, replicating natural deposition processes. It allows the preparation of specimens of a controlled density, and a uniform density profile. The outcome of this method is described as more uniform than moist tamping by the authors.

When air-poured, the density depends on the drop height up to the height where the terminal velocity is reached, then the void ratio is minimum. The drawback of this method is that if the sand is well graded, segregation of particles will occur, yielding less homogeneous samples.

Water pluviation requires less control on the height and the resulting sample is already saturated. However, this method yields loose samples which must be compacted by vibration. Samples with the same dry density behave differently depending on whether this target density was reached only via pluviation or pluviation and subsequent vibration. This procedure consists of pouring the precalculated weight of the sand sample directly in the split mold lined with the membrane and full of water. The height that the sample must have t achieve the desired density is also calculated. Subsequently, the sample is vibrated in a drained condition until the sample contracts to the target height.

2.9. Conclusion

- The build-up of strength in axial pile capacity has been reported in the literature in onshore and offshore driven piles, although the mechanisms taking place are still unclear. Authors attribute this set-up to different mechanisms, including the dissipation of excess pore pressure and the structural changes within the chalk putty are found.

  However, Buckley et al. (2017) characterized the porewater dissipation process as rapid while the axial strength of the piles continues to increase even after 4 months following driving as reported by Ciavaglia et al. (2017). Buckley et al. (2018) also states that aging depends on the shape of the pile or driving mechanism, therefore, on whether chalk putty is formed. It is reported on this publication that primary consolidation finishes before or shortly after driving. However, the effects of creep are still fairly unclear. In contrast, Bundy (2013) characterized the creep behavior as negligible in laboratory tests.

- Buckley et al. (2018) reports null capacity set-up in close-ended jacked piles, thus discarding cementation and redox reactions as means of aging. Total stress in the soil around the shaft during pile jacking

increases marginally compared to the total stress-induced during driving (Buckley et al., 2017, Ciavaglia et al., 2017). As a primary consequence, no puttified zone is recognized after the exhumation of the pile. Additionally, this low-stress regime limits the dissolution of calcium carbonate that may lead to further cementation mechanisms (Neugebauer, 1974) in time in the chalk around the pile shaft. Jacked piles, therefore, may not be taken into account for aging mechanisms.

- In the laboratory, Clayton (1977) shows an increase in strength in his tests as a function of time as an increase in cohesion in triaxial tests, although the water content of the samples in the later tests is not reported. Razoaki (2000) backs up the evolution of the structure of chalk putties as an increase in the yield point in compression and in shear strength. On the contrary, Bundy (2013) does not show set-up of the putty strength using shear box tests. Moreover, despite the increase of undrained shear strength using fall cone, he suggests that loss of water during aging due to leaking of the plastic wrap can lead to changes in consistency that do not reflect the changes in strength only due to sample aging. Bialowas et al. (2018), affirms that aging in chalk does not have an effect in the peak nor the ultimate shear strength of the samples. Finally, Doughty et al. (2018) shows an increase in the peak strength as well as more hardening in aged specimens and thixotropic build-up. Nonetheless, no changes over time were recorded in the specimens tested in the shear box (Doughty, 2016).

- In the literature, several preparation techniques are reported, most start by drying the chalk before crushing ((Bialowas et al., 2018, Bundy, 2013, Clayton, 1977, Razoaki, 2000)) while others (Doughty et al., 2018) involve crushing at sampled moisture content. Moreover, there is no strict follow up of the testing water contents and the effect of compressive efforts on the specimen during preparation and ageing.

- In the preparation and saturation of chalk putty specimens the dry density (or saturated water content) plays a crucial role. As the changes in consistency occur with 6% variation of the water content, this means that the dry density must be controlled in order to yield repeatable results .

- Tests reported in the literature are performed once under each condition, therefore they are unable to show repeatability. More specifically, Doughty et al. (2018) extrapolates yield surfaces based on data from one test. Additionally, only one tested sample is subjected to 200 kPa consolidation pressure after 7 days, with the subsequent difficulty in drawing any conclusion about the aging trend. Furthermore, Clayton (1977), Razoaki (2000), Bundy (2013), Bialowas et al. (2018) test one sample under each condition as well.

- Specimens are tested under arbitrary pressures, for example, Doughty et al. (2018) preserves and tests the samples at 100 kPa and 200 kPa, while Bialowas et al. (2018) consolidates the specimens to 300 kPa prior to set up in the triaxial cell. No meaningful value for the aging pressure is used.

- The behavior of chalk putty can be compared with that of sandy soils in terms of constitutive models (Leddra and Jones, 1990). Moreover, stiffness of the samples is dependent on the mean effective stress (Alvarez-Borges et al., 2019). In summary, the changes in strength as a function of time occur with changes in cementation, which appears as an increase in the effective cohesion as well as yield point in compression (Ciantia, 2018).

3

Research methodology

3.1. Introduction

When piles are driven into chalk, the vibrations and the shear stress induced by this process creates a puttified annulus (Muir Wood et al., 2015). This chalk putty is also created during other construction activities (Clayton, 1977, Razoaki, 2000) and as a result of natural processes. The change of the characteristics over time has drawn interest to a few authors in the past century, and again in the past years with the development of offshore wind farms in the North and Baltic Seas. In the previous chapter, it is described how authors have tried to reproduce these processes in the laboratory, arriving at different conclusions.

The first issue about trying to simulate the behavior of chalk putty in the field is the preparation of specimens that closely replicate those found *in-situ*. To do so, different parameters were targeted, such as the water content (Doughty et al., 2018) attempting to achieve the same as on the field, or building reconstituted specimens (Bialowas et al., 2018). Similar particle size distribution as *in-situ* was targeted by Clayton (1977) and Bundy (2013).

When these preparation methods are examined, it can be observed that uncertainties are induced in the sample preparation techniques, for example when weights are placed on the sample to make it easier to handle and set up on the triaxial apparatus, the targeted dry density of the sample is therefore lost (Doughty, 2016, Razoaki, 2000).

The authors presented in this report mostly focus on triaxial testing of the samples in order to find out the changes in strength and stiffness parameters. Thixotropy is also studied by Bundy (2013) and Doughty et al. (2018), showing an increase of undrained shear strength in time. And shear box tests are also conducted by Bundy (2013) and Doughty (2016). Regarding this, the only study that includes a comprehensive set of tests is Bundy (2013), although not all of them are targeted towards capturing the changes of properties of chalk putty in time.

In this chapter, the objectives of the test program are discussed, giving a better insight into the research questions presented in the first chapter, this includes the discussion about the objectives of the specimen preparation and preservation technique as well as the aim of the test program. Once the objectives are stated, the research methodology is introduced. Finally, the testing program is presented, including a description of each test, a summary of the theory behind it, the test apparatus and the parameters that can be obtained.

3.2. Objectives

In the first chapter, two questions are stated, which this thesis aims to answer. The first one is related to specimen preparation, the second one refers to the behavior of chalk putty over time. The objectives that may be fulfilled in order to provide an answer to those questions are described below.

3.2.1. Objectives of specimen preparation

The specimens that will be prepared must comply with two requirements: the first is to yield saturated samples for testing, and the second is that those samples must have a controlled dry density and close to that measured in the intact samples which are low to medium density chalk. Given that these requirements are fulfilled, the specimen preparation method is evaluated according to the following criteria: quality, the practicality of the method, representativeness, and repeatability. What these criteria assess is stated below:

- Specimen quality: this characteristic assesses the condition of the sample as a whole. This means that the homogeneity is evaluated not only throughout the sample but also the whole batch. The evaluated parameters include particle size distribution or particle density. The ability to control the dry density of the final sample is also of relevance. Additionally, the regularity of the top and bottom surfaces of the specimens is taken into account as well as the robustness of the final sample.
- Preparation method: the simplicity of the preparation technique is evaluated here together with the preparation time, ease of handling the specimen, rate of success. This criterion studies the feasibility of the preparation technique from a practical point of view.
- Repeatability: this quality involves, for example, the use of water with controlled composition, the ability to reach the desired water content/dry density. Use of more than one sample per test type and at each elapsed time ensures that the results are reliable.
- Representativeness: it is defined as the comparability of the specimens to the chalk putty that can be found on the field, and therefore, how the results that will be achieved can be related to the behavior of the chalk putty that is formed due to the effect of soil disturbance. To do so, different water compositions may be tested for thixotropy changes. Furthermore, the results are compared to those obatined by other authors in the literature as it was not possible to collect specimens from the field.

3.2.2. Objectives of the test program

Expansion in the knowledge about the behavior of pile in chalk was attempted in the ALPACA JIP (Jardine et al., 2018) in order to develop a design method similar to those existing in sand and clay. During this research, the setup of axial capacity in driven piles was measured. Considering this, the laboratory test program attempts to measure those parameters that are useful in subsequent pile design.

With this in mind, the testing program must include those tests that capture the important characteristics for pile design and the changes in time of those parameters. In the table below (Table 3.1) the tentative tests, together with the parameters that can be calculated from them and the application in pile design are detailed.

In the tests listed, it can be observed that, in principle, triaxial test and direct simple shear measure the same parameters. Nonetheless, direct simple shear represents better the conditions under axial loads while loads following a different stress path such as lateral are better captured with triaxial tests. Additionally, the shear modulus is captured in direct simple shear tests while Young's modulus is can be derived from triaxial tests (Head, 1980).

The main objective of this program is to capture the changes of these parameters in time, for this reason, the tests will be performed, first, right after the sample is prepared, in order to establish the baseline (Day 1). Subsequent tests will be performed 10 days after, 30, 90, 300 and 1000. From these times the tests up to

Table 3.1: List of tentative tests and parameters that can be correlated from those

Test	*Corrrelated parameters*	*Application in pile design*
Fall cone	Undrained shear strength	Changes in thixotropy, resistance against undrained loads (Axial or lateral)
Constant rate of strain (CRS)	Primary consolidation parameters	Dissipation of pore pressures, drainage behavior. Determination of test pressures for triaxial testing
Triaxial with local strain	Strength parameters (c', ϕ') Large strain stiffness parameters (Young's modulus)	Resistance to axial and lateral load, compressive deformation stiffness
Direct Simple Shear	Strength parameters (c', ϕ') Shear stiffness (Shear modulus)	Resistance against shear, especially axial loads ; deformation against shear
Bender elements	Small strain stiffness (Small strain shear modulus)	Deformation against vibration loads (such as turbine rotation)
Triaxial permeability	Permeability	Dissipation of pore pressures, drainage behavior

90 days are part of the scope of this thesis. The reason for the choice of the test times is that this timing is based on the studies about aging in piles. Build-up started developing as early as 10 days and at least up to for months as shown by Ciavaglia et al. (2017). Tests after 1000 days are optional depending on the results at 300 days, in order to determine the ultimate value of these parameters. In this thesis, due to timing reasons, the results will only be included from the tests up to 90 days. In addition, thixotropy tests will capture the changes in undrained shear strength in the minutes and hours after remolding.

Finally, the last objective of this test program is to show repeatability of the results, this means that each test at each aging time will be performed three times, ensuring that the results obtained are precise. This, together with the objectives of the sample preparation, will help to support the validity of the tests towards proving the hypotheses of this thesis.

3.3. Methodology

To fulfill the objectives listed above, the scope was divided into two phases. The first phase -initial scope- targeted finding a suitable specimen preparation procedure and defining the test conditions for the main scope. Thereafter, the second part of the project -the main scope- was based on undertaking the tests included in the objectives. To do so, the preparation and aging guidelines prescribed were followed for set-up, saturation and aging of the specimens tested.

The initial scope was based on finding the most optimal preparation method for commercial purposes, based on the criteria that are stated in the objectives. To do so, the methods presented in Chapter 2 were examined. For all of them, it was attempted to find a feasible way of adapting to the preparation of chalk specimens. If those were found adequate, a finer adaptation of the method was done in order to determine the preparation moisture content and dry density.

In addition to the determination sample preparation technique, the consolidation pressure was also established by means of testing three specimens in the Constant Rate of Strain oedometer in order to determine the yield pressure of the unaged saturated material - consolidation makes the specimens less fragile to handle but the preconsolidation pressure of the material is not to be surpassed in order to not introduce this variable in the test program.

Furthermore, a batch of index tests were performed on order to attain a preliminary knowledge of what kind of material yielded the crushing and sieving process, in terms of particle size, density, plasticity and salinity of the *in-situ* porewater. In Chapter 4, it is presented the description of the specimen preparation trials together with the results of the tests included in the initial scope.

The testing program, as stated in the objectives, has the aim of capturing the changes in time of parameters that are relevant in the design of piles in order to reproduce in the laboratory the development in pile axial setup measured in the field. To do so, the tests listed and explained below were performed and the relevant parameters were extracted for each specimen to capture the evolution of those parameters in time. As it is stated in the objectives, one of the aims of the project is to characterize the repeatability of the test results. With this in mind, at least three specimens were tested for each of the test types listed.

Capturing of the changes in time is done by means of testing specimens right after the consolidation is achieved in the first place. Then, other specimens were waxed and stored to be tested after 10 days, 30 days and 90 days after consolidation. Although tests of specimens aged 300 and 1000 days are listed in the scope of the test program, they are not included in this report given the duration of the research.

After obtaining the test data, it was processed including the corrections that will be described in the following section for each of the test types. Subsequently, postprocessing of these tests involved the extraction of parameters of the soil such as strength and stiffness in order to quantify the evolution of these parameters in aging time. This allows for an analysis of the consequences of cementation alone in the behavior of samples of chalk putty.

3.4. Test types

3.4.1. Thixotropy

Thixotropy testing measures the changes in undrained shear strength in time on remolded specimens using a fall cone apparatus. The standard for measuring changes in thixotropy with fall cone is BS EN ISO 19901-8-2015 Part 8: Marine soil investigations while the measurement of undrained shear strength is referred to by the following standards: CEN/ISO TS 17892-6:2004 Geotechnical investigation and testing - Laboratory testing of soil - Part 6: Fall cone test and NS 8015: Determination of undrained shear strength by fall-cone testing.

This test is based on a cone that is allowed to fall with its tip toward the specimen, the penetration is subsequently measured and correlated with the undrained shear strength. Thixotropy testing involves measurement of the penetration at different aging times of the specimen in order to capture the change in consistency with time.

Regarding the test device, this is based on a system that allows to suspend a cone of different weights and tip angles by means of a magnet. The cone is suspended in direct contact with the soil, which can be an intact sample, a remoulded sample or in this case, material mixed to a target water content. The soil is then placed in hollow cylinders with detachable base. This allows to extrude the superficial layer of soil before testing in order to minimize the error due to loss of moisture during preservation. In the test, the magnet holding the cone is released, penetrating into the soil. This penetration is measured to the closest 0.5 mm.

The standard indicates that the specimen must be remolded at constant water content, which typically is the water content of undisturbed samples and then placed in jars. In this case, to ensure homogeneity of the specimen the dry crushed chalk was mixed to target water content (26.4%) and left overnight then remixed to ensure that any possible structure is destroyed. Enough specimens must be prepared for testing at each indicated time interval (0 h (initial reading), 1 h, 2 h, 4 h, 8 h, 1 day, 2 days, 4 days, 8 days, 15 days, 30 days and 60 days), although these time intervals are merely a recommendation.

3.4.2. Constant Rate of Strain Compression

This test is classified among the continuous consolidation tests and it provides a method of determination of the magnitude and rate of consolidation of saturated soils by means of a constant strain axial compression ASTM (2012). The tested specimens are submitted to axial compression while radial displacements are retained and the drainage provided along one boundary. The standard that states the procedure of this test is ASTM D4186 – 12 Standard Test Method for One-Dimensional Consolidation Properties of Saturated Cohesive Soils Using Controlled-Strain Loading (ASTM, 2012).

The test is based on the principle that the specimen is gradually loaded by increasing the axial displacement at a constant rate. Consequently, the result is an increase in vertical stress and pore water pressure, which are also logged. The vertical pressure is measured employing a load cell in kN and the pore water pressure in kPa with a pressure transducer hydraulically connected to the sealed boundary. Moreover, the displacement is logged in mm using LVDT transducers. The precision of all of these measurements is 4 decimal places. The suggested layout of the apparatus is reported in the pertinent standard ASTM (2012).

The specimens are prepared according to the standard (ASTM, 2012). In this project, the specimens are obtained from the prepared and aged samples as described in this report and treated as undisturbed samples.

Postprocessing

From CRS tests it is possible to obtain the compression parameters, hydraulic conductivity as well as consolidation coefficient of the tested soil, these include stiffness parameters ($E_{u/r}$ and E_{oed}, which is the stiffness of the soil in K_0 conditions), permeability parameters can also be obtained if the pore water pressure ratio is kept according to the standard and the preconsolidation pressure can be calculated following different methods that will be subsequently presented. These methods comprise those described by Casagrande (1936), Pacheco Silva (1973), Jose et al. (1989) and Wang and Frost (2004). Additionally to those methods, Head (1980) suggests that the preconsolidation pressure can also be determined based on the load where the pore pressure starts increasing (Figure 3.1.).

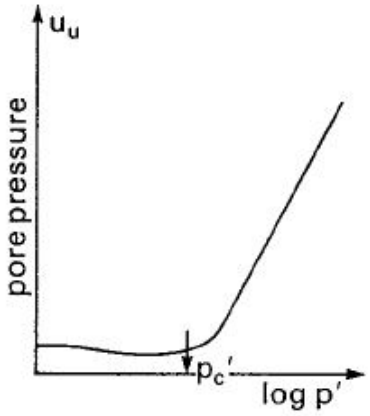

Figure 3.1: Detemination of the preconsolidation pressure in CRS tests based on the change of the pore pressure. Source: Head (1980).

- Casagrande (1936) was the first author to propose a methodology for the determination of the preconsolidation pressure, which is empirical and graphical. This technique is based on the determination of the virgin consolidation line (C_c) and the point of maximum curvature of the result of the consolidation test in the e-log(σ'_v).

- Pacheco Silva (1973) searched for a simplified version of this method since the location of the point of maximum curvature can become poorly defined when the samples are subject to disturbance. With this

in mind, the method proposed by this author takes into account the initial void ratio (e_0) and the virgin consolidation line (C_c).

- Jose et al. (1989) proposes representation of the data in the space log(1+e) - log(σ'_v). In this scale, the data curve appears as two straight lines. The preconsolidation point is at the point of intersection of these two lines. The authors consider this method simpler, more consistent and devoid of human errors.

- Wang and Frost (2004) proposes the determination of the preconsolidation pressure by means of conceiving consolidation in terms of micromechanics. This means that consolidation is the process by which soil particle configuration irreversibly due to consolidation stress. Therefore, the consolidation curve is represented in the strain energy (E) - effective consolidation stress (σ'_v) space. This minimizes the disturbance effects as well as those of the elastic deformation.

3.4.3. Direct Simple Shear

Direct Simple Shear (DSS) is a test that aims to reproduce the strain conditions during simple shear movement of soil, for example in a region of circular failure of a slope or pile capacity testing. This means that the specimen is uniformly strained under simple shear and plane strain conditions. The standard followed in the performance of these tests was ASTM D6528 - 17 Standard Test Method for Consolidated Undrained Direct Simple Shear Testing of Fine Grain Soils (ASTM, 2017a).

The governing principle of this test is subjecting the soil to simple shear, this means that parallel planes remain parallel throughout the test, in-plane strain conditions, deformation of the soil only occurs in one plane, typically the xy plane. The test starts with one or two consolidation phases - overconsolidation conditionsof the soil are reproduced by means of consolidation to a certain pressure and then unloaded to typically the *in-situ* pressure- at designated vertical pressures, then the specimen is sheared at a constant horizontal strain rate, logging the necessary load to keep the rate of strain constant. The volume of the specimen is kept constant as well by means of fixing the vertical plate after the consolidation phase, the changes in vertical stress in the shear stage are recorded. The test apparatus does not allow control of the back pressure and does not possess a pore pressure transducer either. However, according to Bjerrum and Landva (1966) the changes in vertical stress are similar to the changes in pore pressure in undrained tests as long as the rate of strain is low enough to allow for pore pressure equalization within the specimen.

The setup of the test consist of a specimen inside a reinforced membrane or an aluminum ring stack. This is placed on a test device that controls the vertical load on the specimen with a load cell measuring in kN with an accuracy of 0.0001 kN and the displacement with an LVDT which measures up to the closest 0.0001 mm. The horizontal load is applied to one of the plates and the accuracy of both the load cell and the displacement transducer are identical to those measuring the vertical displacement and load. An overview of the test device is described in the test standard (ASTM, 2017a).

Tested specimens are obtained from prepared and aged samples according to this document, specimen preparation was undertaken following the standard specifications for intact material (ASTM (2017a)).

From DSS tests it is possible to compute shear strength and shear stiffness parameters of the soil as well as consolidation behavior.

- Strength parameters from the Mohr-Coulomb model, friction angle and cohesion (ϕ', c'), undrained shear strength.
- Shear stiffness parameters at different ranges of strain, allowing to evaluate the degradation of stiffness.
- In terms of consolidation, the consolidation stage of the test is equivalent to an oedometer test. However, the lack of pore water pressure measurements makes it less suitable to characterize this aspect of soil behavior.

3.4.4. Consolidated Undrained Triaxial

Consolidated Undrained triaxial test measures the stiffness and strength characteristics of a soil specimen by means of subjecting it to consolidation pressure in drained conditions, subsequently, the specimen is sheared at constant volume. The standard that applies to these types of tests is the BS EN ISO 17892-9: 2018 Part 9: Consolidated triaxial compression tests on water-saturated soils (BSI, 2018).

In this test, the specimen is isotropically consolidated at a certain cell pressure, this cell pressure is entirely transmitted to the soil, minus the pore pressure, in saturated condition and it is equal to the minor principal stress (σ'_3) throughout the test. During this stage, the changes in volume and pore pressure are measured. Afterward, in undrained conditions, it is compressed at a constant strain rate and the load to achieve it is recorded. Changes in pore water pressure are also recorded. If local strain gauges are installed, the small strain deformation characteristics can be studied through measuring the deformation of the probe in axial and radial directions.

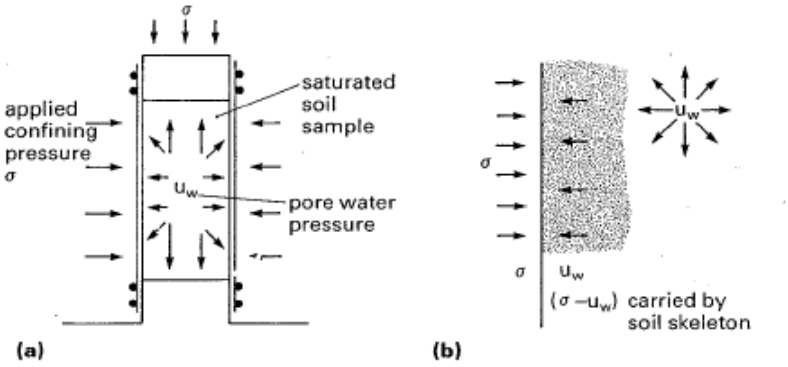

Figure 3.2: Representation of the stress transmission in triaxial tests. Source Head (1980).

The test apparatus is based on a cylindrical specimen located inside a pressure chamber with pumps controlling the pressure inside the cell as well as the pressure in the pores is the material to the closest kPa while the measurements are taken with transducers with 4 decimal places. A load cell measures the axial force on the sample in kN, to the closest 0.0001 kN and displacement is allowed in for compression and extension. The test apparatus is thoroughly described in the test standard BSI (2018).

Given triaxial data, multiple parameters may be determined to fit different soil models. For instance the Mohr-Coulomb model.

- Strength parameters: the strength parameters quantified in the Mohr-Coulomb model are the cohesion and the friction angle of the soil.

- Stiffness parameters: with triaxial tests, Young's Modulus (E) at small strains as well as for larger deformations. It is customary to present Young's modulus at 50% of the strain to failure.

Regarding the preparation of the specimens, the preparation technique is different for undisturbed or remolded specimens. In this case, the sample preparation that applies is the one developed in this report.

This test gives a large amount of information about the behavior of the soil specimens given the number of variables that can be controlled and measured (drainage, measurements of pore pressure...), for example in comparison to the direct shear tests.

3.4.5. Bender Elements

This test allows the calculation of the small strain stiffness of samples in the triaxial cell by means of measuring the shear wave velocity in the soil specimen. This advanced test is not regulated by a standard from an accredited agency.

The test setup consisted of two electromechanical piezoceramic transducer plates located at either end of a triaxial specimen, one of these plates (transmitter) bends when voltage is applied to send a sinusoidal input wave that is then recorded by the other one (receiver) by means generating a voltage when the mechanical impulse arrives (Viggiani and Atkinson, 1995). The travel time of this shear wave is measured allowing the computation of the shear wave velocity.

$v_s = \frac{L}{t}$; where L is the effective distance between the bender elements and t is the travel time.

With the later, the small strain shear modulus (G_{max}) is calculated (Arulnathan et al., 1998).

$G_{max} = \rho \cdot v_s^2$; where ρ is the bulk density of the soil.

With this method it is possible to measure the stiffness at small strains in a fast manner and without disturbing the samples, this means that they can be tested afterward. In this case, the specimens were subsequently sheared in the triaxial cell.

It is worth mentioning the sources of error in these tests and how they can be avoided. The first one is the measurement of the travel time, the first arrival can be obscured by near field effects. Near field effects refer to the coupling of waves that show the same particle motion but different velocities and are attenuated at different rates (Arulnathan et al., 1998). If the ratio between the travel distance and the wavelength is larger than 1 these errors are minimized. Furthermore, in triaxial specimens, indirect travel paths of the waves that are reflected in the soil boundaries can cause interference. In addition to the near field effect, the assumption of planar wavefronts introduces further errors. However, as long as the near field effects are minimized, the results a good estimation of the shear wave velocity in the soil medium.

Finally, for the determination of the travel time, there are several methods, described by Arulnathan et al. (1998). The method chosen in this study is the estimation of the travel time between characteristic peaks of input and output signal. Which can be the first peak, the first trough or zero crossings, as shown in Figure 3.3. As the wavelength increases, the error is reduced as long as the characteristic point chosen is the first positive peak.

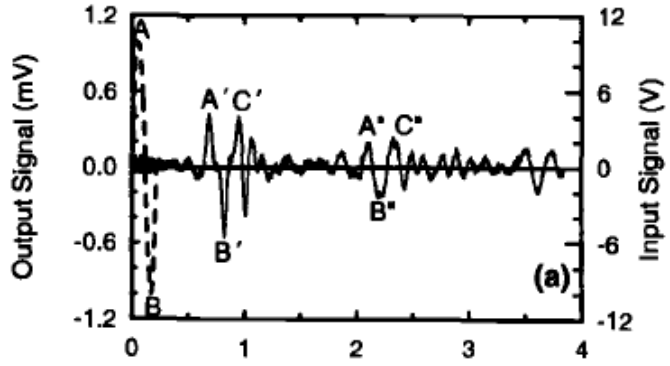

Figure 3.3: Characteristic points of an output sinusoidal shear wave. Source Arulnathan et al. (1998)

4

Specimen preparation and trial phase

4.1. Introduction

These trials intended to find a suitable preparation method, to do so, the preparation methods listed in Chapter 2 were considered. The initial idea was to find a method that yielded samples at a defined water content and then achieve saturation by means of increasing the cell pressure. However, the preparation of samples with a water content close to the plastic limit clumps were formed. When the water content is close to the liquid limit slumping occurs during compaction and the method yielded specimens that were too soft for setting up in the triaxial pedestal. Given the narrow PI range of chalk putty (6-8%) preparing specimens that are not subject to these two issues poses a challenge.

With the objectives listed in the previous chapter in mind, the specimen preparation trials were started. An initial batch 10 kg of chalk was collected evenly spread in depth throughout the same geotechnical unit from the cores from the two boreholes drilled during a site investigation campaign. The material was air-dried, crushed with mortar and pestle, passed through a 425 μm sieve and thoroughly homogenized in one batch. Three subsamples were taken for classification testing, including Atterberg Limits, Particle Size Distribution, Particle Density and Porewater Salinity (BSI, 1990). The results of these tests can be used as an indicator of the uniformity of the batch, together with the information that these tests can provide.

Specimens with lower preparation water content were prepared, these specimens would be subsequently saturated until achieving a Skempton B value of 0.95 (BSI, 2018) using increases of back pressure in the triaxial cell. The downside of this method is that it is very laborious to mix the material with the required amount of water until it becomes uniform, as clumps are formed and it is time-consuming work the mix until it is fine and uniform.

Alternative methods such as wet pluviation were attempted. However, the trial was considered failed as all the water considered to achieve the target preparation water content took up all the dry crushed chalk when only half of the material was introduced. After that, the dry material was accumulating on the top.

Finally, compaction of the dry material was tried, together with flushing and saturation by means of increasing the back pressure. Specimens that result from this preparation are brittle but with careful handling, they do not suffer damage. They are easy to store as they do not deform in time. So it is possible to prepare samples for future use. Since this method seemed the most commercially feasible, it was repeated three times in order to prove that the results are consistent. The next section provides a more exhaustive description of the preparation methods.

4.2. Specimen preparation trials

This section contains an extensive description of the trials towards achieving a suitable specimen preparation technique giving all the specifications and results obtained in each trial. A summary of this section can be found in Table **??** in Appendix A.

- It was agreed to trial specimen preparation using a target water content of 30.0% and a dry density of 1.50 Mg/m^3, assuming a particle density of 2.70 Mg/m^3. Approximately 1 kg of batched material was mixed to 30.0% water content by adding de-ionized water and material in a plastic bag. The material thoroughly mixed and left for 24 hours in a sealed plastic bag. The Ladd undercompaction method was used to prepare a specimen approximately 70 mm in diameter and 135 mm in length. It was found that a target dry density of 1.50 Mg/m^3 was too low for specimen preparation so the target dry density was increased to 1.66 Mg/m^3. The specimen was also unable to support its own weight making testing and storage unfeasible.

- A second specimen was prepared to a target water content of 27.5% and a dry density of 1.66 Mg/m^3, assuming a particle density of 2.70 Mg/m^3. The specimen was also unable to support its own weight making testing and storage unfeasible. A water content test had a result of 27.20%.

- A third specimen was prepared to a target water content of 26.0% and a dry density of 1.66 Mg/m^3, assuming a particle density of 2.70 Mg/m^3. A water content test had a result of 27.1%. The calculation of the density of specimen after preparation showed a dry density of 1.58 Mg/m^3. The specimen set up in a triaxial cell for saturation (BSI, 2018). The cell was pressurized to 300 kPa and the pore pressures allowed to equalize. Bumps in cell pressure of 50 kPa were carried out up to 550 kPa, without application of back pressure, to achieve saturation of the specimen. Saturation was performed during 3 days.

- A fourth specimen was prepared to a target water content of 20.0% and a dry density of 1.58 Mg/m^3, assuming a particle density of 2.70 Mg/m^3. The water content test showed that the water content of the prepared sample was 21.4%. The calculated dry density of the specimen was 1.60 Mg/m^3. Same as with sample number 4, the specimen was set up in the triaxial cell for saturation. The cell was pressurized to 300 kPa and the pore pressures allowed to equalize. Increments in cell pressure of 50 kPa were carried out up to 550 kPa, without application of back pressure, to achieve saturation of the specimen. Saturation was performed Wednesday 24 to 25 April 2019. Back pressure saturation was attempted on this sample, after 16 hours the water intake of the sample was 12 cm^3. The sample did not have a homogeneous water content distribution, being the moisture content higher at the bottom than at the top (Table 2.1)

- A fifth specimen was prepared to a target moisture content of 22.0% and a dry density of 1.58 Mg/m^3, assuming a particle density of 2.70 Mg/m^3. The water content test showed that the water content of the prepared sample was 23.0%. The calculated dry density of the specimen was 1.59 Mg/m^3. Same as with trial number 3, the specimen was set up in the triaxial cell for saturation. The cell was pressurized to 300 kPa and the pore pressures allowed to equalize. Bumps in cell pressure of 50 kPa were carried out up to 550 kPa, without application of back pressure, to achieve saturation of the specimen. Saturation was performed Wednesday 24 to 26 April 2019.

- Trials using the pluviation method (Vaid and Negussey, 1988) were started targeting a water content of 26.0% and a dry density of 1.58 Mg/m^3 assuming a particle density of 2.70 Mg/m^3 for a sixth specimen. The water took approximately half of the calculated weight of the sample before it could not admit more ground chalk. 48 hours after the preparation of the sample, the material settled.

- A seventh specimen was prepared to target a moisture content of 10% and a dry density of 1.58 Mg/m^3 assuming a particle density of 2.70 Mg/m^3. The water content test showed that the water content of the prepared sample was 10.1% The calculated dry density of the specimen was 1.52 Mg/m^3. The specimen was set up for saturation in the triaxial cell, first being flushed with water up to a volume of 132 cm^3,

equal to the estimated volume of pores. After three hours the sample took 120cm ^{3} and stabilized. Saturation with increments of cell and back pressure was commenced up to a Skempton B value of 0.95 or three consecutive readings of 0.9, as per BSI (2018). A Skempton B value of 0.98 was achieved after 5 days of saturation. The saturated sample had top-middle-bottom moisture contents of 25.5%, 25.2%, and 26.4% respectively. The appearance is that the bottom and top of the sample were softer than the middle and the preparation layers can be distinguished with the bare eye.

- An eighth specimen was prepared targeting a water content of 0% and a dry density of 1.58 Mg/m^3, assuming a particle density of 2.70 Mg/m^3. The calculated dry density of the specimen was 1.58 Mg/m^3. The specimen was set up for saturation in the triaxial cell, first being flushed with water, targeting a volume of water introduced equal to the estimated volume of voids (234 cm^3). After 24 h the volume intake was negligible so the saturation of the sample was started. The initial Skempton B value was 0.24. After two days of cell pressure and pore pressure increases, a B value of 0.92 was achieved with a cell pressure of σ_{cell}=500 kPa. The sample was left over the weekend and the final B value was 0.98. The sample was taken down, and top-middle-bottom moisture contents of 25.2%, 25.2%, 25.8%, respectively were measured.

As this last method was deemed suitable as standard sample preparation, 3 trials using the same technique were undertaken in order to demonstrate the repeatability of the method. Trials 9, 10 and 11 were prepared at hygroscopic water content using Ladd undercompaction with a target density 1.58 Mg/m^3 assuming a particle density of 2.71 Mg/m^3, in accordance with the results from index testing. The resulting dry density of the specimens was 1.56 Mg/m^3, 1.58 Mg/m^3 and 1.58 Mg/m^3. Saturation was achieved after 3 days in the cell, including flushing and back pressure increment steps for trials 9 and 10 while trial 11 saturated within 5 days. The samples were taken down and moisture contents were measured.

4.2.1. Results and evaluation

Regarding the sample preparation trials, a summary of all the results is included in Table **??** at the end of this chapter. Ladd undercompaction method with back saturation of the sample seems to be the most feasible technique as the preparation to high moisture content (close to the liquid limit) yields samples that are too soft to set up in the triaxial device or the particles slump when mixed to a target moisture content above 25 %. When the target moisture content is between 20 and 25 % the sample becomes full of voids and uneven. However, the time to achieving saturation of the sample following the back saturation method, according to BSI (2018) is approximately 3 days.

For this reason, the most feasible technique for commercial purposes. Fist of all, because it produces homogeneous specimens. Another advantage is that it is the most simplified technique in terms of preparation, the fact that no water is added before compaction saves much time compared to the other and the saturation time is no longer in comparison to the saturation time of 10% water content at preparation. Additionally, the time that a technician is exclusively working on the specimen is during compaction. The samples are easy to handle as they are hard and no material is lost as long as the specimen is kept in cling film.

4.3. Specimen preparation procedure

In this section, the chosen preparation technique for chalk putty is described step by step. This technique was determined by means of trial and error as described in the previous section. The main advantages of this method in order to choose it was the homogeneity of the specimens and the repeatability along with the ease of preparation and handling as well as the fact that it is not labor-intensive after the chalk is ground.

4.3.1. Material selection, crushing and sieving

Chalk putty from the field is reproduced in the laboratory by means of crushing chalk from the samples extracted on site. Enough material for the planned tests is taken from the rock cores and then air-dried for 2 days. Subsequently, with help of a mortar and a pestle, the dried chalk is crushed and then sieved through the 425 μm sieve with the help of a rubber pestle (Figure 4.1), which ensures that the particle size is smaller than that of fine sand.

Figure 4.1: On the left 425 μm sieve and rubber pestle during sieving process and on the right mortar and pestle for crushing the dry chalk.

In this case, to ensure homogeneity of the material, chalk was obtained from different depths, to ensure homogeneity of the batch, mixing of the material was performed at every stage of the grinding and sieving process. This allows us to average out the properties of the geotechnical unit to be tested.

4.3.2. Ladd undercompaction

Given a batch of crushed chalk, specimens are compacted at hygroscopic moisture content using the Ladd undercompaction method (Ladd, 1978). The compaction is done in 6 layers of which the first one is 3% less dense than the following (Table 4.1). The compacted specimens have a height of 140 mm and 71.66 mm diameter, yielding a dry density of 1.58 Mg/m^3 which corresponds to a medium-density chalk as found in the field.

To prepare the specimens, first, enough material is taken from the batch. To prepare each layer, the crushed chalk is weighted on the scale with the help of a tin tray. Then, the material is poured into the mold, pushing it with a blunt knife and the surface is evened out inside the mold by means of gently shaking it. Compaction is done first with a graduated cylinder and rubber hammer until the layer height is close to the final height and then it is finely adjusted to the indicated height of the layer with an adjustable yoke that is regulated to the indicated height with a caliper. All the materials described are presented in Figure 4.2.

Once the layer is compacted to the right height, the surface is scarified with the blunt knife in order to enhance homogeneity within the specimen. When the final layer is completed the top surface is smoothened by means of rotating the compaction cylinder and compressing with the yoke until a flat, uniform and compact surface is achieved. The mold is then disassembled keeping the specimen in a vertical position (Figure 4.3), Day 1 triaxial specimens had an indentation deep enough to fit the bender elements scraped on either end of the specimen. Afterward, the specimen is weighted and wrapped in cling film for storage until saturation. It is important to keep the specimen in a vertical position as it is dry, cohesionless material, it can break if any tension is induced in the sample.

Table 4.1: Characteristics of the prepared specimens and compaction settings.

Required specimen conditions							
Dry density (Mg/m^3)	*Specimen diameter (mm)*	*Layers*	*Specimen height (mm)*	*Moisture content (%)*	*Particle density (Mg/m^3)*	*Mould height (mm)*	*Undercompaction first layer (%)*
1.58	71.66	6	140.00	0.0	2.71	161.82	3.0
Initial void ratio	*Degree of saturation (%)*	*Volume of voids (cm^3)*	*Bulk density (Mg/m^3)*	*Specimen Area (mm^2)*	*Specimen volume (cm^3)*	*Total mass (g)*	*Difference mould height (mm)*
0.72	0	235.44	1.58	403314	564.64	892.13	21.82

Undercompaction conditions					
Layer	*Undercompaction (%)*	*Final layer height (mm)*	*Cumulative mass (g)*	*Layer mass (g)*	*Yoke setting (mm)*
1	3.0	24.03	148.69	148.69	137.79
2	2.4	47.23	297.38	148.69	114.59
3	1.8	70.42	446.07	148.69	91.40
4	1.2	93.61	594.75	148.69	68.21
5	0.6	116.81	743.44	148.69	45.01
6	0.0	140.00	892.13	148.69	21.82

Figure 4.2: From left to right and top to bottom: tray with material and preparation knife, side view of the preparation mould, top view of the preparation mould and regulable compaction yoke.

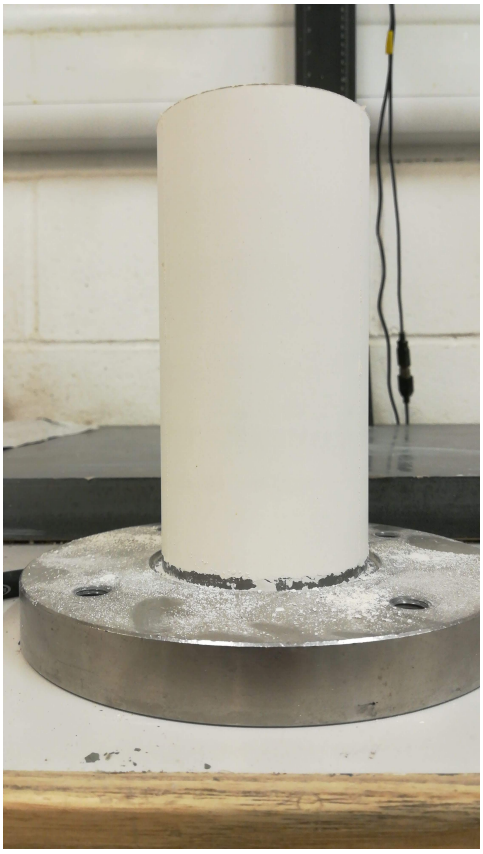

Figure 4.3: Compacted specimen resulting from the described procedure.

4.3.3. Saturation

Specimens were saturated using increases of back and cell pressure in the triaxial cell with a pressure differential of 10 kPa. To do so, first, the specimen is placed on the triaxial apparatus, the membrane and o-rings are put on the specimens and the cell is filled with water, specimens that were tested for Day 1 triaxial had also the local strain sensors installed on the membrane. Subsequently, the cell pressure is set to 50 kPa and the back pressure is set to 40 kPa. A burette is installed in the opposite of the specimen as the back pressure line, preferably the back pressure is installed at the bottom and the burette at the top. Once the cell pressure reaches 50 kPa, the sample is flushed by means of opening for taps. This stage lasts from 8 to 12 hours which means that most of the times the specimen is flushed overnight. The next stage can start when the water level starts rising on the burette.

In the following stages, burette and back pressure lines are closed, the cell pressure is raised by 50 kPa and the B value is calculated ($B = \frac{\Delta U}{\Delta \sigma_{cell}}$). Thereafter, the back pressure is raised by 50 kPa as well and the back pressure line is opened. The specimen is considered saturated when the B-value is equal or higher than 0.95 or higher than 0.9 in three consecutive readings.

Once the specimen is saturated, it is isotropically consolidated to 20 kPa (justification to this value is given in the next section), and taken down for aging or testing. Day 1 triaxial tests were conducted directly after consolidation.

4.3.4. Aging and test preparation

Specimens that were subject to aging are taken down from the cell and wrapped in two layers of cling film with the membrane and porous stones in order to keep the humidity. After, they are wrapped in aluminum

foil, put in a cardboard tube and covered in melted wax to ensure sealing. The samples were then taken into a storage room at a constant temperature of 10°C and humidity (Figure 4.4).

Figure 4.4: Blue box with waxed specimens in the storage room.

After the assigned aging time of each specimen, the corresponding cardboard tube is removed from the cold room at least one hour before testing. The cardboard is opened with a retractable utility knife and the specimen is removed and the wrap is tossed away. If the specimen is to be tested on the triaxial cell, the standard membrane stones, and filter paper are replaced for those suitable for Bender Element measurements. For DSS and CRS tests, the subspecimens can be obtained as if it is an undisturbed sample from the field and preparing the samples following the corresponding standard.

4.4. Test results

4.4.1. Index tests

Three subsamples were taken in order to perform a series of index tests that include particle size distribution, Atterberg limits, particle density, and porewater salinity. These tests give information about the crushed chalk but also about the uniformity of the batch. The results of particle density and Atterberg Limits tests are presented in Table 4.2, the results from the particle size distribution tests are included in Appendix A.

Particle density

The density of the chalk particles was determined according to BS EN ISO 17892-3: 2015 Small pycnometer method (BSI, 2015). The results (Table 4.2) show values ranging from 2.68 Mg/m^3 to 2.73 Mg/m^3. With an average of 2.71 Mg/m^3, this was the value used in data processing throughout the project as it is also a typical value of particle density in chalk.

Particle size distribution

Grain size distribution on the main batch was calculated according to BS 1337-2: 1990 Classification tests (BSI, 1990), using the dry sieve method and sedimentation with a pipette. The result of these tests are shown in Figure A.1 in Appendix A. Particles are all smaller than 212 μm, 80% is silt-sized or smaller and 30% corresponds to clay size.

Atterberg Limits

Plasticity of the batch was determined through Atterberg Limits tests collected in BS 1337-2: 1990 Classification tests (BSI, 1990). Cone penetrometer method was used to measure the liquid limit. The plastic limit method is used to determine the plastic limit. Table 4.2 shows the results obtained from those tests on each subsample. With these Atterberg Limits, these particles behave like a low-plasticity silt, according to the plasticity chart (ASTM, 2017b). This means that 30% of the particles that clay-sized are inactive and therefore behave like silt particles as the ratio between the plasticity index and the clay fraction is 0.24 (Skempton and Northey, 1952).

Table 4.2: Results from particle density and Atterberg limits tests in the trial phase.

Sample	*Particle density* $[Mg/m^3]$	*Liquid limit* *[%]*	*Plasticity index* *[%]*
1BagA	2.73	29	8
1BagB	2.72	28	7
1BagC	2.68	28	7

Pore water salinity

The presence of salinity in the pore-water of the soil was determined following the BS 1377-3: 1990 Chemical and electro-chemical tests (BSI, 1990). This is done first, extracting the salt in the sample by stirring vigorously in a slurry with water an then letting settle. The salinity of the water is measured with a refractometer calibrated for salt content. The results of these tests show that no traces of salt were found in the crushed chalk.

4.4.2. Constant Rate of Strain ofr determination of yield pressure

Consolidation tests were performed during the initial scope of the testing program in order to determine the yield point of the saturated unconsolidated unaged material. This way it would be possible to determine the pressure to which the samples could be isotropically consolidated without changing the yield point or breaking any structure developed.

One specimen was prepared according to the preparation method described in this chapter and subsequently saturated. Following saturation, it was removed from the triaxial apparatus and three CRS tests were performed with the saturated material, these tests were executed complying with ASTM (2012). After setting up of the specimens in the test apparatus, the back pressure was ramped up to 20 kPa with a seating load of 5 kPa. The samples were left at these conditions for one hour before the start of the test. Samples were compressed at a strain rate on 0.7 %/hour, in order to avoid strain rate effects and unloaded at -0.027 %/hour based on Fugro experience (Fugro, 2012). The maximum pressure was 3 MPa, which was considered enough in order to determine the yield point of the unconsolidated specimens and then unloaded to 30 kPa.

Measured data

Constant rate of strain tests measure the load applied to a sample to achieve a certain displacement at a constant rate. In these tests, the data is presented in terms of void ratio and vertical load ($\sigma'_v - e$) in Figure **??** and the changes in pore pressure against vertical load ($\sigma'_v - \Delta U$) in Figure 4.6. The measurements of these parameters allow the determination of the yield point according to the methods presented in the previous chapter.

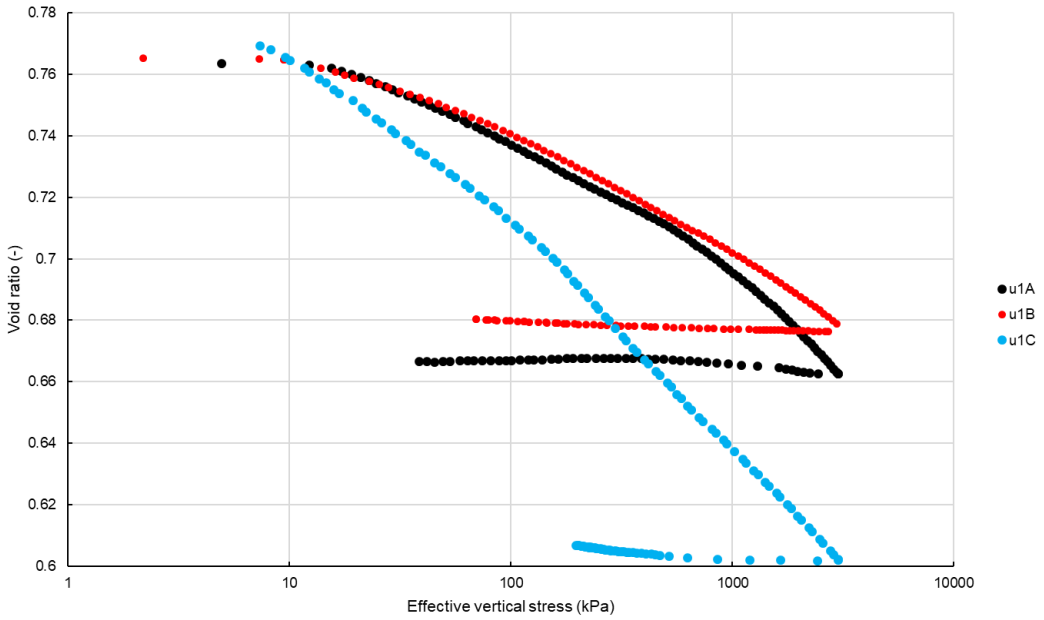

Figure 4.5: Measured stress-void ratio data from unconsolidated and unaged specimens.

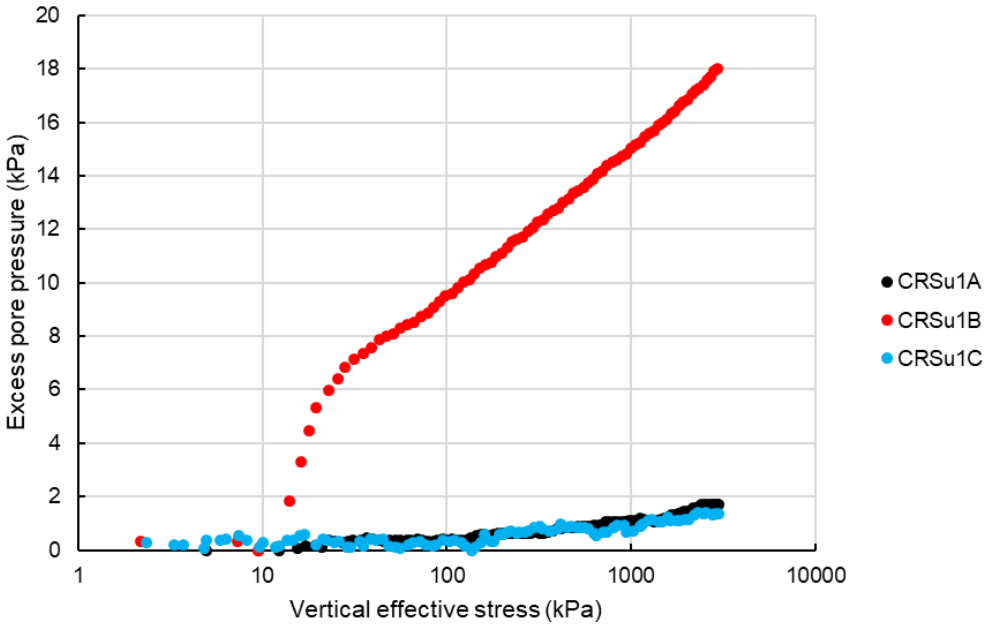

Figure 4.6: Measured stress-excess pore pressure data from unconsolidated and unaged specimens.

Analysis

Given the measured data, the yield pressure of the material was determined for each test following the indications of the methods presented in the previous chapter. In table 4.3, the estimated yield pressures as per the listed authors are presented, these were determined based on the plots presented in Figure 4.5. The average of all the methods is 23 kPa. However, test CRSu3 shows disagreement between the yield points depending on the author. If this is disregarded, the average yield point is 24 kPa.

Furthermore, given the indication of Head (1980) of determination of the yield pressure given the plot $\sigma'_v - \Delta U$, the yield pressure of the specimens CRSu1A and CRSu1C can not be determined effectively. If CRSu1B is assessed using this theory, the yield point would be 12 kPa approximately.

With these test results and the outcome of the subsequent analysis, it was determined that 20 kPa isotropic yield pressure -approximately 80 % of the average yield pressure- was a suitable value to consolidate the saturated specimens prior to aging in the wax in order to make them easier to handle but without disturbing arriving at the virgin consolidation line.

Table 4.3: Determined yield pressures (p'_c) according to Pacheco Silva (1973), Casagrande (1936) and Jose et al. (1989).

	Pacheco Silva (kPa)	***Casagrande (kPa)***	***Log-Log (kPa)***	***Average (kPa)***
CRSu1A	27	23	24	24
CRSu1B	21	26	25	24
CRSu1C	20	37	9	22
			Average	23

4.4.3. Reconstituted Constant Rate of Strain

Compression behavior of the reconsituted material was studied by means of one test, conducted at moisture content equal to $1.25 \cdot LL$, with the objective of determining the slope of the virgin compression line and to observe whether particle crushing occurs when specimens are compressed up to 3 MPa.

With this in mind, dry material was mixed to 35.9% water content and left in the vacuum chamber for 24 hours before tested in order to remove air from the mixture and then remixed to destroy the possible structures formed within the slurry. Then the material was placed in the apparatus and compressed at a rate of 0.7% vertical strain per hour up to 3 MPa effective vertical stress and then unloaded at -0.027%/hour to 30 kPa.

Measured data

The test measures the changes of void ratio with increasing vertical load, as shown in Figure 4.7.

Postprocessing and analysis

With this data it was possible to determine the constrained modulus of the normally consolidated material $E_{oed_{NC}} = 222\ kPa$. Furthermore, given the stress - void ratio response, it is observed that grain crushing does not take place under these test conditions.

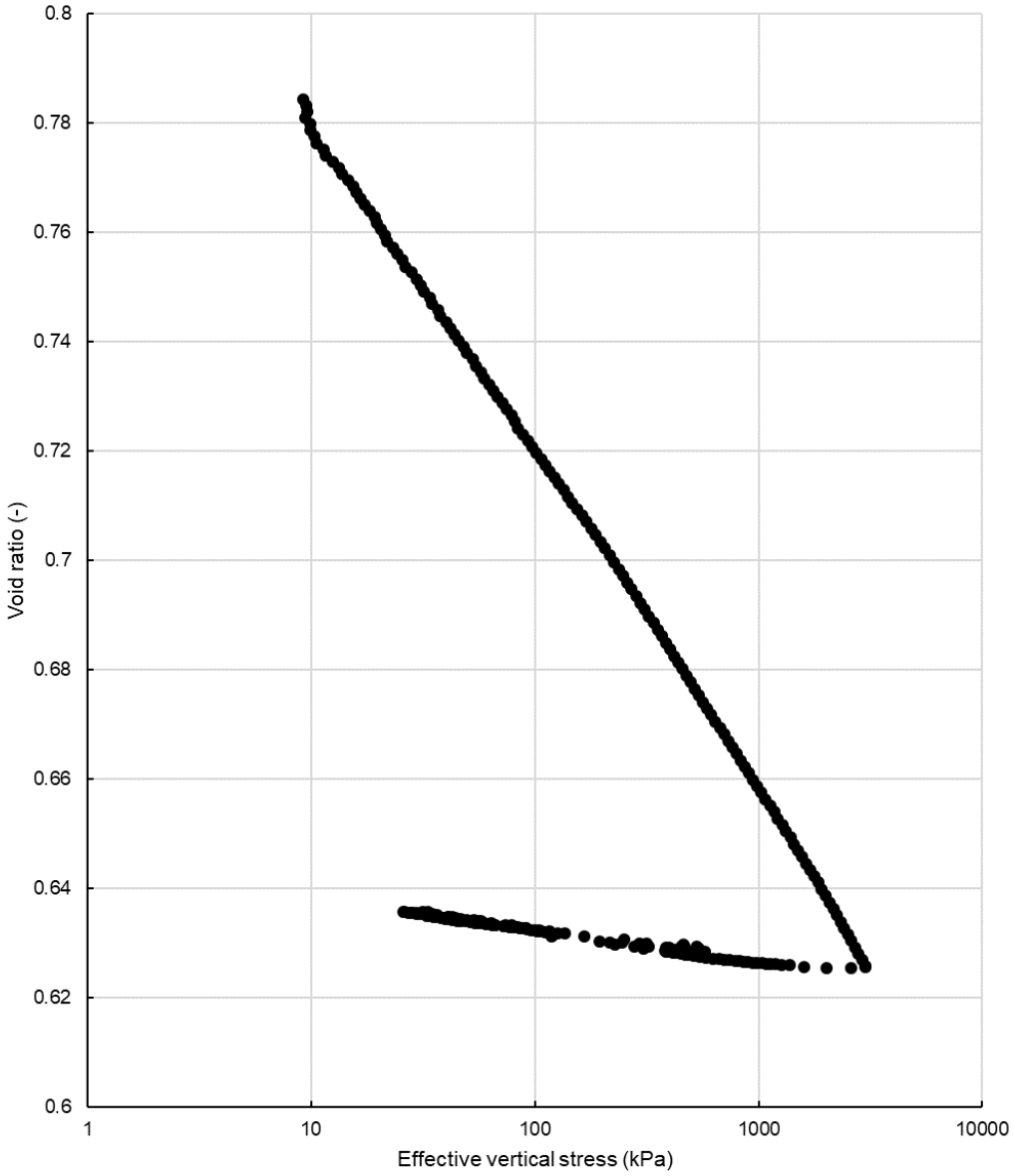

Figure 4.7: Measured stress-void ratio data on the reconstituted CRS specimen.

5

Test results from the main scope, analysis, and interpretation

After the completion of the initial trials, 50 kg of chalk were selected throughout rock cores from the same formation. This material was crushed, sieved and subsequently mixed to obtain a homogeneous batch. This crushed chalk was used for all the tests belonging to the main scope. From this batch, 3 samples were taken for index testing and 5 dry specimens were compacted per aging time, 3 to be tested in the triaxial cell, 1 in Constant Rate of Strain apparatus and another in the Direct Simple Shear device, making a total of 25 dry compacted specimens. Moreover, 3 kg of material was also taken to conduct the Thixotropy tests.

In this Chapter, the results of the main scope are presented along with an analysis and interpretation of those. In total, data are presented for two batches of Thixotropy tests up to 30 days, 11 Consolidated Undrained Triaxial with Bender Element measurements taken after consolidation, 13 Constant Rate of Strain and 10 Direct Simple Shear. For each test, the test conditions are stated. Then, the measured data is presented. The post-processing of the measured data is explained and finally, an analysis of the results is provided and interpretation of the phenomena taking place within the specimens leading to the presented results is included as well. More tests were done, according to the proposed scope, however, outliers are not presented in this analysis.

5.1. Index tests

Three subsamples were taken in order to perform a series of index tests that include particle size distribution and Atterberg limits. These tests were performed in order to characterize the chalk but also to check the uniformity of the batch. The results of particle density and Atterberg Limits tests are presented in Table 4.2, the results from the particle size distribution tests are included in Figure 5.1.

Particle size distribution

Grain size distribution on the main batch was obtained according to BS 1337-2: 1990 - Classification tests (BSI, 1990), using the dry sieve method. The results of these tests are shown in Figure 5.1. Particles are all smaller than 212 μm, 82% is silt-sized or smaller and 28% corresponds to clay size in 1BagA and 1BagB and 15% in 1BagC. D_{50} of the batch is 5 μm.

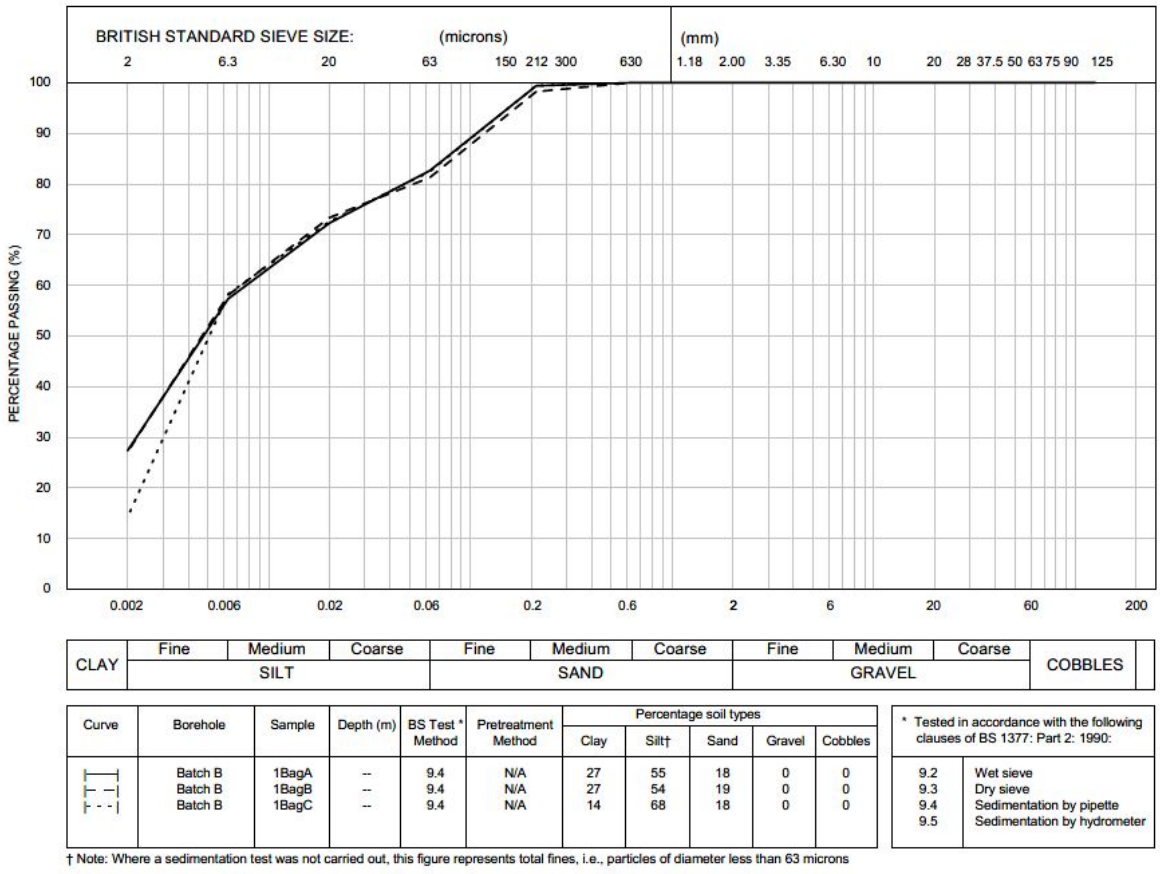

Figure 5.1: Particle size distribution tests for the three subsamples taken from the main batch (Batch B).

Atterberg Limits

Plasticity of the batch was determined through Atterberg Limits tests collected in BS 1337-2: 1990 - Classification tests (BSI, 1990). Cone penetrometer method was used to measure the liquid limit and the plastic limit method to determine the plastic limit. Figure 5.2 shows the results obtained from those tests on each subsample. With these Atterberg Limits, these particles behave like low plasticity silt. However, the liquid limit and the plasticity index of these samples are higher than in the initial batch. Variations in these results may be due to natural variability within the batch or test uncertainties. However, the behavior type is the same on the three subsamples.

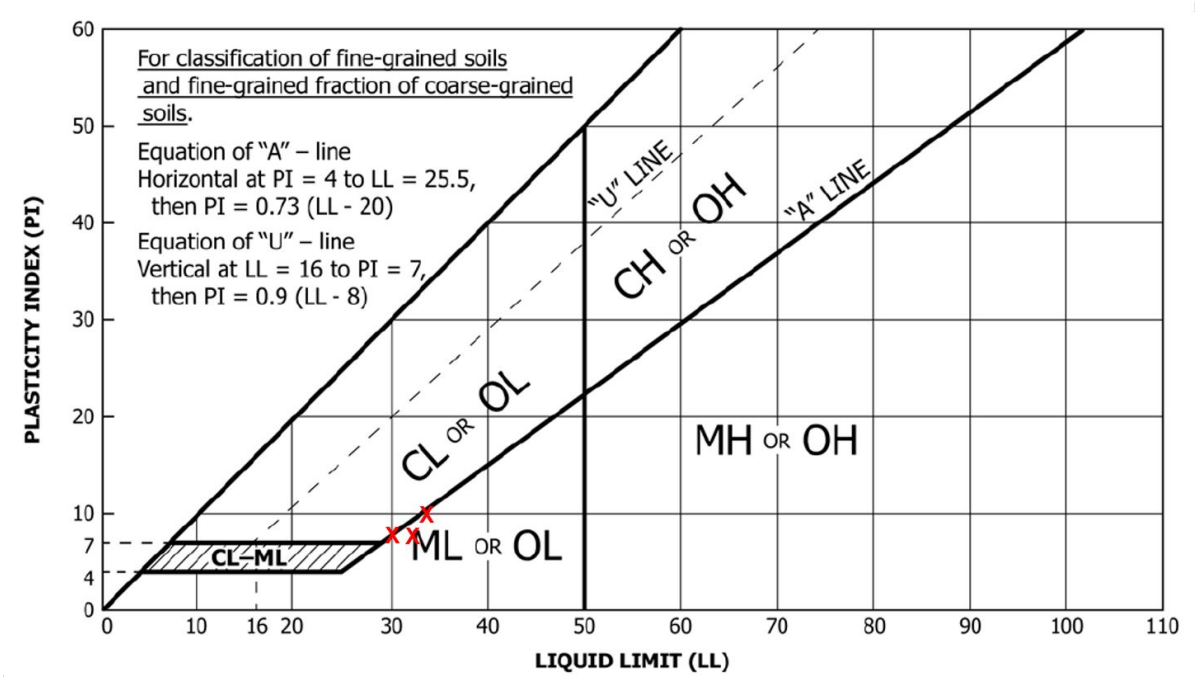

Figure 5.2: Placticity chart showing the plasticity and liquid limit of the subspecimens of the main batch. Source ASTM (2017b).

5.2. Thixotropy

Thixotropy tests were conducted on two types of specimens, the first type was prepared using tap water as pore fluid while the second contained de-ionized water. Tests were performed according to the schedule suggested on the Standard up to 30 days (BSI, 2015). Both batches were mixed to 26.4% water content. During testing, three penetration measurements were taken on each specimen and three specimens were tested per aging time.

5.2.1. Measured data

The tables presented in Appendix B show the measured penetration of the fall cone into the specimens. Table B.2. presents the data of Thixotropy Batch A, mixed with tap water and Table B.3, shows the data obtained from the specimens mixed with de-ionized water (Thixotropy Batch B). It is also presented the water content of each of the specimens against time in Figure B.2.

5.2.2. Post processing

Given the measurement data presented above, it was possible to use the correlations presented in the standards CEN (2004) and Standard Norge (1988) to calculate the correspondent undrained shear strength to each tested specimen. The results applying the ISO conversion are shown in Figure 5.3, while the conversions to Standard Norge can be found in Appendix B.

Additionally, the obtained undrained shear strength with these methods was normalized by the liquidity index. Which is calculated as follows:

$$S_{u_{normalized}} = S_u \cdot \frac{WC-PL}{PI};$$

where WC, PL, and PI stand for water content, plastic limit, and plasticity index respectively. The values of the plastic limit and plasticity index were taken as the average values from Table B.1. The obtained results after this computation are presented in 5.4.

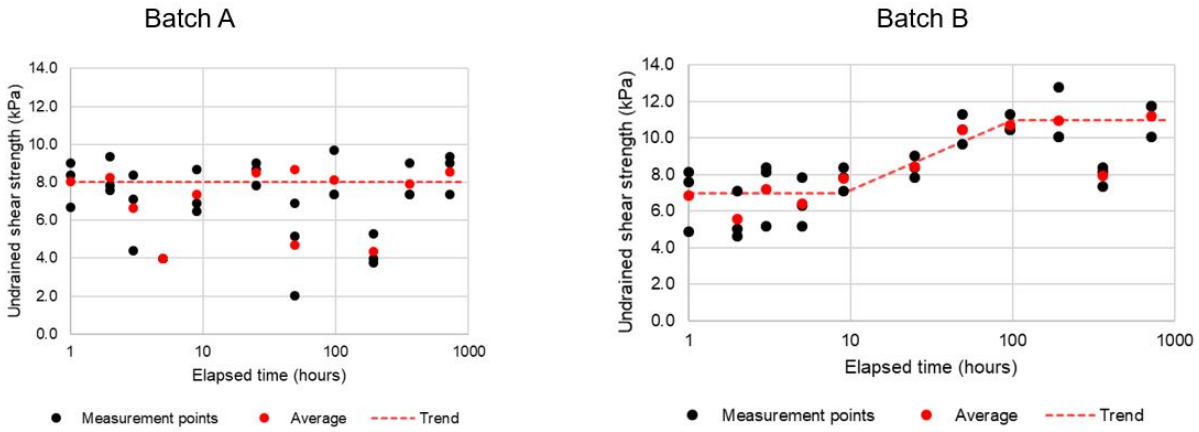

Figure 5.3: Undrained shear strength by the liquidity index in Batch A (left) and Batch B (right) with evolution trend, the conversion from cone penetration to undrained shear strength was calculated according to CEN (2004).

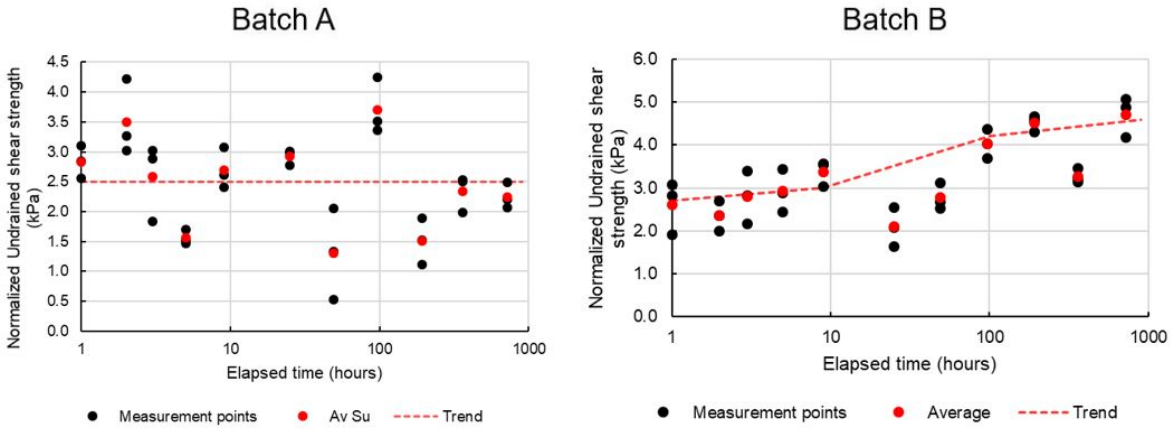

Figure 5.4: Normalized undrained shear strength by the liquidity index in Batch A (left) and Batch B (right) with evolution trend.

5.2.3. Analysis of the results

Assessment of the measured data and calculated results presented above the following observations can be enunciated:

- On one hand, the resulting correlations from Thixotropy Batch A do not show a clear trend, with great variation among specimens tested at the same time as well as the aging evolution of the undrained shear strength. Furthermore, if the water content is normalized by the liquidity index, a trend is not found either
- On the other hand, a slight increase of the average shear strength of the samples mixed with de-ionized water can be detected with a trend of the undrained shear strength evolving from 7 kPa to 10 kPa according to the Standard Norge (1988). Measurement data from this batch also shows a smaller standard deviation. When the normalized undrained shear strength is analyzed, then the increase in the undrained shear strength seems to follow a similar trend.
- Regarding the water content, variations smaller than 1% in the water content of the samples was recorded. However, Batch B shows a higher variation than the former, these variations do not seem to have any correlation with the measurements presented. These variations can be due to inhomogeneous mixing of the batch, though efforts were done to ensure mixing, or due to loss of moisture during storage despite following the guidelines for specimen preservation.

5.2.4. Interpretation

As presented in Figure 5.3 or Appendix B in figures B.6 and B.10, the batch prepared with water solution does not show thixotropic properties while the batch prepared with de-ionized water shows an increase in the normalized undrained shear strength. The value of this parameter evolves from 4 kPa to 7 kPa after 30 days. The shape of this curve is similar to the estimated curve of gain in shaft capacity from the pile tests as shown in Figure 2.5, from the tests reported by Buckley et al. (2018).

The results from the material tested with de-ionized water are very similar to those presented by Doughty et al. (2018) (Figure 2.9), who performed the tests preserving the water from the site as well as the water content. The outcome of this test may be due to the fact that de-ionized water has more capacity to dissolve the Ca^{+} ions than the tap water. On the other hand, the tap water in the area of the test facility is considered hard, with a concentration of calcium carbonate ($CaCO_3$) of 290 ppm, oversaturation of the solution would lead to precipitation of particles (Thames Water Utilities Limited, 2019). However, presence of other solved ions or suspended particles may have inhibited the restructuration process that thixotropy tests measure.

Nevertheless, with de-ionized water, it is possible to see thixotropy but this water composition is not relatable to the conditions in the site. The use of tap water is more similar to the in-situ water composition although more dissolved ions and chemical substances are present in it.

5.3. Constant Rate of Strain

Specimens prepared and aged following the procedure described in this document were tested in the CRS after 1 day (immediately after consolidation), 10 days, 30 days and 90 days after consolidation up to 80% of the measured yield pressure in the initial batch, which was determined 25 kPa. From each sample, at least three CRS test specimens could be trimmed and prepared, following the standard (ASTM, 2017a) and treating the material as an undisturbed sample. These specimens were placed on the test apparatus and, since they were already saturated, were ramped up to a back pressure of 25 kPa with a seating load of 5 kPa over 30 minutes, after which they were left for two hours before starting the test. Subsequently, the tests were started compressing the specimens at a rate of 0.7 %/hour axial strain up to an effective vertical stress of 3 MPa and then unloaded to 30 kPa at a rate of -0.027 %/hour. The choice of the loading strain rate had the objective of eliminating strain rate effects. Regarding the maximum test pressure, a pressure that would allow observation of the yield point and give some margin to draw the virgin compression line was chosen. The unloading strain rate was determined based on previous experience from Fugro (2012). Furthermore, at these rates, the loading part of the test lasted around 12 h and the unloading part 24 h, these time scales were considered acceptable since the main objective of the tests is to determine the yield point of the material at each testing time, as well as the compression moduli and hydraulic conductivity.

5.3.1. Measured data

CRS tests are based on the measurement of the vertical load necessary in order to maintain a constant, predefined rate of compression. As drainage is allowed on one end, the excess pore pressure that may be induced within the specimen is also measured.

For this type of test, the main scope of the project includes testing of three specimens per test time. On Day 1 that was done, however, on Day 10, the test on CRS10A seemed slightly disturbed, judging by the results after the tests were taken. Since some material was left, specimen CRS10D was put up and tested one day later.

Regarding the specimens tested on Day 30, due to improper setup of the apparatuses on specimens CRS30A and CRS30C, while CRS30B suffered the failure of the back pressure controller overnight, all these tests were therefore discarded. For this reason, leftover intact material from DSS30, after the Direct Simple Shear tets were prepared, was used to prepare two CRS specimens (CRS30Ar and CRS30Br). Data is only presented for

CRS30Br - from here on referred to as CRS30B- this is because CRSAr was subjected to a high load during setup, causing disturbance.

Due to the failure of the logging computer, the specimens from Day 90 have limited data. The three specimens were set up, ramped up to 25 kPa back pressure and left under the seating load for two hours. Thereafter, the compression stages were started so that they would take place overnight. However, the computer logging the data of the three CRS apparatuses shut down and therefore, stopped recording while compression of the specimens was not ceased. CRS90A was stopped at 400 kPa effective axial stress, the other two tests (CRS90B and CRS90C) have data until 1600 kPa. The results of these tests are presented with the rest in Figure 5.5. Data from the pore pressure measurements are shown in Figure 5.6. The rest of the measured data that is taken into account for the analysis is shown in Appendix B.

5.3.2. Postprocessing

Following the methods from the authors as presented in Chapter 3, it was possible to extract the yield pressure of the tested specimens. These computed pressures are presented in Table **??**. Regarding the tests from Day 90, given the limited data, up to the 1600 kPa point it seems that the slope of the axial stress-void ratio curve is starting to increase though it is not clear. Moreover, Figure 5.7 shows the average calculated yield point as well as the determined begin of yield.

Table 5.1: Extracted parameters after postprocessing the test data of CRS tests. Not enough data from CRS90 tests is available to determine the end of yield.

Age		*Begin Yield (kPa)*	*End (kPa)*	*P. Silva (kPa)*	*Casagrande (kPa)*	*Log-Log (kPa)*	*Av. (kPa)*
1	***A***	41	1701	261	197	241	233
1	***B***	51	1707	351	328	309	329
10	***B***	47	1752	367	324	277	323
10	***C***	53	1847	218	209	215	214
30	***B***	63	1837	334	460	428	407
90	***B***	79	-	195	359	226	260
90	***C***	95	-	127	367	318	271

In addition to these methods, if the indication from Head (1980) is followed, looking at the point from which pore pressure starts to build up, it is possible to determine the yield point of CRS1B and CRS10D being 275 kPa and 41 kPa respectively. The rest of the specimens do not show a build-up of pore pressured post-yield due to the small rate of vertical strain. This small rate of strain allows the dissipation of the excess pore pressure during loading due to the high permeability of chalk putty.

Moreover, determination of the yield pressure using stress-strain data in chalk putty poses a challenge due to the behavior that can be compared to the compression behavior of silt as described by Nocilla et al. (2006). The transition between the re-compression line and the virgin consolidation line is very gradual and, therefore, the yield point can be identified within a range of values. When the plots are observed, the specimens seem to follow a straight line, then the transitional stage occurs and finally seem to reach the virgin compression line with similarly constrained stiffness. With this in mind, it was attempted to determine the points where yield begins and ends, in order to evaluated how this phenomenon accurs and the evolution over time. The determined start and end of the yield point are shown in Table **??**.

From CRS data it is also possible to extract the constrained compression modulus (E_{oed}) using the data from the axial stress-strain curve. This parameter was determined for the presented tests in the virgin compression part of the curve, yielding the results presented in Table 5.2.

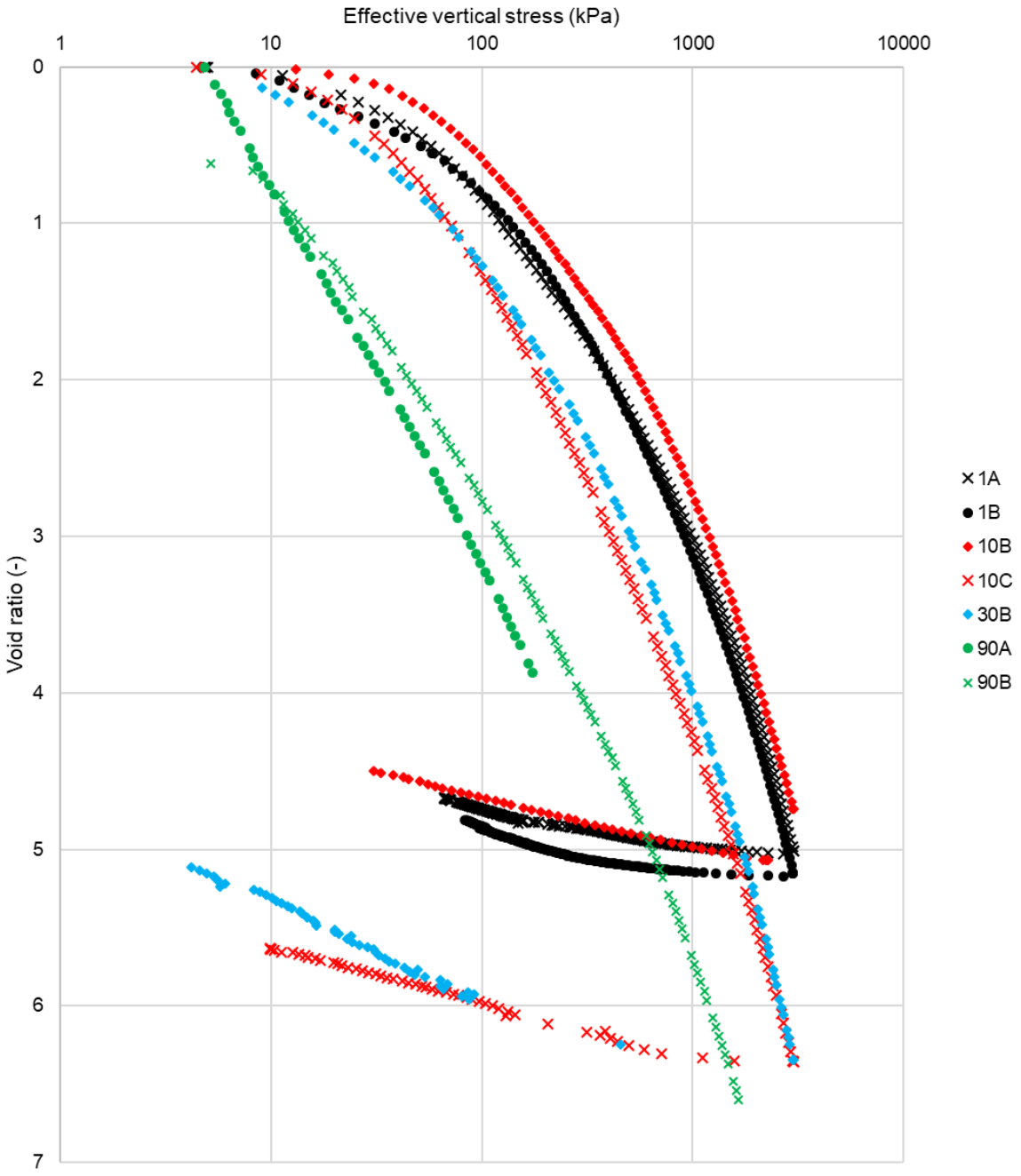

Figure 5.5: Measured stress-strain data on the presented CRS tested specimens, which were used in postprocessing.

5.3.3. Analysis of the results

After evaluation of the test results and postprocessing of those, it can be observed that:

- Tests on Day 1 were isotropically consolidated to 20 kPa and then tested. However, the determined yield point of these specimens ranges between 200 kPa and 320 kPa if the exposed methods for determination of this parameter are applied. Observing the vertical stress-void ratio plots in Figure B.12 it can be seen that:

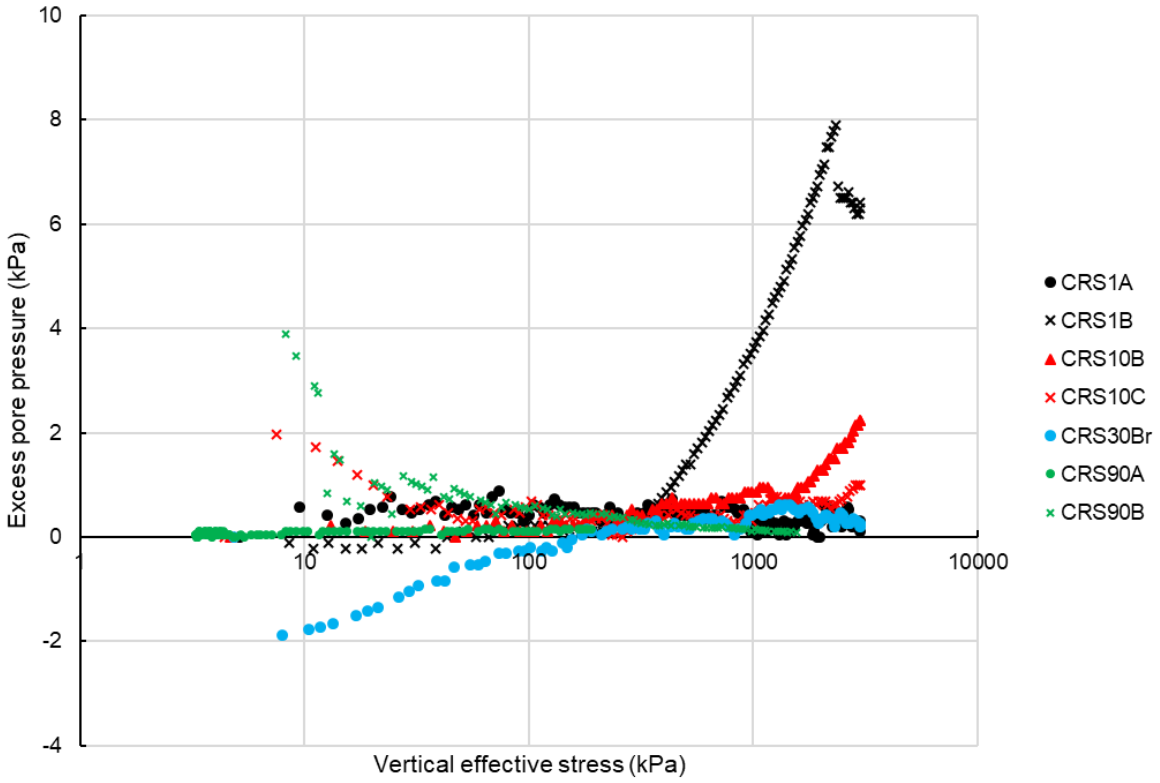

Figure 5.6: Measured stress-excess pore pressure data on all CRS tested specimens

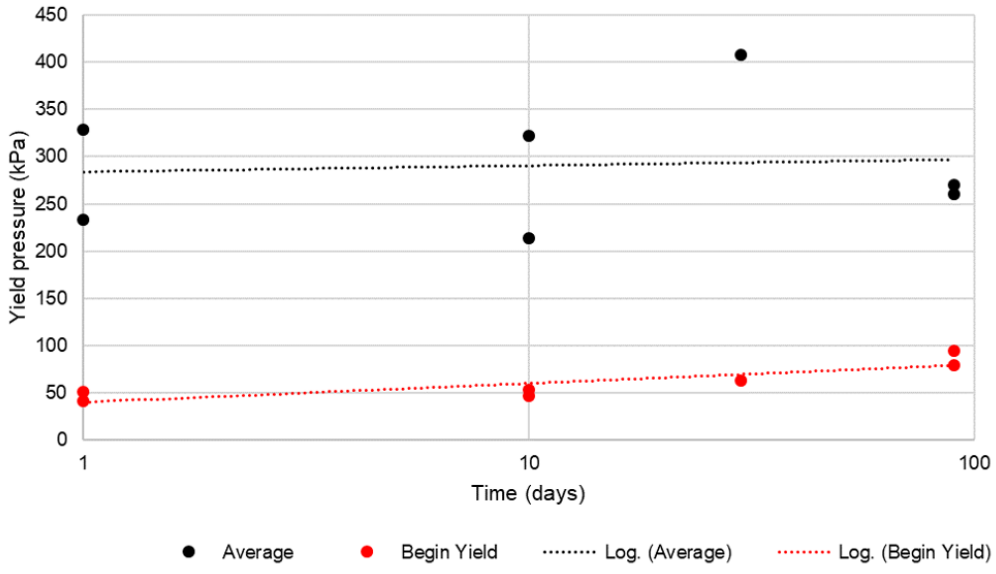

Figure 5.7: Average calculated yield point using the traditional methods and determined begin of yield.

– CRS1A starts from a smaller void ratio than the other two tests, although after 1 MPa it starts converging with CRS1B in terms of void ratio and constrained modulus. It is also noted that the slope of this graph starts to steepen after 30 kPa.

Table 5.2: Parameters of the tests regarding the stiffness. c_c and C_s are determined from the axial stress - void ratio curve while the stiffness moduli are obtained from the axial stres - strain curve.

Age		***C_c***	***C_s***	***E_{oed} (kPa)***	***E_{ur} (kPa)***
1	A	0.08860	0.0104	382	2493
1	B	0.06450	0.0037	531	1995
10	B	0.06475	0.0069	613	2988
10	C	0.06983	0.0060	477	1575
30	B	0.08602	0.0069	462	1301
90	A	0.05	-	31	460
90	B	0.07504	-	280	545
90	C	0.7124	-	250	516

  - CRS1B shows a longer unloading-reloading branch, the stress-void ratio line starts tending towards the virgin compression line after 100 kPa. The final oedometer modulus is similar to that of CRS1C. In the effective stress- excess pore pressure plot of this test (Figure B.13), the yield point of this specimen can be determined at 250 kPa, if this criterion is applied. This is the only test that shows the build-up of pore pressures.

- Regarding the presented tests on Day 10 (CRS10B and CRS10C), as the other two show signs of disturbance, these tests start at similar void ratios, nonetheless, the determined yield point is higher for the specimen CRS10B and it can also be seen in the axial stress-void ratio plot (Figure B.15) that it starts steepening after 50 kPa, the value of the pressure at which the two plots cross. CRS10B has a higher constrained modulus than CRS10C, although the slope of the unloading line is comparable.

- On the test on Day 30 - CRS30B- the determined yield point is higher than in previous tests. Moreover, the slope of the unloading-reloading line in this test is steeper than those with less aging while the oedometer modulus is smaller than previous. The slope of the unloading branch is similar to that measured in previous tests.

- Despite the limited data on Day 90, it is observed in Figure 5.5 that the tests CRS90A and CRS90B tend towards convergence with the rest of the tested specimens. Furthermore, the initial slope of the tests is larger than those on previous dates although an increase in the slope can be observed at higher pressures on tests CRS90B and CRS90C.

5.3.4. Interpretation

- Overall, it can be observed that the response to uniaxial compression of this material is comparable to the behavior presented by Nocilla et al. (2006) on silt. The main features of this type of soil in oedometer tests are the gradual transition between unloading-reloading and virgin compression as well as the non-existence of a unique Normal Compression Line. In this case, rather than one line, normal compression is shown as a range, with parallel virgin compression lines.

- Observing the evolution of the average p_c, it can be seen that it is increasing with time. Although there is dispersion in the data from Day 10 tests and only data from one test on Day 30. However, a positive trend can be observed, with the average yield point evolving from 281 kPa on Day 1 to 365 kPa on Day 10 and 407 kPa on Day 30. On Day 90, it is shown in table 4.3, that the yield point occurs at much lower pressure, although the lack of data reduces the confidence on these determinations.

- The yield point determined using these methods on Day 1 is much higher than that what should be expected given the stress history of the specimens. This is evidence that the traditional methods used in clay are not suitable for this material. When the initial and last point of the transition between the reloading branch and Normal Compression Line an evolution of the initial yield is observed, from 46 kPa to 87 kPa.

- Determination of the yield pressure based on the pore pressure plots is infeasible due to the small rate of strain of the test that does not allow the build-up of excess pore pressure in the majority of the specimens due to the high hydraulic conductivity of putty chalk.
- In time, the tendency seems to be that the initial re-loading branch is steeper with aging and the point from which it starts to tend towards the virgin compression line is at higher axial stresses. The re-loading modulus decreases with age and this is due to the relaxation of the specimens during unconfined aging.
- Regarding the repeatability of the results, on day 1 tests CRS1B and CRS1C are practically overlapping. On day 10, CRS10A and CRS10D yielded similar results while the other two are fairly different, giving a much lower consolidation pressure. On Day 90, tests CRS90A and CRS90B start at a similar void ratio, although the slope of the stress-void ratio plot is slightly different. In contrast, test CR90C starts from a much lower void ratio but the behavior of the specimen is highly comparable to the behavior of CRS90B.
- When the tests are observed in one single plot, the results of CRS10A and CRS10D could be considered outliers, in comparison with the results of the rest of the experiments. However, differences in CRS10D can be because this specimen was tested one day later since some material was left from the other tests. It was preserved employing wrapping it in cling film, aluminum foil and then waxed. However, the disturbance may have occurred during sample handling. More data regarding day 30 or even further aging will help to improve the understanding of the behavior of the samples, and figuring out which results correspond with the actual behavior of the sample and are not affected by disturbance during sample preparation. Test CRS90C was also considered an outlier as the initial void ratio is much lower than that of all the other tests.

In summary, the results from this set of tests show that the yield point increases with elapsed time, however, the softening of the material is observed through a decrease of the stiffness in the re-loading branch of the tests. This can be because the specimens were not preserved under pressure, leading to the relaxation of the material.

5.4. Direct Simple Shear

From aged consolidated specimens subjected to the prescribed aging times, direct simple shear test specimens were obtained following the indications stated in the Standard ASTM (2017a) as undisturbed material. From each of the aged samples, it was possible to obtain 3 to 4 test specimens. These were tested under direct simple shear at a rate of strain of 0.5%/hour (prescribed for high permeability material) after consolidation at σ'_v of 20 kPa, which was applied in a linear ramp during 30 minutes and then left under constant load for 2 hours. Specimens were subsequently sheared to 30% shear strain under undrained conditions. However, data is only presented up to 10% since the error in this test increases with the strain level.

5.4.1. Measured data

Direct Simple Shear tests consist of measuring the necessary horizontal load to keep the specimen shearing at a constant predefined rate. Since there are no pressure sensors to keep track of the pore pressure inside the specimen, the changes in pore pressure are assumed to be equal to the changes in vertical stress that are done in order to keep the specimen volume constant.

With this in mind, at least three specimens were tested per test type and aging time, as stated in the objectives. In this subsection, the results of the DSS tests are presented all together in order to provide an overview of the data trends. These tests are presented in terms of shear stress against shear strain in Figure 5.9, then in terms of excess pore pressure (variations in vertical stress) and shear strain 5.10.

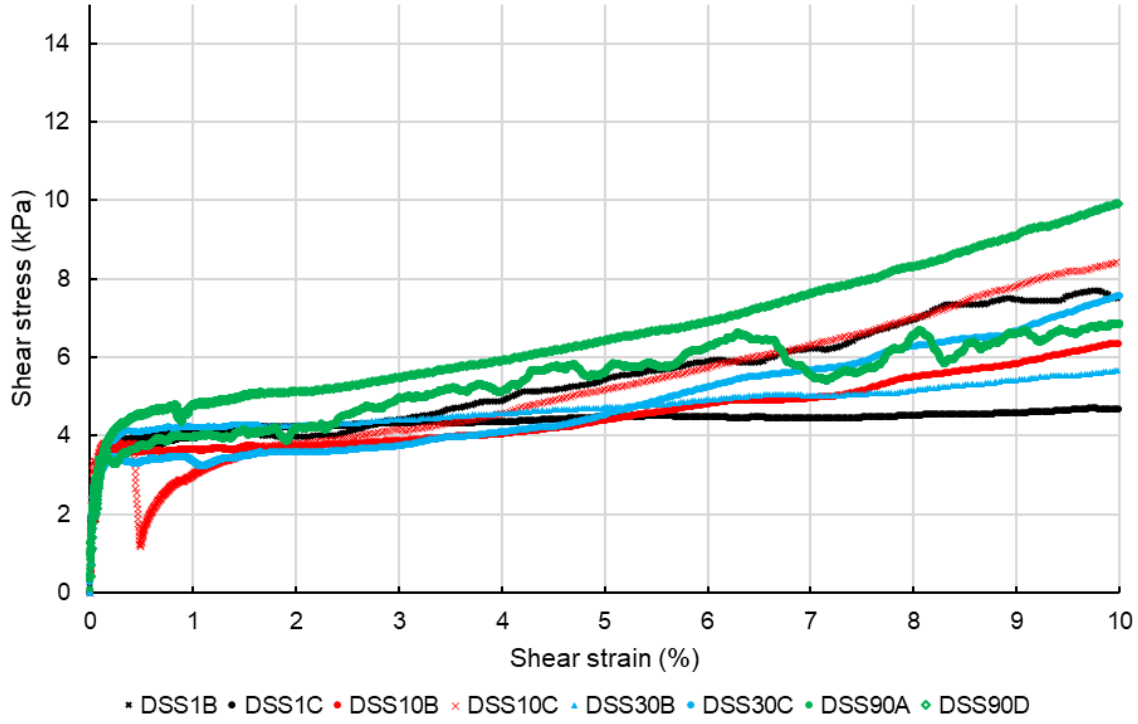

Figure 5.8: Measured stress-strain data on all DSS presented specimens, the measured data is filtered using moving average based on the 20 previous measurements.

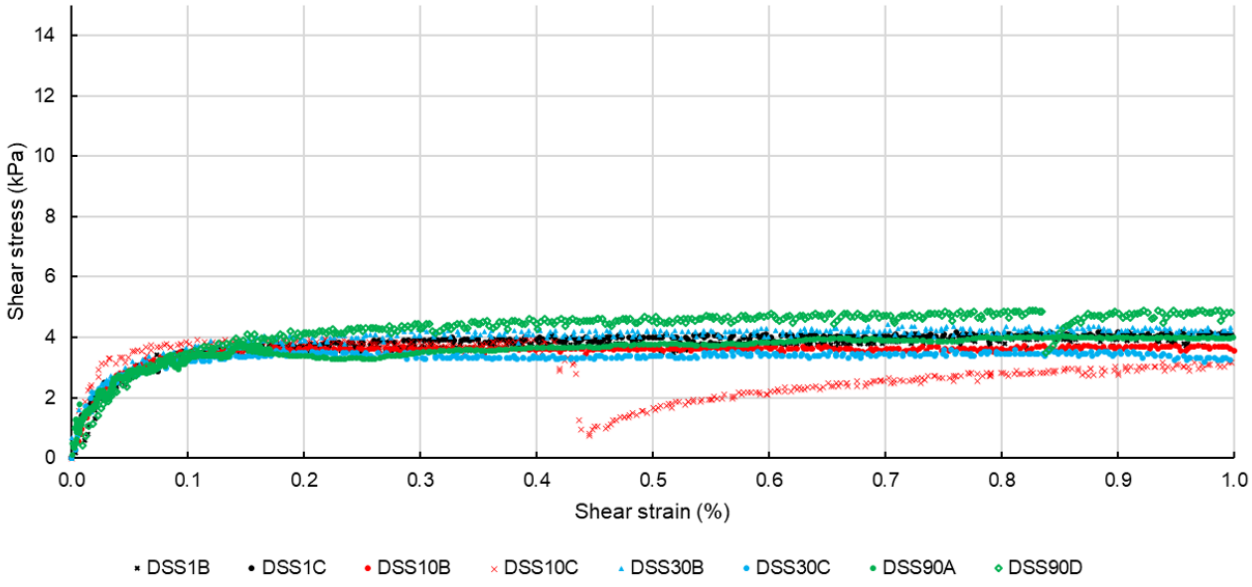

Figure 5.9: Measured stress-strain up to 1% strain data on all DSS presented specimens.

5.4.2. Post processing

Given the plane-strain conditions of DSS tests, it is possible to use the measurement data to calculate the shear modulus, this can be presented at various stages of the test such as initial, at failure or at 10% shear strain. From the recorded data, the stress path of the specimens can be represented in the $\sigma' - \tau$ space (Figure

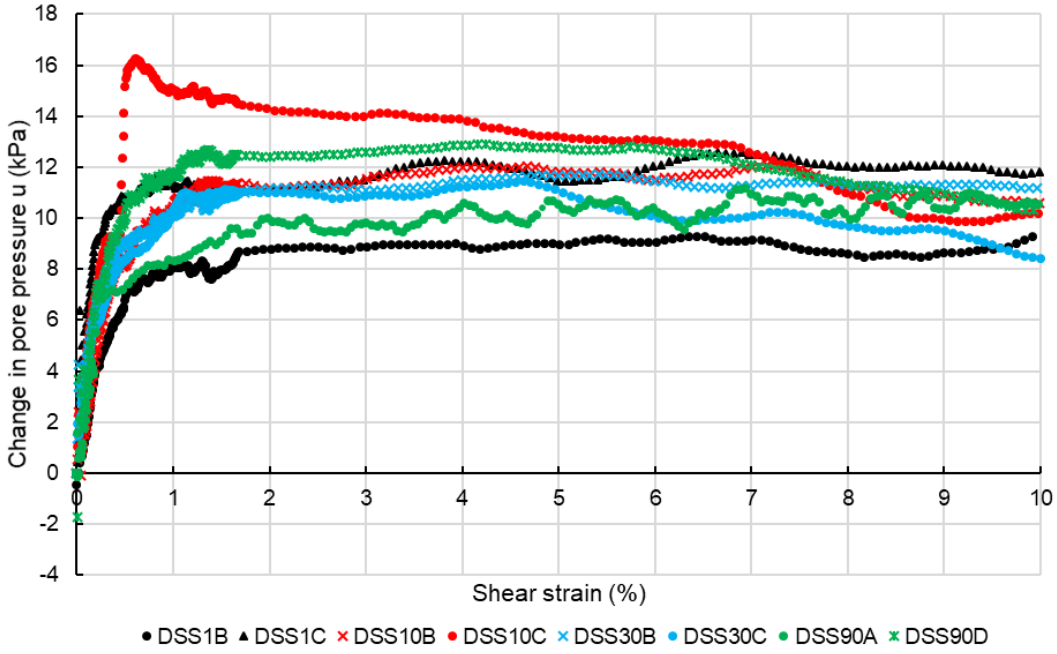

Figure 5.10: Measured stress-change in pore pressure data on all DSS presented specimens.

5.11), from which the Mohr-Coulomb failure envelope can be determined, the average friction angle in the critical state was determined $\phi' = 43°$.

To determine the friction angle at failure, more than one test pressures are needed. However, independently of this, the ultimate friction angle of the material at critical state can be defined. Moreover, given the plot of the changes in pore pressure, the volumetric behavior of the specimens can be properly defined.

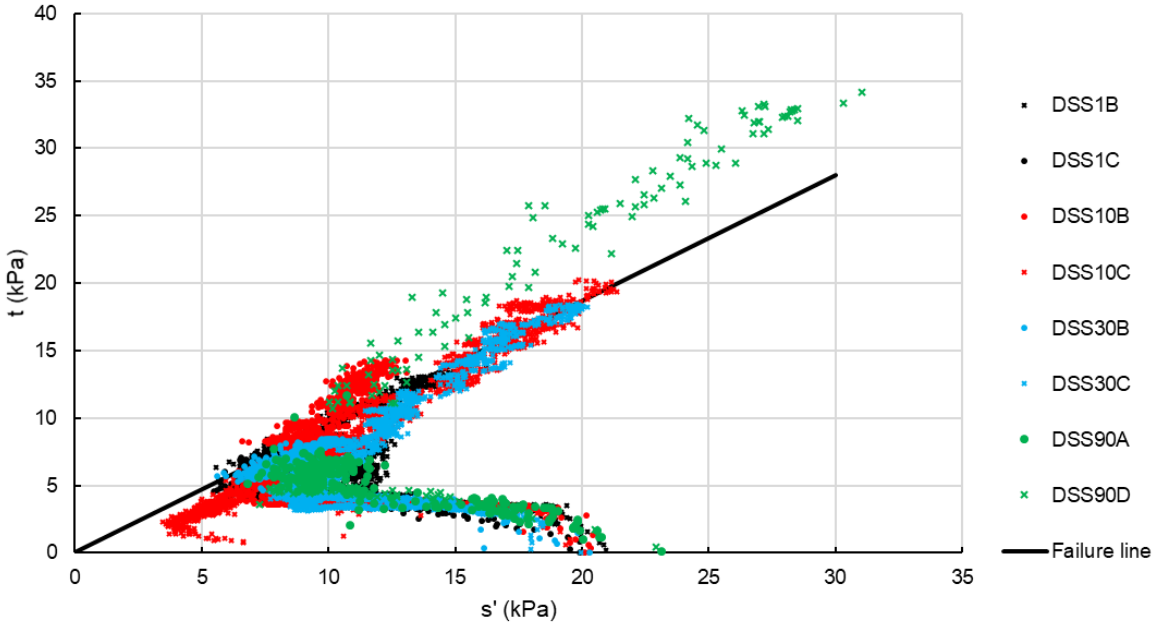

Figure 5.11: sigma'- tau stress path from all selected DSS tests after different aging times, sheared at the same rate, and the position of the failure envelope.

5.4.3. Analysis of results

Given the plots, calculations and parameters calculated above it is possible to state the following:

- On Day 1 in the stress-strain response, there is linear behavior up to 0.02%shear strain followed by a stiffness degradation up to 0.1%, where the shear stress, τ, is 4 kPa. After this point, the critical state is reached. This is confirmed by observing the volumetric response, the specimen contracts initially, with pore pressures rising to 8 kPa and 10 kPa on DSS10B and DSS10C respectively during the first 0.5% strain and then they remain constant throughout the test.

- The specimens tested after 10 days aging show a similar response as the previous, with the linear region lasting up to 0.02% and then there is a degradation of stiffness. However, the shear stress at which critical state is reached is slightly below 4 kPa. Specimen DSS10C shows a peak at 1% strain, followed by an abrupt decrease in shear stress and subsequently sustained hardening which is higher than that of the other specimen. This peak is also present in the change in pore pressure plot as an abrupt increase in pore pressure. Both specimens show dilatant behavior post-failure.

- Regarding the Day 30 tests, the behavior is analogous to the previous two with the exception that the transition between the initial linear region and the degradation of stiffness takes place earlier in the test. Moreover, DSS30C is more dilatant than specimens with less aging time.

- On day 90, the response is comparable as well, with faster degradationof the initial stiffness and slightly higher increase in the pore pressures after which, hardening is more accuse than previous specimens on DSS90D seen in the stress-strain plot as well as the change in pore pressure graph.

- In the $\sigma' - \tau$ plane, the ultimate behavior of the specimens is comparable. With some dispersion in the determined friction angle, the average is 43°, with values ranging between 39° and 47° on the Day average. Nonetheless, the degradation of stiffness takes place earlier on the aged specimens.

- Concerning the repeatability of the data, from a qualitative point of view. There are trends of behavior that seem to be repeated throughout the test. Specimens DSS1A, DSS1B, DSS10A, DSS10B and to a smaller extent DSS30B show a peak after the abrupt strain softening at 4 kPa shear stress which is followed by softening of the sample and then a hardening response in shear. This peak appears at higher strain levels with increasing aging.

5.4.4. Interpretation

Upon the assessment of the analyzed data and the trends that could be identified, the processes laying behind these are explained in this section.

- The tests were first analyzed considering the response in terms of stress-strain and estimated pore water pressure build-up. It was identified that there was not a relevant evolution in terms of the build-up of excess pore pressures with values reaching 11 kPa to 13 kPa during the initial contraction of the specimen. In contrast, attending to the post-failure behavior, specimens tend to be more dilative with age (this phenomenon is not as accused as seen in the triaxial specimens, presented below). The behavior of the specimens is comparable to that shown by Lagioia and Nova (1995) with an initial elastic response, followed by destructuration to finally reach an ultimate hardening or softening stage. This hardening tends to be more accused with elapsed time.

- The decrease in initial stiffness, as well as the shear stress at which the destructuration plateau is reached corresponds to the preservation in unconfined conditions that caused relaxation in the material.

- Representation of the specimens in the $\sigma' - \tau$ plane shows variations, the determined friction angle in critical state is better characterized as a range. The reason for this may be the disturbance of the specimens in handling together with inhomogeneity of the material, compared to triaxial, only a small fraction of the material is tested so the properties are not averaged out.

5.5. Consolidated Undrained Triaxial

Three specimens per test date were saturated by means of increases of cell and back pressure until achieving a Skempton B-value of 0.95 or greater than 0.90 after three consecutive pressure increases (BSI, 2018). The specimens were subsequently isotropically consolidated in the triaxial apparatus to 20 kPa and stored for aging or tested. Before shearing, bender element measurements were taken on each specimen. Specimens were sheared at a constant volume at a rate of 0.01 mm/min up to 15% strain.

The rate of strain was determined according to BSI (2018), which gives the following equation to calculate the maximum axial strain rate (v_{max}):

$$v_{max} = \frac{H_c \cdot \epsilon_{vf}}{F \cdot t_{50}};$$

Where, H_c is the height of the specimen after consolidation, ϵ_{vf} is the estimated strain at failure (in this case, before testing, 10% was estimated as the failure strain), F is a factor that depends on the drainage conditions during isotropic consolidation, in this case, $F = 2.1$ as drainage occurred on one end, and t_{50} is the time taken to consolidate 50%.

To calculate the rate of strain for all of the tests, the first triaxial performed (TXL1A) was taken as a guide. The calculated rate of strain was 0.078 mm/min. A conservative estimate of this value was taken, and therefore, it was decided to shear all the samples at 0.01 mm/min. This way, the test up to 15% would last 35 hours. For Day 1 tests it is a rather long time as the test lasts more than one day. However, it proved the right decision since the aged samples, after slumping and consolidation had a height of 126 mm, yielding a maximum strain velocity of 0.2 mm.

Additionally, two tests on unaged specimens were conducted with the aim of assessing the effect of specimen handling in the results. One specimen was tested immediately after consolidation while the other was removed from the cell and subsequently set up and tested. These tests were deemed necessary given the difference in the behavior of the unaged speciemems compared to the samples subject to aging.

5.5.1. Measured data

In a conventional undrained triaxial test, the parameters that are logged include the axial displacement, axial load, cell pressure, and pore pressure. If local strain gauges are installed, the axial and radial deformations are also measured by means of LVDT transducers. In unaged samples, it was possible to install this type of gauges and this type of data was recorded. However, aged samples were slumping after removing them from the aging wax, and the inability of the sample to stand up straight during the installation of the transducers made it impossible to collect local strain measurements in the aged samples. As a matter of fact, this slumping is significant in terms of determination of the wave velocity with Bender Elements (Figure 5.12). To measure the height of specimens subject to slumping, the displacement was zeroed in the cell with a calibrated block and then the difference in height of the specimen was recorded. As the displacement transducer in the triaxial apparatus only measures displacements relatively rather than on an absolute scale.

In this section, the deviatoric stress (q) data against axial strain (ϵ_v) is presented along with the excess pore pressure against deviatoric stress. It can be observed that the behavior of the Day-1 specimens, which were not removed from the cell since the dry material was placed in the apparatus, is different than the aged specimens. For this reason, they are presented separately. In Figure B.37, the axial strain - deviatoric stress data is presented for Day-1 while in Figure 5.14 the results of the specimens aged 10, 30 and 90 days are shown.

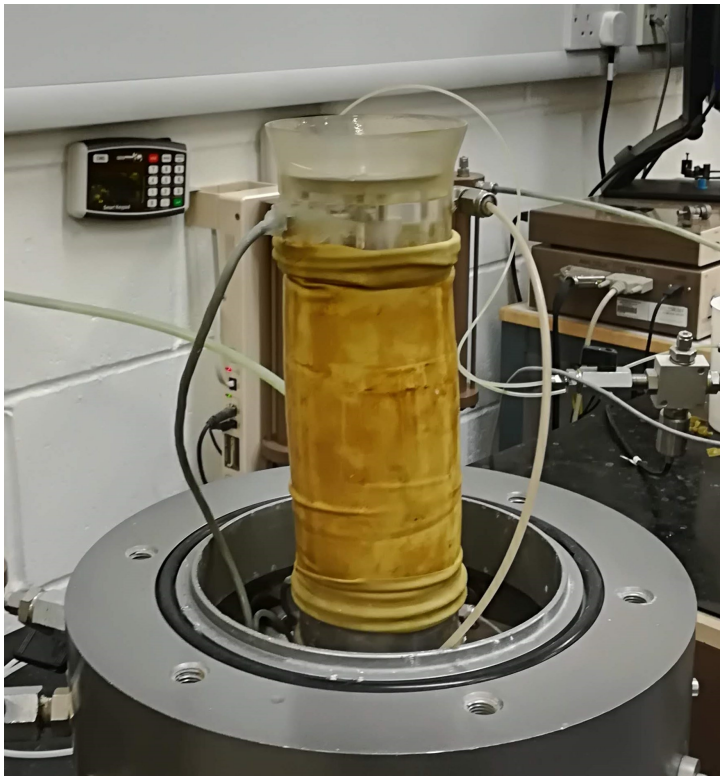

Figure 5.12: Specimen TXL10C experiencing slumping after setup in the triaxial apparatus.

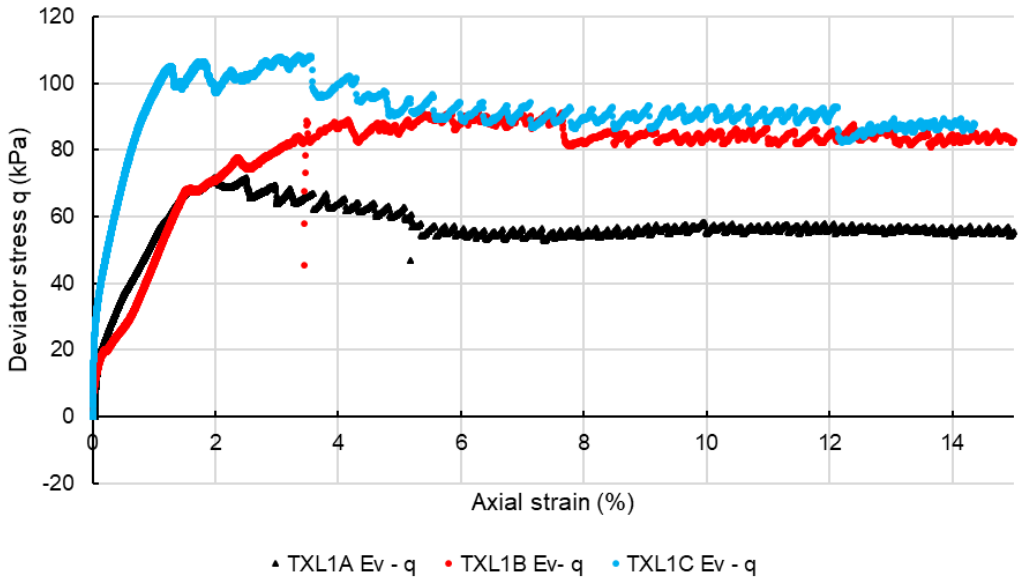

Figure 5.13: Stress-strain relation in triaxial day 1 tests.

In undrained triaxial tests, the volume of the samples is kept constant and the change in pore pressure is measured, which can be compared to the changes in volume in a drained test. Dilative behavior is associated with negative excess pore pressures while contractive with positive changes. The recorded excess pore pressured in Day 1 tests are shown in Figure B.38, while the rest of the tests are presented in Figure 5.16.

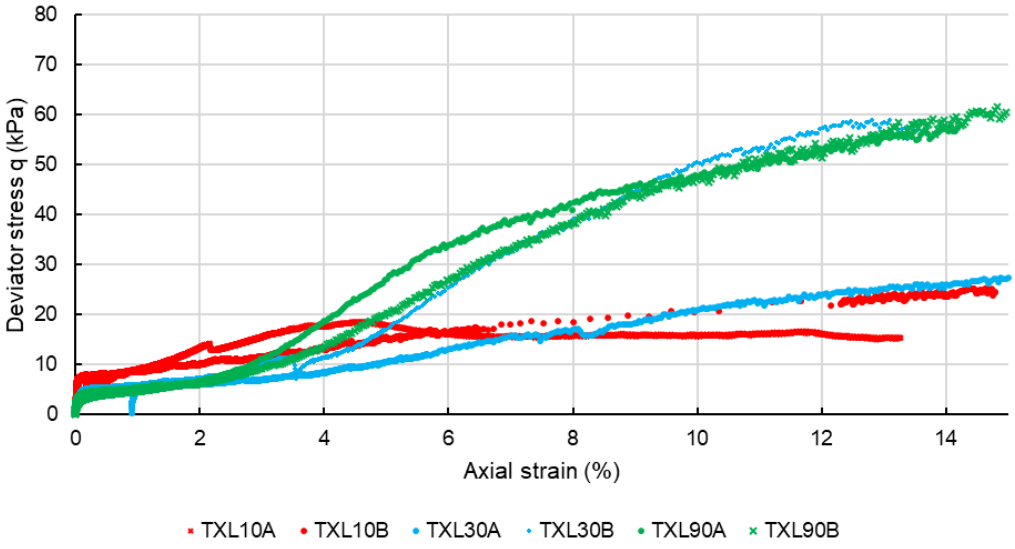

Figure 5.14: Measured deviatoric stress-strain data on all aged triaxial presented specimens.

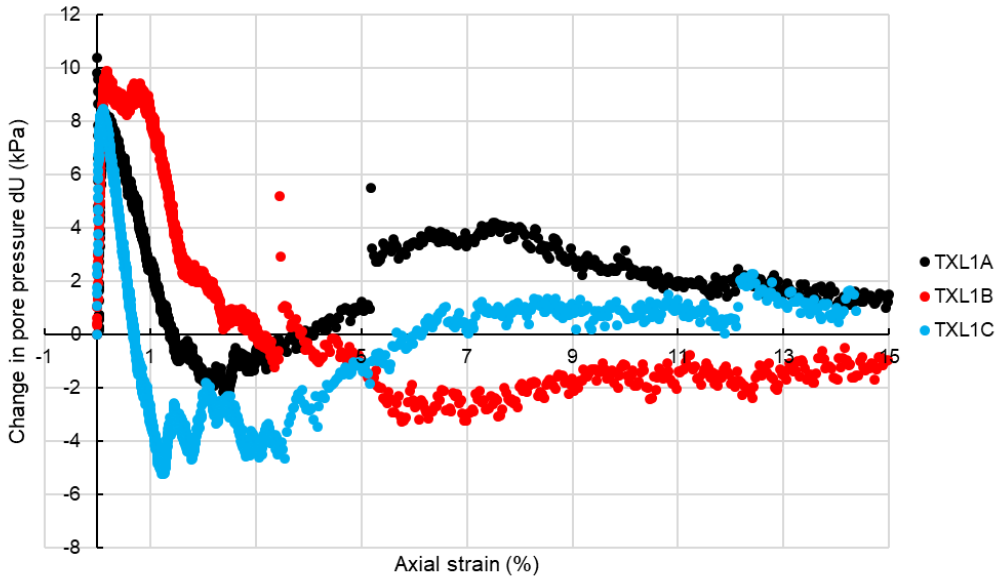

Figure 5.15: Excess pore pressure - strain relation in triaxial day 1 tests.

Furthermore, these measurements were also taken on the unaged specimens that were tested additionally after finding the behavior as different materials. The results obtained from those tests are presented in Figure 5.17 and5.18.

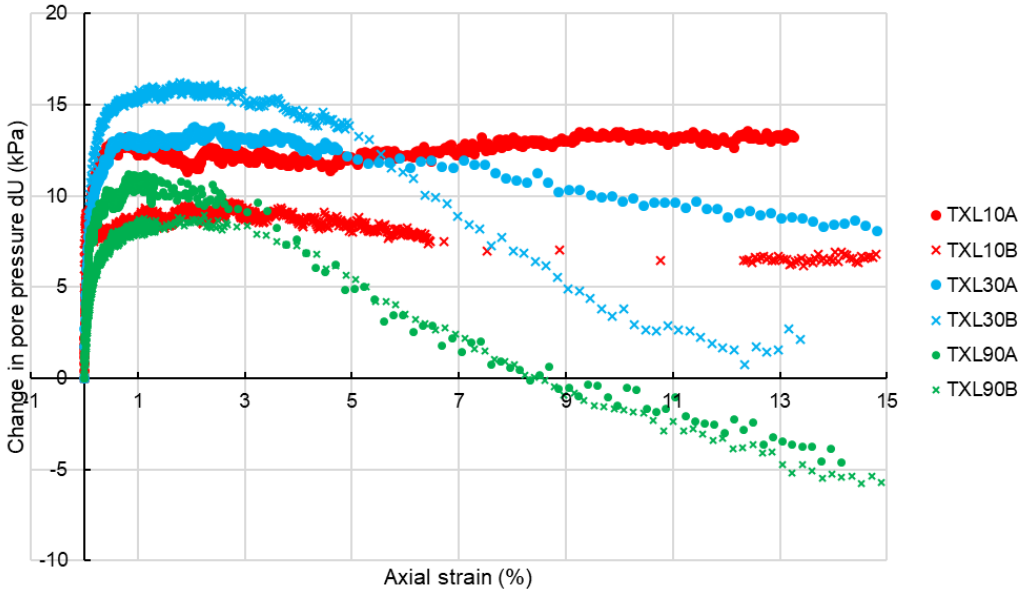

Figure 5.16: Measured deviatoric stress - excess pore pressure data on all aged triaxial presented specimens.

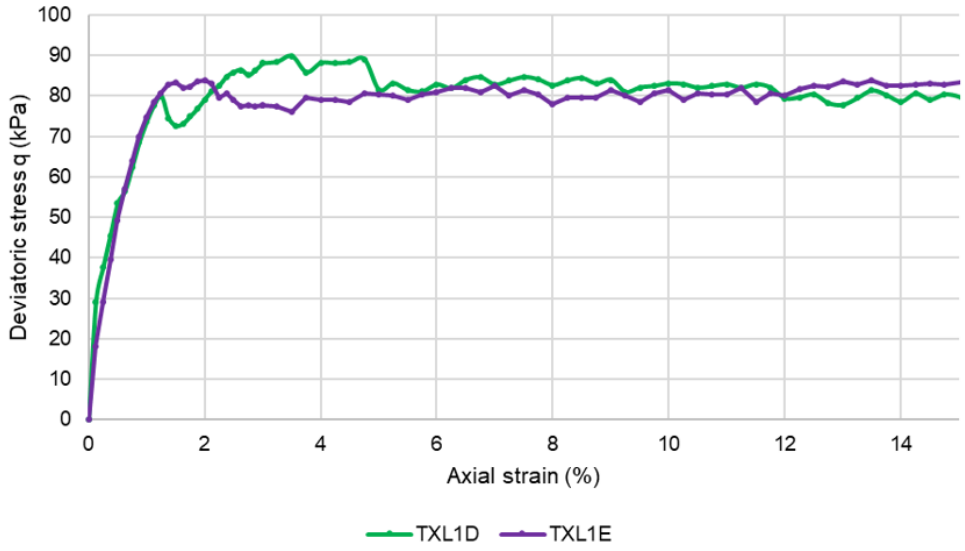

Figure 5.17: Stress-strain relation in triaxial day 1 tests, TXL1D was tested after consolidation and TXL1E was removed from the triaxial cell between consolidation and testing.

5.5.2. Postprocessing

Given the measurement data, it was possible to derive the specimen parameters, so the evolution of these parameters could be understood. It was also possible to calculate the stress path of the soil at each test in the p'-q space. With the data presented in this manner, the critical state friction angle of the material can be determined given the slope of the critical state line using the following equation:

$$M = \frac{6sin\phi_{cs}}{3-sin\phi_{cs}};$$

In Figure 5.19, the results of all the selected tests are presented in the p'-q space. In this case, all of the tests are combined as the critical state friction angle of the material is the same independently of the pre-failure

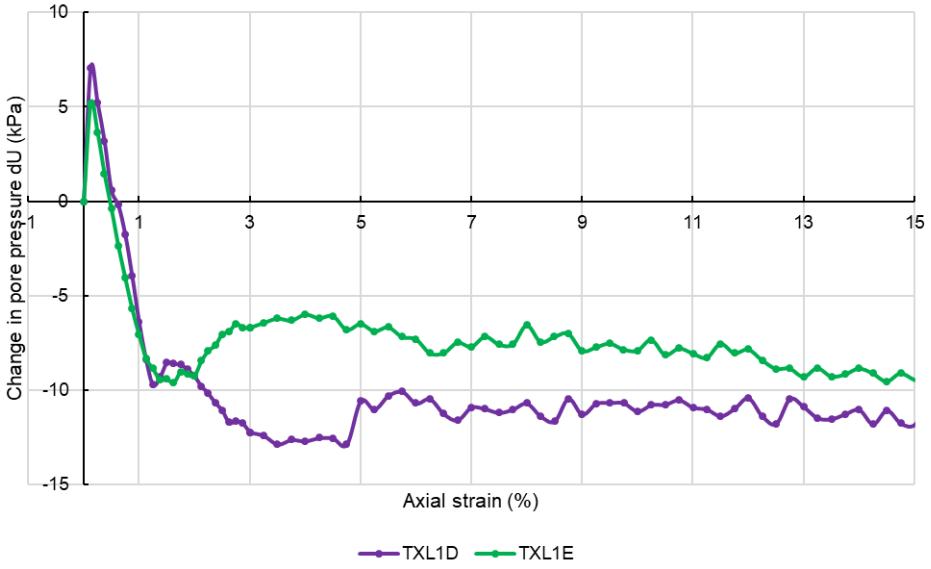

Figure 5.18: Excess pore pressure - strain relation in triaxial day 1 tests, TXL1D was tested after consolidation and TXL1E was removed from the triaxial cell between consolidation and testing..

behavior. The estimated average critical state friction angle is determined $\phi_{cs} = 37.6°$. On the other hand, the individually determined critical state friction angle is shown in Table B.4.

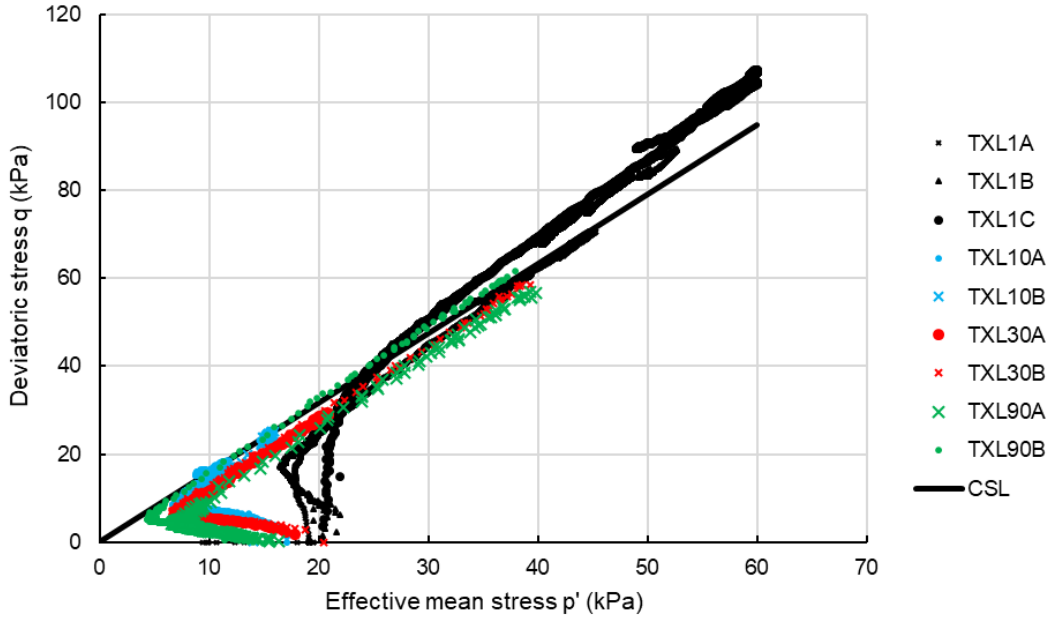

Figure 5.19: p' - q stress path from all selected Triaxial tests after different aging times, sheared at the same rate.

If the data from the triaxial tests is plotted in the s'-t space, the Mohr-Coulomb failure parameters can be correlated with the critical state line in this graph with the following relation:

$$sin(\phi') = tan(\alpha):$$

where α is the slope angle of the failure envelope. These plots, as it was presented in the p'-q space, show that the tests converge when reaching the critical state line. Figure 5.20 represents the stress paths of the

specimens on all presented triaxial tests. In this manner, the average friction angle was calculated $\phi_{cs} = 38°$, which is in agreement with the results obtained analyzing the data in the p'-q space.

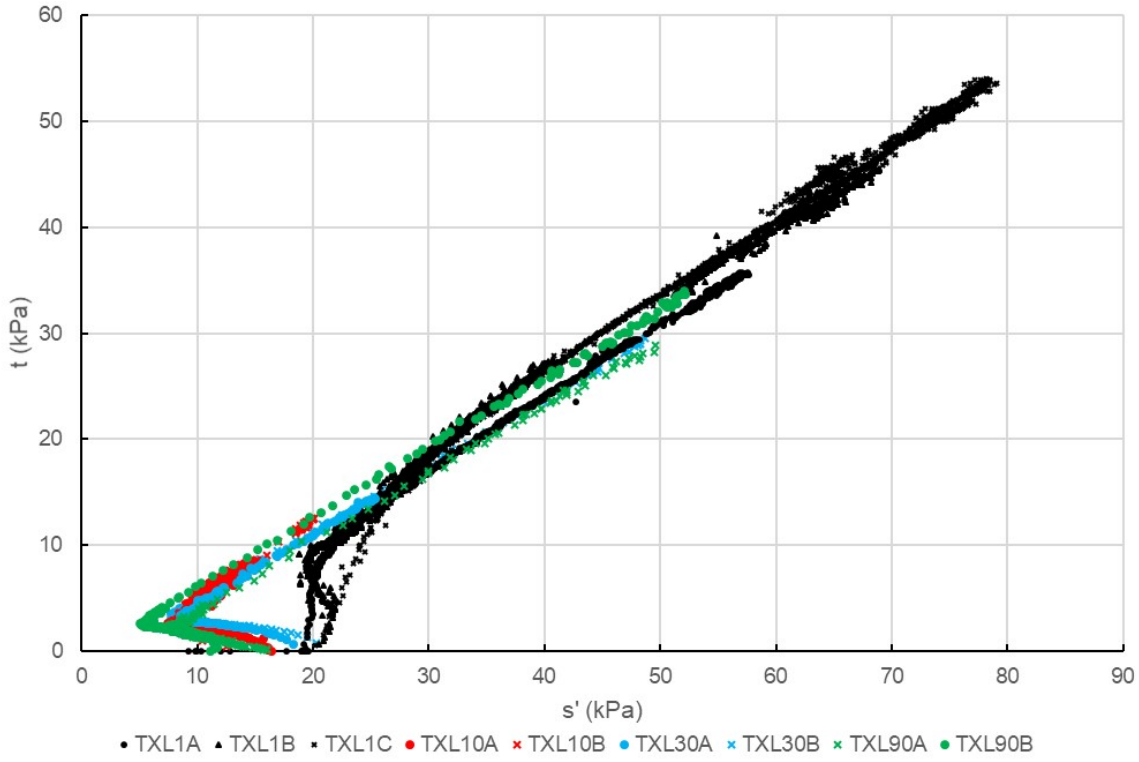

Figure 5.20: s'- t stress path from all selected Triaxial tests after different aging times, sheared at the same rate.

Moreover, stiffness parameter can be extracted from triaxial tests, in common application, the following Young's Moduli of the material are of interest: secant stiffness of the specimen at peak, secant stiffness at 50% axial strain before failure and initial Young's modulus.

5.5.3. Analysis of the results

As can be observed in the plots presented above, the specimens tested on Day 1 behave like a different material than the aged samples in terms of pre-shear, volumetric behavior, undrained shear strength, and stiffness. For this reason, the data of the unaged tests is analyzed separately from the rest in these terms. However, when it comes to the assessment of the ultimate behavior of the chalk putty samples it is found that aged and unaged are comparable.

Moreover, after testing, photographs of the specimens were taken in order to record the failure mechanism. Two types of failure were observed, shear band in Day 1 tests and barrelling on the aged specimens (Figure 5.21).

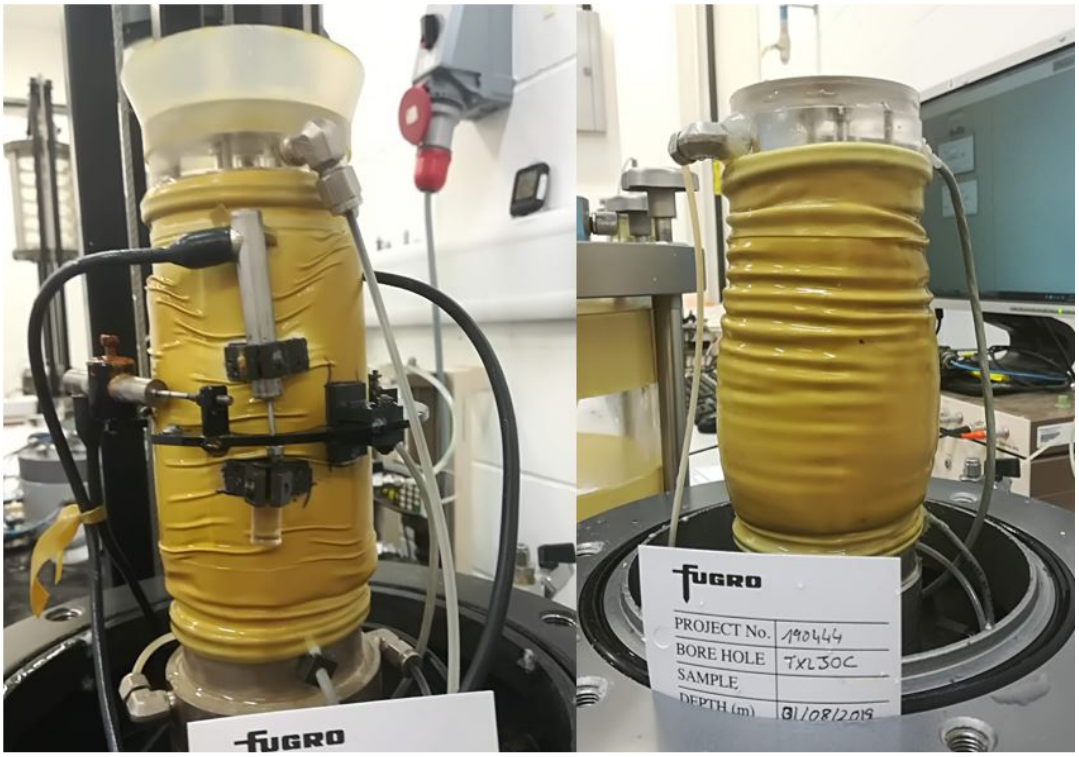

Figure 5.21: Specimen TXL1C on the left experiencing shear band failure and TXL30C on the right showing barrelling type of failure.

First, Day 1 specimens are analyzed:

- TXL1A shows an initial high stiffness until the deviatoric stress reaches approximately 10 kPa. After this point, there is a continuous degradation of the stiffness until the peak strength is reached at 2 % shear strain meaning that the undrained shear strength of the specimen at 20 kPa effective confining stress is 35 kPa. Regarding the volumetric behavior, initial contraction (with 10 kPa excess pore pressure build-up) is succeeded by dilation after 0.02% shear strain, in this stage the pore pressure arrives to -2 kPa values with a shear strain of 1.8%. Subsequently, the specimen shows contractive behavior until 7.5% shear strain and finally, the excess pore pressures remain constant.

- TXL1B, in comparison with the previous, shows a more abrupt degradation of the stiffness at 0.01% shear strain and 10 kPa deviatoric stress. The undrained shear strength of the specimen at 20 kPa effective confinement is 42 kPa. Concerning the volumetric behavior, the specimen is contractive on the initial 0.1%, building pore pressure up to 10 kPa and then there is dilatancy up to 3%. After this, there is a constant volume phase up to 5% shear strain and the specimen undergoes a small dilatant phase before showing contraction steadily until the end of the test.

- TXL1C shows the degradation of stiffness mentioned in the previous two tests at a higher stress level (27 kPa). The undrained shear strength of this specimen is 52 kPa. Regarding the volumetric behavior, it is similar to TXL1A, contractive during linear elastic deformation, then dilative up to 1.2% and followed by a contraction phase up to 6.5% shear strain. After this, the pore pressures remain constant throughout the test.

The aged tests are assessed by aging time:

- In Day 10, both tests show an elastic region up to 0.1%, after which stiffness degrades. This point also corresponds to the initial peak in the graph, giving an undrained shear strength of 3.5 kPa on both specimens. The initial part of the tests also corresponds to an accused increase in pore pressure up to 13 kPa and 9 kPa in TXL10A and TXL10B respectively. After this, the show ultimate behavior until the end of the test being TXL10A slightly dilative and TXL10B slightly contractive.
- The specimens tested after 30 days show an earlier degradation of the stiffness, with the linear elastic region finishing at 0.01% axial strain. Both have an undrained shear strength of 2.5 kPa reaching the peak at 1%. After the peak, a stage where the deviatoric stress remains constant with increasing axial strain is reached up to 2%. In terms of pore pressure, this behavior translates into an initial increase up to 13 kPa and 16 kPa for tests TXL30A and TXL30B respectively and the flat area in the stress-strain curve also coincides with constant pore pressure. Subsequently, pore pressures decrease together with the tangent stiffness, meaning dilatancy of the specimens.
- The 90 Day specimens show lower initial stiffness than the previous tests as well as a lover value of the undrained shear strength 1.75 kPa in TXL90A and 2 kPa in TXL90B. After reaching the peak, the same flat area follows in the stress-strain plots up to 2 % axial strain, after this hardening occurs until the end of the test. In the excess pore pressure plot, it can be observed the initial increase of 11 kPa and 9 kPa in this case. Subsequently, this contractive phase is followed by accused dilation.

At last, in the tests performed in order to evaluate the effect of specimen handling in the results of the Triaxial tests show that the peak strength of a specimen with no handling is 85 kPa and with handling it is 83 kPa. In terms of volumetric behavior, the response is similar and identical to the volumetric behavior of the specimens tested during the main scope of the project. Nonetheless, it can be observed that the stiffness at axial strains below 0.6% is lower on the specimen subject to handling (Figure 5.22).

In what concerns the mobilized friction angle, In the p'-q plots as well as the s'-t plots, there are variations in the slope of the critical state line from test to test with values ranging from 36° to 40°. Giving an average of 38°.

5.5.4. Interpretation

After analyzing the presented data, several trends are identified. The objective of this section is to analyze the processes taking place in the specimen that justify the occurrence of these phenomena:

- The most striking feature of these triaxial tests is the fact that the samples tested on Day 1 have a higher undrained shear strength, stiffness, and a different volumetric behavior compared to the aged specimens. The main reason for this to happen is that these samples are not handled between saturation and testing, instead, they are kept inside the triaxial cell and therefore are undisturbed. This is evidenced in the data, it can be seen that the structure of the specimen is compressed at the beginning of the test, which translates as an increase in pore pressures, once the sample fails the pore pressures decrease indicating high dilatancy. The failure mode of these specimens is different, showing shear planes.
- In all the aged samples, an evolution of the behavior of the material can be detected in time. In terms of volumetric behavior, it can be seen that while Day 10 specimens are ultimately contractive, with elapsed

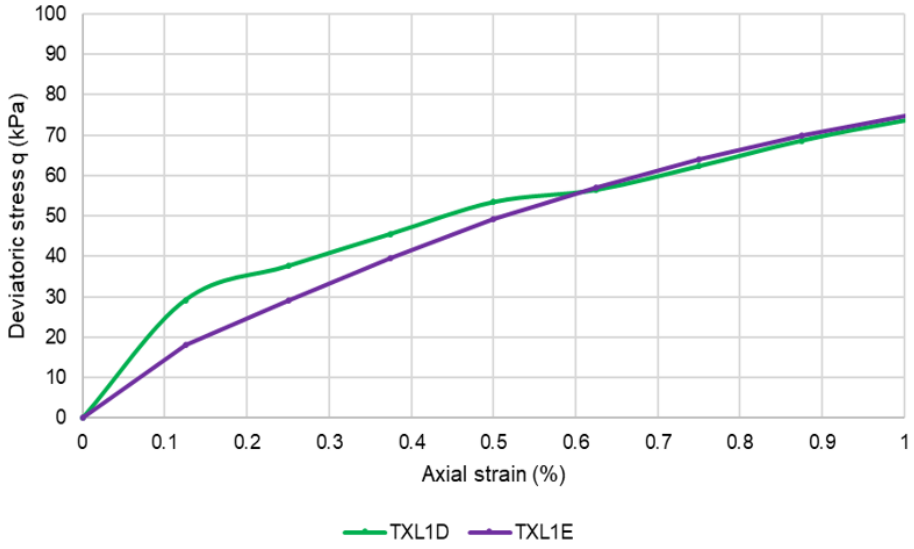

Figure 5.22: Stress-strain relation in Triaxial Day 1 tests up to 1% axial strain, TXL1D was tested after consolidation and TXL1E was removed from the triaxial cell between consolidation and testing.

time, the behavior tends towards increasing dilation. This behavior is comparable to the behavior of the calcarenites studied by Lagioia and Nova (1995), with an initial stage showing elastic deformations, followed by a destructuration phase that shows as a flat area in the stress-straining plots and it is finally followed by hardening or softening ultimate state which is linear in the p'-q plane.

It is possible that this increase in dilatancy is due to growth of the grains due to precipitation of calcium carbonate dissolved in the pore water. This phenomenon would explain why the undrained shear strength or the stiffness don't experience an increase over time as cementation may only take place around the chalk grains but does not create inter-particle bonds.

Regarding the stiffness of the aged specimens, the Young's modulus below 0.1% axial strain tends towards decreasing. This can be explained given the aging conservation conditions without confining pressure.

- There is also a decreasing trend of the variables discussed above even in the aged samples that experience degradation. Peak strength decreases in average but also the stiffness and the deviatoric stress at which abrupt degradation of the stiffness occurs.

- Analysis of tests TXL1D and TXL1E shows that handling of the specimens leads to a decrease in stiffnes up to 1% axial strain. Moreover the specimen that was removed from the cell shows slightlig lower build up of pore pressure in the initial elastic phase (7.5 kPa on TXL1D the degradation of the peak strength is also a consequence of further handling of the specimen when it is transported, wrapped and introduced in the wax cardboard tube, as this difference in the peak strength is not seen in the Direct Simple Shear tests, which are also subject to further handling after removing from the triaxial cell.

- Day 1 specimens have staggered stress-strain response in the post-peak behavior. This staggered graph is also observed at a smaller amplitude in specimens TXL10B and TXL30B. This noise in the results is due to the low pressure of the tests, the measurements are more susceptible to the noise measured in the instrumentation.

5.5.5. Comparison of the results of Triaxial and Direct Simple Shear in the $s' - t/\sigma'_v - \tau$ space

Presentation of the results of triaxial tests in the $s' - t$ space allows drawing the Mohr-Coulomb failure envelope, this means that the friction angle and the effective cohesion can be determined. Regarding DSS, when the data is plotted in the $\sigma'_v - \tau$ space, the same parameters can be extracted and therefore, the behavior of the material can be compared. However, the strength parameters of soil are dependent on the test conditions, which means that the Mohr-Coulomb parameters are not necessarily the same but the behavior of the material can be compared.

The stress path of each of the tests was calculated and the critical state line (CSL) for each triaxial test was estimated as well as the Mohr-Coulomb failure envelope of the DSS tests. The mobilized friction angle of the material is then the angle of the slope of this straight line. The results of the tests are presented per test type in Figures 5.20, 5.11, in Table 5.3 the estimated value of the friction angle (ϕ'), respectively is presented. The cohesion is assumed to be zero. In the results presented, the outlier tests have been eliminated.

Table 5.3: Average estimated effective friction angle of the Mohr-Coulomb failure envelope assuming that the cohesion is negligible.

$\phi'(°)$	***Triaxial***	***Direct Simple Shear***
Day 1	40	41
Day 10	37	48
Day 30	37	41
Day 90	38	47

It is worth mentioning that this analogy between these two test types is not free of uncertainties, mostly regarding the representation of the results of Direct Simple Shear in terms of principal stresses Wroth (1984). This author explains the hierarchy of strength depending on the test from which it is measured using Matsuoka's criterion. In this derivation it is concluded the following relationship between the friction angle measured in triaxial compression and plane strain conditions (simple shear) that can be used for engineering purposes:

$$8\phi'_{ps} \approx 9\phi'_{tc};$$

where ϕ'_{ps} and ϕ'_{tc} are the friction angles expressed in degrees measured in plain strain and simple shear respectively.

- In these plots, it can be observed that the behavior of the specimens in Triaxial compression and Direct Simple Shear in undrained conditions is highly comparable. With an initial dilation behavior up to failure and then reaching the critical state. Behavior which is typical of a dense sand.

- The value of the mobilized friction angle in these specimens is consistent throughout the tests at different dates, although the determined value of this strength parameter for each test type is different. In triaxial tests, ϕ' ranges between 35° and 41° while in DSS the values range between 39° and 46°.

- The measured values of the mobilized friction angle in triaxial tests are higher than those found in the literature. Regarding the friction angle in simple shear, there is no information available about this parameter in chalk putty. Bundy (2013) has performed tests in this material but in the report, no data about Mohr-Coulomb strength parameters is included or plots from which they can be extracted.

- There is not a clear trend regarding the evolution of friction angle or cohesion with aging of chalk putty. Triaxial friction angles stay fairly constant, with variation between specimens while the friction angles measured in the DSS apparatus seem to increase from day 30 to day 90, this variation in the DSS results can be due to variability of the material as well as the limitations of the test.

5.6. Bender element tests

Bender element tests were undertaken on the specimens that were tested in the triaxial apparatus, after the saturation stage on specimens TXL1A and TXL1B and after consolidation stage on all of the samples, including those previously mentioned. This is because the specimens that were subject to aging were consolidated before aging took place. From each specimen, the recorded arrival wave through the medium was logged for at least 10 different wave periods between 0.06 ms and 0.34 ms. From these measurements the best ten are presented, preferably between 0.1 ms and 0.28 ms. Upon analysis of the results, given the difference observed between Day 1 specimens and the aged material, two additional Day 1 tests were conducted one without removing the specimen from the cell (TXL1D) and another where the specimen was taken down after consolidation and placed on the triaxial cell again (TXL1E). From this specimen, bender element measurements were taken before and after removing it. The objective of this trial is to quantify the disturbance caused by specimen handling.

5.6.1. Measured data

The data measured in this test is the change in voltage in the receiver element as a function of time after triggering the transmitter. This recorded sinusoidal wave is presented in Figure 5.23, the different emission frequencies are presented in the same plot. In this chapter only the measurements taken on specimen TXL90A are presented, for the rest of the measurement data refer to Appendix B.

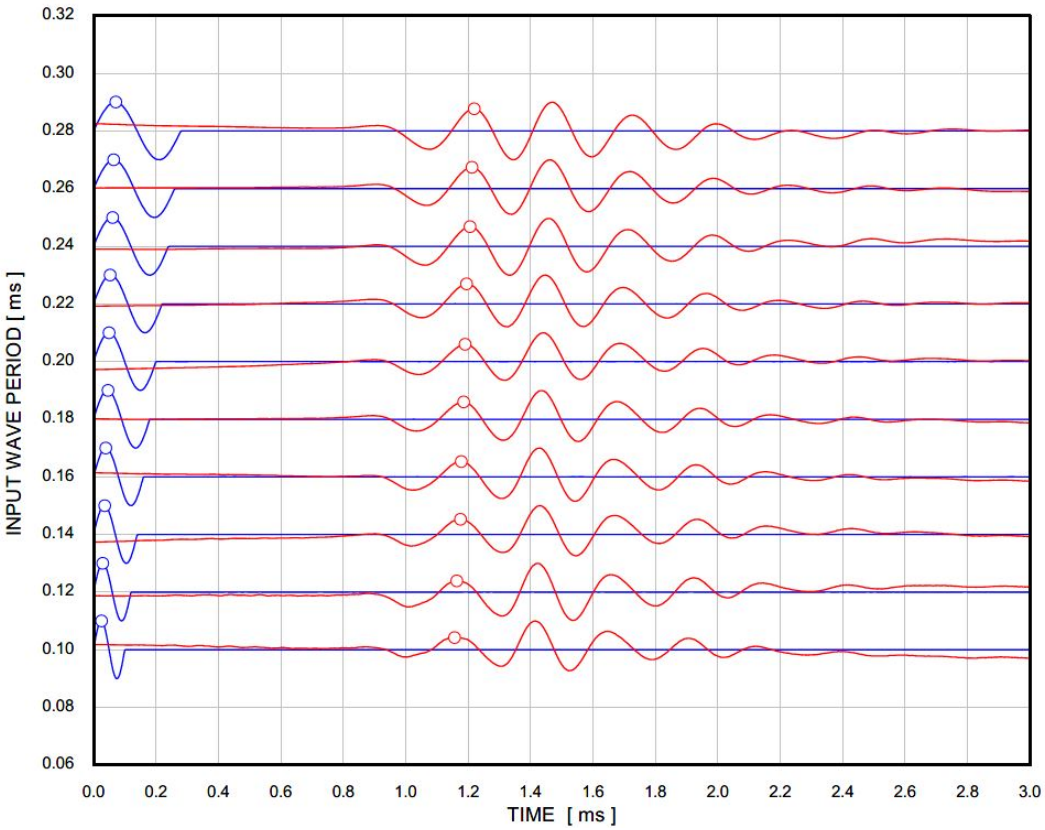

Figure 5.23: Input wave (blue), received signal (red) and determined arrival peak at different frequencies on the Bender Element test taken on TXL90A after consolidation.

5.6.2. Postprocessing

Given the measurement data as presented in Figure 5.23. The travel time was determined by picking the positive peak in the arrival wave. Once this is selected, the shear wave velocity could be calculated, and afterward the initial shear modulus at each wave frequency. In Figure 5.24, the results are presented on Day 1 specimens while the aged specimens are presented in 5.25, together with the measurements taken from the disturbed Day 1 specimen (BE1E-d). Results from the test on TXL10C, where the bender elements were positioned perpendicular to each other instead of parallel, are not presented in the table as no useful data could be extracted from those measurements. Also the results from the bender element measurements before and after removal from the cell are presented in 5.26.

5.6.3. Analysis of the results

After the analysis of the measurement data and the calculated parameters, the following facts were observed:

- In agreement with the triaxial data, degradation of the sample strength takes place due to sample handling. As the average value of G_{MAX} throughout all frequencies decreases abruptly from 130.5 MPa on day 1 to 35.5 MPa on day 10. In Figure 5.26, it can be observed that the initial shear modulus decreases from an average of 142 MPa to 68 MPa after removing from the cell.
- If only the measurements taken on disturbed specimens is accounted for, there is a decrease trend in the average G_{MAX} from 68 MPa on day 1 to 35.4 MPa on Day 10 to 40.3 MPa on Day 30 followed by a decrease in day 90, with an average of 28.9 MPa.
- Despite the efforts to avoid disturbances in the received signal, there is noise present that may have altered the recorded arrival times.

5.6.4. Interpretation

It can be observed that the initial stiffness of the unaged specimens is considerably higher than the aged material, in agreement with the results of the triaxial tests. This is due to the handling of the specimens, being taken down from the triaxial apparatus caused disturbance of the specimens and decrease in the strength and stiffness, including the small-strain stiffness. This is made evident when the measurements taken on TXL1E are taken into account.

Regarding the disturbed Day 1 and aged specimens, there is an decrease in the average stiffness Day 1 to the aged specimens. Within the aged material, the initial stiffness shows an increase from Day 10 to Day 30, followed by a reduction in Day 90. This may be explained by the relaxation of the specimens which was also recorded in other tests, the increase from 10 to 30 days may be explained as natural variability.

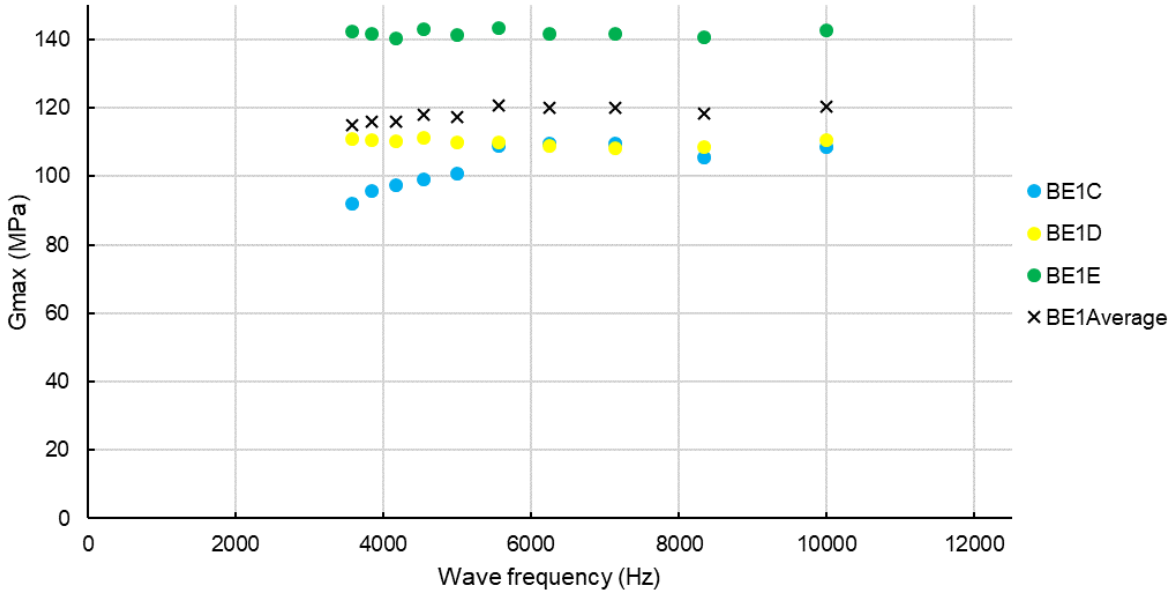

Figure 5.24: Calculated G_{MAX} from wave input at different frequencies for all Day 1 specimens and average G_{MAX}.

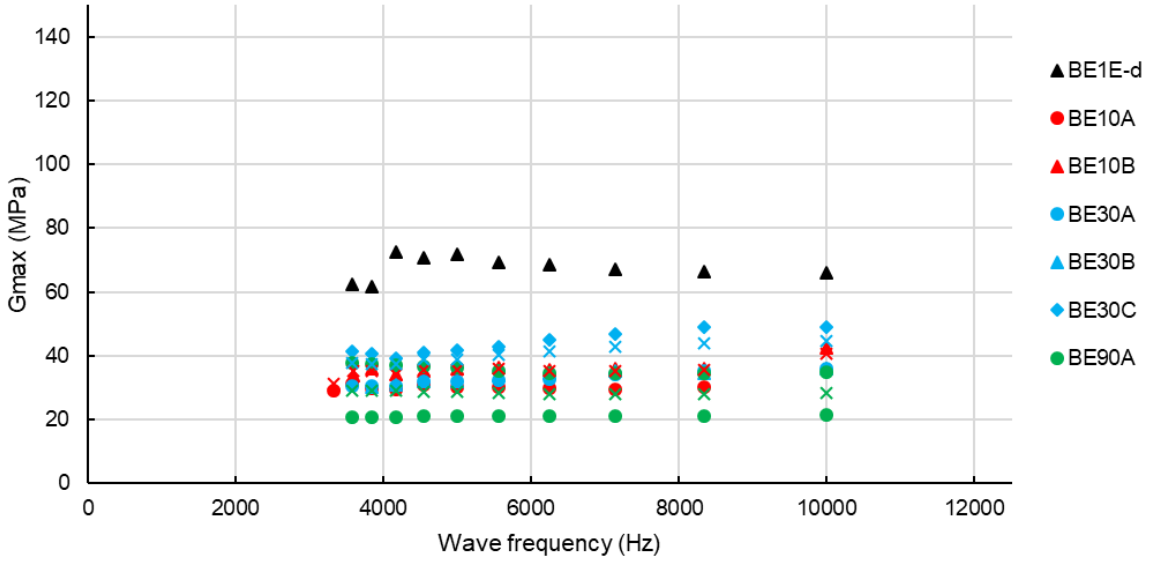

Figure 5.25: Calculated G_{MAX} from wave input at different frequencies for all aged specimens and average G_{MAX} per aging time. Day one specimens are not included in the analysis as the results are not comparable with those of aged specimens.

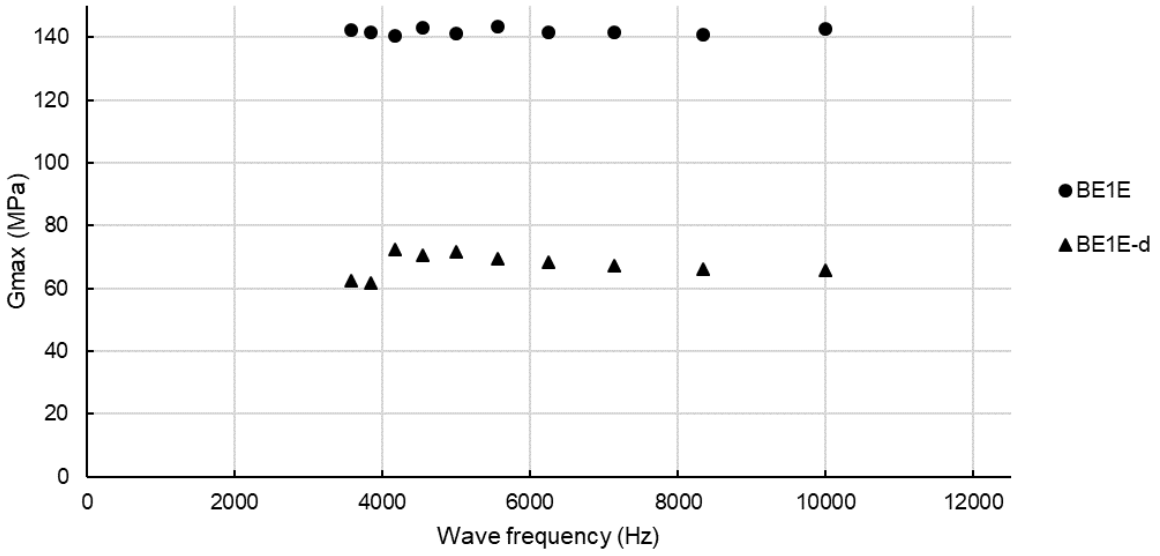

Figure 5.26: Calculated G_{MAX} from wave input at different frequencies from TXL1E before removing from the cell (BE1E) and after removal (BE1E-d).

6

Discussion

6.1. Specimen preparation and aging

An important part of this project was the development of a specimen preparation technique that is commercially feasible at the same time that it yields homogeneous, repeatable and representative specimens. In Chapter 4, the process through which the most suitable method was selected is described along with the preservation conditions and test setup. In Chapter 5, the test conditions and results are presented and an evaluation of these results is done. In this section, it is intended to discuss the the results of the specimen preparation considering the outcome of the tests. Additionally, the aim is to point out which factors from the preparation technique and aging conditions may have influenced the results and in which way.

The compacted dry samples show an average weight of 890.70 g which is 1.4 g below the target weight and a standard deviation of 2.6 g which is 0.3% of the total weight. It should be also taken into account that the Day 1 triaxial specimens had material removed in order to fit the bender elements.This means that the method to produce the compacted samples is highly repeatable, with minimum errors that don't have an impact on the general calculation of the void ratio and dry density. Additionally, the water content measured on the top, middle and bottom of these specimens show consistent values, they can be found in Table **??**.

Regarding the results of the saturation process, as it was not possible to take the water content of the specimens after saturation and consolidation in order to not disturb the material, the way of comparing the homogeneity of the process is by means of comparing the saturation data available. Some specimens were saturated in advanced triaxial cells with logging options for this stage. However, other specimens were saturated in less computer-controlled devices that do not allow logging during saturation stages. This means that data was recorded by hand and when, left overnight, there was not the possibility of monitoring the samples. Therefore, the saturation processes can be compared by the number of cell and back pressure increment steps that were taken before achieving saturation and, thus, the cell pressure when saturation was reached. On average, the cell pressure at saturation was 547 kPa, most specimens achieve saturation at 500 kPa and 550 kPa although the value ranges from 450 kPa in TXL90A and TXL90B to 800 kPa in DSS1. The reason for this variation may be found in the duration of the flushing stage (in some specimens end of flushing took place overnight) as it does not seem to be connected to the dry weight at compaction.

After saturation and consolidation of the specimens, those assigned for it were stored for aging in the conditions described in Chapter 4. It was shown in the test results that this process had limited effect on the strength and strain parameters of the material, which will be analyzed in depth in subsequent sections. Nonetheless, it is relevant to analyze the effect of aging and the devised aging conditions in the index properties of the specimen. It was possible to measure the water content (using leftover material) and bulk density

of the specimens tested in CRS and DSS. With this information and the particle density, the void ratio of the specimens can be computed. Observation of these results shows that the water content and void ratio increased with aging in some of the specimens. A clear example of this is the evolution of the void ratio in the DSS specimens. Nonetheless, it should be pointed out that the water content taken from this specimens only belongs to a small fraction of the sample, assuming that the specimen is homogeneous. A reason for this increase, given that the specimens are completely sealed is that water migrated from the porous stone into the specimens.

Analysis of the evolution of the stiffness of the specimens in the different tests indicates that the material is relaxing with increasing aging as the deformation moduli in most tests (CRS, DSS, triaxial) follows a decreasing trend. This is due to the unconfined aging conditions, chalk putty is a non-cohesive material, therefore, when it is preserved without confining pressure the structure does tends to collapse.

Another conclusion that can be drawn from this overview, is the fact that material that was saved from one specimen and tested later on to make up for a failed test was disturbed and had water losses although it was preserved in cling film, aluminum foil and a layer of wax; although it was not kept in a wax cardboard tube. All the tests conducted with this material were classified as outliers and discarded.

Table 6.1: Summary of preparation characteristics and index properties of the specimens before and after aging. WC of the triaxial specimens was not taken after aging as it would disturb the sample.

Specimen	***Dry weight (g)***	***Max pressure at saturation (kPa)***	***Aging (days)***	***WC (%)***	***Void Ratio (-)***	***Dry density (Mg/m3)***	***Comments***
DSS1A			1	28.95	0.719	1.58	
DSS1B	891.84	800	2	26.43	0.621	1.67	Tested with leftover DSS1
DSS1C			1	28.95	0.787	1.52	
DSS10A			9	27.03	0.727	1.57	
DSS10B	890.8	550	9	27.03	0.725	1.57	
DSS10C			9	27.03	0.716	1.65	
DSS30A			29	27.55	0.822	1.49	
DSS30B	889.9	500	29	27.55	0.806	1.5	
DSS30C			29	27.55	0.778	1.52	
DSS90A			90	29.97	0.802	1.5	
DSS90B	890.63	550	90	30.79	0.827	1.49	
DSS90C			90	30.34	0.828	1.48	
DSS90D			92	27.06	0.767	1.53	Tested with leftover CRS90
CRS1A			1	27.85	0.784	1.519	
CRS1B	891.54	600	1	27.1	0.783	1.52	
CRS1C			1	27.6	0.77	1.534	
CRS10A			10	26.89	0.777	1.525	
CRS10B	892.04	550	10	27.44	0.788	1.515	
CRS10C			10	27.36	0.771	1.53	
CRS10D			11	25.32	0.661	1.632	Tested with leftover CRS10
CRS30B	889.9	500	29	27.3	0.792	1.51	Tested with leftover DSS30
CRS90A			92	28.23	0.769	1.532	
CRS90B	891.57	600	92	27.43	0.786	1.52	
CRS90C			92	27	0.722	1.54	
TXL1A	891.04	450	1		0.716	1.58	
TXL1B	891.33	500	1		0.716	1.58	
TXL1C	886.8	650	1		0.717	1.58	
TXL10A	892.61	550	10		0.717	1.58	
TXl10B	892.85	500	10		0.717	1.58	
TXL10C	891.66	500	10		0.716	1.58	
TXL30A	894	550	30		0.717	1.58	
TXL30B	885.08	600	30		0.729	1.57	
TXL30C	883.48	500	30		0.734	1.56	
TXL90A	891.39	600	90		0.716	1.58	
TXL90B	892.9	450	90		0.716	1.58	
TXl90C	892.43	700	90		0.716	1.58	Consolidated to 200~kPa

6.2. Thixotropy

Evolution of the undrained shear strength was studied through fall cone tests with the objective of observing the changes in this parameter as well as to evaluating the influence of different water contents in the changes in of this parameter. The idea was to test three batches: with tap water, de-ionized water and saline solution to the salt concentration found in the pores. Since there was no salt found in the pores, the scope was limited to the first two water compositions.

The results reveal that the batch prepared with water solution does not show thixotropical properties while the batch prepared with de-ionized water presents an increase in the normalized undrained shear strength. The value of this parameter evolves from 4 kPa to 7 kPa after 30 days, according to the ISO Standard (BSI, 2015).

In the literature, authors reported the increase in undrained shear strength of chalk putty specimens. Bundy (2013) studied thixotropical behavior of chalk slurries by means of fall cone tests, these show a decrease of the penetration of the fall cone from 23 mm to less than 5 mm after 2000 hours (Figure 2.12). The weight and shape of the fall cone is not given, therefore, the value of the undrained shear strength cannot be derived. Moreover, in contrast with other authors as well as with the results obtained in this project, in which after one month the undrained shear strength seems to have reached the upper limit, in this case the measurement after 50 days presents a significant increase.

The results obtained by Doughty et al. (2018) show that an increase takes place up to 28 days. However, the value tested in that date is significantly higher than previous. If this value is disregarded, the trend observed is similar to that presented in this report. And also, to the capacity gained in the tested piles. Further research would involve testing the evolution of undrained shear strength in time spans similar to the pile tests.

6.3. Compression

Constant Rate of Strain tests were performed on chalk putty on the initial scope and the main batch. The initial scope comprised testing of unaged material at target dry density and unconsolidated in order to determine the yield pressure of the slurry. After analysis of these results, isotropically consolidated to 20 kPa aged material was tested at the different designated aging times. Due to technical complications, one Day 30 test can be presented while the tests from Day 90 only logged data up to 1600 kPa in the best of the cases. Nonetheless, it is possible to analyze and interpret the results, this assessment is collected in the previous Chapter.

Despite the fact that performance of CRS or incremental oedometer tests in different aging time of the specimens is not reported in the literature, Razoaki (2000) shows the compression path during isotropic consolidation of the specimens previous to triaxial testing. On the specimens that were aged under drained conditions and an unknown axial stress, it can be observed that a reloading branch is developed together with the evolution of the yield stress. The material also tends towards more abrupt rupture at yield. The undrained aged specimens also show a slight increase in the yield point, that could be interpreted as the formation of a structure in the material (Figure 6.1.). Instead, in this project, the yield point tends to increase while the transition between unloading and reloading is smoother with elapsed time. Moreover, only one specimen is presented per aging time by this author, therefore the repeatability of the result is unknown.

Furthermore, Bialowas et al. (2018) conducted oedometer tests in reconstituted specimens up to 10 MPa, after this, it was concluded that the stress at which particle breaking takes place is 2 MPa. In the test carried out in this project, there is no evidence of this phenomenon taking place. However, according to Hardin (1985), particle crushing depends on several factors, the ones that may lead to different results in this case include the particle size distribution and the void ratio.

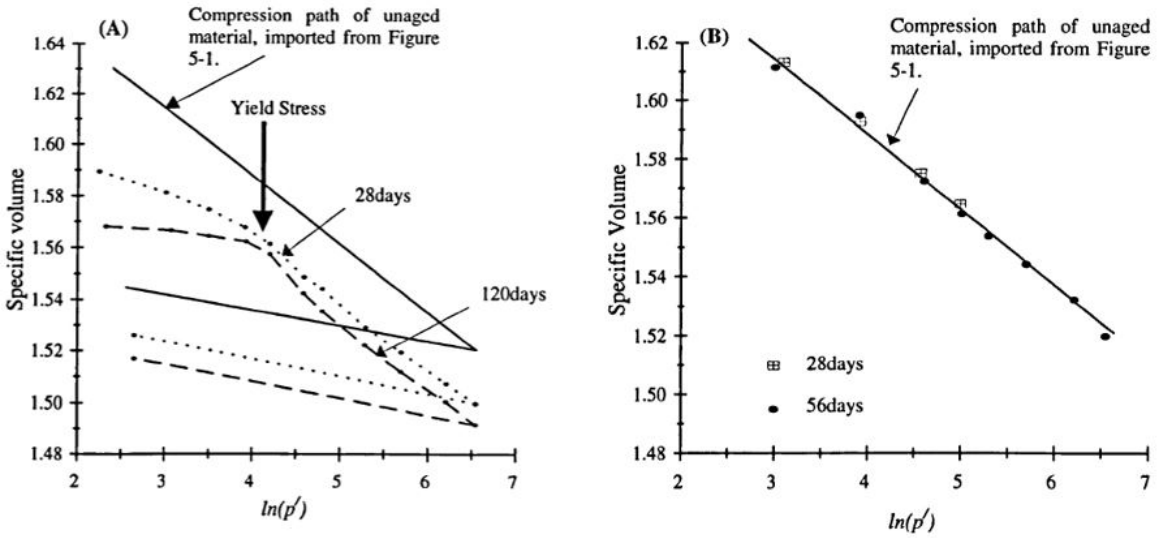

Figure 6.1: Isotropic compression paths for aged material. (A) drained aging and (B) undrained aging. Source Razoaki (2000).

6.4. Strength and volumetric behavior

The performance of Consolidated Undrained Triaxial and Direct Simple Shear tests allows the study of the strength characteristics of this material and the volumetric behavior in shear. The results of nine triaxial tests and eight Direct Simple Shear tests at four different elapsed times were evaluated in order to determine the strength characteristics of chalk putty, as a material and in time. As it is mentioned in the analysis of the results of the previous chapter, in light of the Day 1 tests keeping the specimen in the cell and removing it there is relaxation due to testing and the volumetric response does evolve with time. No increase in the peak strength is found through this tests, agreeing with the results of Bialowas et al. (2018). Nonetheless, changes in the volumetric behavior can be tracked in time. In this section, the strength and volumetric behavior of the tested specimens is discussed by test type comparing them with the results obtained by other authors in the literature.

6.4.1. Consolidated Undrained Triaxial

The strength of the specimens in triaxial testing conditions can be analyzed in several ways, from undrained tests, the undrained shear strength can be estimated. Mohr-Coulomb strength parameters (cohesion and friction angle) may be calculated presenting the data in the $\sigma' - \tau$ space, or from the data in the $s' - t$ plot. Presenting the stress path in the p - q' graph the critical state parameters can be obtained.

Upon analysis of the data obtained on the triaxial tests it was determined that the tests from Day 1 should be assessed separately from those on the aged specimens. The most distinctive feature of the unaged tests is the high undrained shear strength which ranges between 35 kPa and 52 kPa. Bundy (2013) conducted undrained triaxial tests on unaged specimens with similar preparation and no handling involved, obtaining similar values of the undrained shear strength (Figure 6.2.) Moreover, the variation in the ranges is similar as well.

Upon analysis of the aged specimens, it was possible to conclude that the ultimate strength of the specimens as well as the peak strength do not seem to be influenced by time in the tests conducted. Nontheless, it could be observed that there is an evolution in the volumetric behavior, with specimens showing more dilatancy in time as well as post-yield hardening.

Razoaki (2000) performed drained and undrained tests at 27 and 56 days. In the presented results, the stress-strain behavior of the material is similar to that of the specimens presented here. Despite this, relaxation is

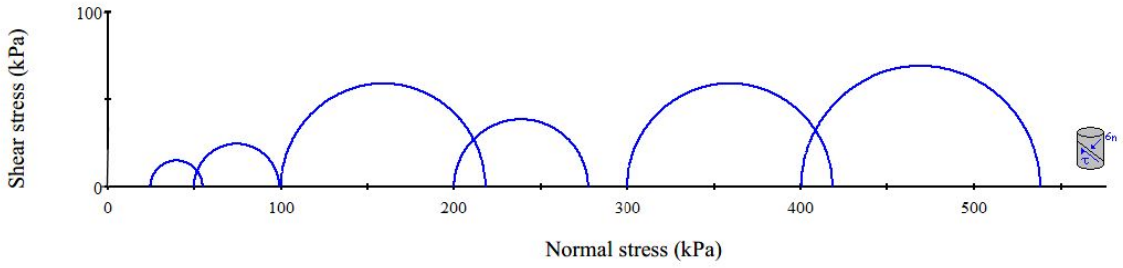

Figure 6.2: Mohr circles at failure from undrained triaxial tests on chalk putty. Source Bundy (2013)

observed, with specimens showing similar peak strength but softening in the post-peak behavior and becoming more contractive.

Bialowas et al. (2018) studied the effect of aging as well as the effect of confinement and overconsoldation. In the tests presented in this publication regarding the study of aging, very limited changes were observed in terms of peak strength and ultimate strength. This is in agreement with the results here presented. However, in these tests there is no evolution of the volumetric behavior in time.

In contrast, Doughty et al. (2018) found an increase in the peak strength as well as increased hardening with age. The tested specimens show a comparable response in terms of volumetric behavior to the ones presented in this report, with an initial linear behavior followed by destructuration and increased hardening in time (Figure 6.3).

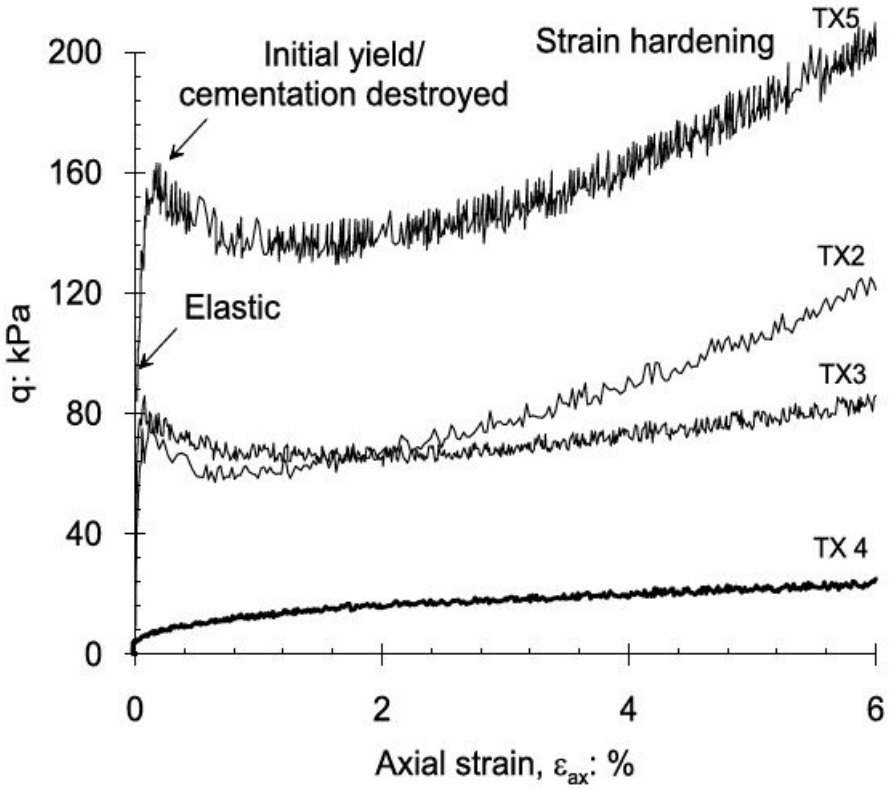

Figure 6.3: Stress-strain plots triaxial tests on chalk putty 0 days of aging corresponds to TX4, 7 days with TX3, 14 days with TX2, all of them aged and tested with 100 kPa effective cell pressure. TX5 is aged 5 days and the effective cell pressure 200 kPa. Source Doughty et al. (2018)

In summary, the tests results found in the literature show similarities with those presented in this report. First, the undrained shear strength of undisturbed specimens is in agreement to the results presented by Bundy (2013). The volumetric behavior and evolution of it is also recorded by other authors in the recent literature.

6.4.2. Direct Simple Shear

Direct Simple Shear tests were analyzed in terms of $\sigma' - \tau$, in this plot it is possible to draw the Mohr-Coulomb failure envelope. It can be observed that all the presented results behave similarly, and the friction angle at critical state has similar values. The estimated friction angles are presented in Table 5.3. While the global average friction angle was determined 43° in the critical state. Other Direct Simple Shear thests are not reported in the literature although there is records of shear box, these have been conducted by Bundy (2013) and Doughty (2016).

Bundy (2013) carried out simple shear tests at different times on specimens consolidated to 100 kPa finding the peak shear strength ranging between 72.8 kPa and 75.1 kPa, with no significant reduction taking place after the peak is reached. This last feature is also observed in the tests conducted in this project. Furthermore, this author also performed ring shear tests at different confining pressures, concluding that the failure envelope is dependent on the confining stress. The friction angle evolves from approximately 31° at pressures between 50 and 150 kPa to around 36° at pressures ranging between 400 and 600 kPa. The values found are much lower than the 43° determined in this report even though these tests yield similar values of the friction angle in sands according to Okada et al. (1998). Nontheless, the determined friction angle of the specimens in this project is higher than by Bundy (2013) and, the results from DSS tests are in agreement with those obtained in Triaxial.

Doughty (2016) conducted shear box tests in chalk putty material up to 28 days, concluding that no evolution of the properties in time was captured. In the ultimate strength, all the specimens converge in a common critical state, as presented in this report. A peak is found after 28 days aging although the repeatability of testing is unclear. Moreover, the data in these tests is considerably scattered, with variations of the initial void ratio.

6.5. Stiffness

From triaxial and Direct Simple Shear tests it is possible to extract data of the stiffness of the specimens. Triaxial tests allow the calculation of the Young's modulus of the tested material at a certain strain level for the stress level at which the test is done. On the other hand, from shear box tests, the shear modulus is extracted with the same variables, strain and stress level. Furthermore, the stiffness at very small strains of the specimens (G_{MAX}) was investigated by means of performing bender element tests on the consolidated triaxial specimens. Findings when exploring the changes in this variable throughout the tests and in time are shown in the previous Chapter.

In the Direct Simple Shear tests, it was found that the stiffness is dependent on the level of strain. Starting with a linear portion on the initial 0.02% shear strain, then softening occurs, which is related to destructuration of the material and then hardening or softening at higher strain levels. It is not possible to compare the measured stiffness with Bundy (2013) as it is not included in the published report. However, the description of the behavior is similar to the ring shear tests conducted by this author. Doughty (2016) reports similar behavior in shear box tests, with no evolution of the stiffness appearing over time.

In the analysis of the stiffness in the Triaxial tests it can be observed that there is a region with higher stiffness up to 0.02% axial strain after which the tangent stiffness is continuously degraded. Over time, the stiffness in this region decreases, which is identified with a relaxation of the specimens due to unconfined preservation. On the contrary, although the authors in the literature identified a similar pattern in the degradation

of stiffness with increasing strain, over time Razoaki (2000), Bialowas et al. (2018) and Doughty et al. (2018) measured increase in the stiffness up to 1% axial strain. Furthermore, Doughty et al. (2018) detected that the degradation of stiffness occurs at higher strains in aged specimens. Specific values of the stiffness cannot be compared as it is highly dependent on the effective stress level.

With respect to the stiffness measured with Bender Elements, there is a decrease in the specimens that have been taken down from the triaxial cell with respect to those that are not removed from the cell between consolidation and testing. While the trend shows a decrease of the initial stiffness in the aged specimens. In specimens aged under pressure, Bialowas et al. (2018) finds that the stiffness at very small strains increases with creep.

7

Conclusions

Chalk putty is a soil-like material that is formed when intact chalk is disturbed. Recently it has become of special interest due to the construction of offshore wind farms in the North Sea as chalk strata are found in the layers where the turbine foundations are designed in projects in offshore France, United Kingdom, Denmark, Germany and Poland. When piles are driven into these chalk layers, a disturbed area is created around the pile. Several pile tests reported in the literature show increased shaft capacity as early as 10 days after driving and after 4 months this increase still takes place.

Although it is a widespread affirmation in the scientific publications that chalk properties improve over time, laboratory replications of this phenomenon are scarce and the results are inconclusive. In the first place, authors have not proved that their proposed specimen preparation techniques yield repeatable results as only one test is presented for each test condition. Moreover, the conclusions derived after the test programs are diverse. In the most recent publications, Bialowas et al. (2018) states that ageing does not have an effect on increased undrained shear strength whereas Doughty et al. (2018) claims the opposite.

Testing specimens of chalk putty is a very challenging issue as it is a very soft material (undrained shear strength less than 5 kPa), which behaves as a slurry even at medium densities. It liquefies easily when being worked, for instance when preparing sub-specimens. The low range of plasticity leads to formation of clumps when the water content is close to the plastic limit and to slumping when close to the liquid limit. Furthermore, the strength is highly dependent on the dry density of the material. This creates uncertainties in the characteristics of the specimen during preparation and testing.

The objectives of this project were two: first, to develop a specimen preparation technique that yielded repeatable specimens and, once this is achieved, to study the time dependency of the mechanical behavior of the prepared specimens. To do so, the first phase of the project involved preparation trials and orientation tests where different techniques were investigated as well as the preparation parameters and initial tests in order to decide the test conditions. The main phase of the testing program comprises an extensive set of tests after 1 day, 10 days, 30 days and 90 days. The tests aim to capture the possible changes of the hydromechanical properties in time. This batch of tests includes: Triaxial with Bender Elements, Direct Simple Shear, Constant Rate of Strain and Thixotropy. In the literature, triaxial tests are the most widely reported, there are also results of simple shear tests and thixotropy. However, Constant Rate of Strain tests to track changes over time in the response under constrained uniaxial compression had not been done in the past.

Upon execution and assessment of the outcome of the two phases of the project, it is possible to derive conclusions about the results achieved and the factors influencing those; these are presented in this Chapter.

7.1. Specimen preparation

The first research question was posed with the objective of finding a repeatable specimen preparation method which is also suitable for commercial purposes. Representativeness of the prepared specimens is also an aspect taken into account in the evaluation of the resulting specimen. Upon execution of the preparatory phase, dry compaction and saturation in the triaxial cell was the method deemed more satisfactory. Following the end of the test program, the following observations have been made about the specimen preparation, aging conditions and all the aspects related to the setup of the tests:

- The compacted and saturated specimens are of almost identical characteristics in terms of water content and void ratio prior to aging. Conservation only in wax disturbs the specimens as they are not kept under pressure and storage. This causes relaxation of the material, leading to a decrease of the stiffness in the linear phase of the test with increasing aging time. Nevertheless, preservation in the triaxial cell is not feasible for commercial purposes.

- Regarding the representativeness of the tested specimens, the preparation technique yields specimens that represent an average of this chalk unit as the dried and crushed chalk is thoroughly mixed. The variations within the index tests on the subsamples are small (2% in the Plasticity Index and 10% in the content of clay-sized material in the Particle Size Distribution test) and can be accounted on natural variability and the uncertainty of the test. Moreover, the density of the compacted chalk is low to medium, which reproduces the values recorded from field data , and the water content at full saturation, 26.4%, is in agreement to with the field measurements from undisturbed chalk as well. There is no data available on the bulk density, water content and particle size distribution in the remolded annulus around the pile, therefore, it is not possible to check these parameters against field data. On the other hand, drying at a maximum temperature of 50°C ensures that the chemical structure of the chalk remains unchanged.

- Chemistry of the pore water may have an influence in the results obtained from the tests as shown in the results from Thixotropy tests. While tests with tap water do not show thixotropical increase of the undrained shear strength, tests on the specimens mixed with de-ionized water show an increase from 2.8 kPa to 4.5 kPa on the undrained shear strength normalized by the liquidity index. Nonetheless, specimens prepared with de-ionized water are not representative of the site conditions although the introduction of additional chemical component is prevented. Analysis of the groundwater chemistry might reveal a component in the tap water that inhibits thixotropy or whether the thixotropical increase of undrained shear strength is neglibile with *in-situ* chemistry.

- As it can be observed in the divergence of the results from Day 1 and the rest of the dates in the Triaxial test, there is disturbance of the specimen when these are depressurized and removed from the triaxial apparatus. This process leads to a decrease in initial stiffness of 52%, as measured with Bender Elements. Additionally, further handling of the specimens, for instance in the preparation of Direct Simple Shear tests, leads to increased disturbance. For this reason there is a larger decrease between the undrained shear strength in Day 1 (38 kPa -52 kPa) and aged Triaxials (3 kPa) compared to Day 1 and aged Direct Simple Shear, where peak strength values remain within the same range (4 kPa - 5 kPa).

- Finally, unconfined preservation in cardboard tubes leads to relaxation of the samples due to the behavior as a cohesionless granular material. This relaxation is evident in the initial shear stiffness as measured with Bender Elements (from 68 MPa on the unaged disturbed Triaxial specimen TXL1E to 28.9 MPa after 90 days of aging). Moreover, the undrained shear strength measured in Triaxial tests decreases from values between 38 kPa and 52 kPa and 3 kPa on aged specimens with the same confining stress.

7.2. Test results and aging

Given the results from the tests presented and analyzed in Chapter 5 and discussed in Chapter 6, the finding from these are related to the behavior of chalk putty in the different tests and its similarities with the common soil types as well as the evolution of the properties that could be studied in time.

First, the findings on the behavior of chalk putty are presented for each test type:

- The index tests show a material whose particle sizes range from fine sand to clay; the clay-sized portion of the material composing 30% of the mass. Atterberg Limits tests establish that the behavior of the clay to silt-sized fraction is that of a low plasticity silt (the Liquid Limit is at 31% and the Plasticity Index 9%), with inactive clay-sized grains.
- Thixotropy tests reveal an increase in the undrained shear strength in the specimens prepared with de-ionized water. The results measured after 30 days show an increase from 2.8 kPa to 4.5 kPa which means that the thixotropy strength ratio is 1.6, with not much increase expected after that time. In the samples saturated with tap water, this strengthening is undetectable.
- The Constant Rate of Strain tests showed that the behavior in compression of chalk putty is similar to a silt as not all the vertical stress - void ratio responses of the specimens converge in a unique normally consolidated line. Furthermore, the transition between reloading response and the virgin compression cannot be assigned to one unique point but a range of pressures. This means that the determination of the yield point using the methods commonly used in engineering practice for clays are not completely applicable in chalk since the estimated yield pressures are too large given that the stress history of the specimens is known.
- Consolidated Undrained Triaxial tests show that the behavior of the material is close to that of a dense sand, with a critical state effective friction angle equal to 38° and an initial contractive response followed by contraction or dilation, which are assumed based on the variation of the pore pressures, depending on the aging time. The volumetric behavior as well as the stress-strain response shows similarities to the behavior described by Lagioia and Nova (1995) in calcarenites, with an initial elastic response, followed by destructuration after yield an an ultimate hardening/softening response.
- In the Direct Simple Shear the behavior is highly comparable to triaxial tests, with similar stress-strain and volumetric response. The estimated ultimate effective friction angle is 43°, which is in agreement with the theory when compared to the friction angle measured in the triaxial tests.

Regarding the test results and the effect of aging in the properties of the specimens it can be concluded that the changes in the properties is limited compared with the results obtained in the field. Test by test, the evolution of the properties in time is here enumerated.

- Thixotropic gain of strength can be seen in the specimens mixed with de-ionized water although this gain is not comparable to the results from the field as on the field the shaft resistance is more than twice as large after 10 days. Nonetheless, the shape of the "set-up" curve is analogous to the observations made *in-situ*.
- In the Constant Rate of Strain compression tests, a slight increase in the yield point is observed. This increase in the yield point is detected with the traditional methods used in engineering as well as the alternative proposed in this project, selecting the beginning and end of yield. With the methods reported

in the literature, the yield point increases on average from 280 kPa to 300 kPa while the beginning of yield as proposed in this report evolves from 46 kPa on average on Day 1 to 87 kPa on Day 90. Furthermore, the end of yield evolves from 1705 kPa on Day 1 to 1836 kPa on Day 30, data from Day 90 is not available). It is also observed that the stiffness of the specimens during reloading decreases in time which is due to the relaxation of the specimens during aging in the wax. The transition between reloading and normally consolidated becomes less accused with increasing aging time.

- In Direct Simple Shear and Triaxial tests, the response of chalk putty over time is comparable. On one hand, there is no increase in the peak strength. On the other hand, the critical state behavior evolves from contractive with softening in the post-peak region in the unaged and Day 10 tests to dilative in further aged specimens. A hypothesis that may justify this phenomenon is cementation taking place around the grains or the presence of aragonite crystals as reported by Clayton (1978). Finally, the critical state friction angle remains constant over time.

Based upon the two different trends that were identified in the literature review and the obtained results it can be said that, in agreement with Bialowas et al. (2018), there is no evidence that inter-granular cementation takes place in the specimens studied in the laboratory. On the other hand, there are similarities in the ultimate response as presented by Doughty et al. (2018) with increasing dilation over time. However, the specimens studied in this project were preserved under no pressure while the results presented in the literature show consolidation of the specimens up to an arbitrary pressure. There is the possibility that these pressures are below those that the pile exerts into the chalk after driving. Investigation of the effects of these aging conditions is suggested.

In the literature review, it is presented a constitutive model of chalk developed by Ciantia (2018). This model presents the cementation of the material as an expansion of the yield locus. The bond between particles gives the material tensile strength while the yield point is also displaced to higher pressures. None of these effects seem to take place in the studied chalk putty as there is no sign of displacement of the yield locus in time in the p' - q plots (Figure 5.19). However, an slight increase in the yield point is detected although the phenomenon behind this feature is unclear.

7.3. Further research

During the development of this project there were decisions that have been taken based on the criteria based on the objectives. For example, it is not feasible in commercial terms to compact intact chalk from the field or preserve the specimens for aging in the triaxial cell. Additionally, hypotheses have been derived based on the results which must be validated. These and other suggestions for further research are here collected.

- Aging under K_0 condition using molds with applied load on the top. Specimen disturbance while setting up the tests may also be avoided by means of using a soluble glue and therefore it would be possible to install the specimen in the cell without removing the mould. This device may also allow the installation of local strain measurement gauges in the aged specimens. This was not possible in this project due to the slumping of the soft material while being installed.

- In the literature, the isotropic compression values when preserving the samples in the cell are arbitrarily assigned. In this case this variable was discarded. Nonetheless, numerical calculations or field measurements of the pressure exerted from the pile into the soil in order to determine the aging pressure are recommended.

- Determination to what extent the specimen preparation method influences the behavior of the tested specimens, this means preparing specimens using different methods in order to evaluate the degree of representativeness of each prepared specimen and the influence of each assumption in the results.
- As the results from the thixotropy tests are dependent on the chemistry of the pore water, analysis of the water chemistry from the site is suggested. Also, the use of water with this composition in the thixotropy tests is advised in order to determine the thixotropical properties of the chalk in conditions closer to those *in-situ*. Furthermore, study of the thixotropy with alternative tests that are not as susceptible to the inhomogeneities of the material and a shear method allowing direct calculation of the strength instead of using correlation such as the laboratory vane.
- Regarding the validation of the specimens in terms of representativeness, collection of samples belonging to the chalk putty which results from pile driving, in order to check the particle size distribution *in-situ*. A more feasible option is to drive plates in the same manner as Muir Wood et al. (2015) and study the resulting chalk putty.
- Measurement of the Particle Size Distribution after aging in order to check whether cementation around the grains is the cause of increased dilatancy over time.
- SEM imaging of the specimens in order to assess the changes in structure in the chalk putty samples over time.

Bibliography

F.J. Alvarez-Borges, B N. Madhusudhan, and D.J. Richards. Stiffness of Destructured Weak Carbonate Rock. In *Micro to MACRO Mathematical Modelling in Soil Mechanics*, pages 1–9. Birkhauser, 2019. doi: 10.1007/978-3-319-99474-1_1.

R. Anderton. *A dynamic stratigraphy of the British Isles: a study in crustal evolution.* Allen & Unwin, 1979.

R. Arulnathan, R.W. Boulanger, and M.F. Riemer. Analysis of bender element tests. *Geotechnical Testing Journal*, 21(2):120–131, 1998.

ASTM. Astm d5311-92. *Standard Test Method for Load Controlled Cyclic Triaxial Strength of Soil", Annual Book of ASTM Standards*, pages 1167–1176, 2004.

ASTM. *D4186-12 Standard Test Method for One-dimensional Consolidation Properties of Saturated Cohesive Soils Using Controlled-strain Loading.* ASTM International, 2012.

ASTM. *D6528 - 17 Standard Test Method for Consolidated Undrained Direct Simple Shear Testing of Fine Grain Soils.* ASTM International, 2017a.

ASTM. *D2487 - 17 Standard Practice for Classification of Soils for Engineering Purposes (Unified Soil Classification System).* ASTM International, 2017b.

P. Barbosa, M. Geduhn, R. Jardine, F. Schroeder, and M. Horn. Full scale offshore verification of axial pile design in chalk. In *Frontiers in Offshore Geotechnics III*. 2015. doi: 10.1201/b18442-64.

G.A. Bialowas, A. Diambra, and D.F.T. Nash. Stress and time-dependent properties of crushed chalk. *Proceedings of the Institution of Civil Engineers - Geotechnical Engineering*, 171(6):530–544, 2018. ISSN 1353-2618. doi: 10.1680/jgeen.17.00168.

L. Bjerrum and A. Landva. Direct simple-shear tests on a norwegian quick clay. *Geotechnique*, 16(1):1–20, 1966.

P.G.H. Boswell. The thixotropy of certain sedimentary rocks. *Science Progress (1933-)*, 36(143):412–422, 1948.

BSI. BS 1377: 1990 Methods of Test for Soils for Civil Engineering Purposes. *London: BSI*, 1990.

BSI. BS ISO 17892-3:2015 Geotechnical investigation and testing — Laboratory testing of soil — Part 3: Determination of particle density. *Geotechnical investigation and testing - Laboratory testing of soil*, 2015.

BSI. BS EN ISO 17892-9:2018 Consolidated triaxial compression tests on water saturated soils. *Geotechnical investigation and testing - Laboratory testing of soil*, 2018.

R.M. Buckley, R.J. Jardine, S. Kontoe, T. Liu, E. Ushev, B.M. Lehane, T. Pine, F.C. Schroeder, and P. Barbosa. Field Investigations into the Axial Loading Response of Displacement Piles in Chalk. In *Offshore Site Investigation Geotechnics 8th International Conference Proceedings*. 2017. doi: 10.3723/osig17.1178.

R.M. Buckley, R.J. Jardine, S. Kontoe, and B.M. Lehane. Effective stress regime around a jacked steel pile during installation ageing and load testing in chalk. *Canadian Geotechnical Journal*, 2018. ISSN 0008-3674. doi: 10.1139/cgj-2017-0145.

S. Bundy. *Geotechnical properties of chalk putties*. PhD thesis, University of Portsmouth Portsmouth, UK, 2013.

T.M. Carrington, G. Li, and M.J. Rattley. A new assessment of ultimate unit friction for driven piles in low to medium density chalk. In *Proc. 15th Eur. Conf. Soil Mech. & Geotech. Eng*, pages 825–830. Amsterdam, The Netherlands, 2011.

A. Casagrande. The determination of pre-consolidation load and it's practical significance. In *Proc. Int. Conf. Soil Mech. Found. Eng. Cambridge, Mass., 1936*, volume 3, page 60, 1936.

CEN. ISO/TS 17892-6:2004 Laboratory testing of soil - Part 6 : Fall cone test. 2004.

M.O. Ciantia. A constitutive model for the hydro-chemo-mehcanical behavior of chalk. In *Engineering in Chalk*, pages 275–281. ICE publishing, 2018.

F. Ciavaglia, J. Carey, and A. Diambra. Time-dependent uplift capacity of driven piles in low to medium density chalk. *Géotechnique Letters*, 2017. doi: 10.1680/jgele.16.00162.

C.R.I. Clayton. Some properties of remoulded chalk. In *Proceedings of the 9th International Conference on Soil Mechanics and Foundation Engineering*, pages 65–68. 1977.

C.R.I. Clayton. *Chalk as fill*. PhD thesis, Surrey University, 1978.

C.R.I. Clayton and M.C. Matthews. Deformation, diagenesis and the mechanical behaviour of chalk. *Geological Society, London, Special Publications*, 29(1):55–62, 1987.

L.J. Doughty. Laboratory Testing of Chalk. Technical report, Imperial College London, 2016.

L.J. Doughty, R.M. Buckley, and R.J. Jardine. Investigating the effect of ageing on the behaviour of chalk putty. *ICE Publishing*, (September), 2018. doi: 10.1680/eiccf.64072.695.

J.A. et al. Lord. *PRJ PR 11 "Foundations in Chalk"*. CIRIA, London, 1994.

I.L Fabricius. Chalk: composition, diagenesis and physical properties. *Bulletin of the Geological Society of Denmark*, 55:97–128, 2007.

Fugro. Laboratory Testing Report, Pile Test Site, Chalk Specific Testing, St-Nicholas-at-Wade, Kent, UK. Fugro Report No. D34001-2. Technical report, Fugro Geoconsulting Limited, Wallingford, 2012.

K. Gavin, R. Jardine, K. Karlsrud, and B. Lehane. The effects of pile ageing on the shaft capacity of offshore piles in sand. In *Frontiers in Offshore Geotechnics III*. 2015. doi: 10.1201/b18442-8.

B.O. Hardin. Crushing of soil particles. *Journal of geotechnical engineering*, 111(10):1177–1192, 1985.

K.H. Head. *Manual of Soil Laboratory Testing*. Pentech Press London, 1980. ISBN 0-7273-1302-9.

L.K. Hermansen, H.and Thomas, J.E. Sylte, and B.T. Aasboe. Twenty five years of Ekofisk reservoir management. In *SPE Annual Technical Conference and Exhibition*, 1997.

R. Jardine, R. Buckley, S. Kontoe, P. Barbosa, and F. C. Schroeder. Keynote lecture: Behaviour of piles driven in chalk. 2018.

J.P. Johnson, D.W. Rhett, and W.T. Siemers. Rock mechanics of the Ekofisk reservoir in the evaluation of subsidence. In *Offshore Techonology Conference*, 1988.

B.T. Jose, A. Sridharan, and B.M. Abraham. Log-log method for determination of preconsolidation pressure. *Geotechnical Testing Journal*, 12(3):230–237, 1989.

R.S. Ladd. Preparing test specimens using undercompaction. *Geotechnical Testing Journal*, 1(1):16–23, 1978.

R. Lagioia and R. Nova. An experimental and theoretical study of the behaviour of a calcarenite in triaxial compression. *Géotechnique*, 45(4):633–648, 1995.

L.Z. Lakshtanov, D.V. Okhrimenko, O.N. Karaseva, and S.L.S. Stipp. Limits on calcite and chalk recrystallization. *Crystal Growth & Design*, 18(8):4536–4543, 2018.

M.J. Leddra and M.E. Jones. Steady-state flow during undrained loading of chalk. In *Chalk*, pages 145–252. Thomas Telford Publishing, London, 1990.

J.A. Lord, C.R.I. Clayton, and R.N. Mortimore. *Engineering in chalk*. CIRIA, 2002.

H.B. Madsen and L. Stemmerik. Diagenesis of flint and porcellanite in the maastrichtian chalk at stevns klint, denmark. *Journal of Sedimentary Research*, 80(6):578–588, 2010.

McGraw-Hill and S.P. Parker. *McGraw-Hill Dictionary of scientific and technical terms*. McGraw-Hill New York, 2003.

J.K. Mitchell. Fundamental aspects of thixotropy in soils. *Transactions of the American Society of Civil Engineers*, 126(1):1586–1620, 1961.

A Muir Wood, B Mackenzie, D Burbury, M Rattley, C Clayton, M Mygind, K. Andersen, C. Thilsted, and M. Liingaard. Design of large diameter monopiles in chalk at Westermost Rough offshore wind farm. In *Frontiers in Offshore Geotechnics III*. 2015. doi: 10.1201/b18442-99.

J. Neugebauer. Some aspects of cementation in chalk. *Pelagic Sediments: on Land and under the Sea*, 1: 149–176, 1974.

A. Nocilla, M.R. Coop, and F. Colleselli. The mechanics of an italian silt: an example of 'transitional'behaviour. *Géotechnique*, 56(4):261–271, 2006.

Y. Okada, K. Sassa, and H. Fukuoka. Comparison of shear behaviour of sandy soils by ring-shear test with conventional shear tests. In *Environmental Forest Science*, pages 623–632. Springer, 1998.

F Pacheco Silva. *Uma nova construção gráfica para determinação da pressão de pré-adensamento de uma amostra de solo*. IPT, 1973.

J. Puig. Problemes de terrassement dans la craie. *BULL. LIAIS. LAB. PONTS CHAUSS.*, (63), 1973.

R.N. Razoaki. *Effect of ageing on mechanics of chalk slurries*. PhD thesis, University of Portsmouth, 2000.

A.W. Skempton and R.D. Northey. The sensitivity of clays. *Geotechnique*, 3(1):30–53, 1952.

C. Sorgi and V. De Gennaro. Water-rock interaction mechanisms and ageing processes in chalk. In *Advances in Data, Methods, Models and Their Applications in Geoscience*. IntechOpen, 2011.

Standard Norge. NS 8015 Determination of undrained shear strength by fall-cone testing. *Geotechnical Testing. Laboratory Methods*, 1988.

Thames Water Utilities Limited. Water Quality Report. Technical report, Reading, UK, 2019. URL `http://twmediadevcdn.azureedge.net/waterquality/WQReport{_}ZO241{_}Wallingford.pdf`.

Y.P. Vaid and D. Negussey. Preparation of Reconstituted Sand Specimens. In *Advanced Triaxial Testing of Soil and Rock*. 1988. doi: 10.1520/stp29090s.

G. Viggiani and J.H. Atkinson. Interpretation of bender element tests. In *International Journal of Rock Mechanics and Mining Sciences and Geomechanics Abstracts*, volume 8, page 373A, 1995.

T. Waltham. *Foundations of engineering geology*. CRC Press, 2002.

L.B. Wang and J.D. Frost. Dissipated strain energy method for determining preconsolidation pressure. *Canadian geotechnical journal*, 41(4):760–768, 2004.

C.P. Wroth. The interpretation of in situ soil tests. *Geotechnique*, 34(4):449–489, 1984.

S. Yang and K.H. Andersen. Thixotropy of marine clays. *Geotechnical Testing Journal*, 39(2):331–339, 2015.

A

Results from trial phase

A.1. Specimen preparation trials

Table A.1: Summary of specimen preparation trials.

Trial	*Preparation Water Content [%]*	*Achieved Water Content [%]*	*Target Dry Density [Mg/m^3]*	*Achieved Dry Density [Mg/m^3]*	*Compaction Method*	*Saturation Method*	*Notes*
1	30.0	-	1.50	1.66	Ladd Undercompaction	-	Slumped, could not hold it own weight
2	27.5	27.2	1.66	-	Ladd Undercompaction	-	Slumped, could not hold it own weight
3	26.0	26.3 (Top) 26.6 (Middle) 26.7 (Base)	1.66	1.58	Ladd Undercompaction	Constant water content	Slumping during triaxial setup. WC and split photo taken after saturation
4	20.0	20.4 (Top) 21.1 (Middle) 21.1 (Base)	1.58		Ladd Undercompaction	Back pressure	Sample took 12 cm3 during back pressure saturation. WC and split photo taken after saturation
5	22.0	22.4 (Top) 23.7 (Middle) 23.0 (Bottom)	1.58		Ladd Undercompaction	Constant water content	Number of slumps created voids within the sample. WC and split photo taken after saturation
6	26.0	-	1.58			-	Sample takes all the water after adding 50% of the dry material, settling of the particles 48h after preparation
7	10.0	25.5 (Top) 25.2 (Middle) 26.4 (Bottom)	1.58	1.52	Ladd Undercompaction	Back pressure	Back pressure increments of 50 kPa until acceptable B value. WC and split photo taken after saturation. Sample appears uneven the top and the bottom are softer than the middle and the distinct layers can be distinguised.
8	0.0	25.2 (Top) 25.2 (Middle) 25.8 (Bottom)	1.58	1.58	Ladd Undercompaction	Back pressure	Even appearance. Saturation achieved within 3 days of cell and back pressure increases. WC and split photo taken after saturation.
9	Hygroscopic	26.8 (Top) 25.7 (Middle) 26.3 (Bottom)	1.58	1.56	Ladd Undercompaction	Back pressure	Even appearance. Saturation achieved within 3 days of cell and back pressure increases. WC and split photo taken after saturation.
10	Hygroscopic	26.4 (Top) 25.7 (Middle) 26.3 (Bottom)	1.58	1.58	Ladd Undercompaction	Back pressure	Even appearance. Saturation achieved within 3 days of cell and back pressure increases. WC and split photo taken after saturation
11	Hygroscopic		1.58	1.58	Ladd undercompaction	Back pressure	

A.2. Particle size distribution

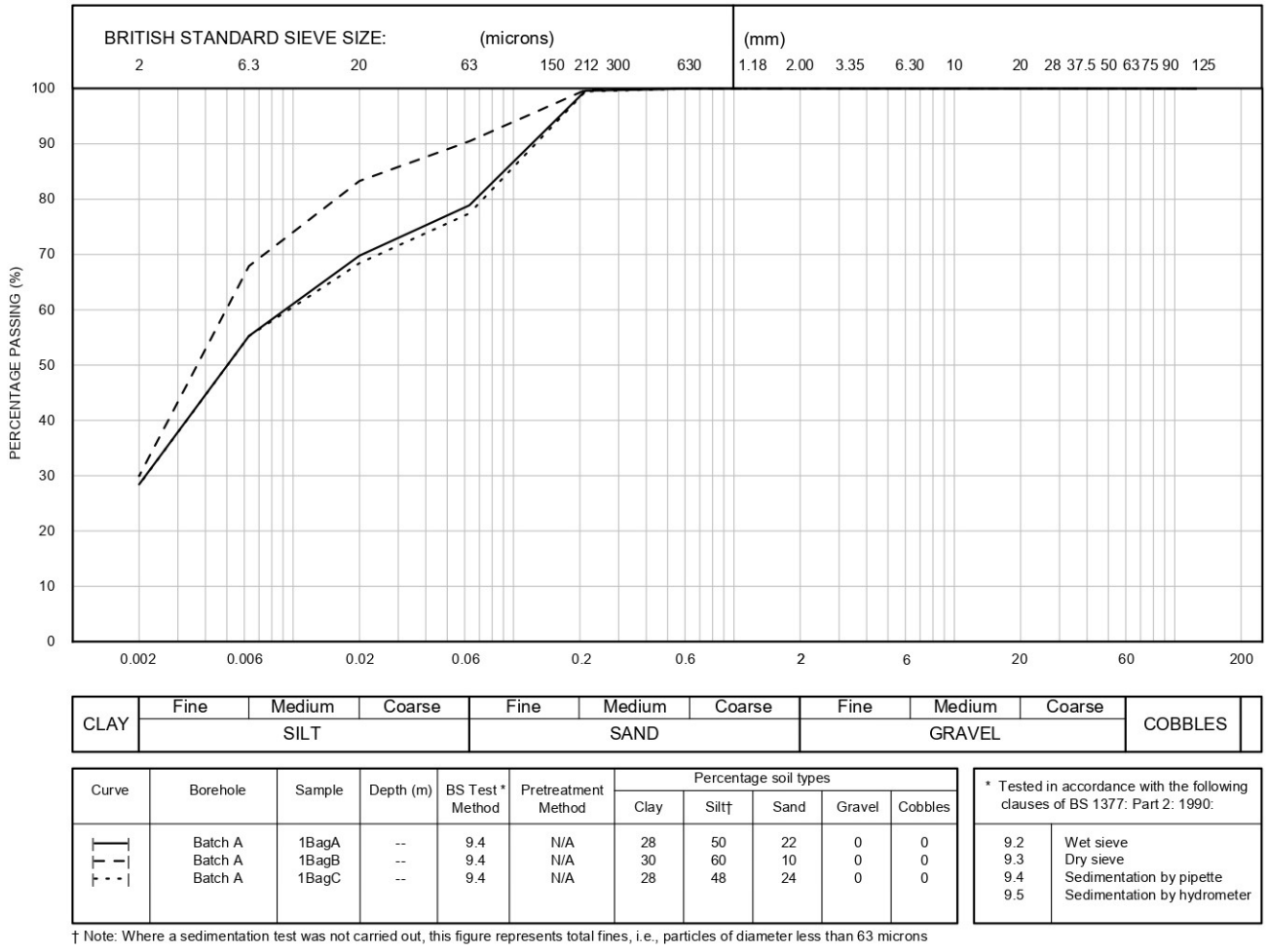

Curve	Borehole	Sample	Depth (m)	BS Test * Method	Pretreatment Method	Percentage soil types				
						Clay	Silt†	Sand	Gravel	Cobbles
├──┤	Batch A	1BagA	--	9.4	N/A	28	50	22	0	0
├ ─ ┤	Batch A	1BagB	--	9.4	N/A	30	60	10	0	0
├ - - ┤	Batch A	1BagC	--	9.4	N/A	28	48	24	0	0

* Tested in accordance with the following clauses of BS 1377: Part 2: 1990:

9.2	Wet sieve
9.3	Dry sieve
9.4	Sedimentation by pipette
9.5	Sedimentation by hydrometer

† Note: Where a sedimentation test was not carried out, this figure represents total fines, i.e., particles of diameter less than 63 microns

Figure A.1: Particle size distribution tests from the three subsamples taken from the trial batch

A.3. Sample pictures from trials

Figure A.2: Intact photo of trial 3

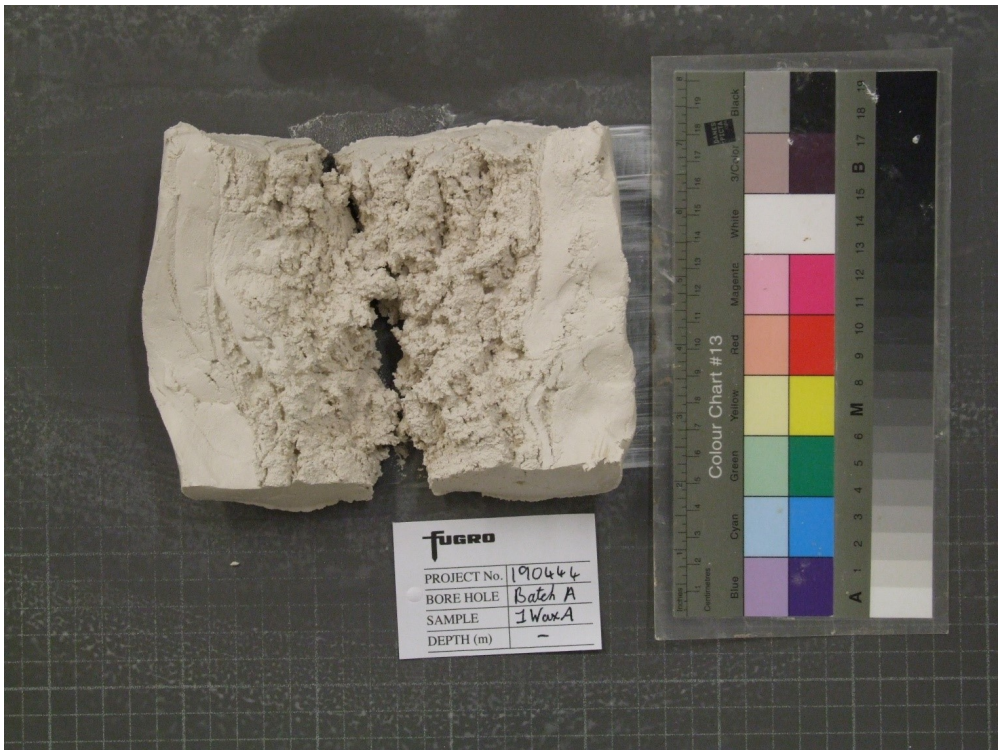

Figure A.3: Split photo of trial 3

Figure A.4: Intact photo of trial 4

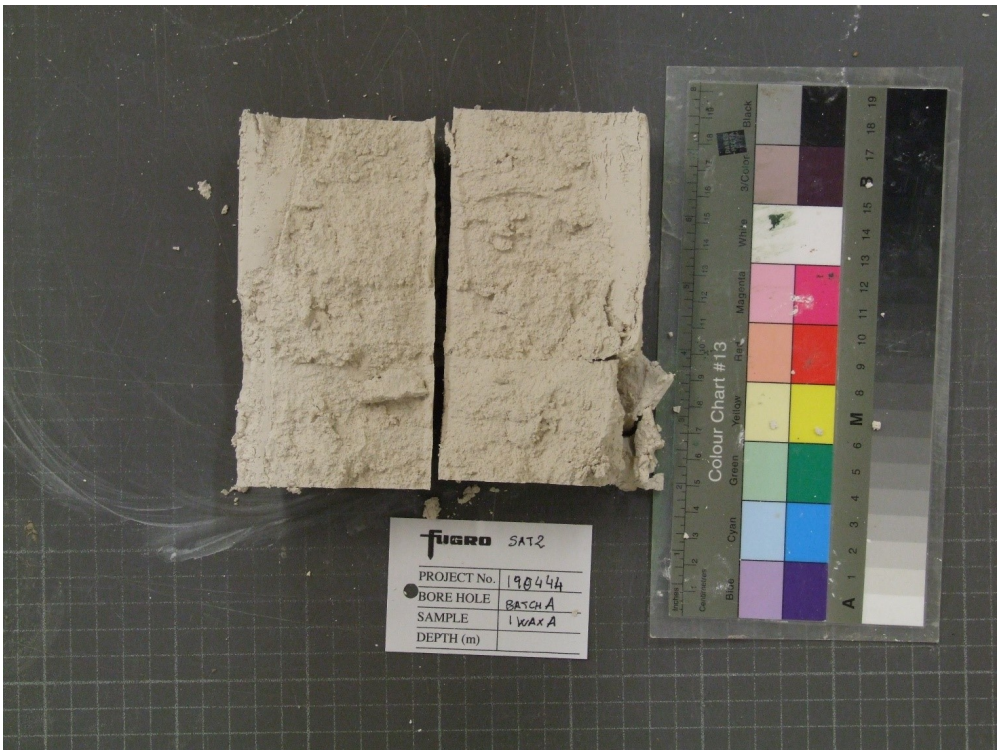

Figure A.5: Split photo of trial 4

Figure A.6: Intact photo of trial 5

Figure A.7: Split photo of trial 5

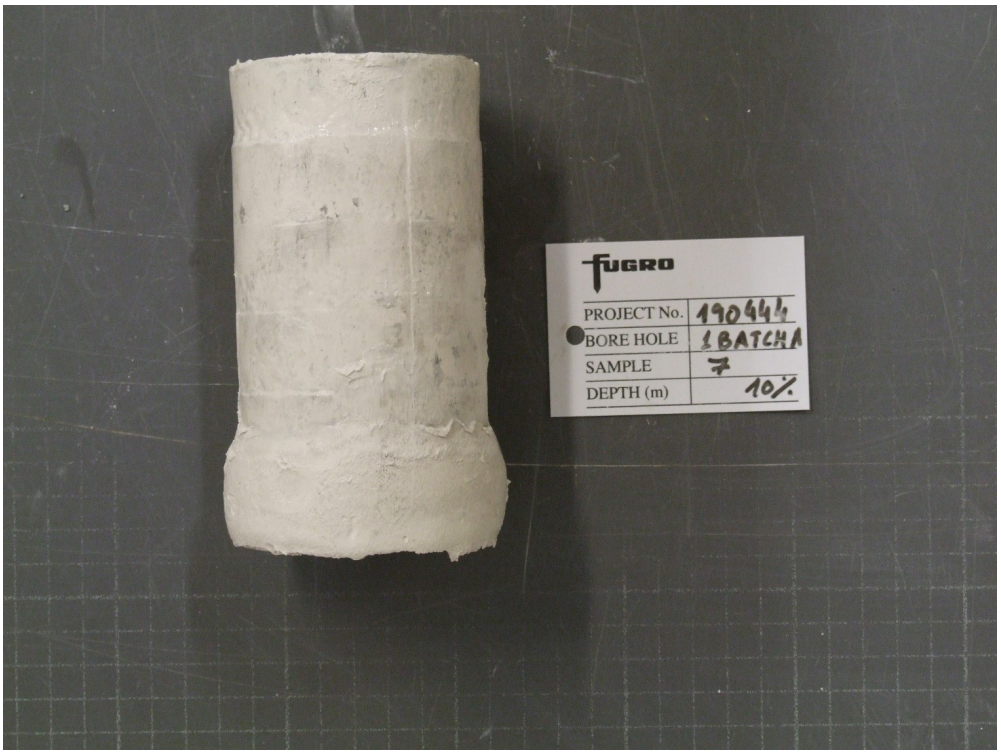

Figure A.8: Intact photo of trial 7

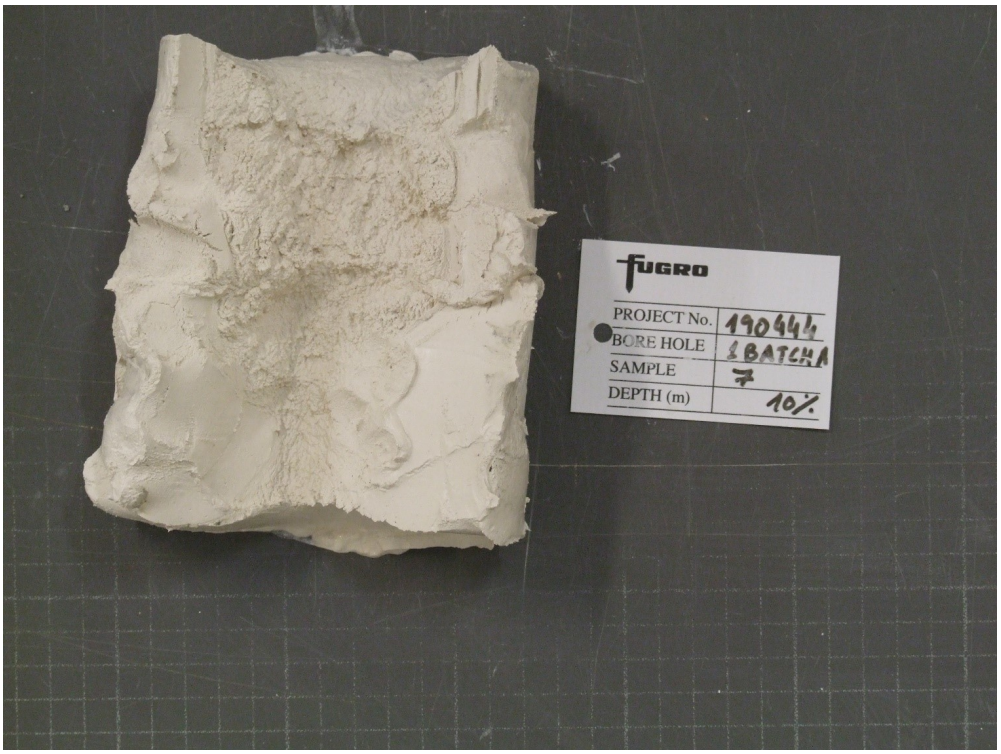

Figure A.9: Split photo of trial 7

Figure A.10: Intact photo of trial 8

Figure A.11: Split photo of trial 8

Figure A.12: Split photo of trial 9. Intact photo is missing.

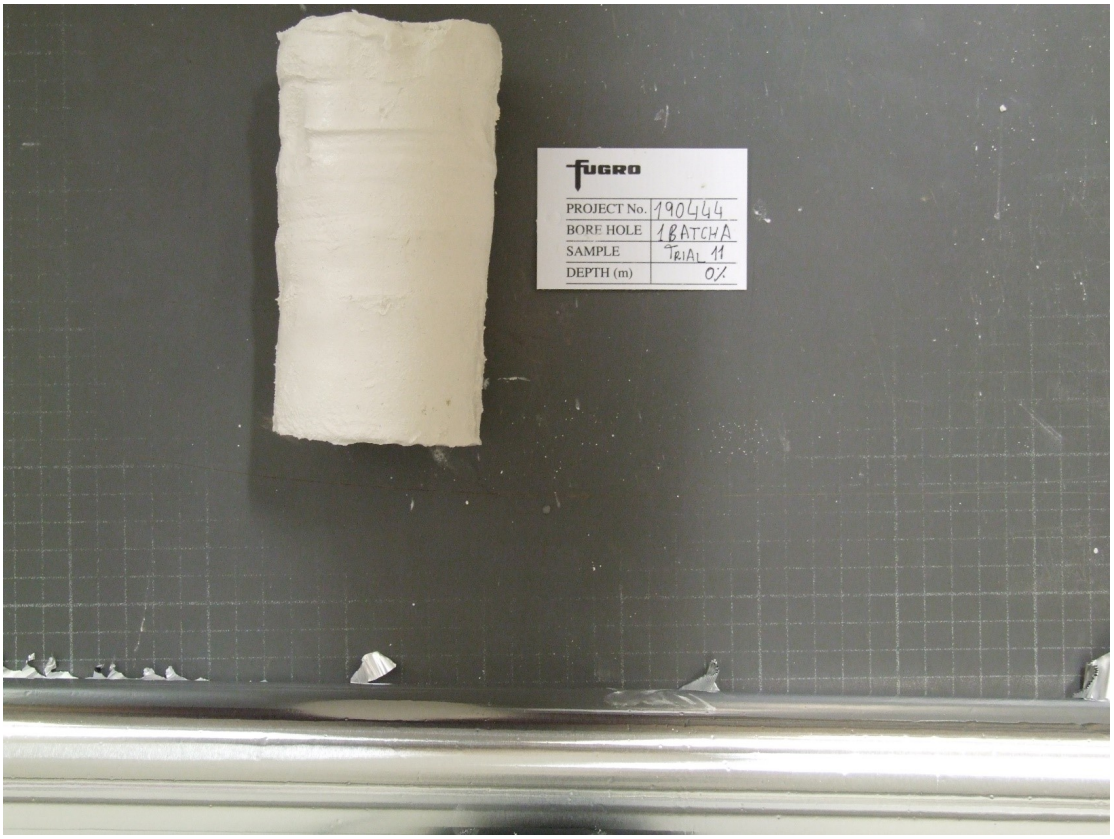

Figure A.13: Intact photo of trial 10

Figure A.14: Split photo of trial 10

Figure A.15: Intact photo of trial 11

Figure A.16: Split photo of trial 11

B

Results from main scope

B.1. Index tests

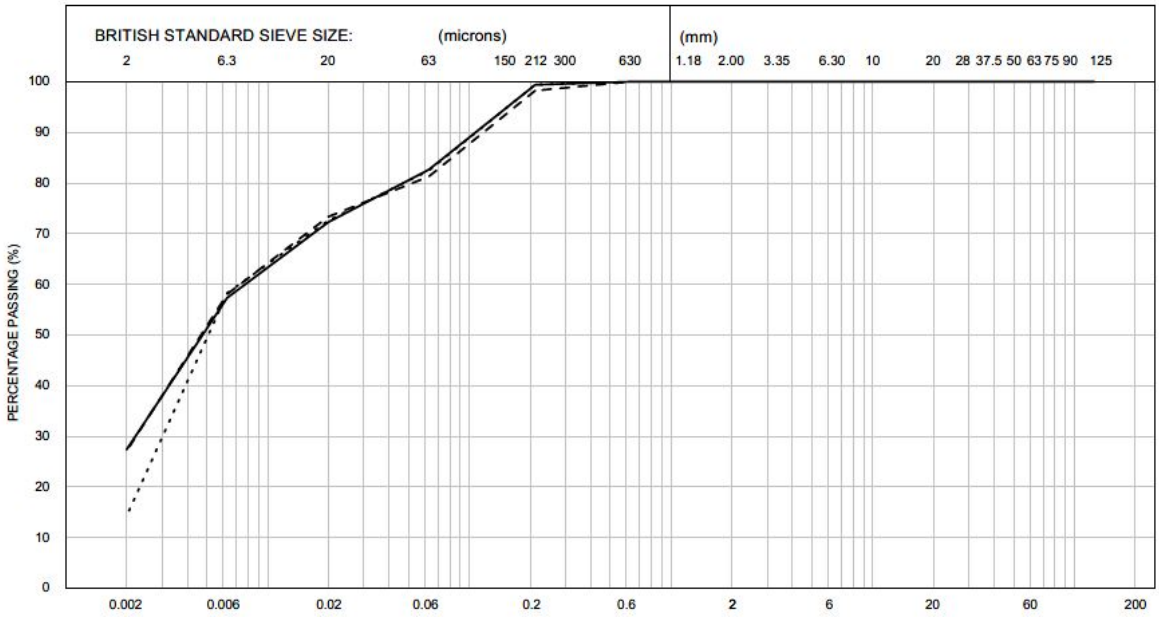

Curve	Borehole	Sample	Depth (m)	BS Test * Method	Pretreatment Method	Percentage soil types				
						Clay	Silt†	Sand	Gravel	Cobbles
├──┤	Batch B	1BagA	--	9.4	N/A	27	55	18	0	0
├ ─ ┤	Batch B	1BagB	--	9.4	N/A	27	54	19	0	0
├ - - ┤	Batch B	1BagC	--	9.4	N/A	14	68	18	0	0

† Note: Where a sedimentation test was not carried out, this figure represents total fines, i.e., particles of diameter less than 63 microns

* Tested in accordance with the following clauses of BS 1377: Part 2: 1990:

9.2	Wet sieve
9.3	Dry sieve
9.4	Sedimentation by pipette
9.5	Sedimentation by hydrometer

Figure B.1: Particle size distribution tests for the three subsamples taken from the main batch (Batch B).

Table B.1: Atterberg Limits of the subsamples taken from the main batch

Sample	*Liquid limit [%]*	*Plasticity index [%]*
1BagA	33	10
1BagB	31	8
1BagC	30	8

B.2. Thixotropy

Table B.2: Measured penetration on Thixotropy Batch A specimens.

	Test 1		***Test 2***		***Test 3***	
Time (hours)	Cone (g)	Average penetration (mm)	Cone (g)	Average penetration (mm)	Cone (g)	Average penetration (mm)
0	100	10.8	100	9.7	100	9.3
1	100	10.2	100	10.0	100	9.2
2	100	9.7	100	10.5	100	13.3
4	60	6.3	60	6.3	60	6.3
8	100	11.0	100	9.5	100	10.7
24	100	10.0	100	9.3	100	9.5
48	100	10.7	100	12.3	60	8.8
96	100	9.0	100	10.3	100	10.3
192	100	12.2	60	6.3	60	6.5
360	100	10.3	100	10.3	100	9.3
720	100	10.3	100	9.2	100	9.3

Table B.3: Measured penetration on Thixotropy Batch B specimens.

	Test 1		***Test 2***		***Test 3***	
Time (hours)	Cone (g)	Average penetration (mm)	Cone (g)	Average penetration (mm)	Cone (g)	Average penetration (mm)
0	100	9.8	100	12.7	100	10.2
1	100	12.5	100	13.0	100	10.5
2	100	9.7	100	12.3	100	9.8
4	100	10.0	100	12.3	100	11.2
8	100	10.5	100	9.7	100	10.0
24	100	9.7	100	9.3	100	10.0
48	100	8.7	100	9.0	100	8.3
96	100	8.3	100	8.7	100	8.7
192	100	7.8	100	8.8	100	8.8
360	100	9.7	100	10.3	100	9.8
720	100	8.2	100	8.2	100	8.8

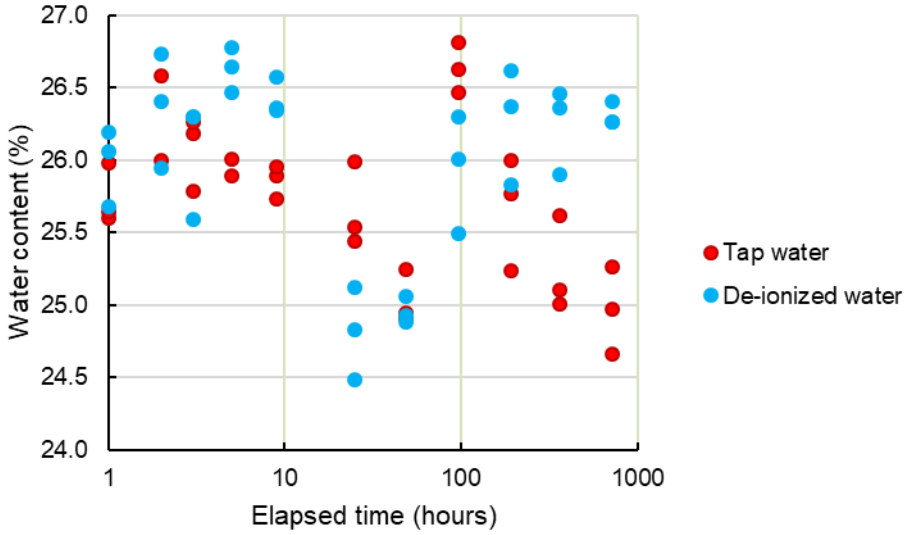

Figure B.2: Measured water content of Thixotropy Batch A and Batch B specimens.

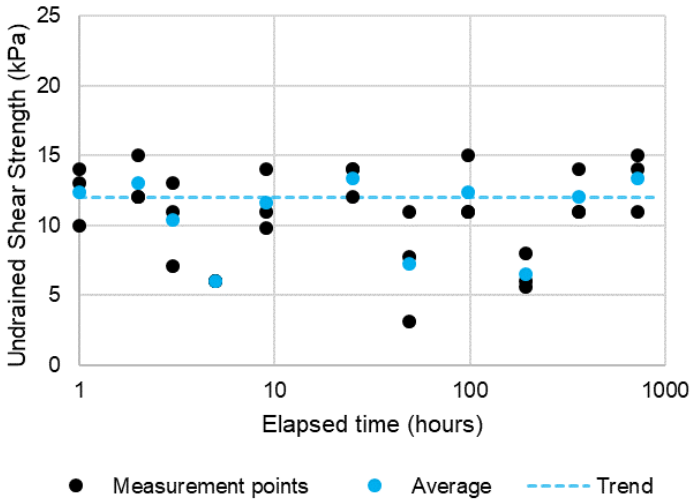

Figure B.3: Calculated Undrained shear strength according to NS 8015 on Batch A specimens.

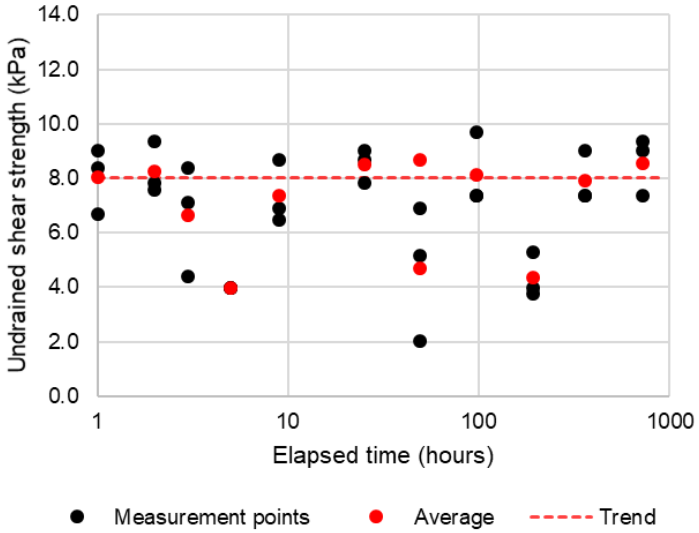

Figure B.4: Calculated Undrained shear strength according to ISO/TS 17892-6:2004 on Batch A specimens.

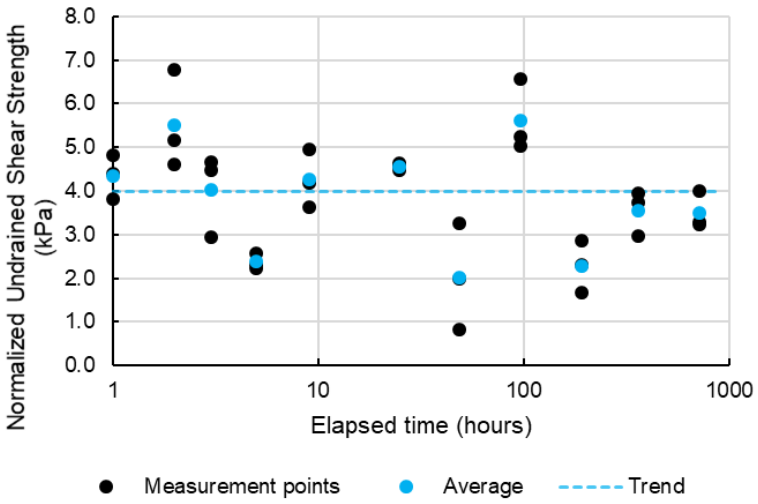

Figure B.5: Calculated Undrained shear strength according to NS 8015 on Batch A specimens normalized by the liquiity index.

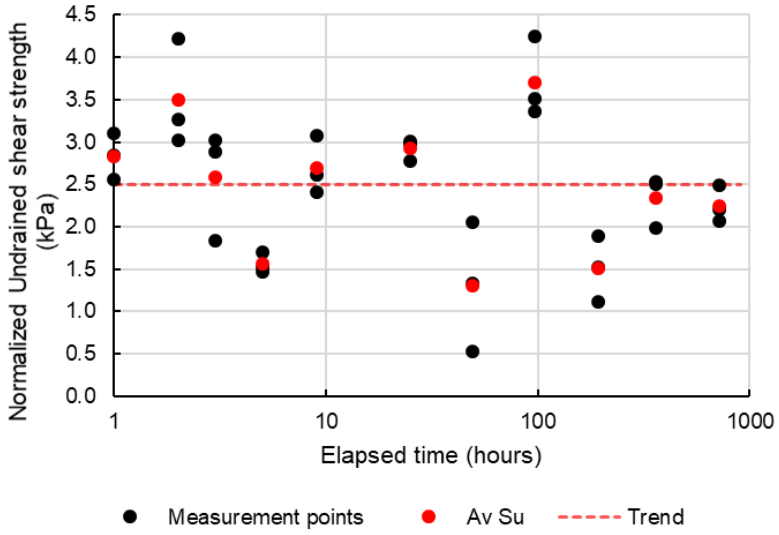

Figure B.6: Calculated Undrained shear strength according to ISO/TS 17892-6:2004 on Batch A specimens normalized by the liquidity index.

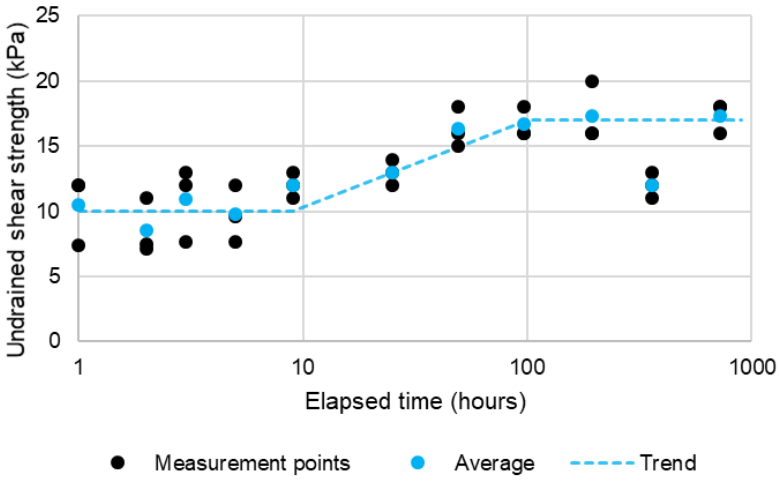

Figure B.7: Calculated Undrained shear strength according to NS 8015 on Batch B specimens.

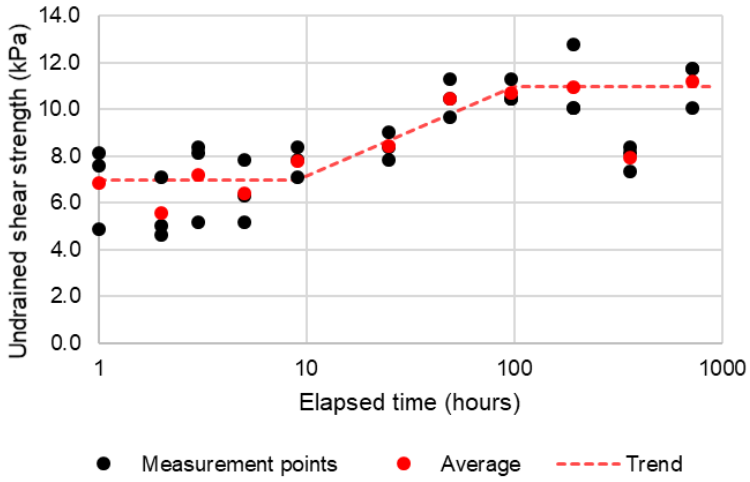

Figure B.8: Calculated Undrained shear strength according to ISO/TS 17892-6:2004 on Batch B specimens.

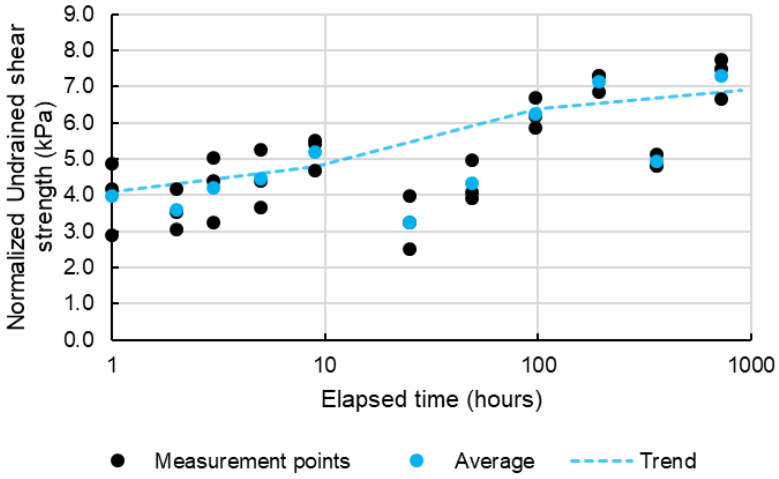

Figure B.9: Calculated Undrained shear strength according to NS 8015 on Batch B specimens normalized by the liquiity index.

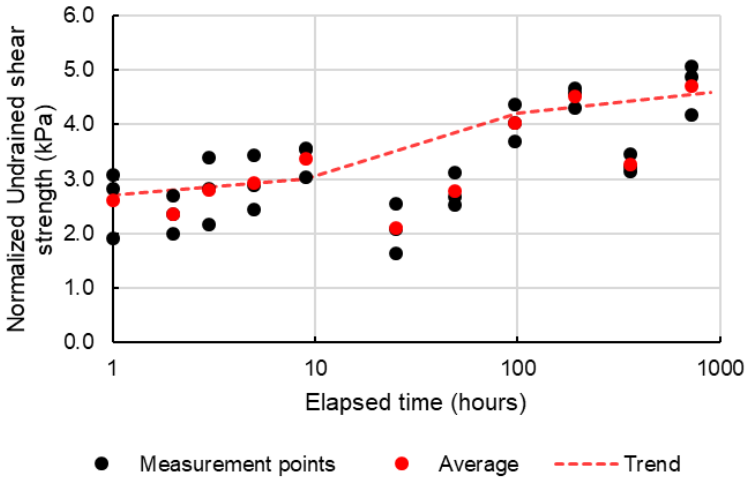

Figure B.10: Calculated Undrained shear strength according to ISO/TS 17892-6:2004 on Batch B specimens normalized by the liquidity index.

B.3. Constant Rate of Strain

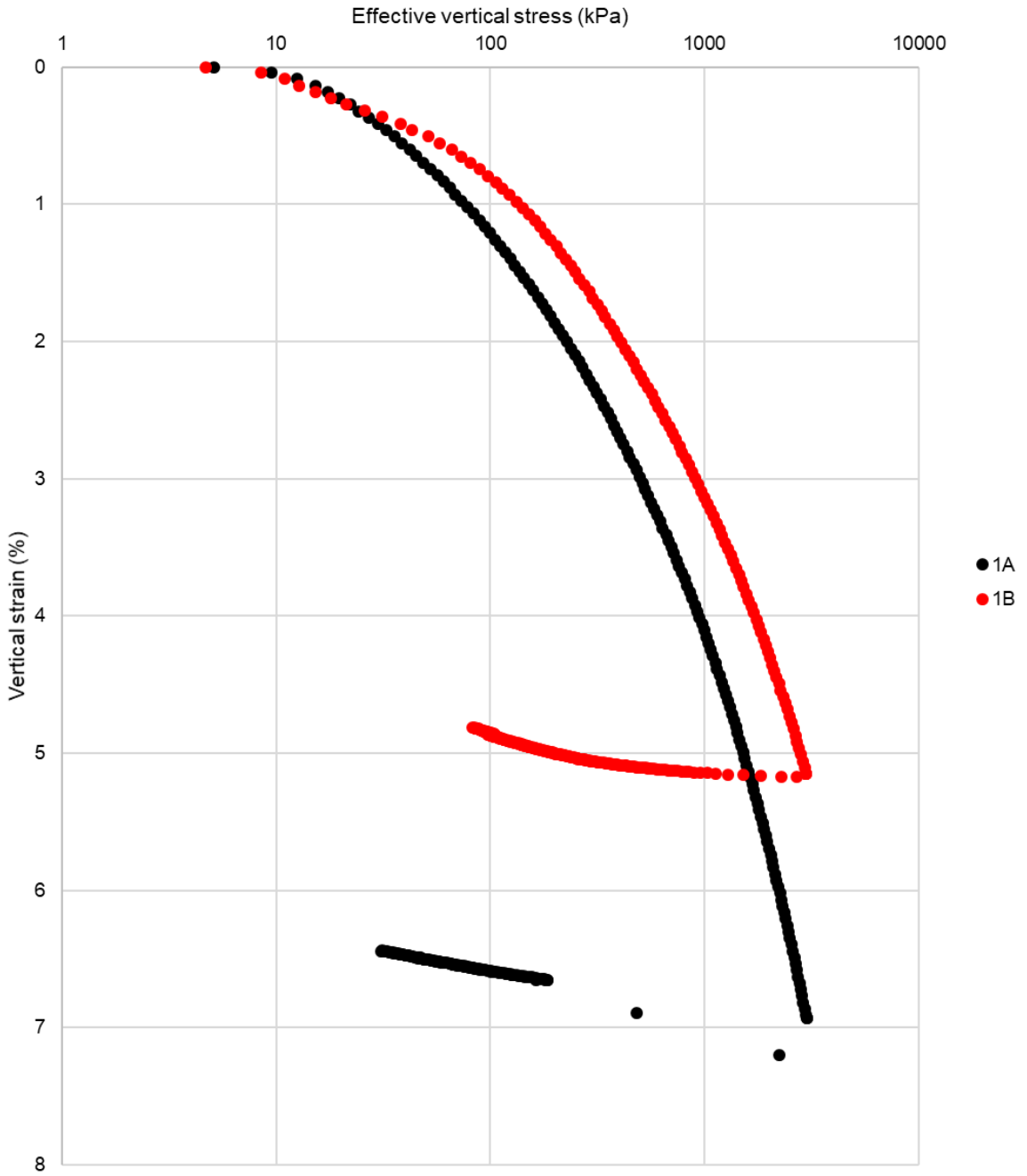

Figure B.11: Measured stress-strain data from specimens on day 1.

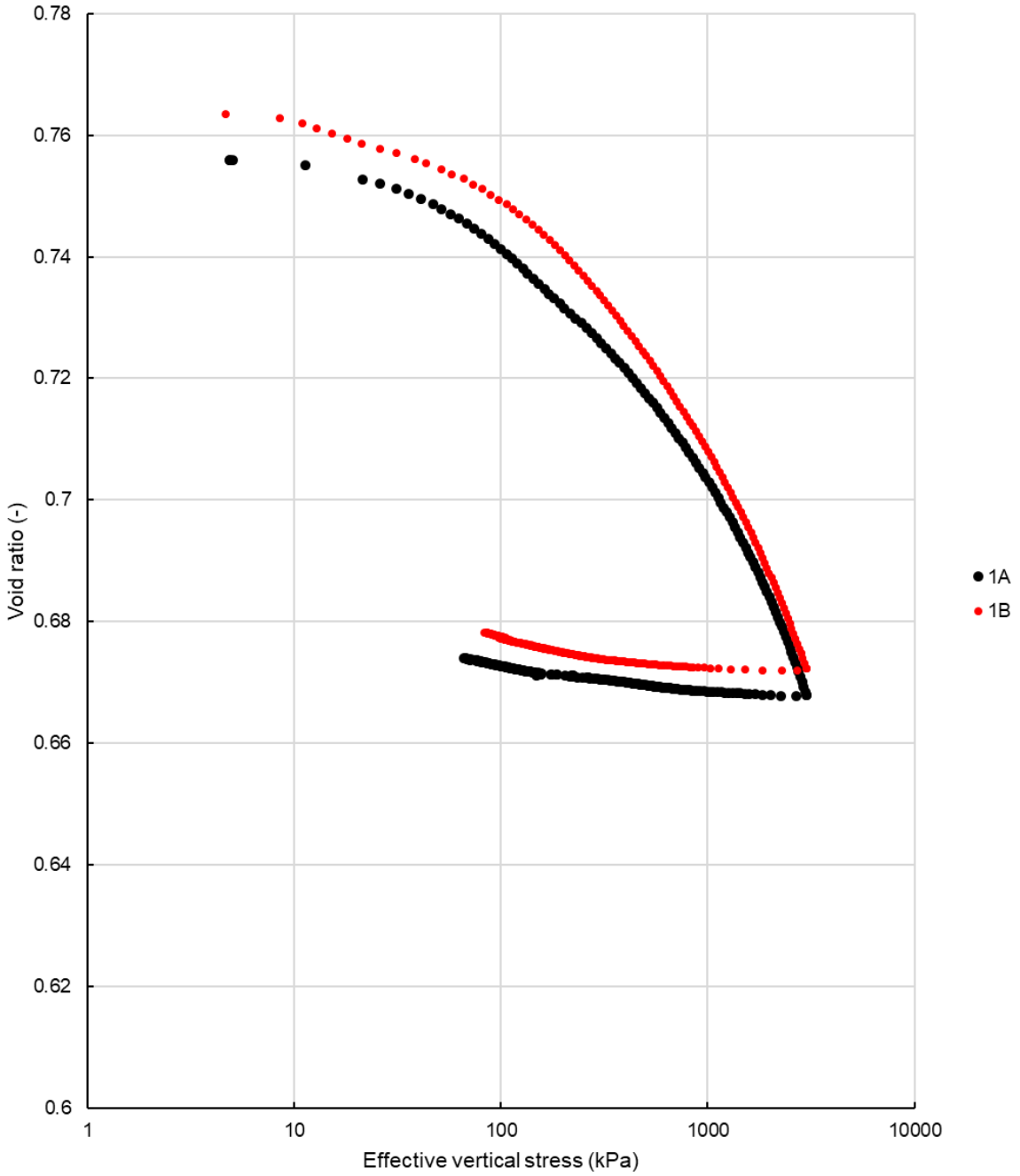

Figure B.12: Calculated stress-void ratio data from specimens on day 1.

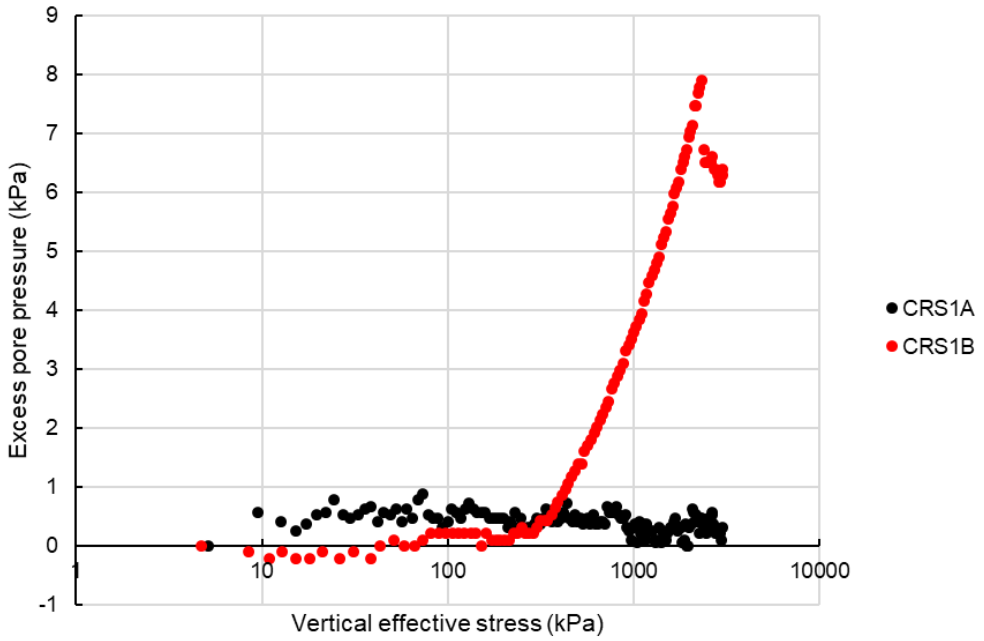

Figure B.13: Measured stress-pore pressure data from specimens on day 1.

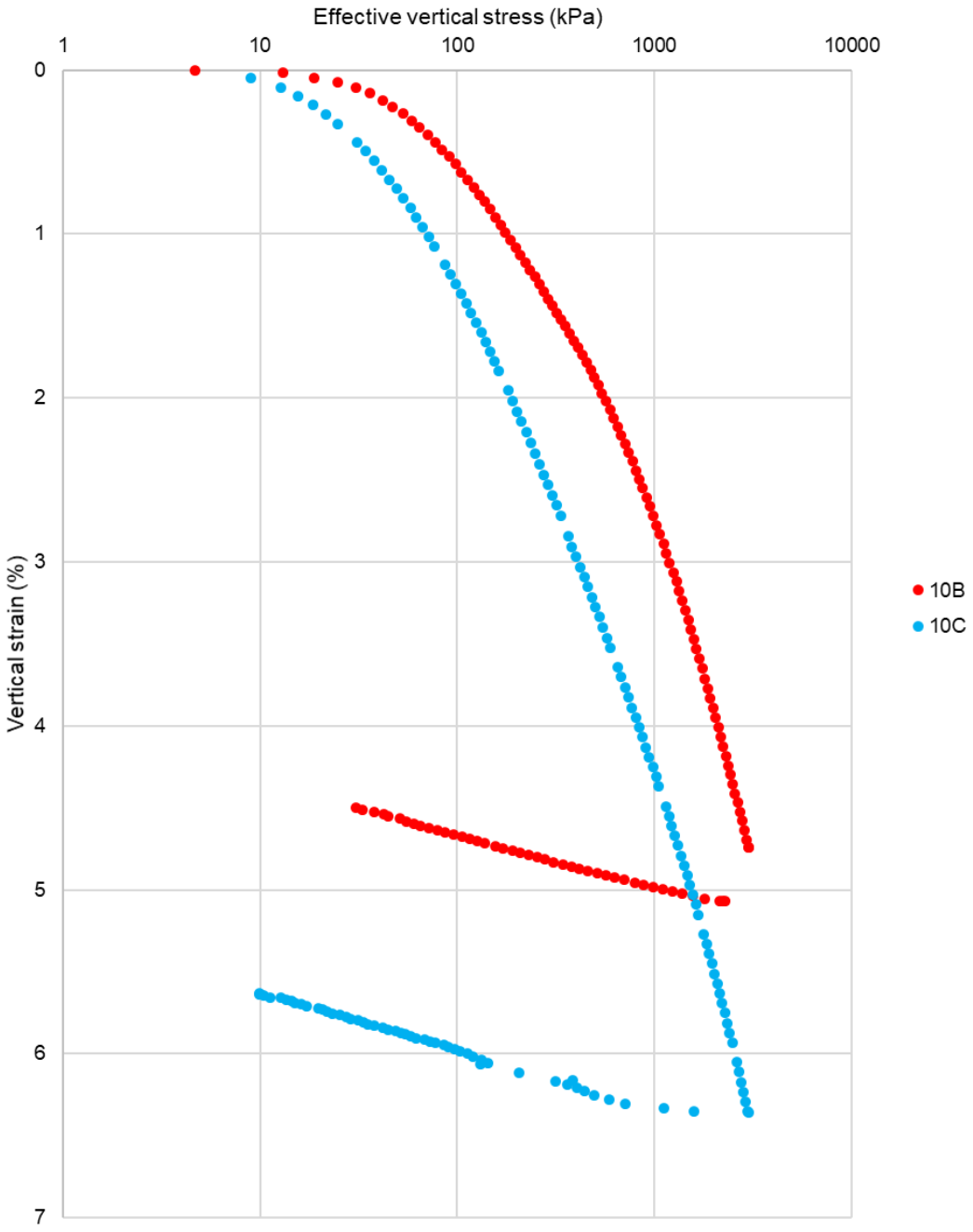

Figure B.14: Measured stress-strain data from specimens on day 10.

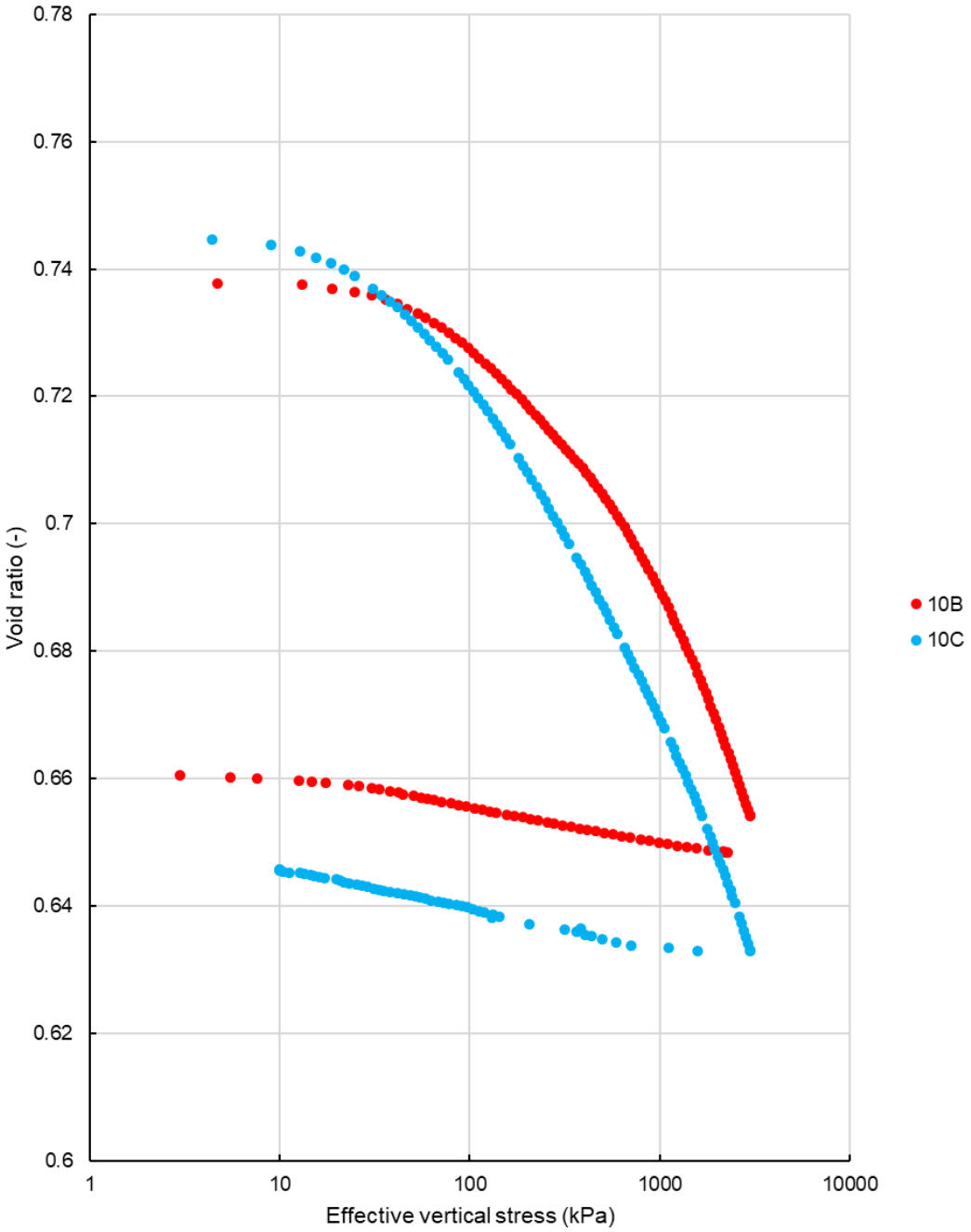

Figure B.15: Calculated stress-void ratio data from specimens on day 10.

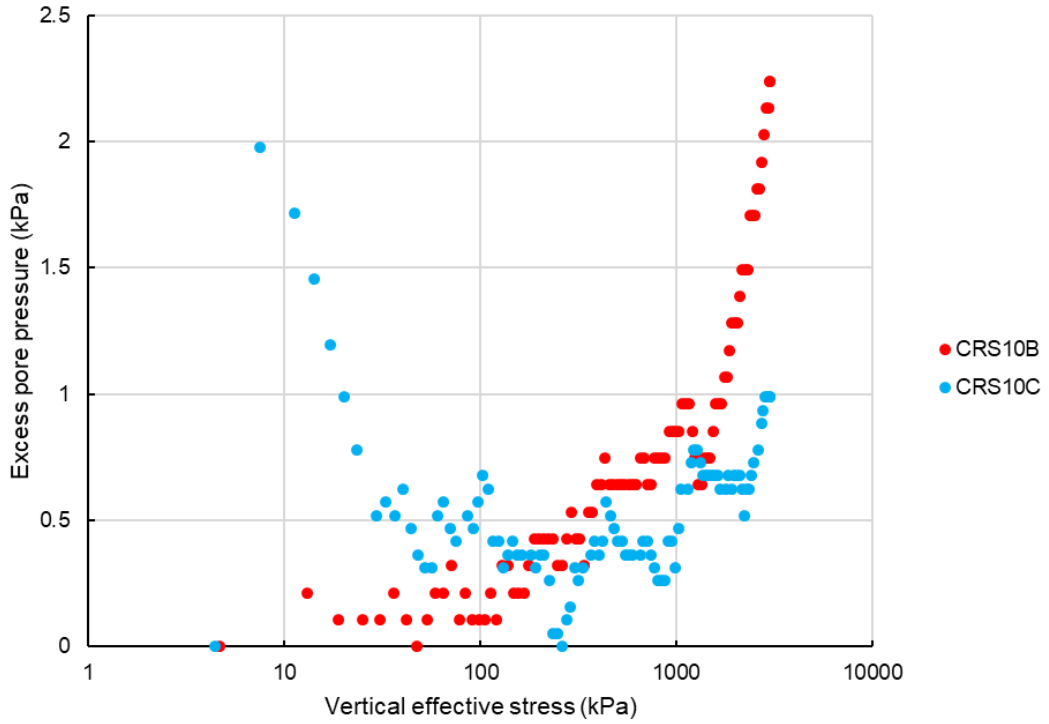

Figure B.16: Measured stress-pore pressure data from specimens on day 10.

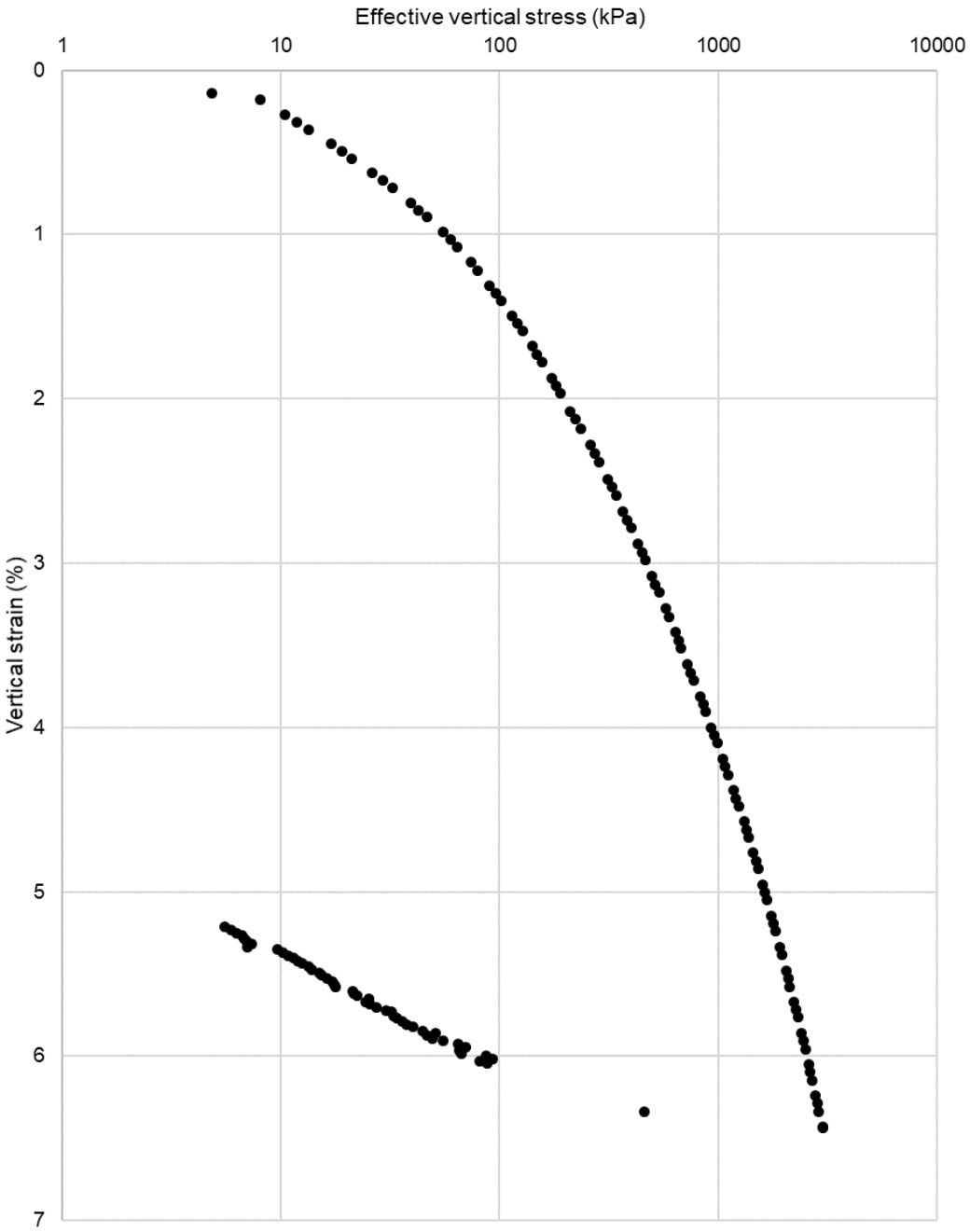

Figure B.17: Measured stress-strain data from specimens on day 30.

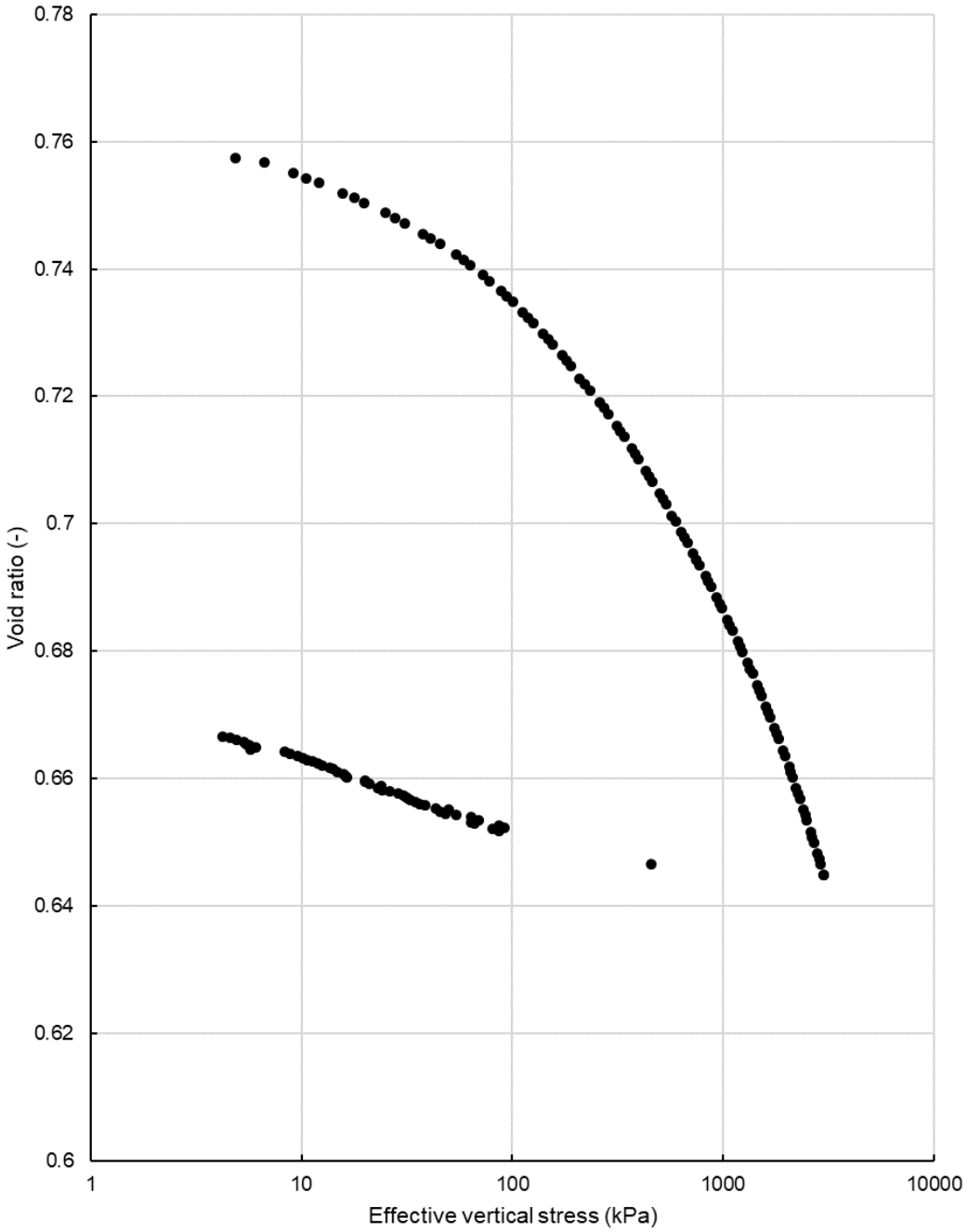

Figure B.18: Calculated stress-void ratio data from specimens on day 30.

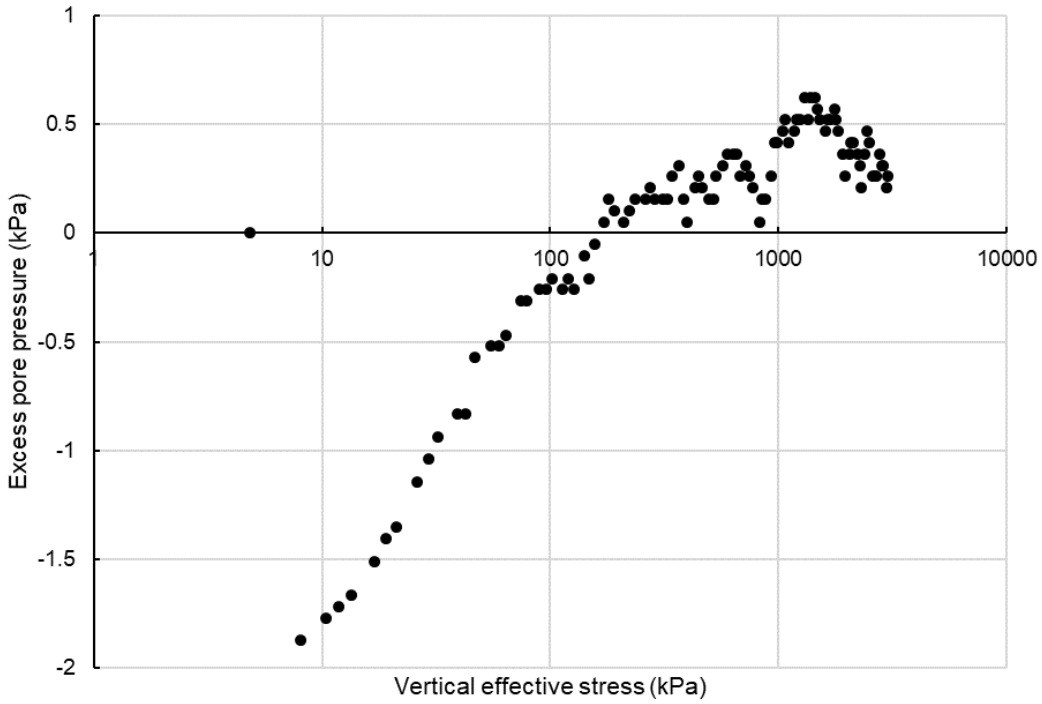

Figure B.19: Measured stress-pore pressure data from specimens on day 30.

B.4. Direct Simple Shear

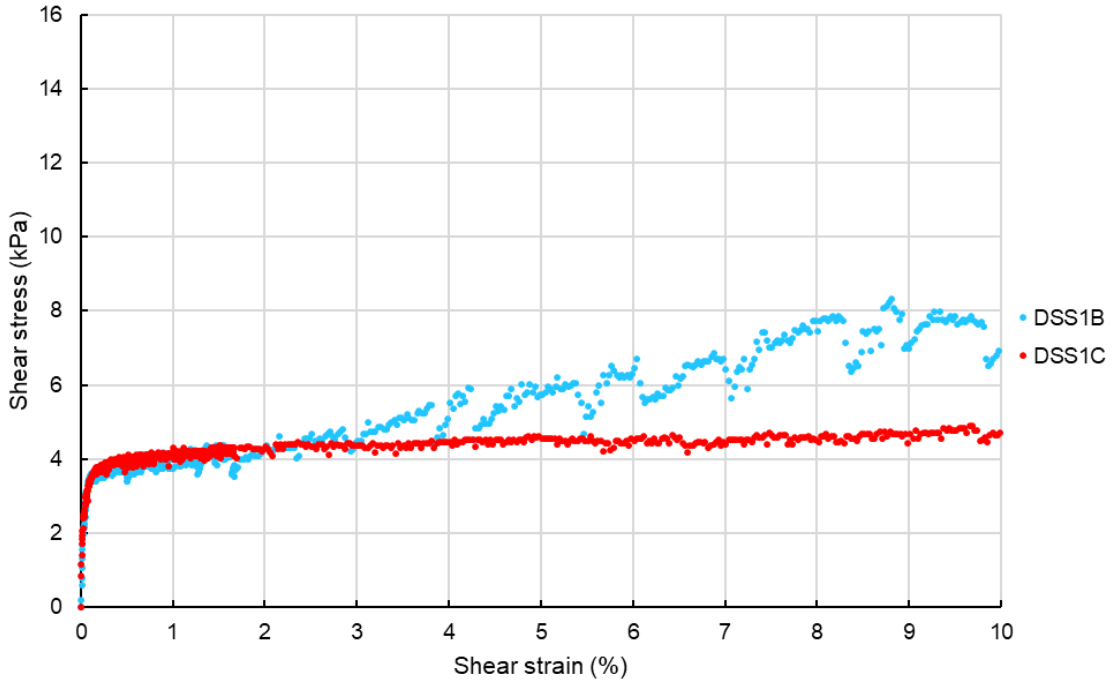

Figure B.20: Stress-strain relation in DSS day 1 tests.

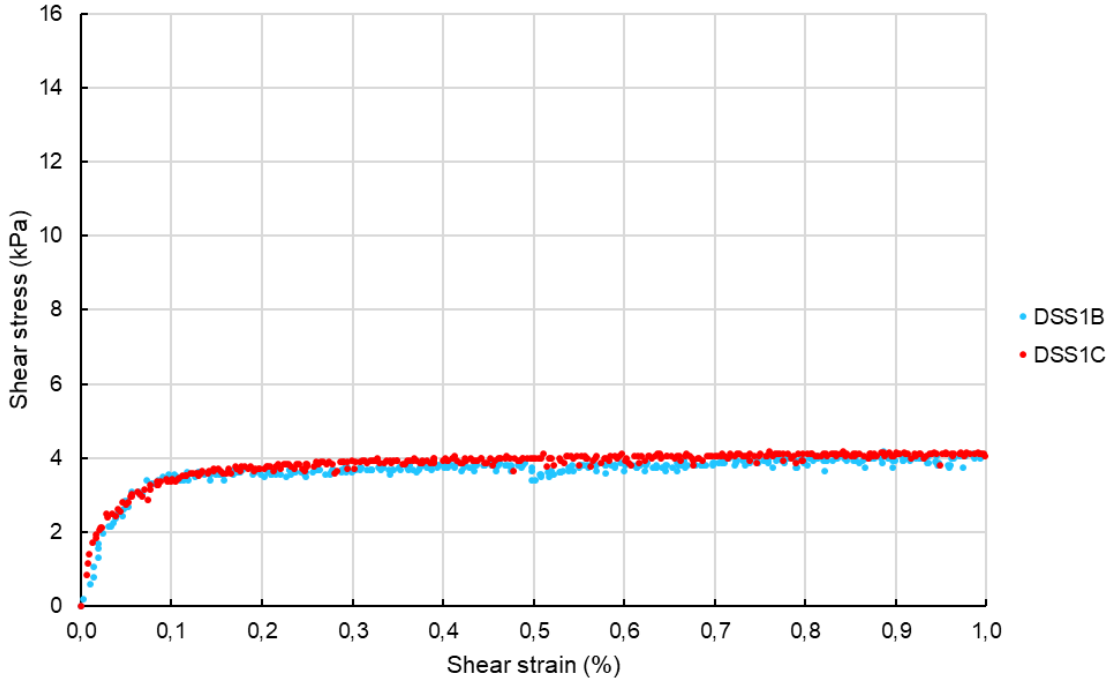

Figure B.21: Stress-strain relation in DSS day 1 tests up to 1% strain.

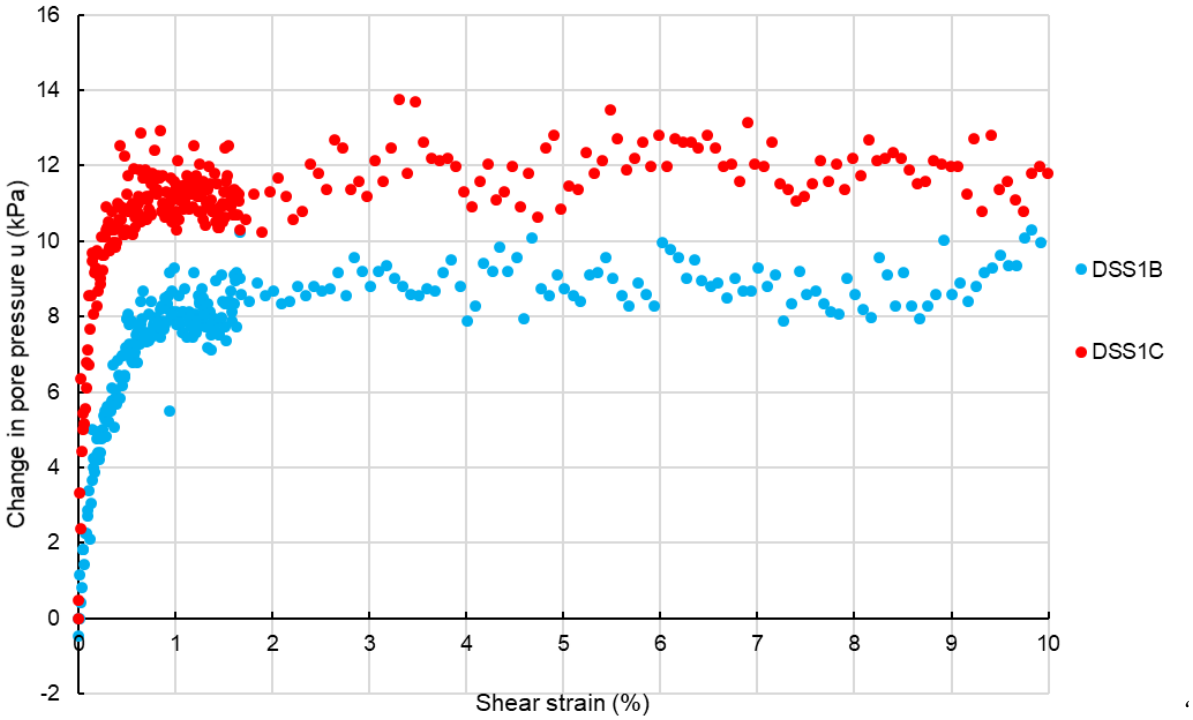

Figure B.22: Stress-excess pore pressure relation in DSS day 1 tests.

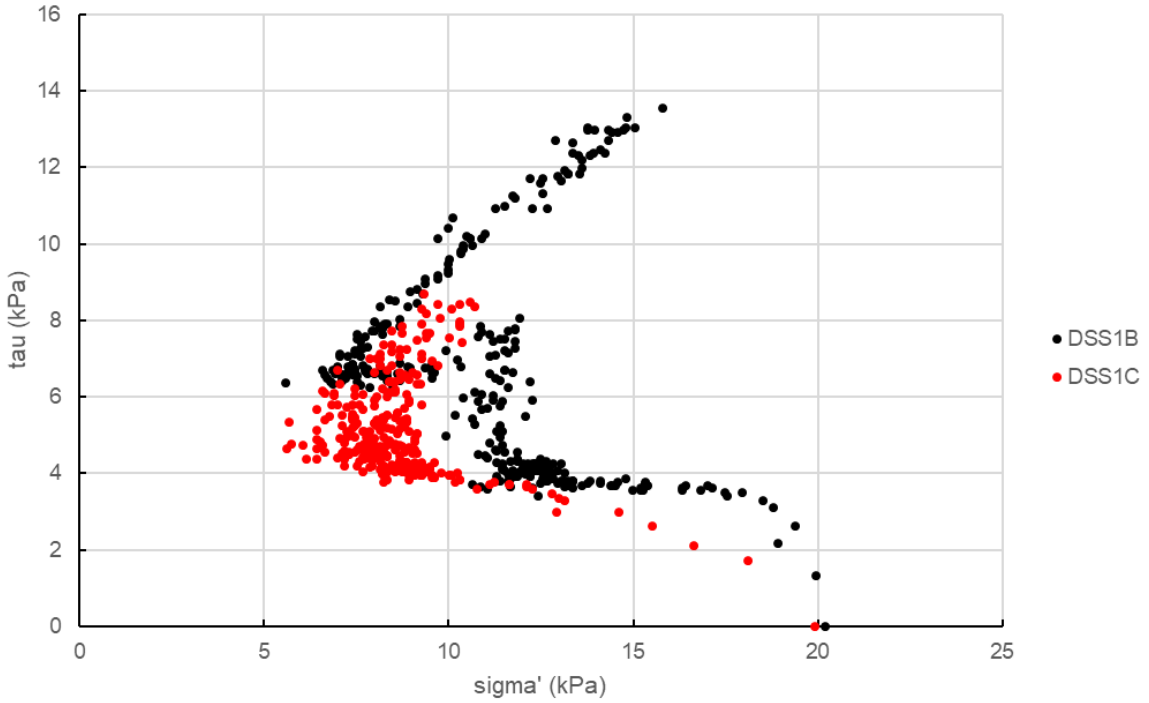

Figure B.23: $\sigma' - \tau$ relation in DSS day 1 tests.

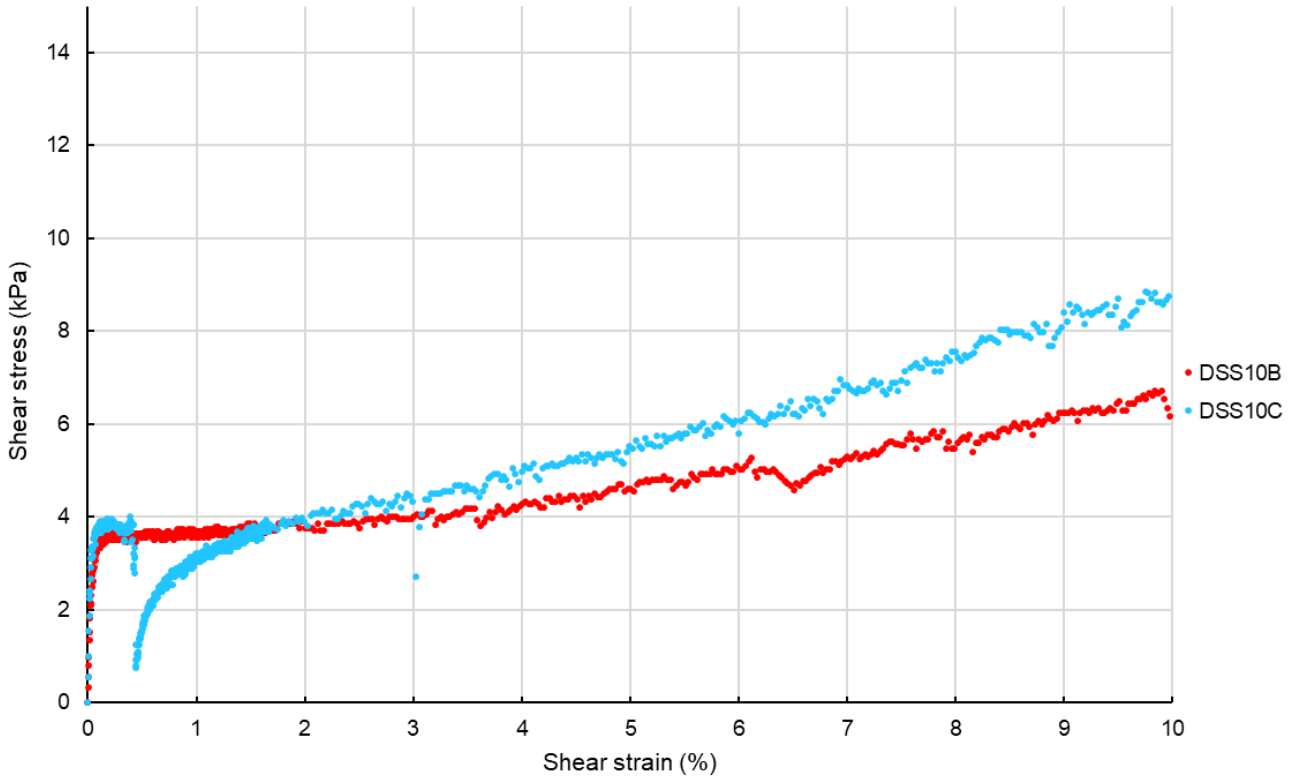

Figure B.24: Stress-strain relation in DSS day 10 tests.

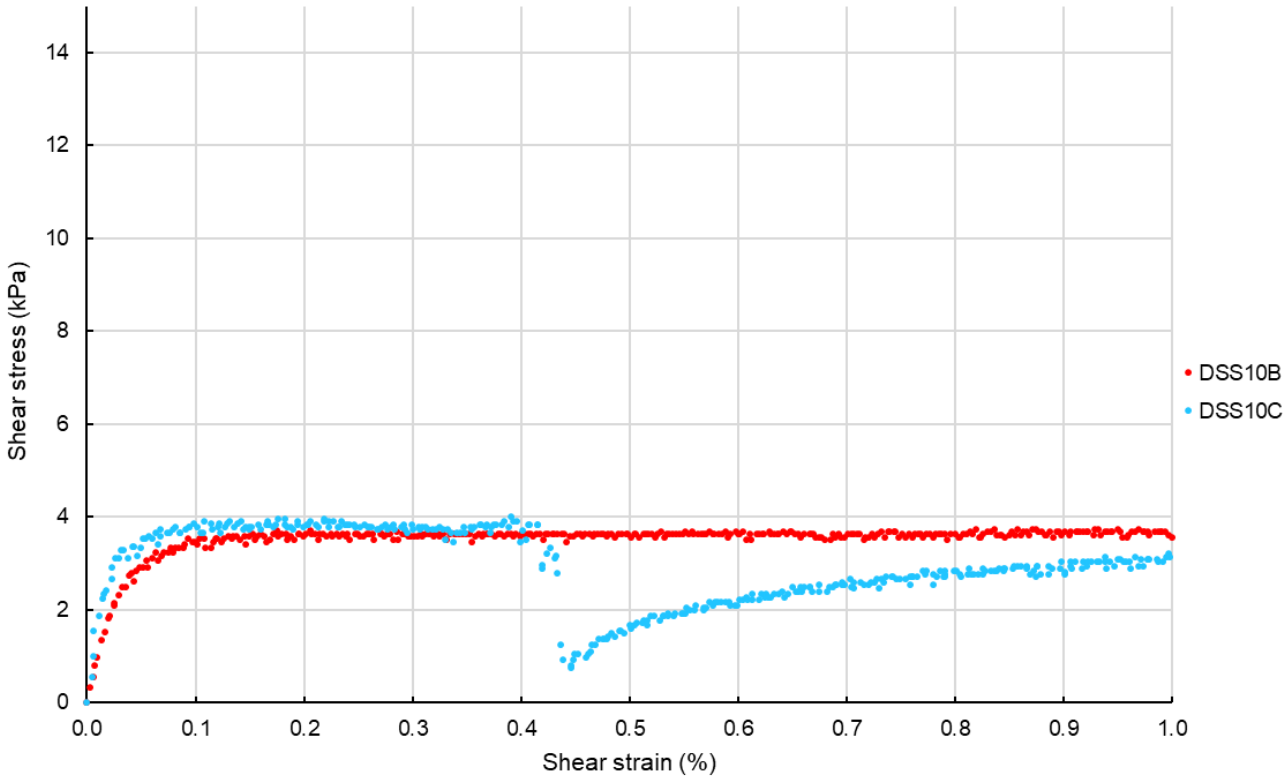

Figure B.25: Stress-strain relation in DSS day 10 tests up to 1% strain.

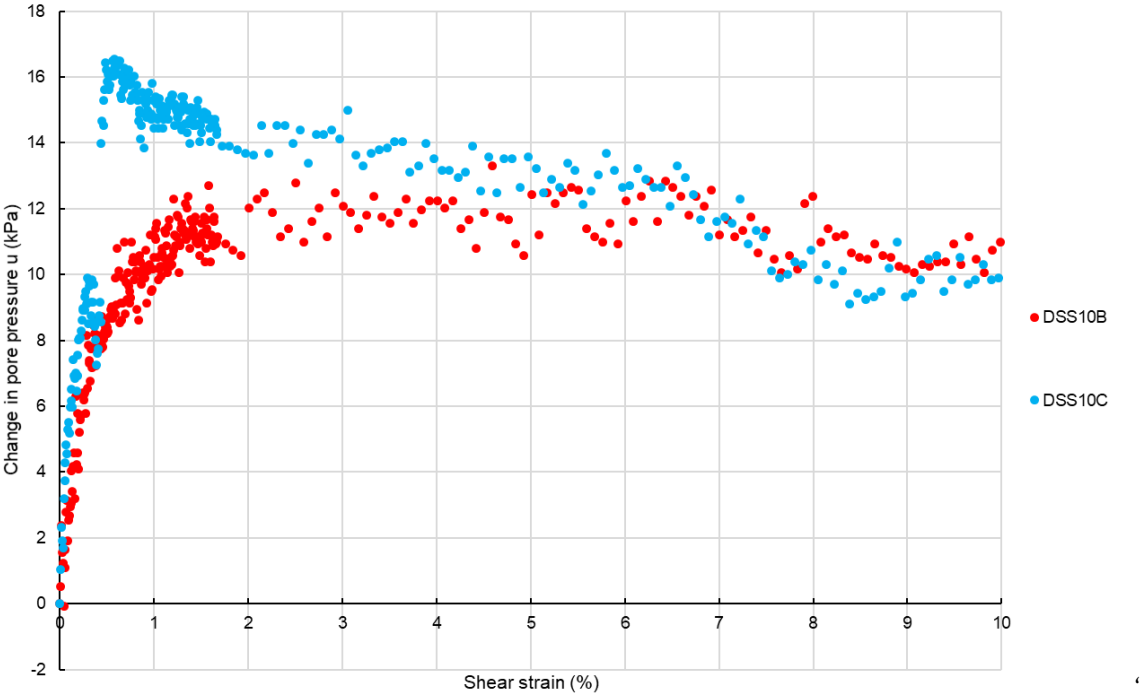

Figure B.26: Stress-excess pore pressure relation in DSS day 10 tests.

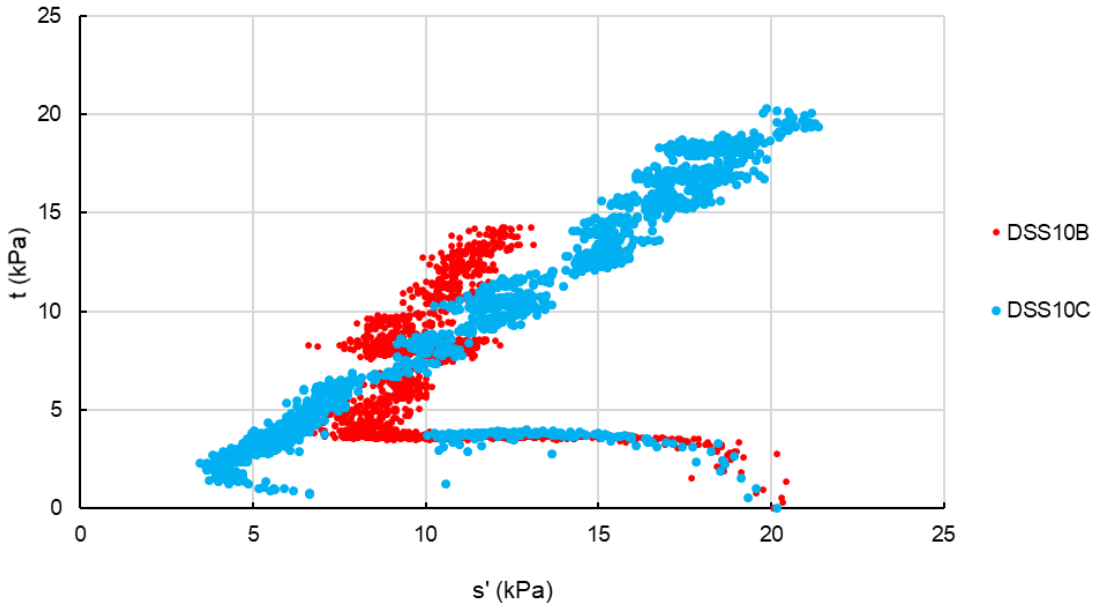

Figure B.27: $\sigma' - \tau$ relation in DSS day 10 tests.

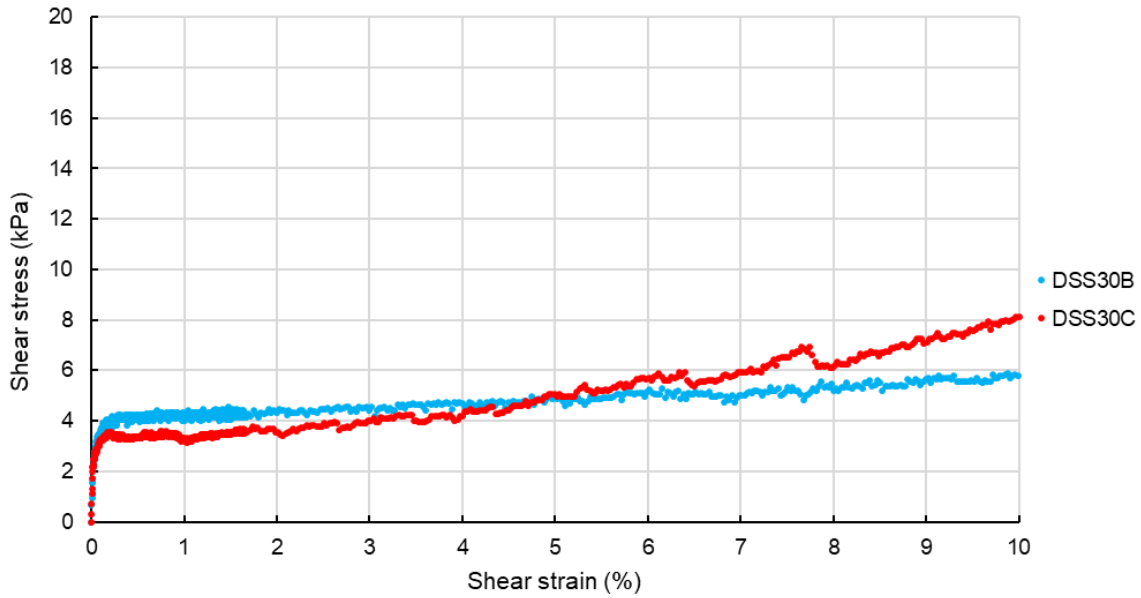

Figure B.28: Stress-strain relation in DSS day 30 tests.

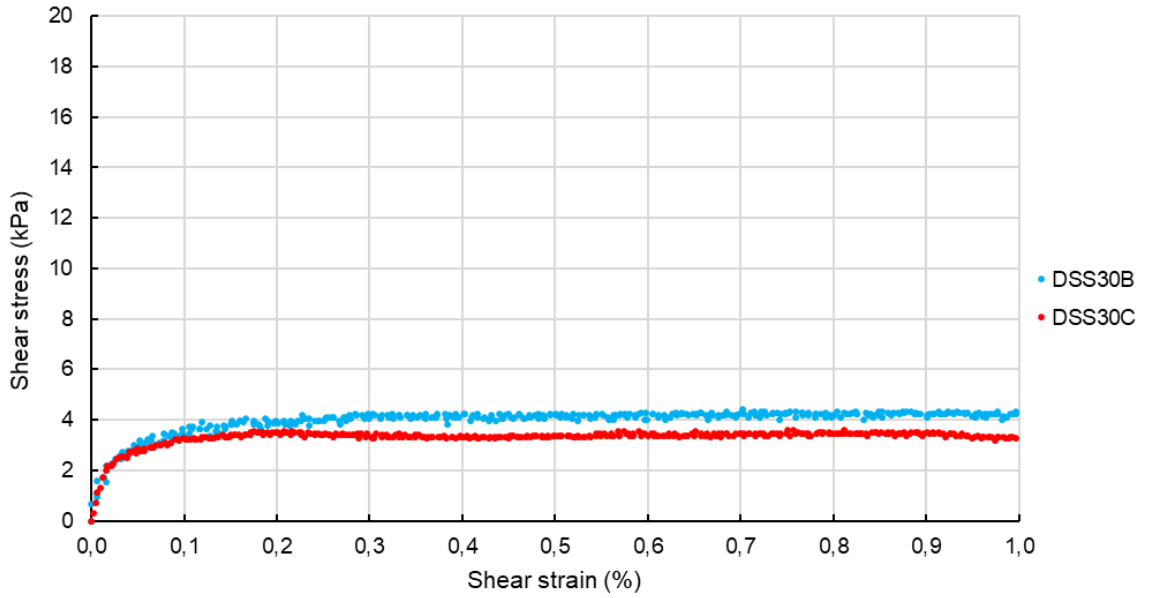

Figure B.29: Stress-strain relation in DSS day 30 tests up to 1% strain.

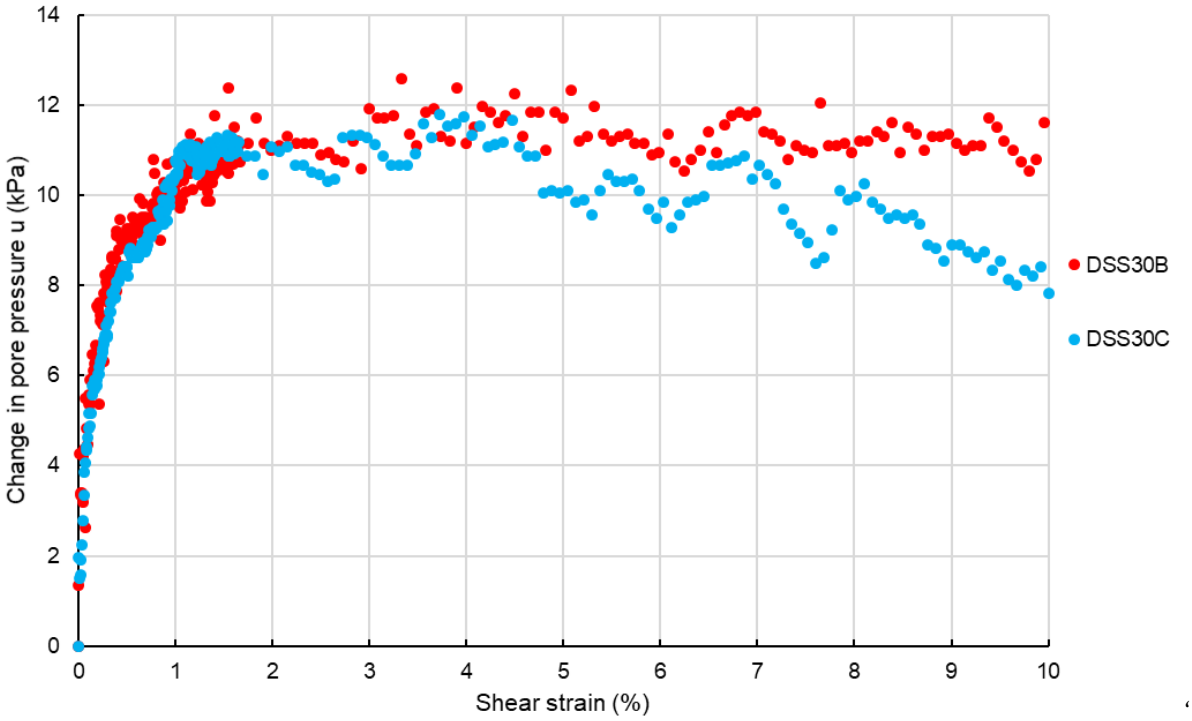

Figure B.30: Stress-excess pore pressure relation in DSS day 30 tests.

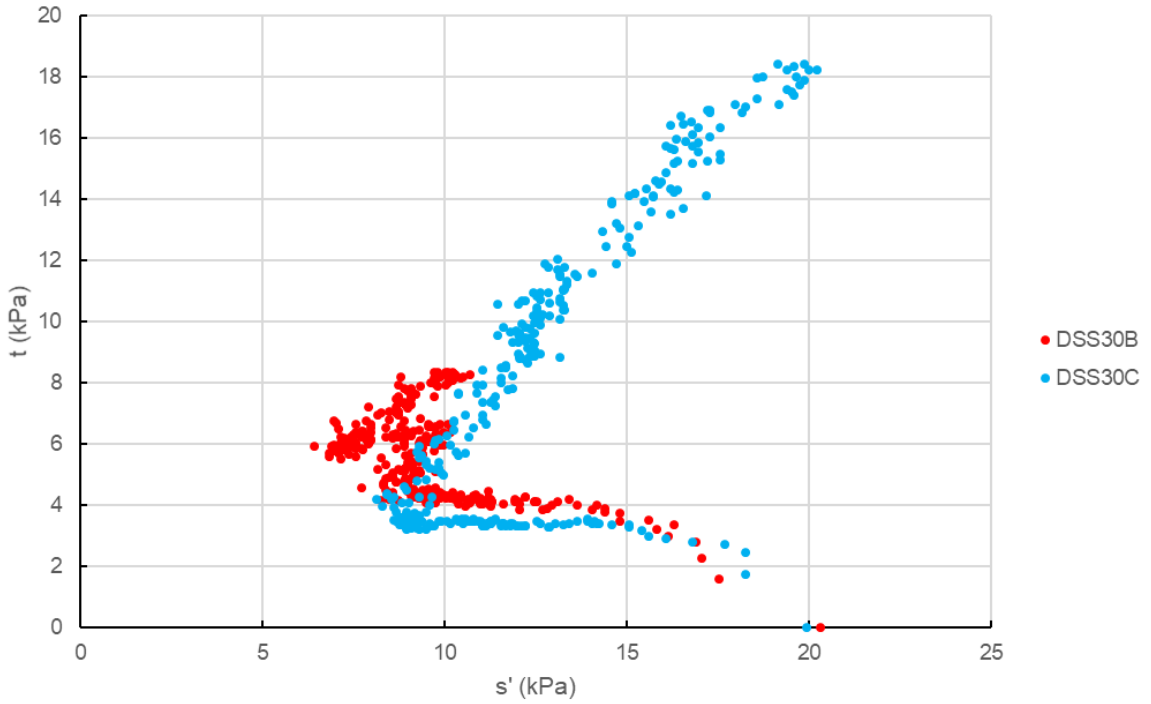

Figure B.31: $\sigma' - \tau$ relation in DSS day 30 tests.

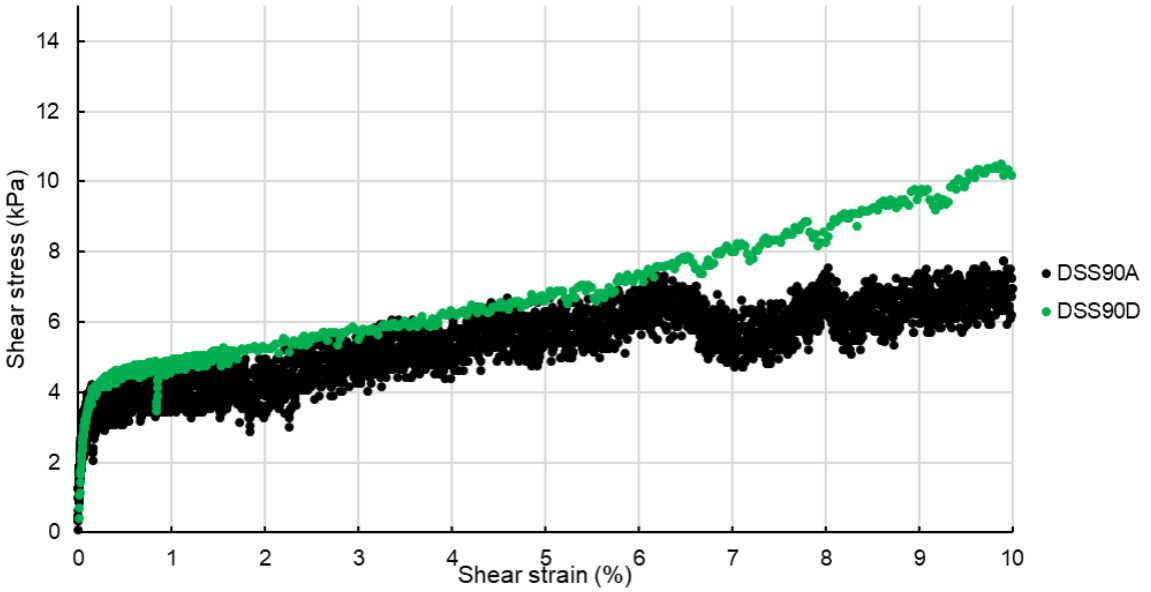

Figure B.32: Stress-strain relation in DSS day 90 tests.

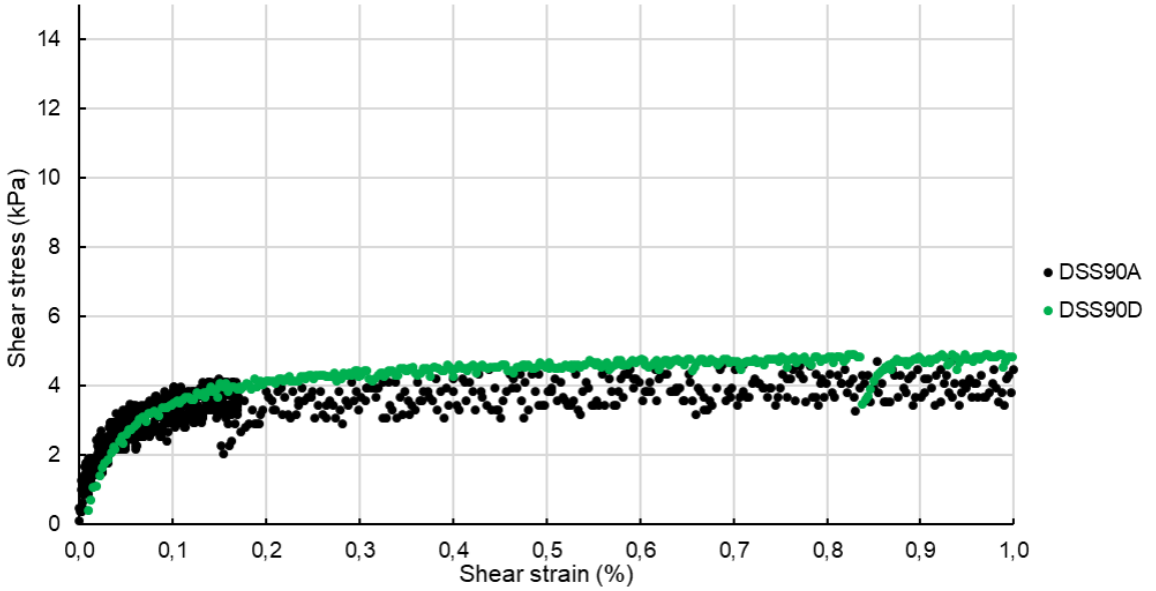

Figure B.33: Stress-strain relation in DSS day 90 tests up to 1% strain.

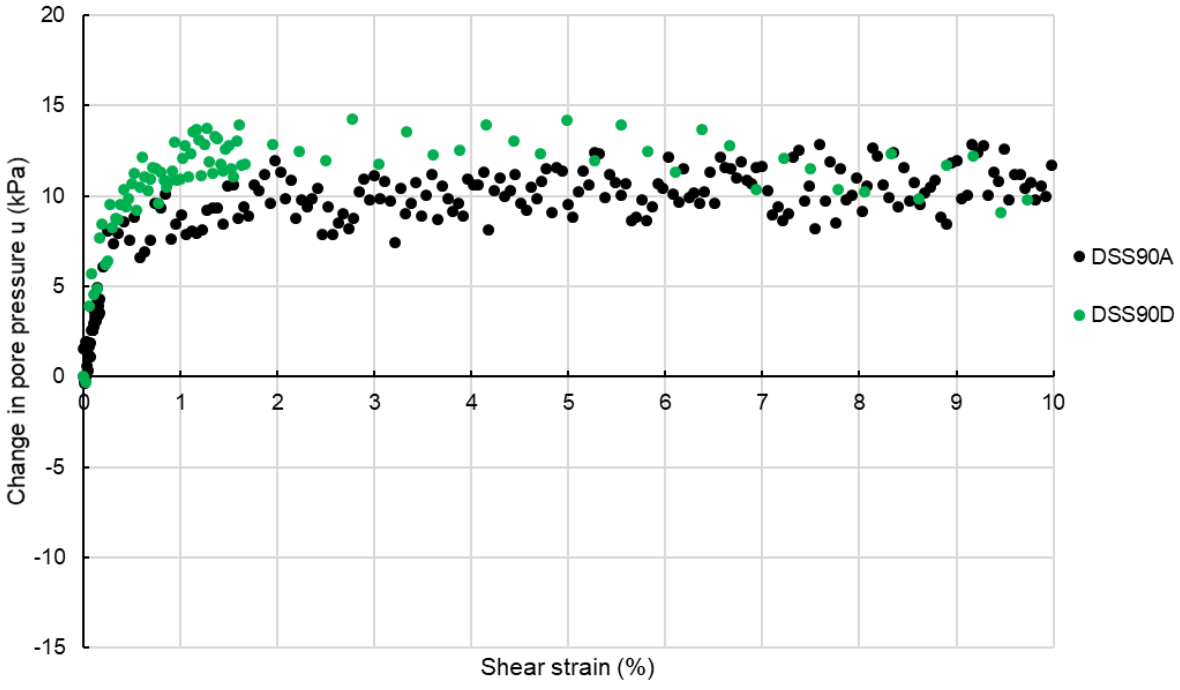

Figure B.34: Stress-excess pore pressure relation in DSS day 90 tests.

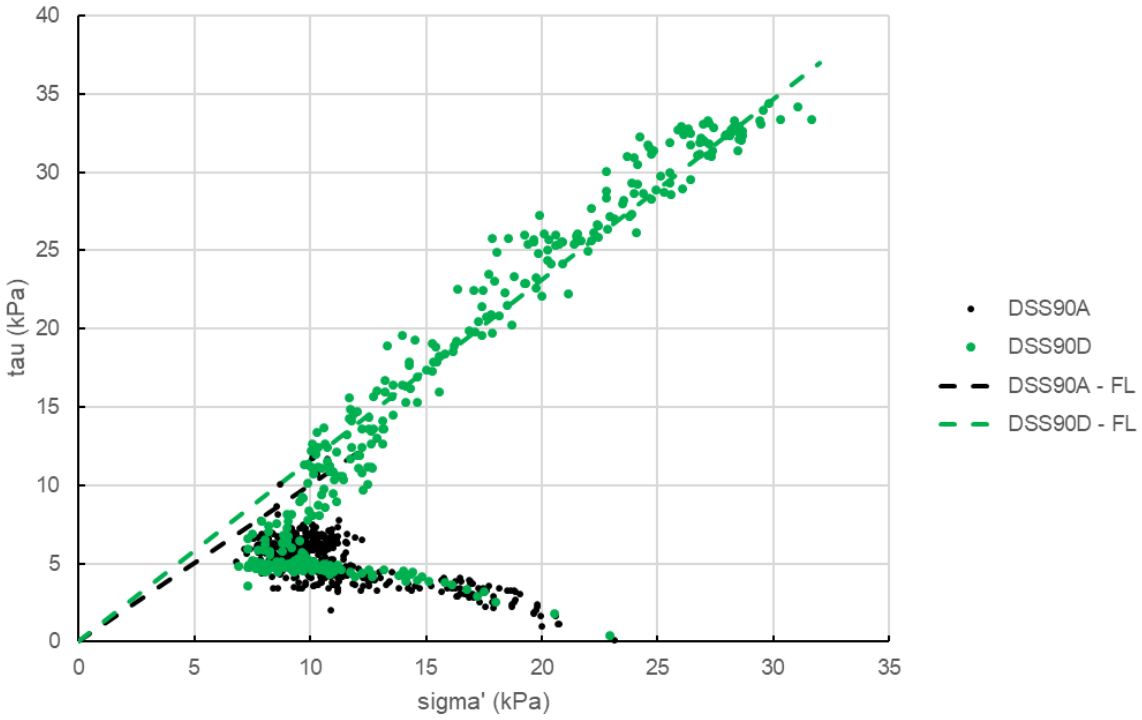

Figure B.35: $\sigma' - \tau$ relation in DSS day 90 tests.

B.5. Triaxial

Table B.4: Slope (M) of the Critical State Line in the p'-q space and value of the critical state friction angle of each triaxial test.

Test	***M***	$\phi_{cs}(^{\circ})$
TXL1A	1,58	38,7
TXL1B	1,67	40,7
TXL1C	1,74	42,4
TXL10A	1,60	39,2
TXL10B	1,57	38,5
TXL30A	1,42	35,0
TXL30B	1,51	37,1
TXL90A	1,45	35,7
TXL90B	1,64	40,0

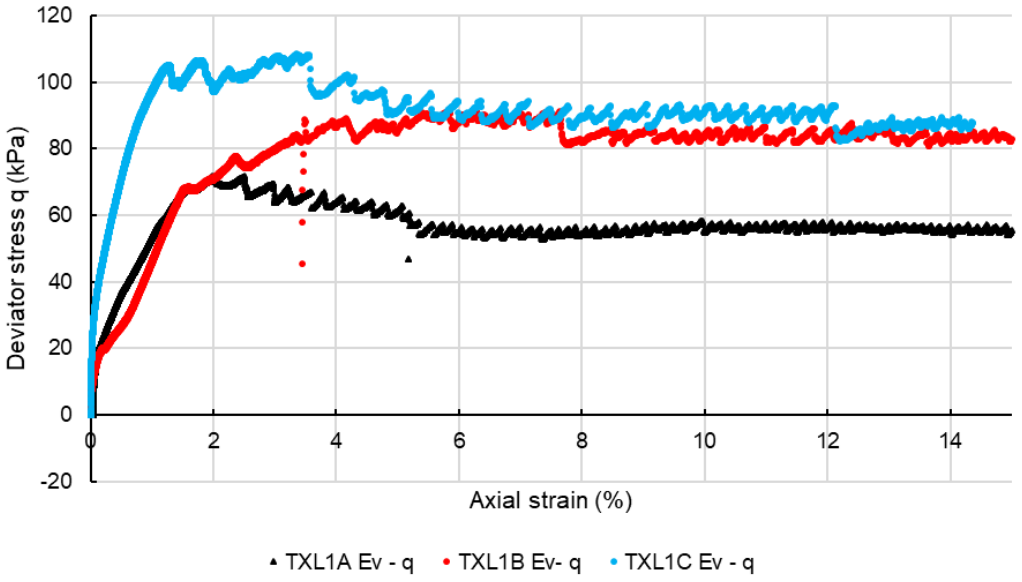

Figure B.36: Stress-strain relation in triaxial day 1 tests.

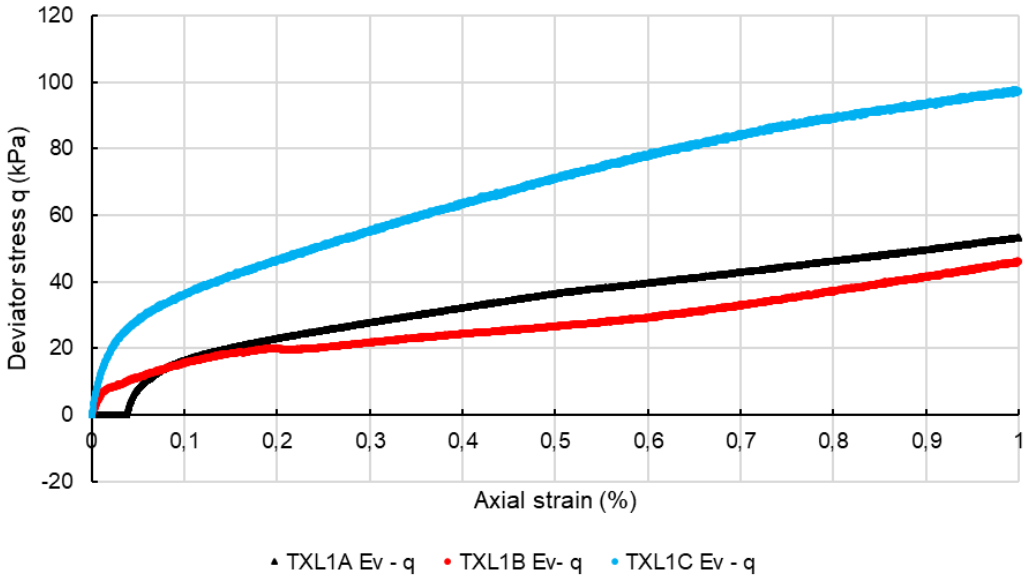

Figure B.37: Stress-strain relation in triaxial day 1 tests up to 1% strain.

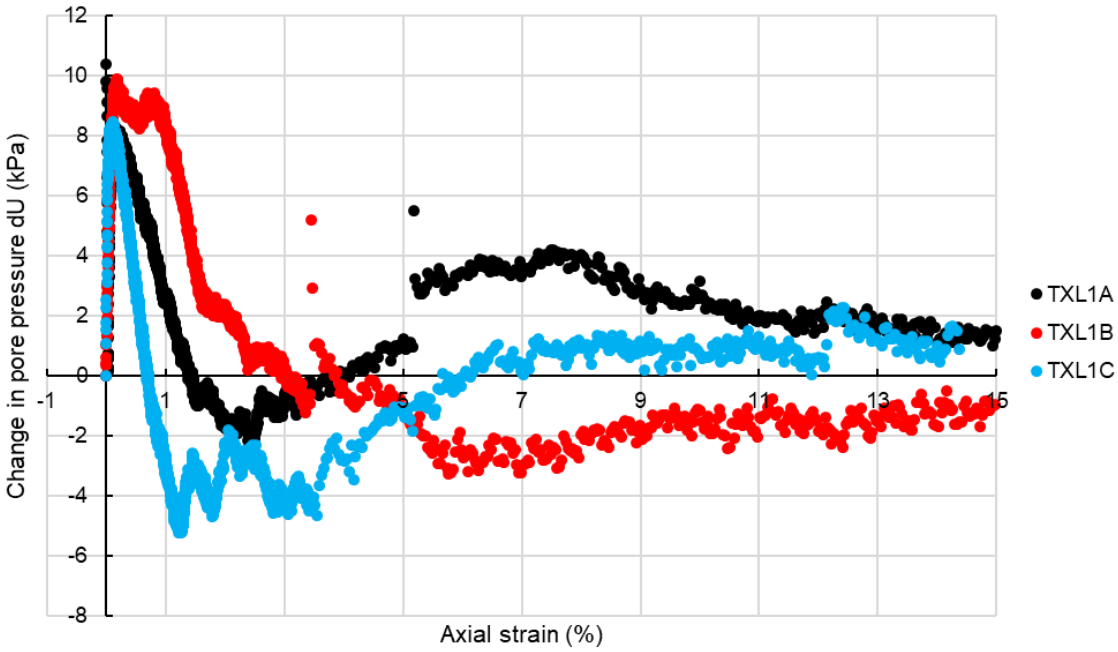

Figure B.38: Excess pore pressure - strain relation in triaxial day 1 tests.

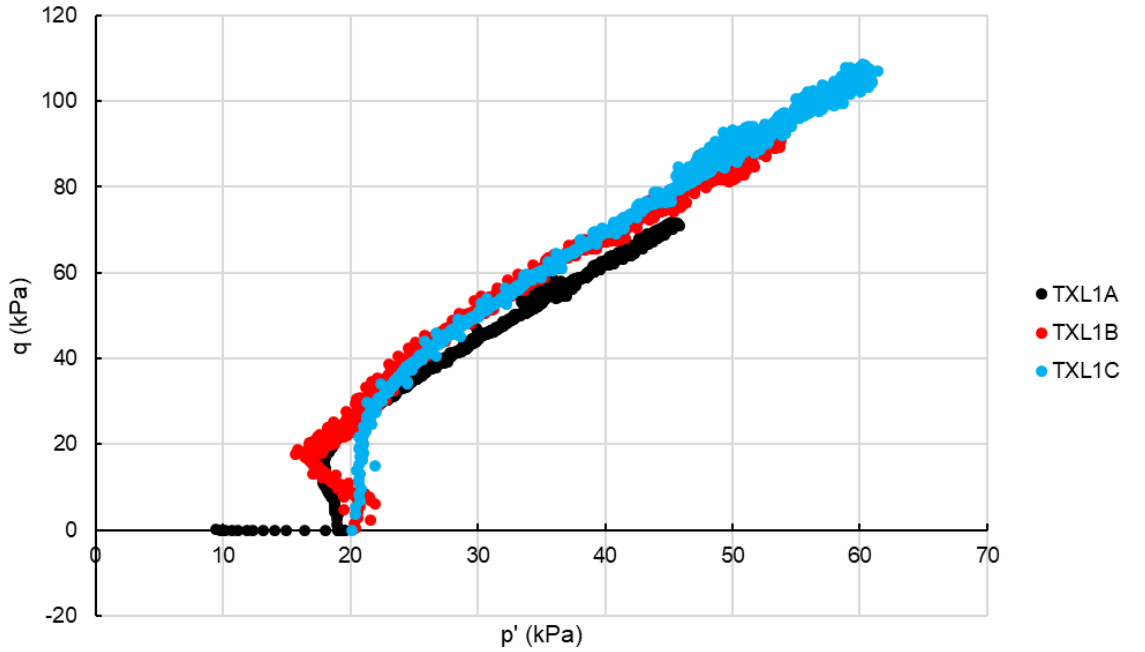

Figure B.39: Stress path in the p'-q space in triaxial day 1 tests.

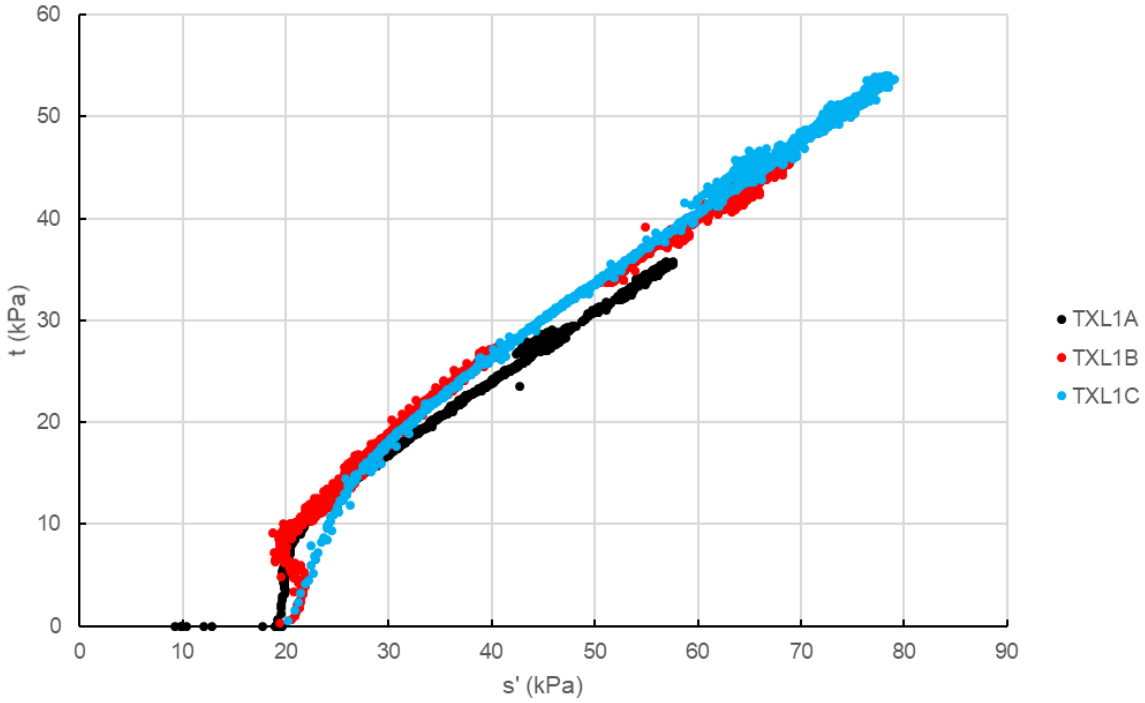

Figure B.40: Stress path in the s'-t space in triaxial day 1 tests.

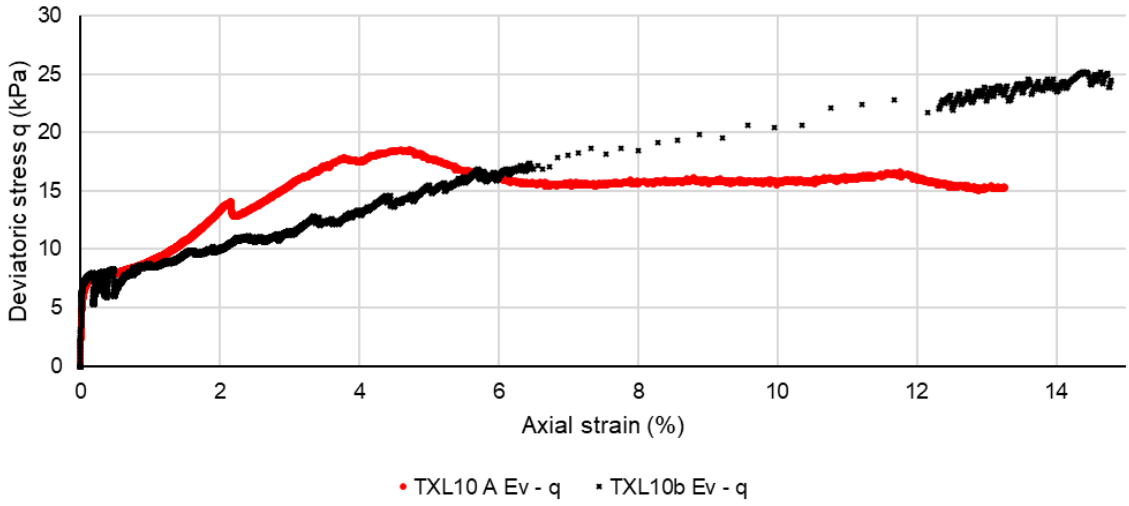

Figure B.41: Stress-strain relation in triaxial day 10 tests.

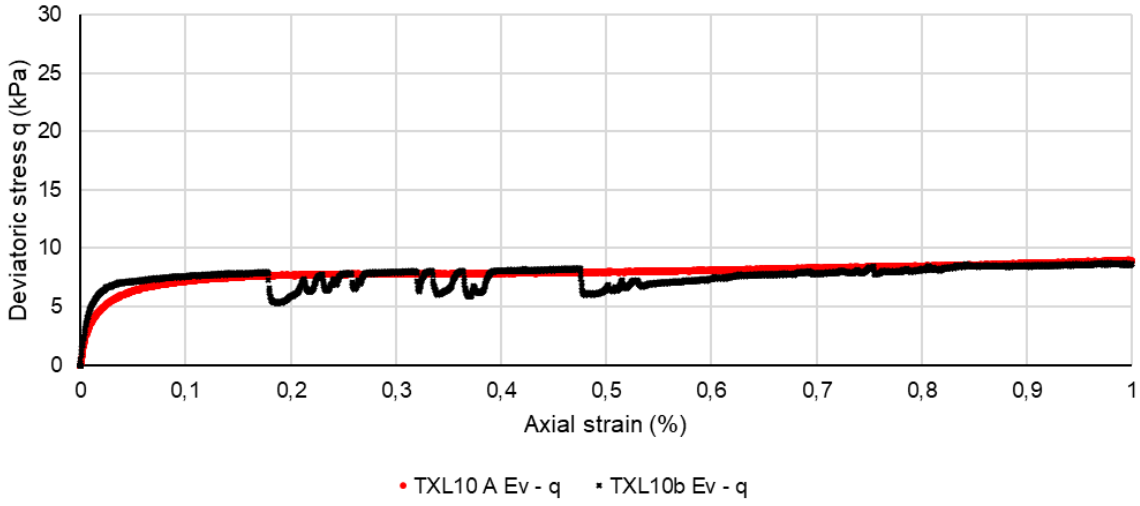

Figure B.42: Stress-strain relation in triaxial day 10 tests up to 1% strain.

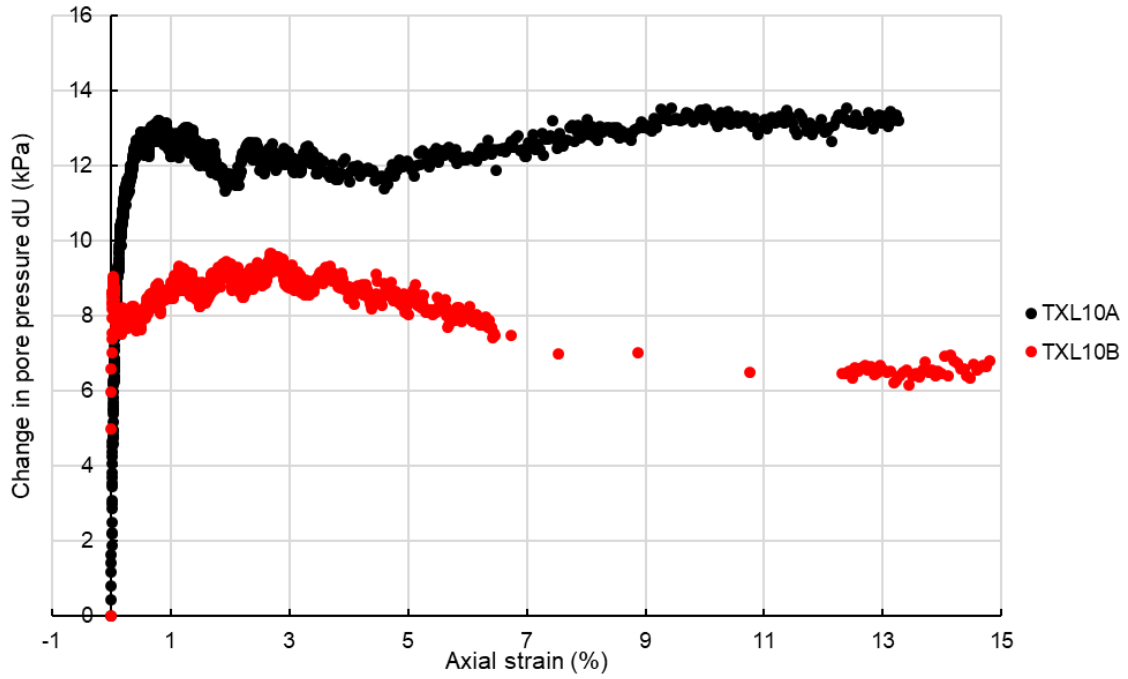

Figure B.43: Excess pore pressure - strain relation in triaxial day 10 tests.

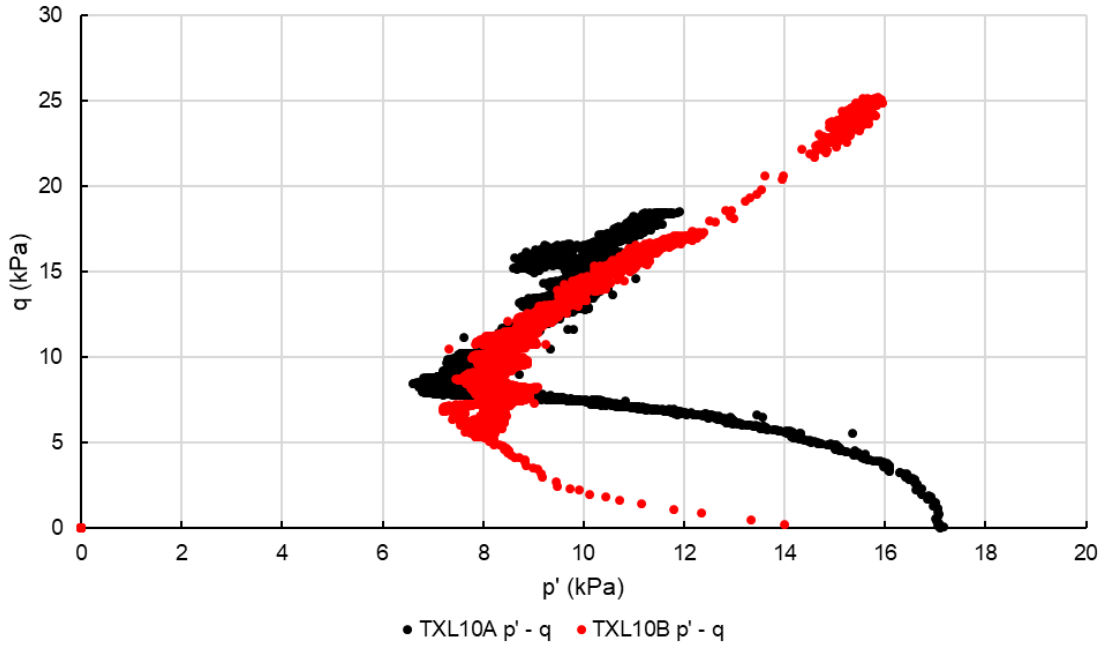

Figure B.44: Stress path in the p'-q space in triaxial day 10 tests.

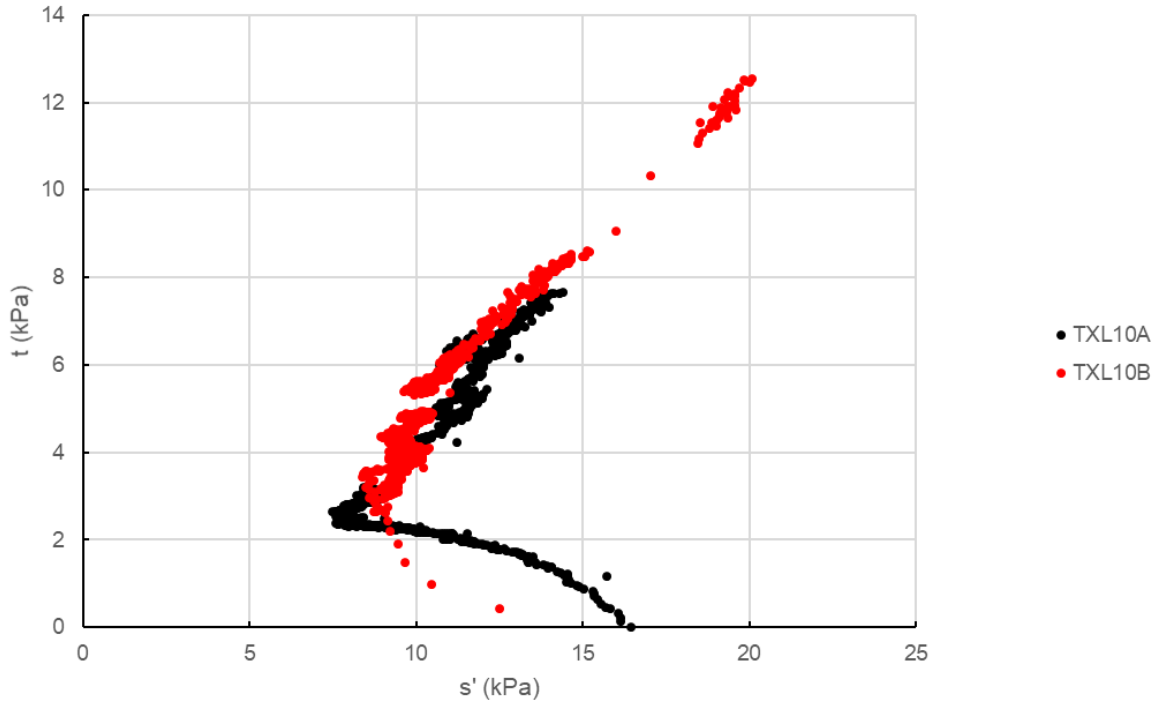

Figure B.45: Stress path in the s'-t space in triaxial day 10 tests.

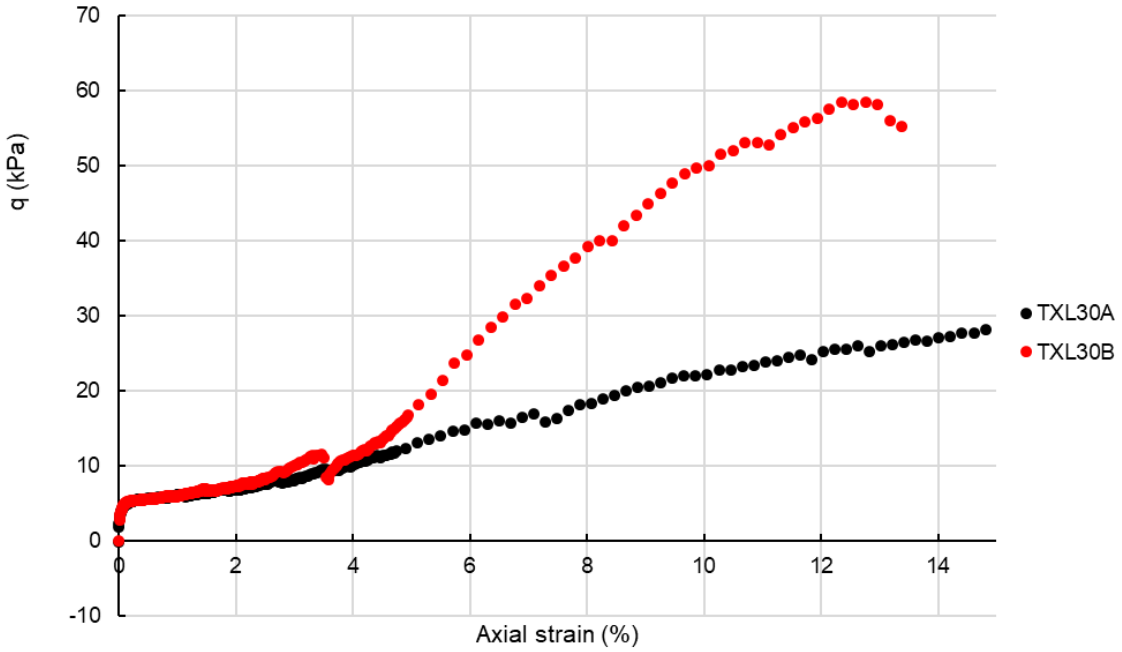

Figure B.46: Stress-strain relation in triaxial day 30 tests.

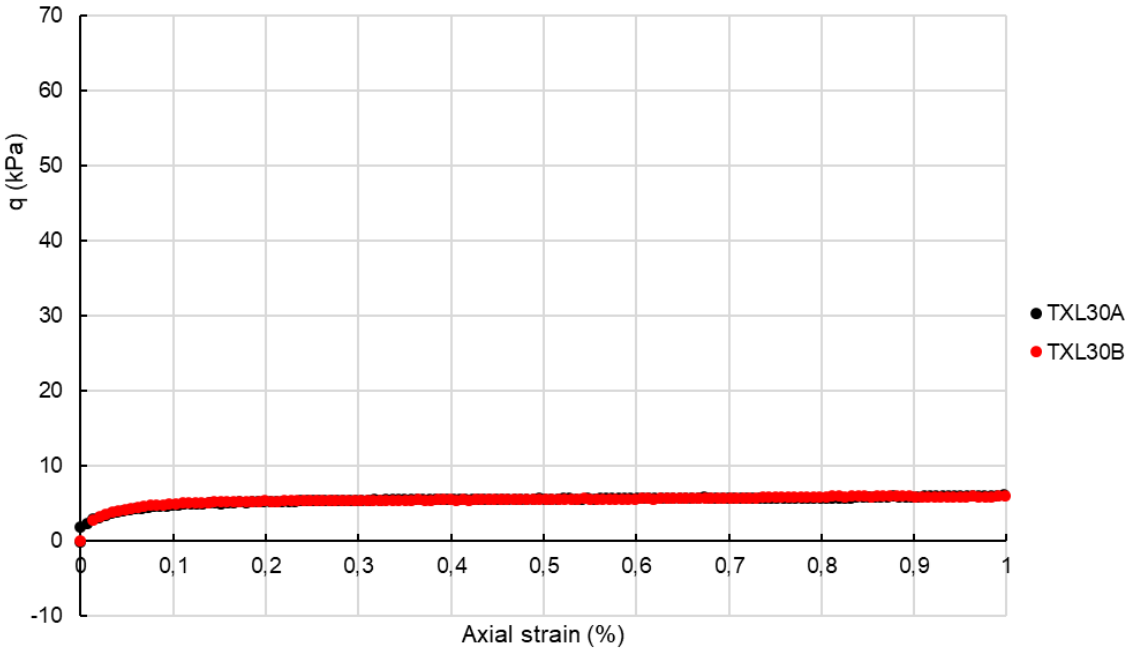

Figure B.47: Stress-strain relation in triaxial day 30 tests up to 1% strain.

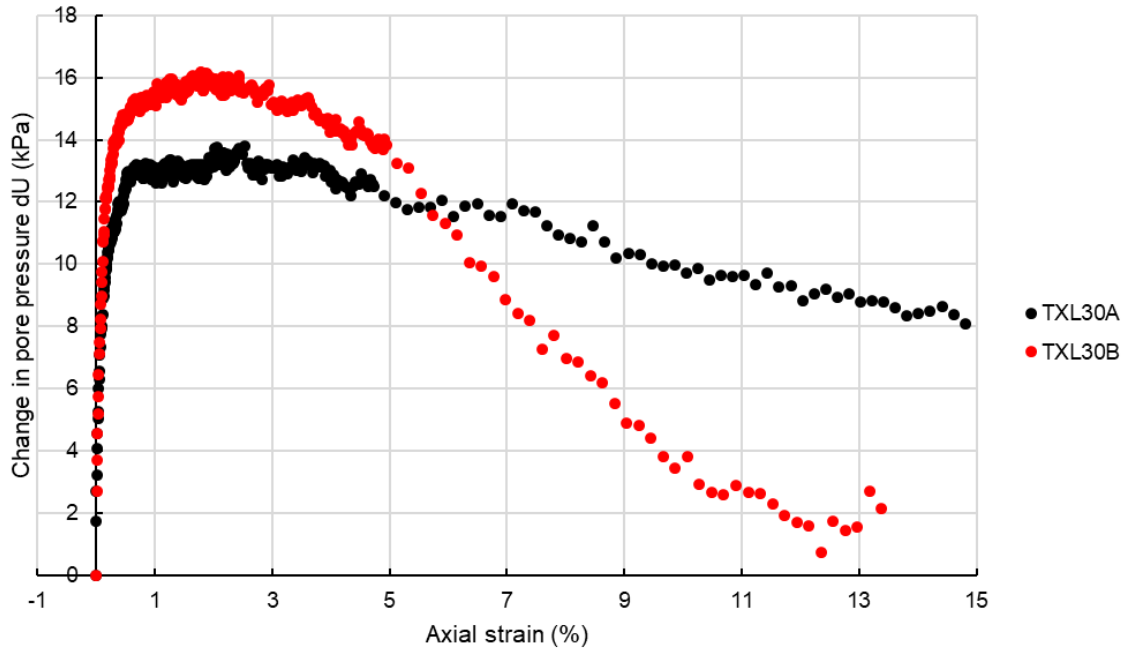

Figure B.48: Excess pore pressure - strain relation in triaxial day 30 tests.

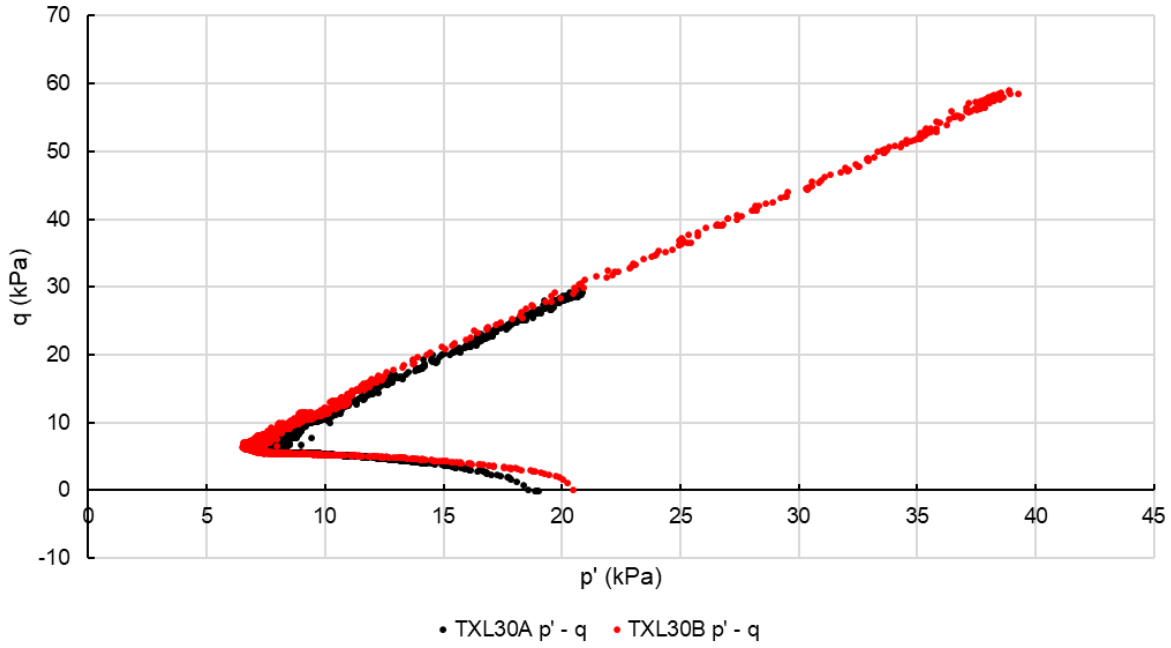

Figure B.49: Stress path in the p'-q space in triaxial day 30 tests.

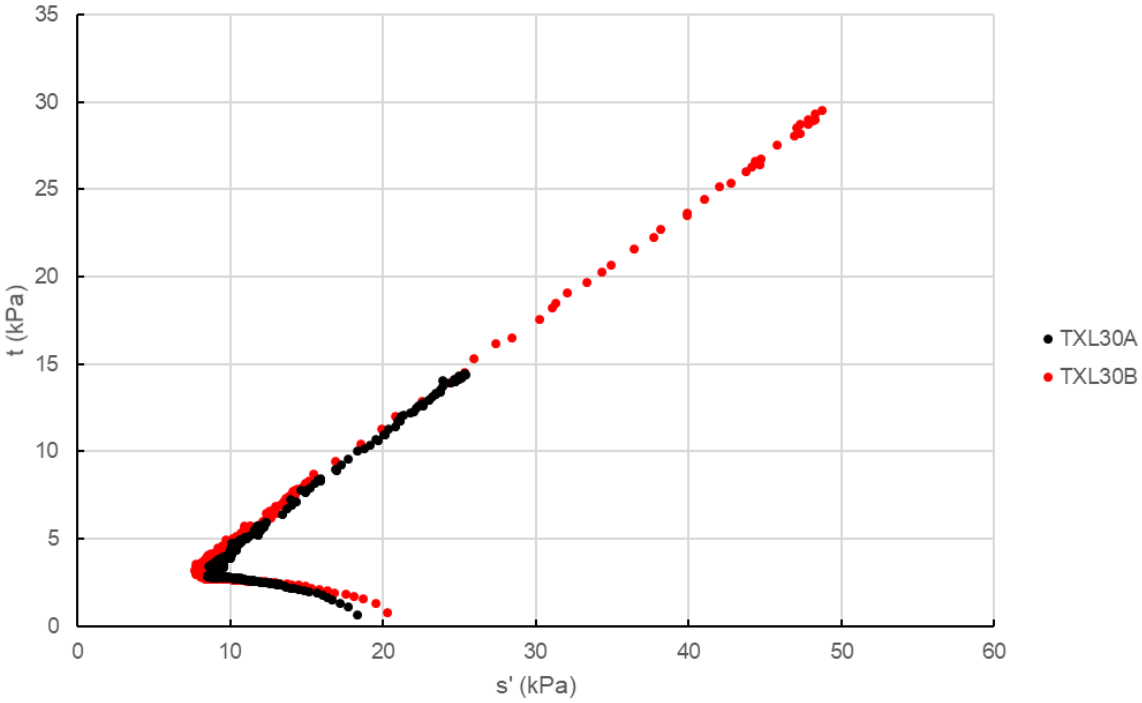

Figure B.50: Stress path in the s'-t space in triaxial day 30 tests.

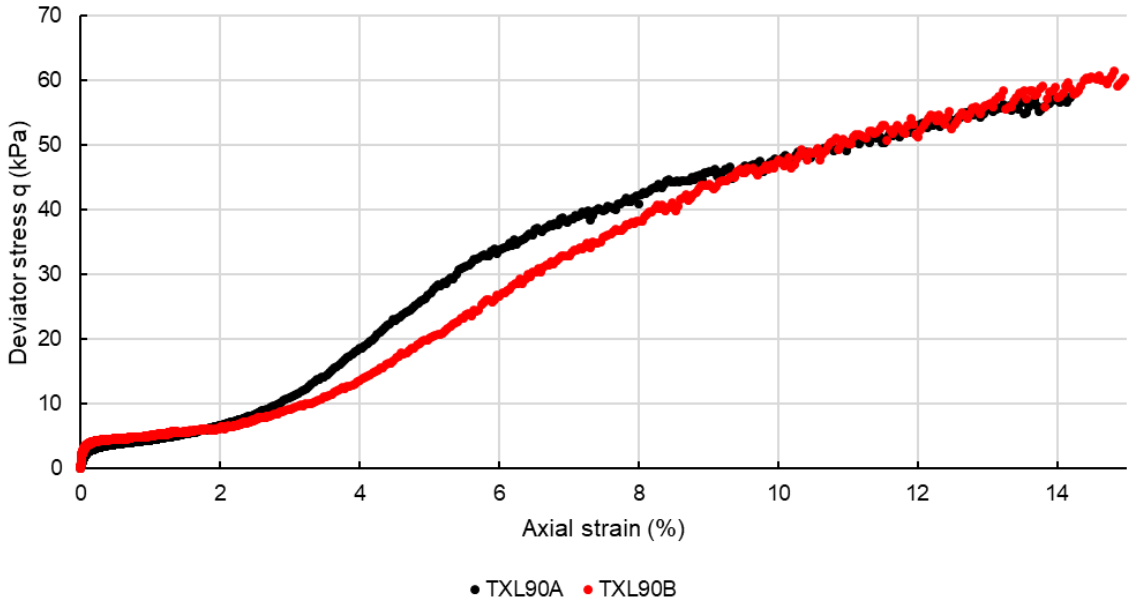

Figure B.51: Stress-strain relation in triaxial day 90 tests.

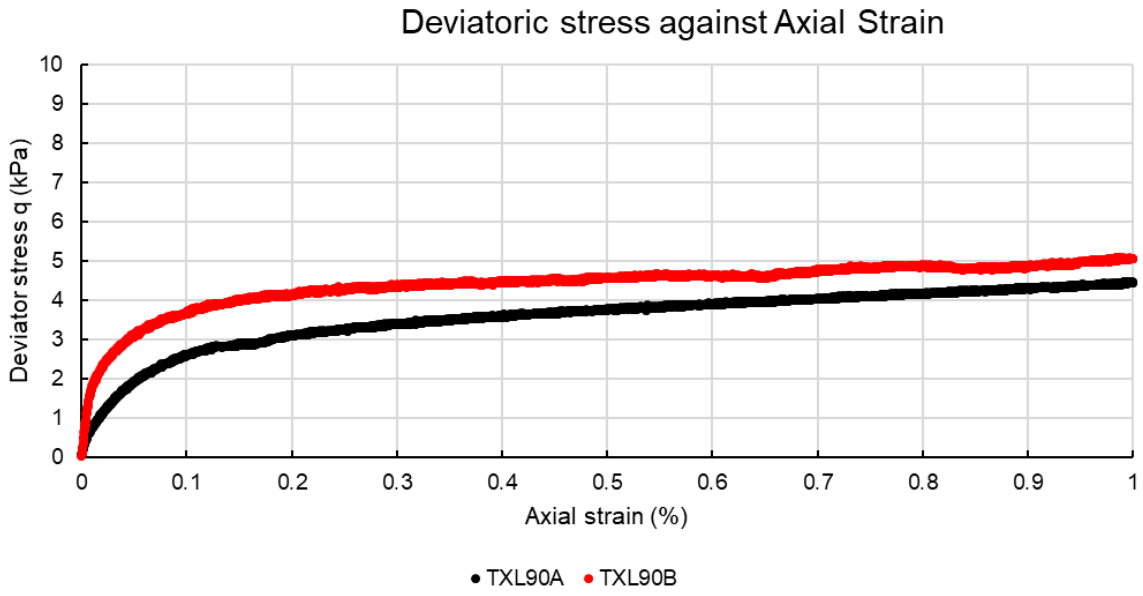

Figure B.52: Stress-strain relation in triaxial day 90 tests up to 1% strain.

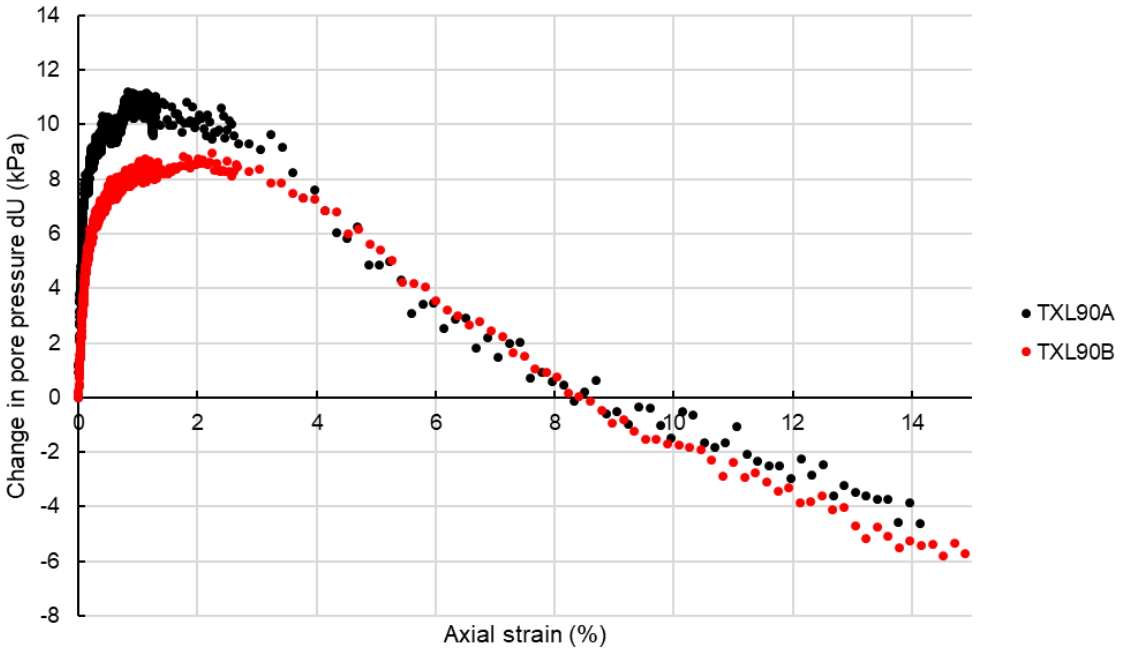

Figure B.53: Excess pore pressure - strain relation in triaxial day 90 tests.

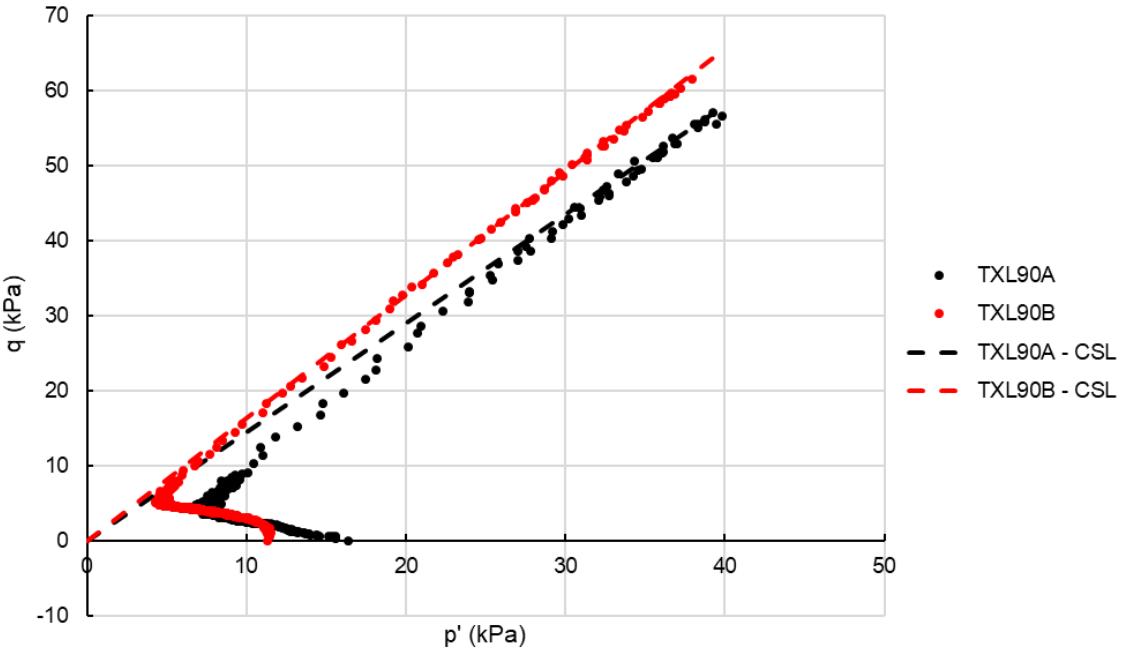

Figure B.54: Stress path in the p'-q space in triaxial day 90 tests.

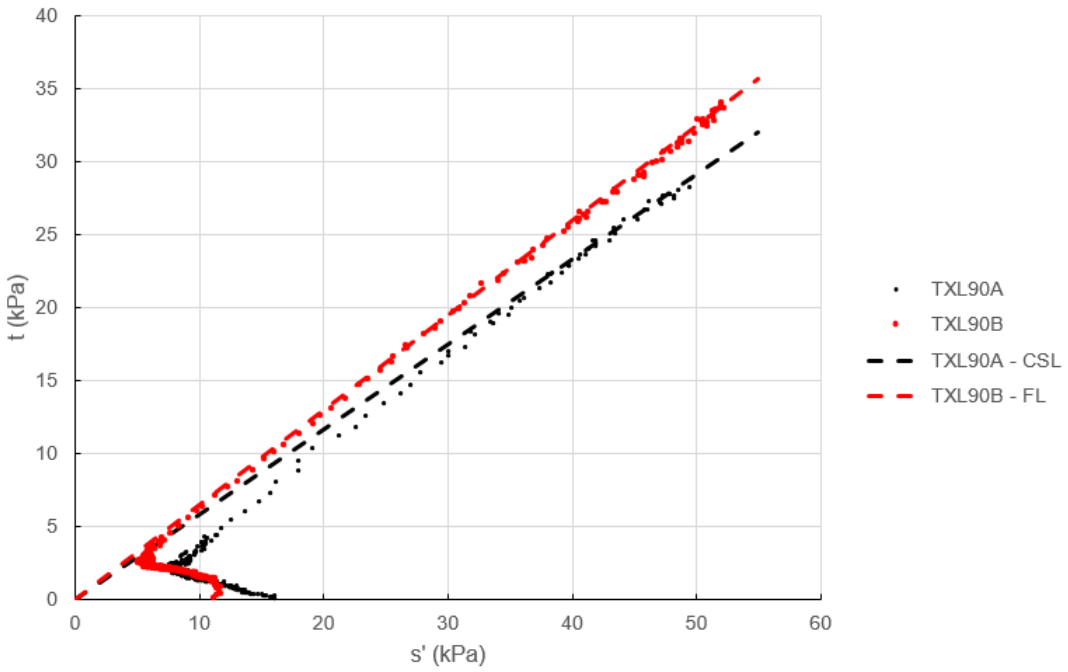

Figure B.55: Stress path in the s'-t space in triaxial day 90 tests.

B.6. Bender Elements

Table B.5: G_{MAX} calculated at different frequencies from the bender elements taken on Day 1 specimens after consolidation

Frequency (Hz)	***TXL1A***	***TXL1B***	***TXL1C***	***Average (Mpa)***	***St Dev***
50000	433.77			433.77	0.00
25000	452.91	97.05		274.98	177.93
16667		95.64		95.64	0.00
12500	292.64	94.25		193.45	99.20
10000	200.76	91.24	108.40	133.47	48.10
8333		89.47	105.55	97.51	8.04
7143	39.44	87.59	109.66	78.89	29.32
6250	39.07	86.83	109.44	78.45	29.34
5556		87.13	109.02	98.08	10.95
5000		55.59	100.92	78.25	22.66
4545	39.12	53.77	99.26	64.05	25.61
4167	38.40		97.29	67.84	29.45
3846	38.17		95.89	67.03	28.86
3571	38.66		92.04	65.35	26.69
			Average	130.48	101.73

Table B.6: G_{MAX} calculated at different frequencies from the bender elements taken on Day 1 specimens after consolidation

Frequency (Hz)	***TXL10A***	***TXL10B***	***Average***	***Standard deviation***
10000		40.47	40.47	0.00
8333	32.19	38.80	35.49	3.31
7143	31.70	38.89	35.30	3.60
6250	31.85	38.39	35.12	3.27
5556	32.30	39.27	35.78	3.48
5000	32.30	38.94	35.62	3.32
4545	33.07	38.25	35.66	2.59
4167	31.52	36.97	34.25	2.72
3846	31.78	38.85	35.31	3.54
3597	33.54	36.50	35.02	1.48
3333	31.16		31.16	0.00
		Average	35.38	2.04

C

Sample photographs

C.1. Constant Rate of Strain

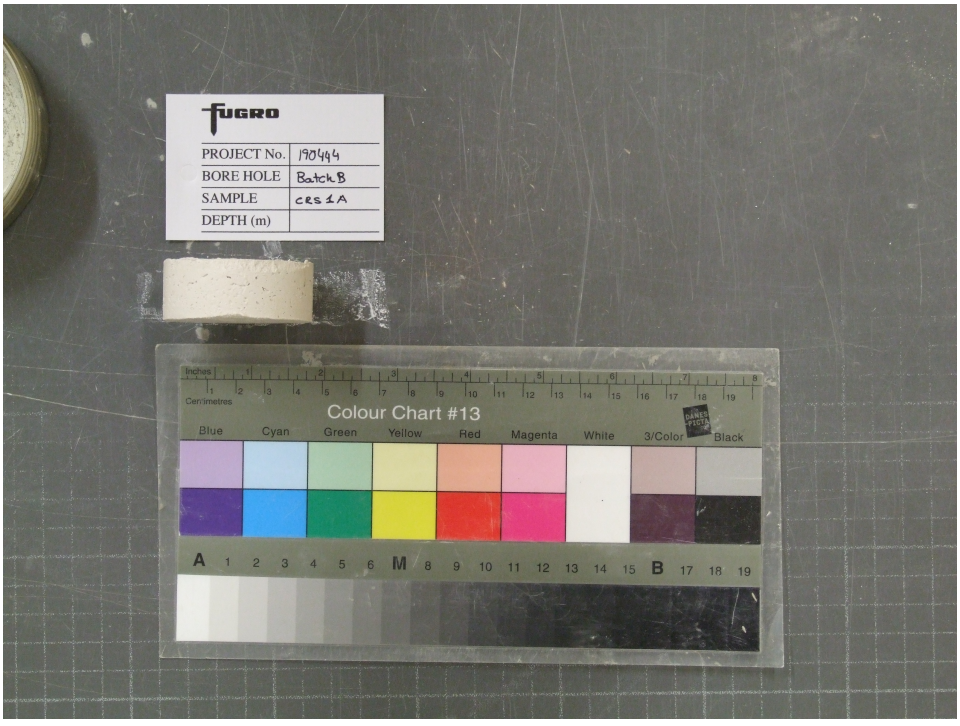

Figure C.1: Sample photo CRS1A.

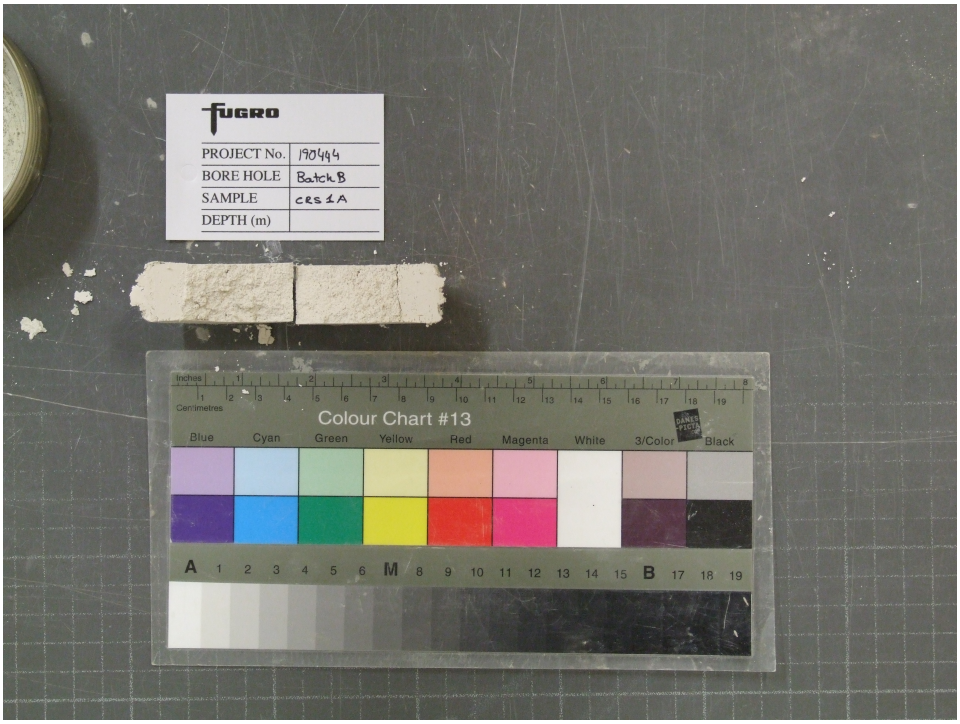

Figure C.2: Split sample photo CRS1A.

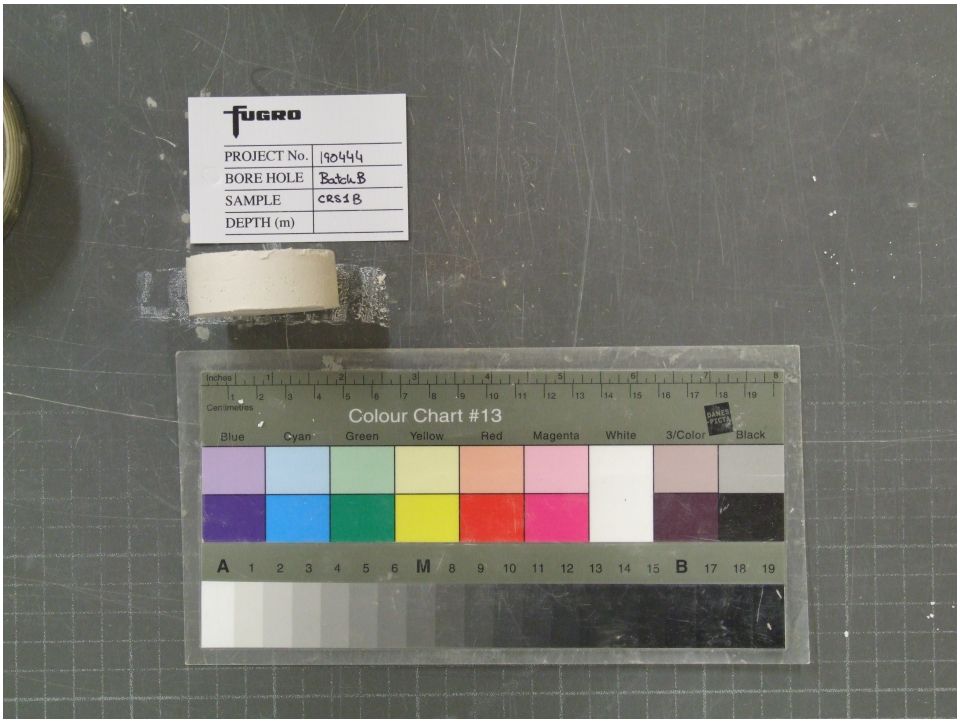

Figure C.3: Sample photo CRS1B.

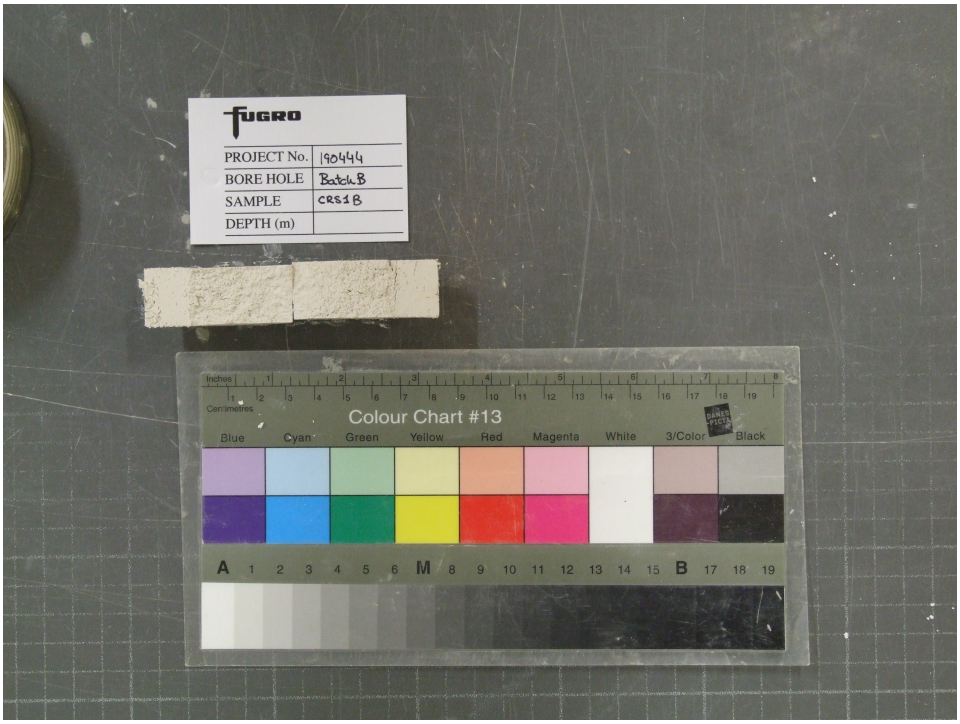

Figure C.4: Split sample photo CRS1B.

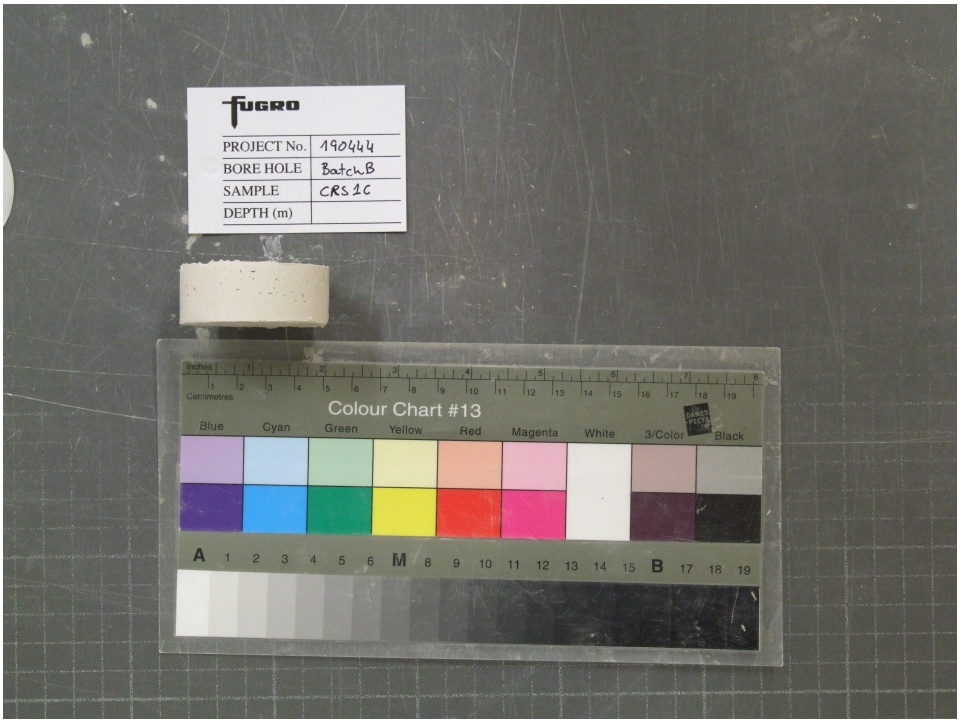

Figure C.5: Sample photo CRS1C.

Figure C.6: Split sample photo CRS1C.

Figure C.7: Sample photo CRS10A.

Figure C.8: Split sample photo CRS10A.

Figure C.9: Sample photo CRS10B.

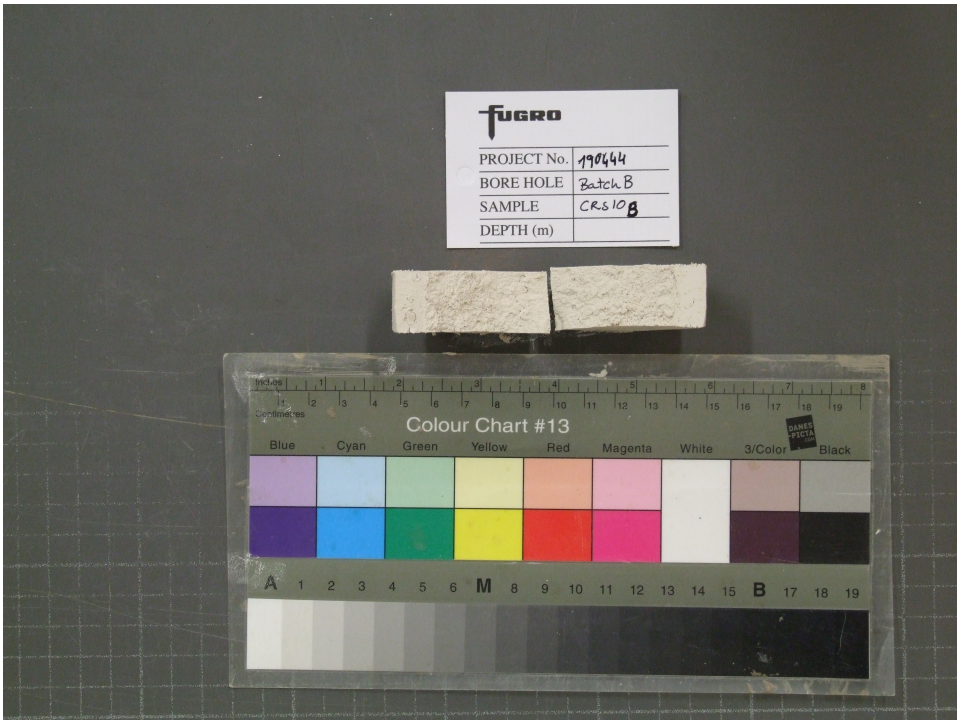

Figure C.10: Split sample photo CRS10B.

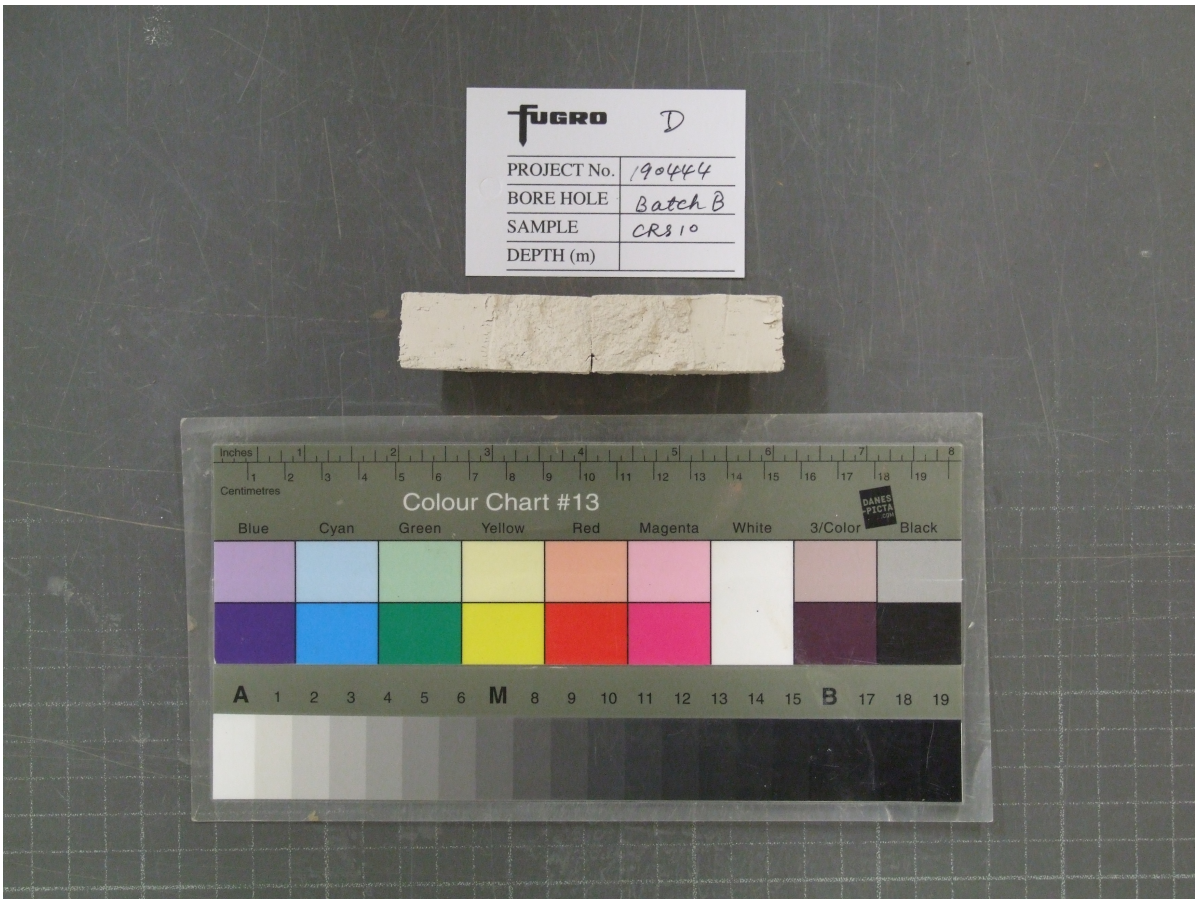

Figure C.11: Split sample photo CRS10D.

Figure C.12: Sample photo CRS30B.

Figure C.13: Split sample photo CRS30B.

C.2. Direct Simple Shear

Figure C.14: Sample photo DSS1A.

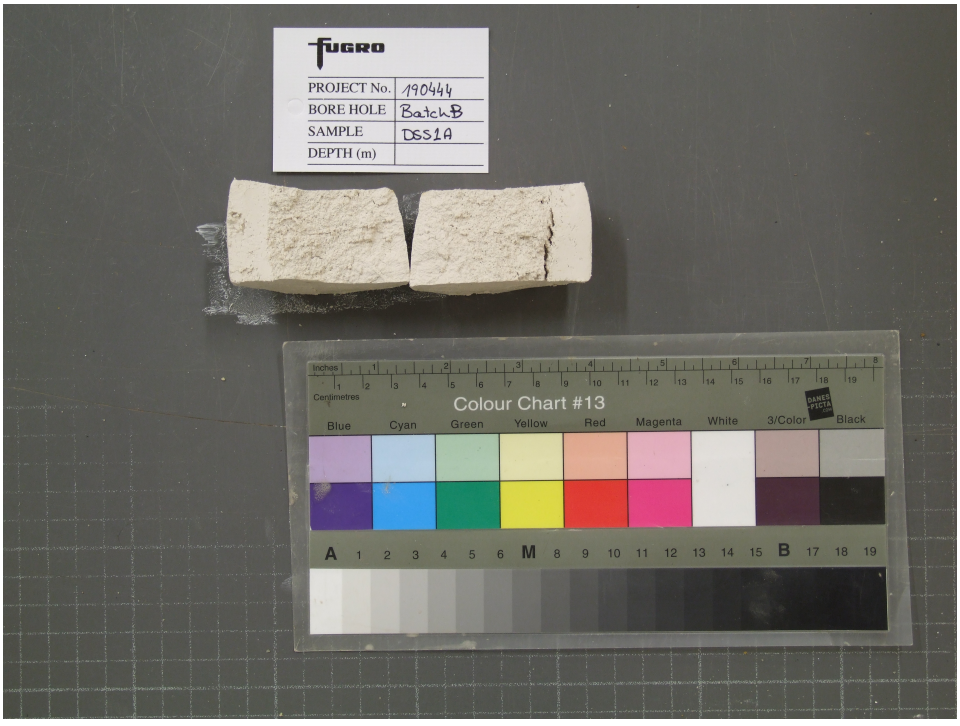

Figure C.15: Split sample photo DSS1A.

Figure C.16: Sample photo DSS1B.

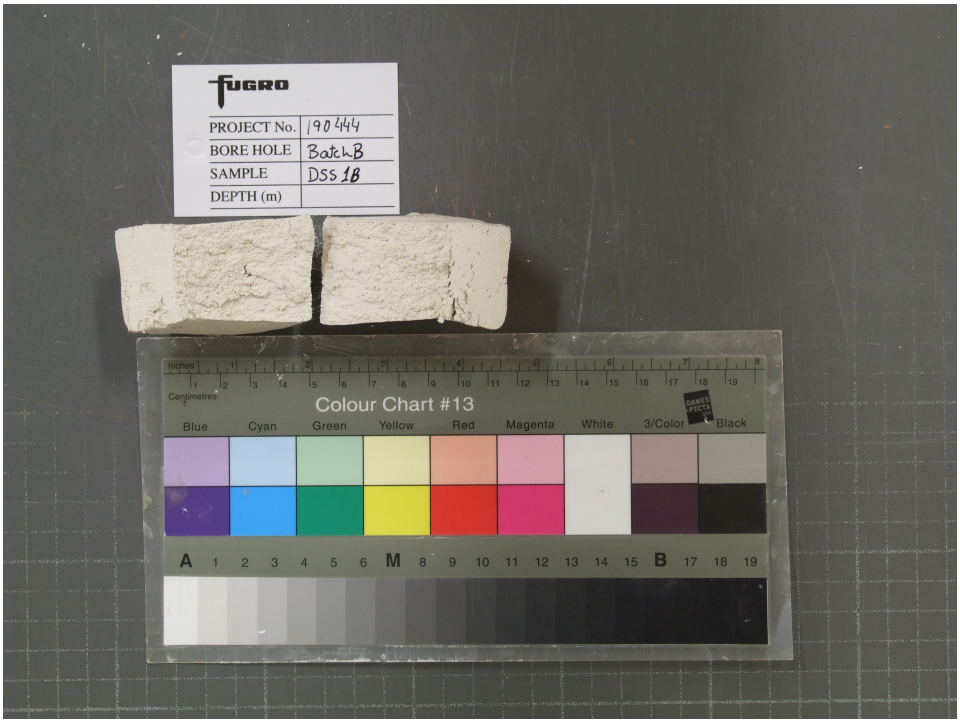

Figure C.17: Split sample photo DSS1B.

Figure C.18: Sample photo DSS1C.

Figure C.19: Split sample photo DSS1C.

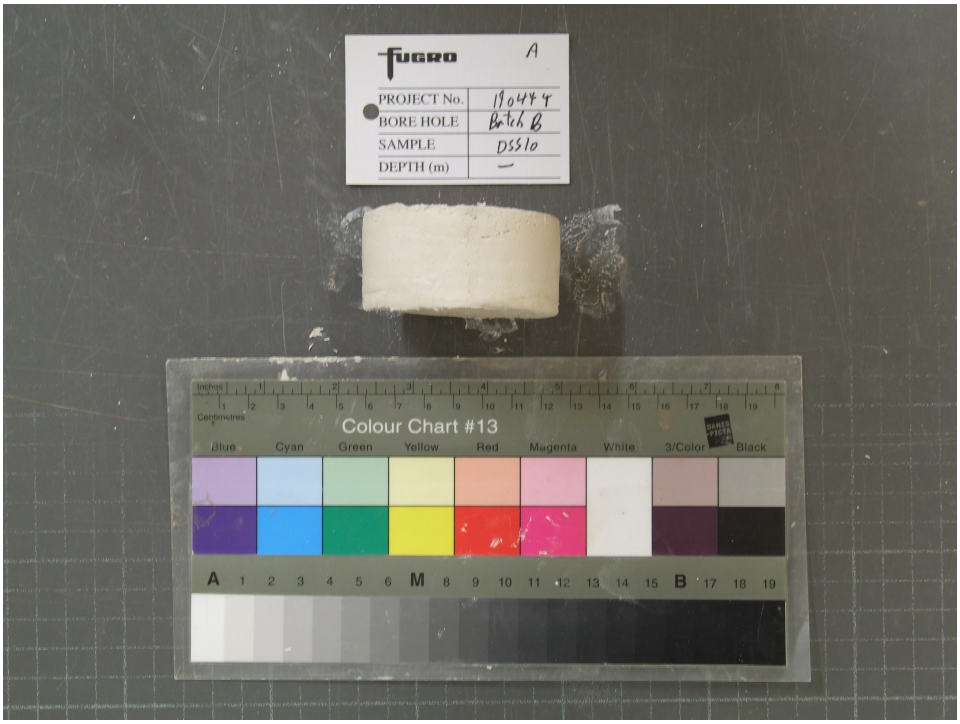

Figure C.20: Sample photo DSS10A.

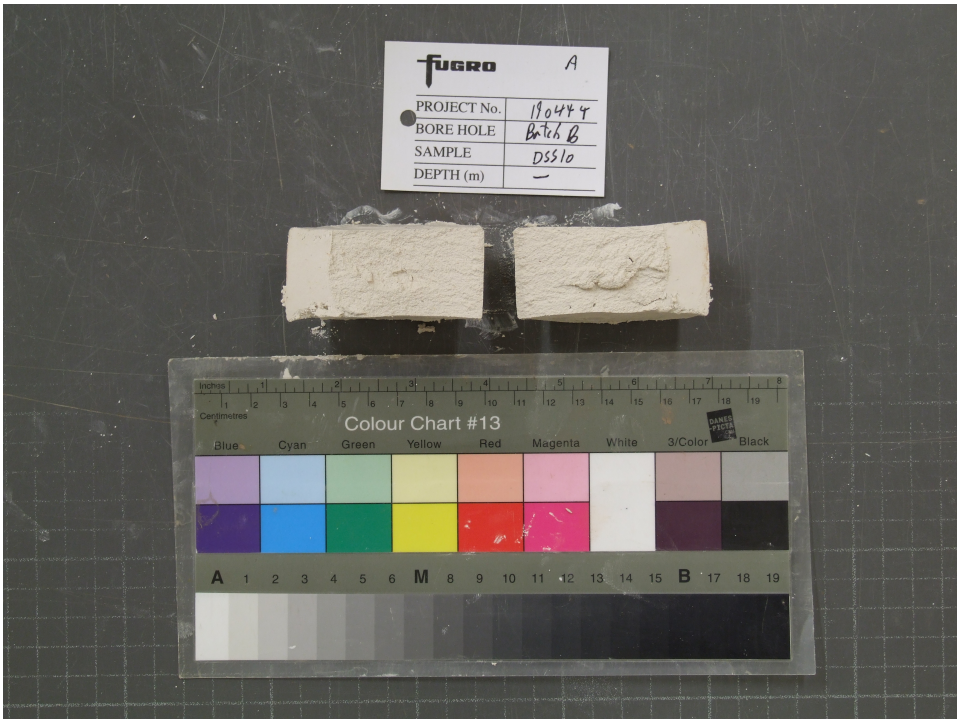

Figure C.21: Split sample photo DSS10A.

Figure C.22: Sample photo DSS10B.

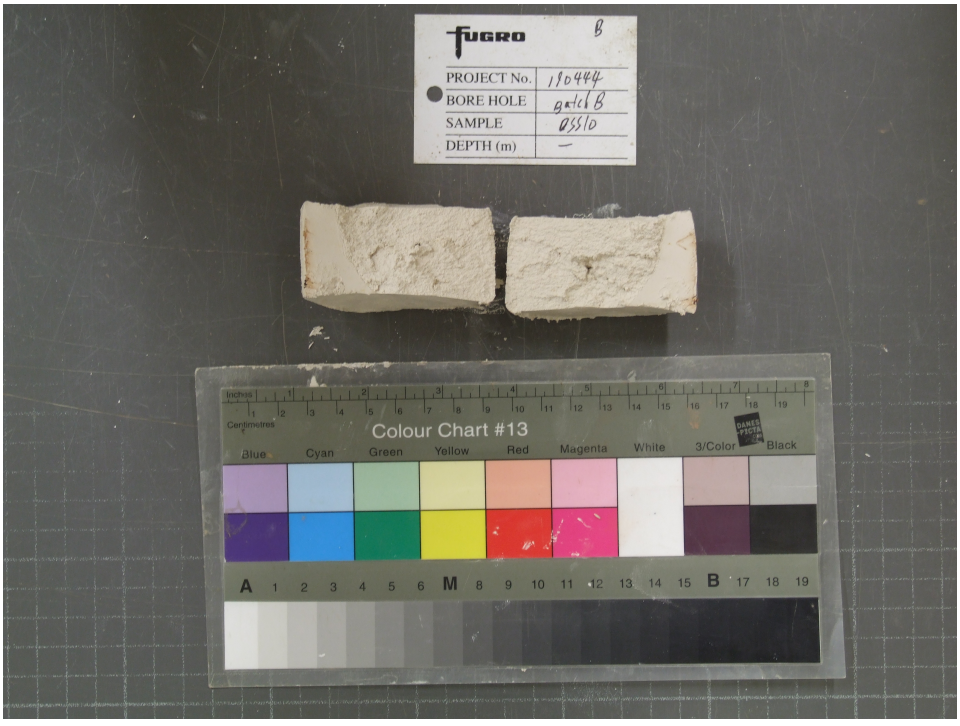

Figure C.23: Split sample photo DSS10B.

Figure C.24: Sample photo DSS10C.

Figure C.25: Sample photo DSS30A.

Figure C.26: Split sample photo DSS30A.

Figure C.27: Sample photo DSS30B.

Figure C.28: Split sample photo DSS30B.

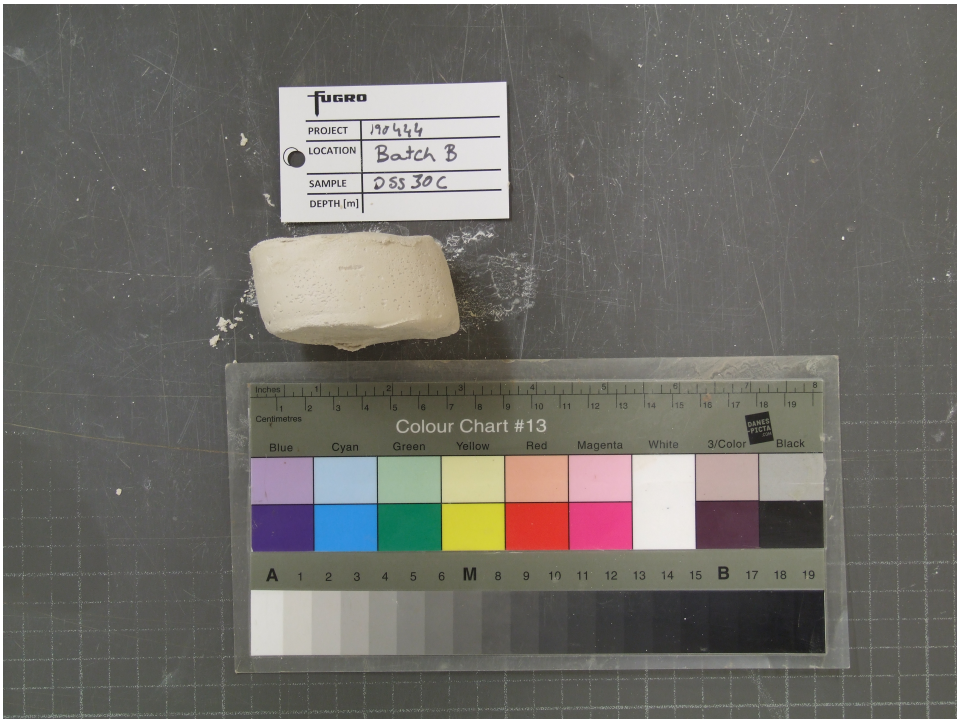

Figure C.29: Sample photo DSS30C.

Figure C.30: Split sample photo DSS30C.

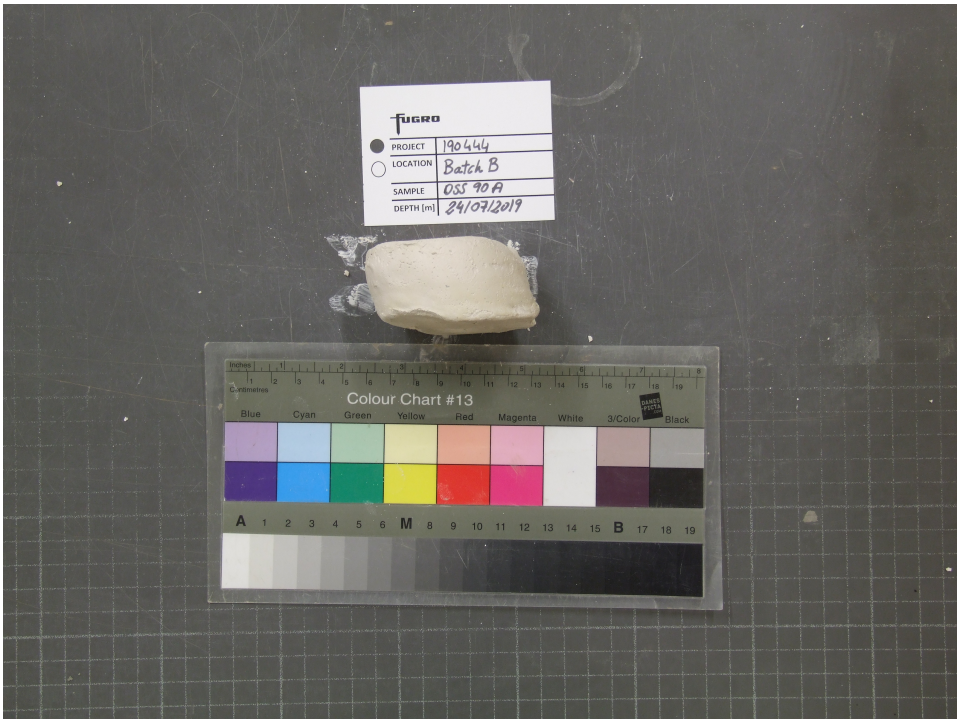

Figure C.31: Sample photo DSS90A.

Figure C.32: Split sample photo DSS90A.

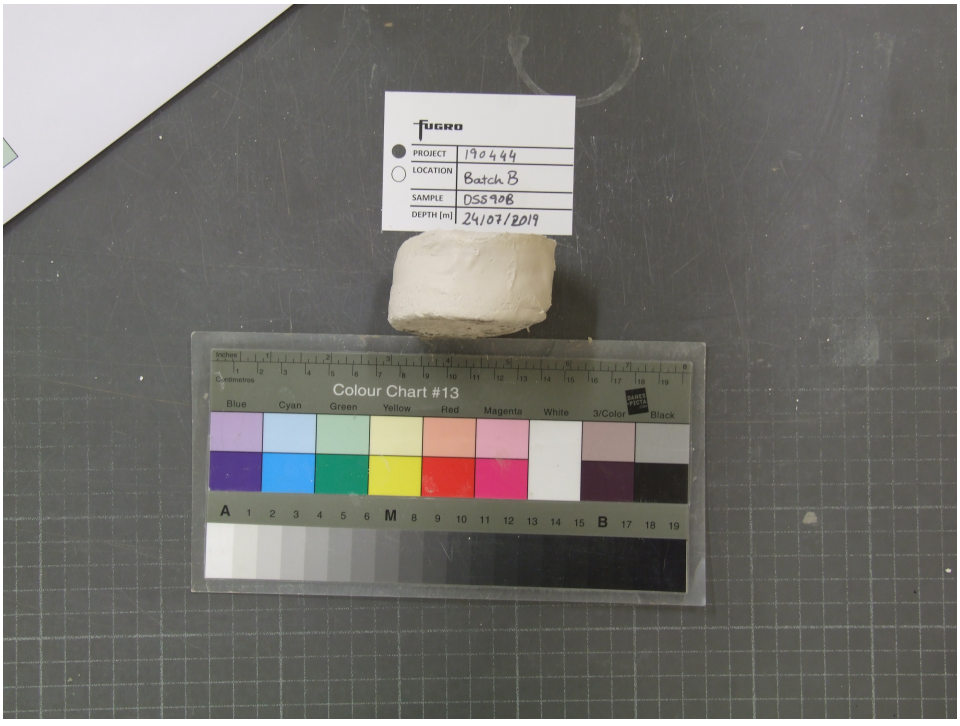

Figure C.33: Sample photo DSS90B.

Figure C.34: Split sample photo DSS90B.

Figure C.35: Sample photo DSS90C.

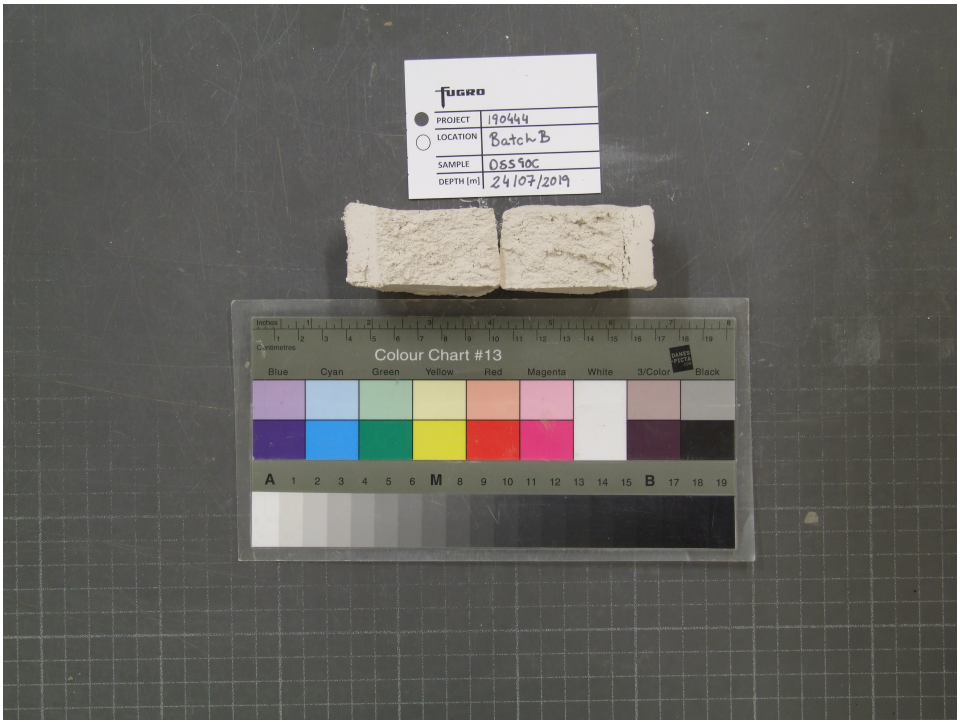

Figure C.36: Split sample photo DSS90C.

C.3. Consolidated Undrained Triaxial

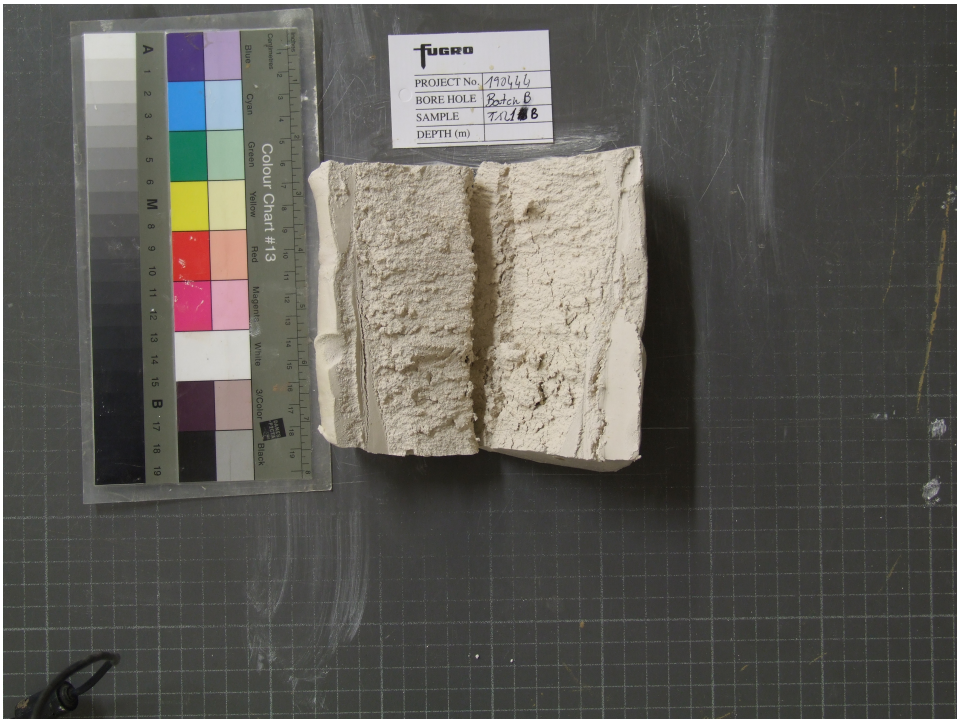

Figure C.37: Sample photo TXL1B.

Figure C.38: Split sample photo TXL1B.

Figure C.39: Sample photo TXL1C.

Figure C.40: Split sample photo TXL1C.

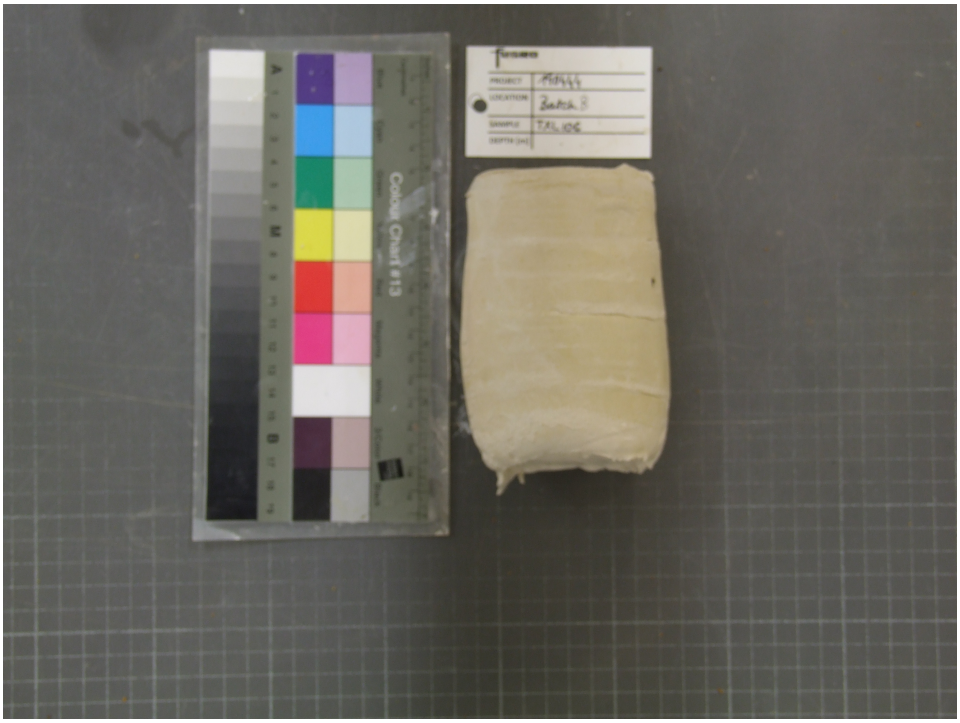

Figure C.41: Sample photo TXL1D.

Figure C.42: Split sample photo TXL1D.

Figure C.43: Sample photo TXL1E.

Figure C.44: Split sample photo TXL1E.

Figure C.45: Sample photo TXL10A.

Figure C.46: Split sample photo TXL10A.

Figure C.47: Sample photo TXL10B.

Figure C.48: Split sample photo TXL10B.

Figure C.49: Sample photo TXL30A.

Figure C.50: Split sample photo TXL30A.

Figure C.51: Sample photo TXL30B.

Figure C.52: Split sample photo TXL30B.

Figure C.53: Sample photo TXL30C.

Figure C.54: Split sample photo TXL30C.

Figure C.55: Sample photo TXL90A.

Figure C.56: Split sample photo TXL90A.

Figure C.57: Sample photo TXL90B.

Figure C.58: Split sample photo TXL90B.